



## THESIS APPROVAL

### GRADUATE SCHOOL, KASETSART UNIVERSITY

Doctor of Philosophy (Food Science)

DEGREE

Food Science

FIELD

Food Science and Technology

DEPARTMENT

TITLE: The Effect of Freeze-dried Mango Structure on  $\beta$ -carotene Degradation During Storage

NAME: Mr. Nathdanai Harnkarnsujarit

THIS THESIS HAS BEEN ACCEPTED BY

THESIS ADVISOR

( Associate Professor Sanguansri Charoenrein, Ph.D. )

THESIS CO-ADVISOR

( Assistant Professor Tanaboon Sajjaanantakul, Ph.D. )

THESIS CO-ADVISOR

( Mrs. Sasitorn Tongchitpakdee, Ph.D. )

DEPARTMENT HEAD

( Assistant Professor Wannee Jirapakkul, Ph.D. )

APPROVED BY THE GRADUATE SCHOOL ON \_\_\_\_\_

DEAN

( Associate Professor Gunjana Theeragool, D.Agr. )

THESIS

THE EFFECT OF FREEZE-DRIED MANGO STRUCTURE ON  
 $\beta$ -CAROTENE DEGRADATION DURING STORAGE



NATHDANAI HARNKARNSUJARIT

A Thesis Submitted in Partial Fulfillment of  
the Requirements for the Degree of  
Doctor of Philosophy (Food Science)  
Graduate School, Kasetsart University

2012

ณัฐดนัย หาญการสุจริต 2555: ผลของโครงสร้างมะม่วงทำแห้งเยือกแข็งต่อการสลายตัวของสารบีตาแคโรทีนในระหว่างการเก็บรักษา ปริญญาคุญบัณฑิต (วิทยาศาสตร์การอาหาร) สาขาวิทยาศาสตร์การอาหาร ภาควิชาวิทยาศาสตร์และเทคโนโลยีการอาหาร อาจารย์ที่ปรึกษาวิทยานิพนธ์หลัก: รองศาสตราจารย์สงวนศรี เจริญเหรียญ, Ph.D. 190 หน้า

งานวิจัยนี้มีวัตถุประสงค์เพื่อศึกษาผลของโครงสร้างอาหารทำแห้งเยือกแข็งและค่าออสโมติกแอคทีวิตีต่ออัตราการสลายตัวของสารบีตาแคโรทีนที่พบตามธรรมชาติในอาหาร รวมถึงการบรรจุลงในระบบจำลองที่ประกอบด้วยสารคาร์โบไฮเดรต งานวิจัยประกอบด้วย 5 ส่วน ได้แก่ การศึกษาในมะม่วงซึ่งเป็นตัวแทนระบบอาหารจริง (ส่วนที่ 1 และ 2) และของผสมที่ประกอบด้วยวุ้น มอลโตเดกซ์ทรินและน้ำตาล (กลูโคส ฟรุกโตสและซูโครส) ซึ่งเป็นตัวแทนของระบบจำลองผลไม้ (ส่วนที่ 3, 4 และ 5) จากการศึกษาพบว่าการสลายตัวของสารบีตาแคโรทีนเป็นไปตามจลนศาสตร์ลำดับที่ 1 การเก็บรักษามะม่วงแห้งเยือกแข็งที่ระดับออสโมติกแอคทีวิตีต่ำกว่าหรือเท่ากับ 0.4 ทำให้เกิดการสูญเสียสีน้ำตาลหลังจากเก็บรักษาในระยะหนึ่ง ซึ่งเกิดจากการตกผลึกของน้ำตาล โดยขึ้นชั้นผลจากการวิเคราะห์ด้วยการเลี้ยวเบนของรังสีเอกซ์เรย์และภาพถ่ายจากกล้องจุลทรรศน์อิเล็กตรอน และยังพบการเพิ่มขึ้นของอัตราการสลายตัวของสารบีตาแคโรทีนเมื่อความชื้นเพิ่มขึ้นจากระดับดังกล่าว นอกจากนี้พบการลดลงของอัตราการสลายตัวของสารบีตาแคโรทีนในมะม่วงแห้งเมื่อความชื้นในระหว่างการเก็บรักษาเพิ่มขึ้น จากออสโมติกแอคทีวิตี 0.1-0.4 ซึ่งสอดคล้องกับการยุบตัวหรือการเกาะตัวกันของผนังมะม่วง การใช้สภาวะในการแช่เยือกแข็งต่างๆสามารถควบคุมโครงสร้างของมะม่วงแห้งให้มีความพรุนและการยุบตัวได้ โดยการยุบตัวของมะม่วงทำแห้งเยือกแข็งในสภาวะกลาสสามารถเพิ่มความคงตัวของสารบีตาแคโรทีนได้เมื่อเทียบกับระบบที่มีรูพรุน เนื่องจากโครงสร้างที่ยุบตัวช่วยป้องกันการซึมผ่านของออกซิเจนไปสัมผัสกับสารบีตาแคโรทีน สำหรับระบบของผสมวุ้น มอลโตเดกซ์ทรินและน้ำตาลนั้นพบว่าการเปลี่ยนแปลงอุณหภูมิการแช่เยือกแข็งและขนาดโมเลกุลมีผลต่อความพรุนและการยุบตัวของโครงสร้าง โดยที่น้ำตาลมีอิทธิพลในการลดอุณหภูมิกลาสทรานซิชันและอุณหภูมิเริ่มต้นของการหลอมละลายของน้ำแข็ง นำไปสู่การยุบตัวของโครงสร้างระหว่างการทำแห้ง อย่างไรก็ตามน้ำตาลมีอิทธิพลในการกำกับโครงสร้างของรูพรุนในระบบที่ไม่ยุบตัว ในระบบโมเดลซึ่งอยู่ในสภาวะกลาสพบว่าความพรุนมีอิทธิพลหลักต่อความคงตัวของสารบีตาแคโรทีนทั้งแบบผลึกและแบบที่ละลายในไขมัน รูพรุนที่เล็กจะมีผนังบางรวมถึงพื้นที่ผิวที่มาก จึงมีโอกาสสัมผัสกับออกซิเจนในปริมาณสูงและทำให้มีอัตราการสลายตัวสูง นอกจากนี้ยังพบว่าเวลาที่ใช้ในการคลายตัวของโมเลกุลหรือรีแลกเซชัน ซึ่งวิเคราะห์จากเครื่องวัดการเคลื่อนที่เชิงกลมีความสัมพันธ์กับอัตราการสลายตัวของสารบีตาแคโรทีนในระบบที่เก็บรักษาที่อุณหภูมิสูงกว่าอุณหภูมิกลาสทรานซิชัน และการเพิ่มขนาดของอนุภาคไขมันซึ่งมีสารบีตาแคโรทีนละลายอยู่โดยการเกาะกลุ่มจะช่วยลดปริมาณพื้นที่ผิวที่สัมผัสกับออกซิเจน ซึ่งช่วยเพิ่มความคงตัวของสารบีตาแคโรทีนในระบบอาหารอาหารทำแห้งเยือกแข็ง

Nathdanai Harnkarnsujarit 2012: The Effect of Freeze-dried Mango Structure on  $\beta$ -carotene Degradation During Storage. Doctor of Philosophy (Food Science),  
Major Field: Food Science, Department of Food Science and Technology.  
Thesis Advisor: Associate Professor Sanguansri Charoenrein, Ph.D. 190 pages.

The main objective of this research was to investigate the effect of freeze-dried food structures and water activity ( $a_w$ ) on the rate of  $\beta$ -carotene loss as naturally dispersed in foods as well as the encapsulated components in carbohydrate systems. The research was divided in five parts which composed of the study in mango as a real food (part 1 and 2) and the agar-maltodextrin-sugar (glucose, fructose and sucrose) mixtures as fruit model systems (part 3, 4 and 5). The results indicated that the degradation of  $\beta$ -carotene in freeze-dried materials followed first order kinetics. Freeze-dried mango powders stored at  $a_w \geq 0.4$  showed the loss of initially sorbed water as a result of sugar crystallization which was confirmed by the X-ray powder diffraction as well as scanning electron microscope. In addition, increased rate of  $\beta$ -carotene degradation was observed above such  $a_w$ . The  $\beta$ -carotene loss decreased as increased  $a_w$  from 0.1 to 0.4 which was coincident with the collapse or sticky of mango powder. The various freeze-drying conditions effectively controlled the porosity and structural collapse of freeze-dried mangoes. The structural collapse of glassy freeze-dried mangoes showed an effective stabilization of  $\beta$ -carotene by the prevention of oxygen permeation to expose with  $\beta$ -carotene. Various freezing temperature and molecular size of solutes influenced the porosity and structural collapse of freeze-dried agar-maltodextrin-sugars systems. Sugars depressed the glass transition and onset temperatures of ice melting of maximally-freeze-concentrated systems and affected collapse during freeze-drying, but controlled microstructure of non-collapsed solids. In the glassy solids, pore microstructure had a major effect on stability of both crystalline and oil-dispersed  $\beta$ -carotene in solids. Smaller pores corresponding to thinner membrane walls and a larger surface area allowed more oxygen accessibility through solids and led to a higher  $\beta$ -carotene loss. The relaxation times derived from dynamic mechanical analysis correlated well to the rate of  $\beta$ -carotene degradation above glass transition temperature. Moreover, the coalescence of dispersed lipid increased the size of droplets and reduced surface area for oxygen exposure which effectively enhanced  $\beta$ -carotene stability in freeze-dried foods.

---

Student's signature

---

Thesis Advisor's signature

## ACKNOWLEDGEMENTS

This research was financially supported by the Thailand Research Fund through the Royal Golden Jubilee Ph.D. program during December 2007 to May 2012. I could not deny that it was a very hard time at the beginning of my Ph.D. study as I was a newly graduated student and took part in the Ph.D. program; however, over years with kind help and support from my advisors, colleagues, friends and family, this research and my Ph.D. was achieved.

In the first place I would like to express my grateful gratitude to my thesis advisor, Assoc. Prof. Dr. Sanguansri Charoenrein for her advice, encouragement and valuable suggestion to achieve not only the research work but fulfill the skill in the real life as a good person. I appreciate for her belief in my ability and gave me chance to conduct Ph.D. research. It was really a great and joyful time working with her. Furthermore, this research would not be achieved without my thesis co-advisor, Prof. Yrjö H. Roos. I would grateful to him for his guidance, advice and uncountable useful comments on my research. Since the first time we met in Thailand until my stay at UCC, he always kindly taught very useful knowledge and abilities to conduct research. He inspired me to be a good scientist and always encouraged the student to explore the world of food scientist.

I would like to thanks my thesis committees, Asst. Prof. Tanaboon Sajjaanatakul for his valuable comments and suggestion in fulfillment of Ph.D. as well as Dr. Sasitorn Tongchitpakdee and her graduated students for their support on analytical techniques. I appreciate the guidance and encouragements from all the faculties of the department of Food Science and Technology, KU. I appreciate Prof. Vanna Tulyathan and Asst. Prof. Wannee Jirapakkul for their kind willing to be my defense thesis examiner as well as their kind comments and suggestions on this research.

I sincerely thank my colleagues at the laboratory 2411, 2412, 2413 KU for their kind help, support and encouragements as well as the Material Science laboratory at UCC for their support and research skills. I appreciate all the support from the technician at KU and UCC.

Finally, I would like to thank my family for their encouragement, support and gladly sacrifice during the time of my Ph.D. study.

Nathdanai Harnkarnsujarit

April 2012



## TABLE OF CONTENTS

	<b>Page</b>
TABLE OF CONTENTS	i
LIST OF TABLES	ii
LIST OF FIGURES	iv
INTRODUCTION	1
OBJECTIVES	5
LITERATURE REVIEW	7
MATERIALS AND METHODS	50
Materials	50
Methods	53
RESULTS AND DISCUSSION	72
CONCLUSIONS	145
RECOMMENDATION	148
LITERATURE CITED	149
APPENDIX	173
CURRICULUM VITAE	188

## LIST OF TABLES

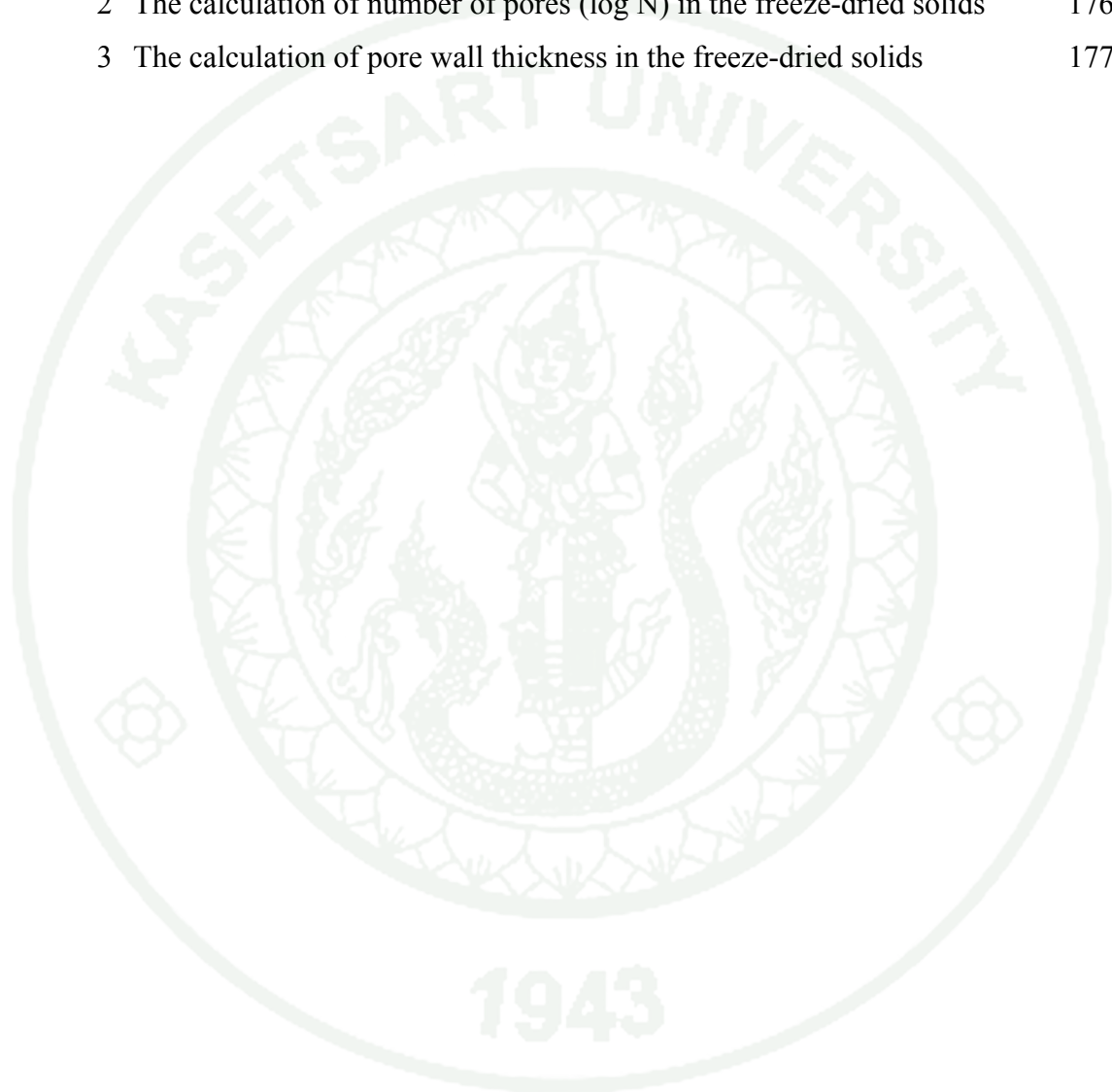
Table	Page
1 The nutritional qualities of fresh mangoes	39
2 Freeze-drying protocols and obtained freeze-dried mango and agar gel (2% and 4% w/w) structures	83
3 Rate constant of $\beta$ -carotene degradation in freeze-dried mangoes stored at 11% and 22% RVP	92
4 Glass transition ( $T_g'$ ) and onset temperature of ice melting ( $T_m'$ ) of maltodextrin–agar gels with and without sugars, and compression characteristics of freeze-dried solids frozen at $-20^\circ\text{C}$ prior to freeze-drying	94
5 Freezing properties derived from freezing profiles: supercooling temperature ( $T_s$ ) and freezing temperature ( $T_i$ ) of fresh maltodextrin-agar gels with and without sugars frozen at $-20^\circ\text{C}$ , $-40^\circ\text{C}$ and $-80^\circ\text{C}$ prior to freeze-drying	97
6 Water content and glass transition temperature ( $T_g$ ) of freeze-dried maltodextrin (M40:DE6, M100:DE11 and M250:DE25.5) and maltodextrin-sugar (glucose, fructose, sucrose and sugar mixture (glucose: fructose: sucrose; 1:1:4) systems (M100: sugars; 1:1) at various $a_w$ ,	112
7 Brunauer-Emmet-Teller (BET) monolayer water content ( $m_m$ ) and critical water activity, $a_w$ , which depressed the glass transition temperature, $T_g$ , of freeze-dried solids to room temperature ( $24^\circ\text{C}$ )	119

### Appendix Table

1 Zeroth-, first- and second-order rate constants ( $k$ ) and coefficients of determination ( $R^2$ ) of $\beta$ -carotene degradation in freeze-dried maltodextrin solids (M40, M100, M250) prefrozen at various temperature ( $-20^\circ\text{C}$ , $-40^\circ\text{C}$ and $-80^\circ\text{C}$ ) during storage at anhydrous condition at $25^\circ\text{C}$	175
---	-----

**LIST OF TABLES (Continued)**

<b>Appendix Table</b>	<b>Page</b>
2 The calculation of number of pores (log N) in the freeze-dried solids	176
3 The calculation of pore wall thickness in the freeze-dried solids	177





## LIST OF FIGURES

Figure	Page
1 Enthalpy and volume of various states of materials and the changes of heat flow around glass transition region as measured by DSC	9
2 Changes in dielectric and mechanical properties of materials at and above the glass transition	13
3 State diagram showing various cooling behavior of food materials at various concentration	17
4 The original stability map of food showing the relative rate of reactions and moisture content as a function of water activity	19
5 Phase diagram of water showing the classical freeze-drying pathway	25
6 Typical state diagram supplemented with the freeze-drying pathway of a freeze-concentrated solution to be freeze-dried ( $X=20\%$ )	28
7 Light micrograph of ripe mango mesophyll cell showing the typical color of mango chromoplasts, some starch grains, soft cell wall and vacuole, and cortex cells of carrot root showing typical color and structure of the crystalline type of chromoplasts	40
8 Structure of all trans- $\beta$ -carotene	41
9 $\beta$ -carotene degradation pathway and their products	42
10 Water content and water sorption isotherms of freeze-dried mango powder at various RVP levels at $25^{\circ}\text{C}$	74
11 X-ray diffraction pattern of freeze-dried mango powder: uncrystallized, stored at 11.3% RVP, 43.2% RVP, 57.6% RVP, and 68.9% RVP for 7 d at $25^{\circ}\text{C}$	76
12 X-ray diffraction pattern of freeze-dried mango powder stored at 68.9% RVP for 7 d at $25^{\circ}\text{C}$ compared to XRD standard peaks of sucrose, fructose, and glucose	77
13 SEM images of freeze-dried mango powder: uncrystallized, stored at 11.3% RVP, 43.2% RVP, 57.6% RVP and 68.9% RVP for 7 d at $25^{\circ}\text{C}$	78
14 First-order rate constant of $\beta$ -carotene degradation at various $a_w$ , at $25^{\circ}\text{C}$	80

## LIST OF FIGURES (Continued)

Figure	Page
15 Freeze-drying temperature profile of mangoes with the application of freeze-drying protocols 1: freezing at -35°C and shelf temperature of -40°C, protocol 2: freezing at -35°C and shelf temperature of -15°C and protocol 3: freezing by immersion in liquid nitrogen and shelf temperature of -40°C	84
16 Stereomicrographs of freeze-dried mangoes using freeze-drying protocol 1: freezing at -35°C and shelf temperature of -40°C, protocol 2: freezing at -35°C and shelf temperature of -15°C and protocol 3: freezing by immersion in liquid nitrogen and shelf temperature of -40°C at a magnification of 10x	85
17 Stereomicrographs of freeze-dried agar gel surface with the application of freeze-drying protocol 1: freezing at -35°C and shelf temperature of -40°C of 2%w/w, 4%w/w, protocol 2: freezing at -35°C and shelf temperature of -15°C of 2%w/w, 4%w/w and protocol 3: freezing by immersion in liquid nitrogen and shelf temperature of -40°C of 2%w/w, 4%w/w at a magnification of 10x	86
18 SEM images of cross-sectioned freeze-dried mangoes using freeze-drying protocol 1: freezing at -35°C and shelf temperature of -40°C, protocol 2: freezing at -35°C and shelf temperature of -15°C and protocol 3: freezing by immersion in liquid nitrogen and shelf temperature of -40°C at a magnification of 10x	89
19 Degradation of $\beta$ -carotene in freeze-dried mangoes as a result of various freeze-drying protocols during storage at 11% and 22% RVP	90
20 Freezing profiles of maltodextrin–agar gels and maltodextrin–agar gels with sugars at freezing temperatures of -20°C, -40°C and -80°C	96
21 SEM micrographs of freeze-dried maltodextrin–agar systems: M40 frozen at -20 °C, -40 °C and -80 °C; M100 frozen at -20°C, -40°C and -80°C; and M250 frozen at -20°C, -40°C and -80°C prior to freeze-drying at 250x magnification	98

## LIST OF FIGURES (Continued)

Figure		Page
22	Number of pores and wall thickness as a function of pore diameter of freeze-dried maltodextrin–agar systems with and without sugars	100
23	SEM micrographs of freeze-dried maltodextrin–agar (M100) solids with glucose, fructose and sucrose frozen at $-20^{\circ}\text{C}$ prior to freeze-drying at 100x magnification	102
24	Appearance of freeze-dried solids: maltodextrin (M40:DE6, M100:DE11 and M250:DE25.5); maltodextrin (M100) with sugar (glucose, fructose, sucrose and mixture) at the ratio of 1:1 frozen at $-20^{\circ}\text{C}$ , $-40^{\circ}\text{C}$ and $-80^{\circ}\text{C}$ prior to freeze-drying	105
25	Compressive force–displacement curves of ‘anhydrous’ freeze-dried maltodextrin–agar systems: maltodextrin M40:DE6; M100:DE11; M250:DE25.5 frozen at $-20^{\circ}\text{C}$ , $-40^{\circ}\text{C}$ and $-80^{\circ}\text{C}$ prior to freeze-drying	108
26	Compressive peak force and modulus of ‘anhydrous’ freeze-dried maltodextrin–agar systems (M40, M100 and M250) frozen at $-20^{\circ}\text{C}$ , $-40^{\circ}\text{C}$ and $-80^{\circ}\text{C}$ prior to freeze-drying as a function of dextrose equivalent (DE)	109
27	SEM micrographs of freeze-dried maltodextrin systems (M100) prefrozen at $-20^{\circ}\text{C}$ , $-40^{\circ}\text{C}$ and $-80^{\circ}\text{C}$ prior to freeze-drying at 100x magnification indicate pore size and wall thickness of the solids	111
28	The $\alpha$ -relaxation time ( $\tau_{\alpha}$ ) of freeze-dried maltodextrin-sugar systems (M100: sugar; 1:1) at anhydrous and 0.44 $a_w$ at $24^{\circ}\text{C}$ . The $\tau$ values were derived from the loss modulus of dynamic mechanical measurements at frequencies of 0.5, 1, 5, 10, 20 Hz	114
29	Log $\alpha$ -relaxation time ( $\tau_{\alpha}$ ) and first-order rate constants ( $-k$ ) of $\beta$ -carotene degradation in porous freeze-dried maltodextrin-sugar (glucose, fructose, sucrose and sugar mixture (glucose: fructose: sucrose; 1:1:4) systems (M100: sugars; 1:1) as a function of difference between storage temperature and glass transition temperature ( $T-T_g$ )	116

## LIST OF FIGURES (Continued)

Figure	Page	
30	Log $\alpha$ -relaxation time ( $\tau_\alpha$ ) and first-order rate constants (-k) of $\beta$ -carotene degradation in porous freeze-dried maltodextrin (M40:DE6, M100:DE11 and M250:DE25.5) and maltodextrin-sugar (glucose, fructose, sucrose and sugar mixture (glucose: fructose: sucrose; 1:1:4) systems (M100: sugars; 1:1) as a function of water activity, $a_w$	117
31	First-order rate constants (k) of $\beta$ -carotene degradation in freeze-dried maltodextrin-sugar systems (glucose, fructose, sucrose and sugar mixture (glucose: fructose: sucrose; 1:1:4) (M100: sugars; 1:1) prefrozen at -20°C and -80°C prior to freeze-drying and stored at 24°C in anhydrous condition and 0.11 $a_w$	120
32	First-order rate constants (k) of $\beta$ -carotene degradation in freeze-dried maltodextrin systems (prefreezing at -20°C, -40°C and -80°C) as functions of solid pore diameter and wall thickness stored at anhydrous condition, 0.22 and 0.44 $a_w$ at 24°C	122
33	Freezing profile of maltodextrin-agar gels containing dispersed emulsion of $\beta$ -carotene at freezing temperature of -20°C, -40°C and -80°C with onset of ice melting temperature ( $T_m'$ ) of maltodextrin systems	126
34	Influence of freezing at -20°C, -40°C and -80°C, and freeze-drying on average particle size $d_{32}$ of $\beta$ -carotene emulsion in various maltodextrin solids (M40:DE6, M100:DE11 and M250:DE25.5)	127
35	Appearance of freeze-dried $\beta$ -carotene emulsions after freeze-drying and subsequent storage for 24 days at 0.75 $a_w$ at room temperature (24°C) with the corresponding T- $T_g$ values referring to the difference between storage temperature and glass transition temperature	128
36	Average particle size $d_{32}$ of $\beta$ -carotene emulsion in various freeze-dried maltodextrin solids (M40:DE6, M100:DE11 and M250:DE25.5) prefrozen at -20°C, -40°C and -80°C prior to freeze-drying and storage under anhydrous, 0.33 and 0.75 $a_w$ at room temperature (24°C) for 24 days	129

## LIST OF FIGURES (Continued)

Figure	Page
37    Appearance of freeze-dried agar-maltodextrin (M040, M100 and M250) solids containing dispersed oil-dissolved $\beta$ -carotene particles prefrozen at -20°C, -40°C and -80°C prior to freeze-drying	131
38    First-order rate constants for $\beta$ -carotene degradation in freeze-dried maltodextrin systems prefrozen at -20°C, -40°C and -80°C prior to freeze-drying stored at anhydrous, 0.33 and 0.75 $a_w$ condition at room temperature (24°C)	135
39    Schematic diagram shows the microstructure formation (porous and collapsed structure) of freeze-dried solids as reflected by the process parameters (freezing and freeze-drying) and solid components	137
40    Schematic diagram shows the effect of solid microstructure on the stability of $\beta$ -carotene in freeze-dried solids	141
41    Schematic diagram shows the effects of water on the stability of $\beta$ -carotene in freeze-dried systems	142
42    Water accelerates sugar crystallization causing the cell wall disruption of mangoes	144

### Appendix Figure

1    Experimental HPLC chromatogram shows the eluting peak and retention time (~3.5 min) of $\beta$ -carotene in freeze-dried mangoes	177
2    Experimental standard curve for $\beta$ -carotene analysis using a HPLC	177
3    First and second DSC scan of freeze-dried mangoes stored under anhydrous and 0.11 $a_w$ conditions	178
4    Particle size distribution of dispersed phase of emulsion (40:60 oil: water) containing 0.02%w/w $\beta$ -carotene after homogenized with a two-stage valve homogenizer prior to mixing with maltodextrin systems	179



## LIST OF FIGURES (Continued)

Appendix Figure	Page
5 DSC thermograms of mango juice and freeze-dried mangoes stored at various relative vapor pressure (RVP) with the corresponding $T_g$ values	180
6 DSC thermogram of fresh mango juice showing phase and state transitions of mangoes	181
7 DSC thermograms of agar-maltodextrin (M100) and agar-M100-fructose systems shows the ice melting peak during a heating scan and some experimental parameters	182
8 DSC thermograms of freeze-dried maltodextrin-sugar systems (M100: sugar, 1:1) at $0.44a_w$	183
9 The loss modulus as a function of temperature of anhydrous freeze-dried maltodextrin (M100)-sugar systems at a frequency of 0.5 Hz	183
10 The loss modulus as a function of temperature of $0.44a_w$ freeze-dried maltodextrin (M100)-sugar systems at a frequency of 0.5 Hz	184
11 The rate constant for $\beta$ -carotene degradation in freeze-dried maltodextrin systems (M40:DE6, M100:DE11, M250:DE25.5) as a function of dextrose equivalent at $25^\circ\text{C}$	185
12 Retention (%) of $\beta$ -carotene in sugar-maltodextrin systems prefrozen at $-20^\circ\text{C}$ and $-80^\circ\text{C}$ during storage at anhydrous and 11% RVP at $25^\circ\text{C}$	186
13 Particle size distribution of lipid particles in maltodextrin systems (M040, M100 and M250) measured with a laser diffraction particle size analyzer at 0 day and 24 days of storage at various $a_w$ (0, 0.33 and $0.75a_w$ )	187

# THE EFFECT OF FREEZE-DRIED MANGO STRUCTURE ON $\beta$ -CAROTENE DEGRADATION DURING STORAGE

## INTRODUCTION

$\beta$ -carotene is a functional lipid soluble compounds, which contributes to provitamin A precursors and possesses an antioxidant function. This lipophilic molecule is naturally a pigment and exists in foods in various physical forms, as it may be noncrystalline in lipid droplets in mangoes and it appears in crystalline forms, e.g., in carrots and tomatoes (Harris and Spurr, 1969; Vásquez-Caicedo *et al.*, 2006). The molecular structure consists of high amount of unsaturated double bonds contributing to oxygen sensitivity and degrades continually during storage. Therefore, an improved stabilization of  $\beta$ -carotene can help preserve product color as well as the nutritional qualities.

Water sorption and glass transition ( $T_g$ ) of solids often play key roles as determinants of physicochemical properties of amorphous materials and low water food stability. The freezing and dehydration processes, e.g., spray-drying and freeze-drying produce amorphous form of food solids as a result of rapid water removal. The phase and state transitions in food materials are strongly dependent on the hydrophilic components. As most of the soluble solids present in food particularly fruit are low molecular weight sugars (glucose, fructose, and sucrose), organic acids, and free amino acids, these compounds mainly responsible for the phase and state transition properties of amorphous foods. Water is a strong plasticizer of amorphous hydrophilic solids causing increases in their free volume and molecular mobility, which affect rates of deteriorative changes during storage (Le Meste *et al.*, 2002). The molecular motions above  $T_g$  increased instantly in glass-forming solids which contained small molecular weight sugars. Various structural changes including sugar crystallization and structural collapse have been shown to increase as temperature increases above  $T_g$  ( $T-T_g$ ) (Bellows and King, 1973; Levi and Karel, 1995; Roos, 1995).

Freeze-drying is capable to preserve high quality materials food of good appearance with well-retained flavor and nutritional quality as well as the encapsulation of functional food components. A successful freeze-drying process retains the volume of the material which, in the dry state, is usually highly porous, brittle and hygroscopic, and excellent rehydration properties. However, the inappropriate freeze-drying conditions lead to the structural collapse of freeze-dried solids and hence the loss of appearance and rehydration capacity (Levi and Karel, 1995). Collapse in freeze-drying has been shown to be directly related to the decreasing viscosity of amorphous solids as a result of plasticization by temperature and unfrozen water above the  $T_m'$  (Roos, 1995) which affects significantly the microstructure of freeze-dried foods and may be related to the stability of active components in freeze-dried systems.

Structural properties of freeze-dried foods are primarily formed in the prefreezing step and affect, e.g., porosity and strength of solids of freeze-dried foods as well as entrapment of functional food components. The possibilities for the manipulation of ice crystal size during freezing are numerous, i.e., the initial ice nucleation conditions can be chosen to control the ice crystal size with subsequent thermal treatment to satisfy ice sublimation requirements during the freeze-drying process. The ice crystal size needs to allow optimum heat and mass transfer properties during dehydration as well as appropriate porosity for product stability and rehydration. During freeze-drying, the ice sublimation temperature needs to be maintained below the collapse temperature,  $T_c$  (Flink and Karel, 1972; Bellows and King, 1973), which is known to correlate with the onset temperature of ice melting in maximally freeze-concentrated systems,  $T_m'$  (Roos, 1995; 2010). The  $T_m'$  values of food components vary substantially and are typically low for sugars, particularly monosaccharides. However, there is still lack of investigation on the sugar components effect on the structure formation of freeze-dried foods.

The highly porous structures of freeze-dried products elevated high rehydration capacity which may, however, enhance the oxygen exposure of dispersed components and accelerate oxidation. In the present literature, there were limited

studies on the effect of the freeze-dried food structure including porosity on dispersed bioactive component degradation. Moreover, the stability of  $\beta$ -carotene and other carotenoids in dehydrated solids at various  $a_w$  has been addressed in several studies reporting varying results (Tsimidou and Biliaderis, 1997; Selim *et al.*, 2000; Serris and Biliaderis, 2001; Prado *et al.*, 2006; Ramoneda *et al.*, 2011). The differences of sensitivity of each polymer to humidity led to differences in physico-chemical characteristics, such as collapse, and subsequent impact on the stability of encapsulated compounds. Moreover, the explanation on how these factors, e.g., water and components, affect to  $\beta$ -carotene stability is still incomplete. The stability of  $\beta$ -carotene during storage has been investigated in various food and model systems (Desobry *et al.*, 1997, 1999; Elizalde *et al.*, 2002; Prado *et al.*, 2006; Lavelli *et al.*, 2007; Ramoneda *et al.*, 2011); however, there is no study available on the effect of storage  $a_w$  on the stability of  $\beta$ -carotene in freeze-dried mangoes as well as the correlation between freeze-dried solid structures and molecular mobility above  $T_g$  on  $\beta$ -carotene stability.

The development of functional food ingredients and foods require deep understanding of the critical relationships between food structure, quality, shelf life, delivery characteristics and bioavailability of active components. The manipulation of matrix porosity possibly affects the stability of  $\beta$ -carotene by altering its exposure to oxygen. This research aimed to investigate the effect of freeze-dried solid structures and water activity on the stability of dispersed  $\beta$ -carotene in both crystalline and non-crystalline forms as naturally distributed in plants and encapsulated in carbohydrate matrices. Understanding a possible relationship between microstructures and  $\beta$ -carotene retention may help to increase stabilization of such compounds and other functional lipid ingredients in dehydrated food system. This contributes to higher nutritional benefits upon consumption as well as the retention of product color which significantly affects the consumer acceptance. The stabilization of functional substances by structural modification benefits the production of health promoting ingredients as well as the freeze-dry food industries.

## Hypotheses

As, the degradation of  $\beta$ -carotene is strongly dependent on the oxygen availability, the microstructures and water sorption would alter the oxygen accessibility through freeze-dried matrices which subsequently impact the stability of dispersed  $\beta$ -carotene in freeze-dried solids. The specific hypotheses for each parts of this research are as follows.

Part 1 based on the hypothesis that the water plasticization accelerates the crystallization of amorphous sugar components during storage above  $T_g$  of solids which subsequently impact the stability of  $\beta$ -carotene in freeze-dried mangoes.

Part 2 was hypothesized that the modification of matrix microstructure namely the structural collapse would enhance the storage stability of  $\beta$ -carotene in freeze-dried mangoes by altering the oxygen permeation and diffusion through solids.

Part 3 was based on 2 hypotheses: (i) the ice nucleation is strongly dependent on solid components (sugars and polymers) and, therefore, would control the microstructure formation of freeze-dried materials by altering the freezing properties, and (ii) The freezing process possibly manipulate the pore morphology of freeze-dried solids by control the rate of ice nucleation.

Part 4 hypothesized that the stability of dispersed crystalline form of  $\beta$ -carotene in the glassy solids is strongly dependent on the porosity of matrices. Moreover, the water plasticization would increase the molecular mobility and structural changes of solids which control the degradation of  $\beta$ -carotene.

Part 5 was hypothesized that the stability of dispersed emulsion form of  $\beta$ -carotene (non-crystalline form) in freeze-dried solids not only influenced by the porosity of solids but also the stability of dispersed lipid particles and the size of droplets which could alter the surface area for exposure of molecular oxygen.



## OBJECTIVES

The main objective of this research was to investigate the effect of freeze-dried food structures and water activity on the stability of dispersed  $\beta$ -carotene in dehydrated solids. Mango (*Mangifera indica*) was studied as a case of real food and the sugar-polymer mixtures were considered as food model systems. The results are divided in 5 parts with the specific objectives as the following.

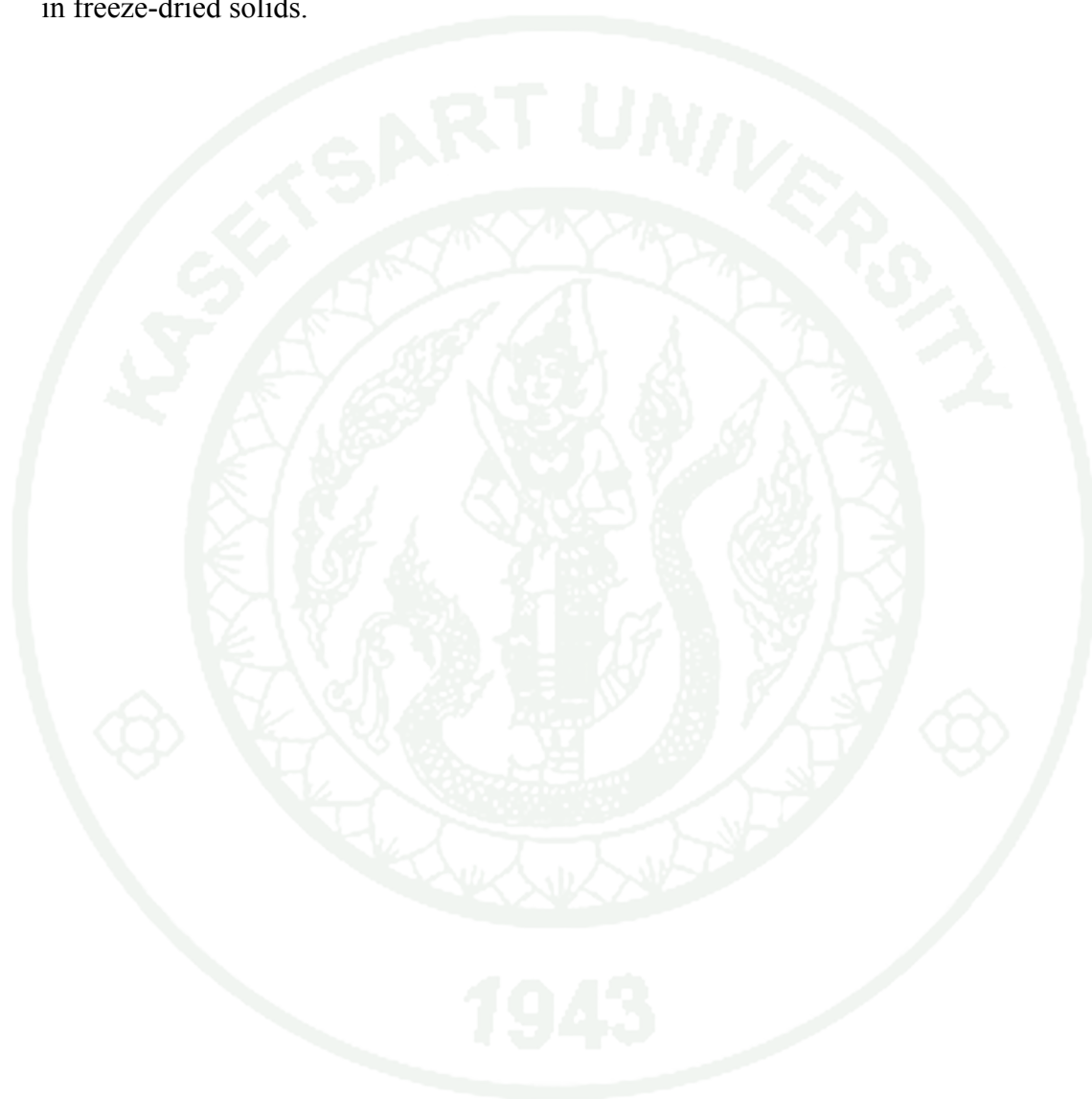
The objective of part 1 was to monitor the sugar crystallization and  $\beta$ -carotene stability in freeze-dried mangoes stored at various levels of  $a_w$ .

The objective of part 2 was to investigate the effects of structural collapse during freeze-drying on  $\beta$ -carotene stability in freeze-dried mangoes. The collapsed as well as non-collapsed structures of freeze-dried mangoes were manipulated by various freeze-drying protocols.

The objective of part 3 was to investigate the effects of freezing and carbohydrate composition on the structure of freeze-dried solids. The matrices used were maltodextrin and maltodextrin-sugar systems serving as fruit-type food models. Maltodextrin at different dextrose equivalents (DE6, 11 and 25.5) and sugars (glucose, fructose and sucrose) were used. These matrices were frozen using different freezing temperatures and freeze-dried at similar pressure-temperature conditions.

The objectives of part 4 were to investigate the effects of freeze-dried solids structures (porosity and collapse), water activity and carbohydrate solids composition on stability of dispersed crystalline  $\beta$ -carotene particles. Various porosities as well as levels of structural collapse of the freeze-dried matrices were produced by varying freezing parameters and matrix formulation.

The objectives of part 5 were to investigate the effect of porosity as well as the particle size of dispersed oil on the stability of oil-dissolved  $\beta$ -carotene particles dispersed in freeze-dried matrices. Particle size of reconstituted freeze-dried  $\beta$ -carotene emulsion was monitored coincided with the analysis of  $\beta$ -carotene stability in freeze-dried solids.



## LITERATURE REVIEW

### 1. Phase and state transitions of food materials

Phase transition is physical changes of materials namely solid-liquid-gas transformation whereas state transitions refers to the non-equilibrium changes between two configurations, typically in the solid state, i.e., amorphous-crystalline and glass-rubber transitions. Food materials are complex systems often composed of compounds that have various phase behavior or they may contain compounds that are or become phase separated, e.g., carbohydrates, lipids, protein and water. These components may all exist in different states or phases or in phases separated from each other. Water is the major components in most foods which exhibits phase transition of its own, e.g., freezing and evaporation, and has several effects on phase and state transition of other food components as well as on related food stability and quality (Witschi, 1996). The impact of water on food stability is often referred as a strong plasticizer of hydrophilic amorphous components which contributes to an increasing free volume and molecular mobility of the systems. Typically, food solids are in an amorphous metastable state, due to rapid removal of water by drying or freezing. An amorphous state of a material refers to its random, disordered molecular structure which is very sensitive to changes in temperature and moisture content.

Food materials undergo various phase and state transitions during processing and storage. This work focused on the freeze-drying process with the corresponding phase transition of water into ice and vapor. The state transition of interest is the glass transition between the solid “glassy” state and the supercooled “rubbery” state of amorphous materials.

#### 1.1 Glass transition and plasticization

Glass transition is a reversible transformation in the state (glassy↔rubbery) of amorphous materials occurs over a temperature range. In the cooling of a liquid-like material, glass transition results in solidification to a glassy

substance (vitrification); whereas, in a heating process, glass transition results in increasing translational mobility of molecules and the concomitant appearance of liquid-like characteristics of the substance (Roos, 2010a,b). Food materials may be considered as stable in their solid “glassy” state (Roos, 1993b), which is characterized by an extremely high viscosity ( $10^{12}$  Pa s) which are able to support their own weight. When the temperature of the glass is increased to glass transition temperature ( $T_g$ ), this material changes to rubbery state with a decreased viscosity ranging from  $10^6$  -  $10^8$  Pa s (Bhandari and Howes, 1999). These changes in viscosity and flow properties affect stickiness and caking of powders, crispness of amorphous solids, and crystallization as well as the rate of diffusion-controlled reactions in amorphous food systems (Roos, 2003). The transition between glass and rubber material causes various changes as shown in Figure 1.

Roos (2010b) stated that the liquid and crystalline states are equilibrium states. A supercooled liquid can retain the amorphous, disordered liquid-like structure. Molecules of such supercooled materials become frozen to form a solid glass structure below the glass transition temperature range. The glassy state of a material can show freezing of the molecules at various heat contents and volumes depending on the cooling process. The glass transition in a differential scanning calorimetry (DSC) measurement appears as an endothermic step change corresponding to a heat capacity change,  $\Delta C_p$ , over the glass transition temperature range (Figure 1). Enthalpy and volume relaxations are typical of glass transition measurements, as they indicate the appearance of translational mobility around the glass transition and the concomitant ability of the material to respond to increasing temperature. Hence, an endothermic or exothermic change with a corresponding volume change may appear, depending on the differences of the thermodynamic properties of the glassy and supercooled liquid-state at the glass transition (Roos, 2010b).

The hydrophilic phase of solids have major role on the  $T_g$  values of the bulk systems. The  $T_g$  is affected by the molecular weight of solid components. Therefore, the small molecular weight substances including sugar and acids contribute to low  $T_g$  of solids (Roos, 1995). Moreover, water is a strong plasticizer of

hydrophilic component which significantly decrease  $T_g$  of the systems. These small molecular weight substances increase the free volume of solids which is the places, space or holes that are not occupied by the molecules and are available for the molecular movement. Gordon-Taylor as well as more complicated Couchmann and Karasz equation have been used to predict the  $T_g$  of binary mixtures as well as the water plasticization effect on  $T_g$ . However, several studies indicated that Gordon-Taylor relationship (Eq.1) was successful to predict water content dependence of  $T_g$  (Roos and Karel, 1991b; Roos, 2010b).

$$T_g = \frac{(w_1 T_{g1} + k w_2 T_{g2})}{(w_1 + k w_2)} \quad (\text{Eq.1})$$

where  $T_{g1}$ ,  $T_{g2}$  and  $w_1$ ,  $w_2$  refer to glass transition temperature and weight fractions of components 1 and 2, respectively. The parameter  $k$  is a constant

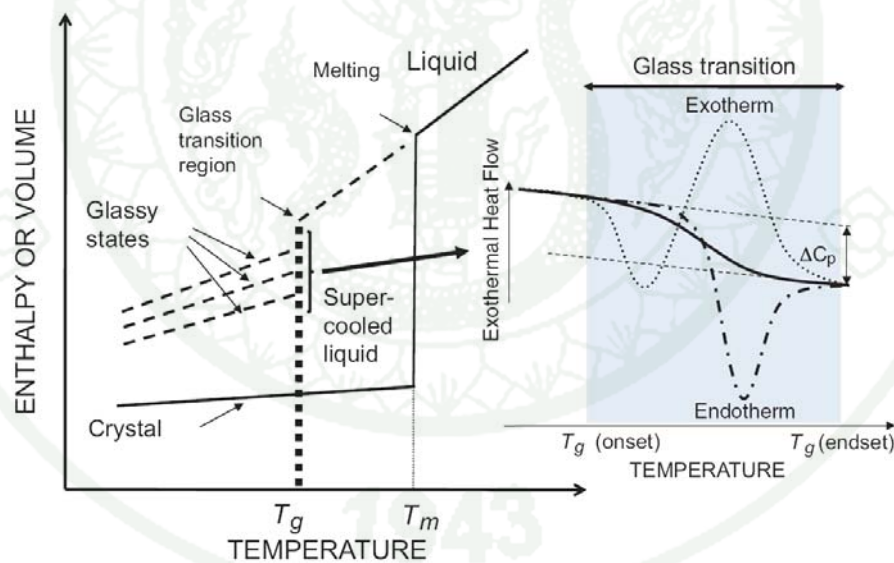


**Figure 1** Enthalpy and volume of various states of materials and the changes of heat flow around glass transition region as measured by DSC.

**Source:** Roos (2010b)



## 1.2 Structural relaxation

Amorphous materials show various relaxations when exposed to an external, oscillating small stress (Roos, 2010b). The relaxation time ( $\tau$ ) refers to the time that is necessary for the recovery towards equilibrium conditions in materials after perturbation of an external disturbance (Champion *et al.*, 2000; Roos, 2009). The main relaxation associated with the glass transition is known as  $\alpha$ -relaxation. The  $\alpha$ -relaxation appears as a dramatic decrease in modulus observed from a rapid decrease in storage modulus and increase in loss modulus with increasing temperature (Figure 2). These changes are frequency-dependent and follow the nonequilibrium, time-dependent nature of the glassy and supercooled liquid forms (Roos, 2010b). The relaxation also take place in the glassy state which so called ‘sub- $T_g$  relaxation’ or ‘secondary relaxation’. In the glassy state, the mobility is local, restricted to vibration of atoms or bonds (Roudaut *et al.*, 2004). The  $\tau$  can be extremely long in the glassy state, but they may dramatically decrease within and above  $T_g$  as a result of increasing molecular mobility (Roos, 2008; 2009). Several studies discussed about the sub- $T_g$  relaxation ( $\beta$ ,  $\gamma$ , etc.) in biopolymers and low molecular weight sugars using the mechanical or impedance spectroscopy (Noel *et al.*, 1996, 2000; LeMeste *et al.*, 2002; Shinyashiki *et al.*, 2008; Roudaut *et al.*, 2004). These types of relaxations also give rise to endothermic features on DSC curves.

Roudaut *et al.* (2004) pointed out that the relaxation studies are classically used to probe the molecular motions. As a result, the lower  $\tau$  refers to a higher molecular mobility. Therefore, the  $\alpha$ -relaxation time ( $\tau_\alpha$ ) may potentially be an effective parameter to indicate molecular mobility above  $T_g$ . In this work, the  $\alpha$ -relaxation time was related to the degradation of dispersed  $\beta$ -carotene in freeze-dried solids (Part 4 and 5).

Mechanical properties of amorphous solids change dramatically around glass transition. Williams *et al.* (1955) suggested an empirical relationship describing the temperature dependence of mechanical properties, e.g., viscosity and relaxation time above  $T_g$  known as Williams-Landel-Ferry (WLF) equation (Eq.2). It was

reported to be applicable over the temperature range from  $T_g$  to  $T_g + 100^\circ\text{C}$  (Levine and Slade, 1986). Levi and Karel (1995) demonstrated a well correlation between relaxation time of structural collapse during storage above  $T_g$  and the difference between  $T-T_g$  of carbohydrate matrix.

$$\log a_T = \log \left( \frac{\tau}{\tau_g} \right) = \log \left( \frac{\eta}{\eta_g} \right) = \frac{-C_1(T - T_g)}{C_2 + (T - T_g)} \quad (\text{Eq.2})$$

where  $\eta$  and  $\eta_g$  are the viscosity at  $T$  and  $T_g$ , respectively;  $\eta_g$ ,  $C_1$  and  $C_2$  are fitting parameters.  $C_1$  and  $C_2$  values fluctuate slightly around their ‘universal values’ ( $C_1 = 17.4$  and  $C_2 = 51.6$ ) given by Williams *et al.* (1995). These universal constants have been commonly used for many synthetic polymers. However, Peleg (1992) discussed several problems regarding the use of average constants in the WLF equation. He found the disagreement of prediction above  $T_g$  for  $20\text{-}30^\circ\text{C}$  (Witschi, 1999). Angell *et al.* (1994) proposed that the universal value for  $C_1$  was probably true if the constant is applied for the viscosity ( $C_1 \approx 17$ ) or relaxation time ( $C_1 \approx 16$ ) data. The parameters  $C_2$ , however, vary upon solid components and used to classify the ‘strong-fragile’ of polymers as stated by Angell (1997).

### 1.3 Glass transition and relaxation measurements

Glass transitions and relaxations of amorphous materials may be measured with calorimetric, dielectric, mechanical, and spectroscopic techniques. In most studies, glass transitions are reported as results of measurements of thermodynamic changes during heating of a glassy system to above its glass transition. Most  $T_g$  reported for foods and other materials have been determined using a DSC showing a change in heat capacity over the material specific glass transition. As the glass transition is the kinetic phenomenon, the experimental  $T_g$  shift with the scan speed. The transition temperature is often taken as the onset or mid-point temperature of the step change in heat capacity. Moreover, other properties of materials changing dramatically around the glass transition include modulus and viscosity, volume and thermal expansion, and dielectric properties (Witschi, 1999; Roos, 2010b).

The glass transition appears as a change in enthalpy and volume in the measurement of thermodynamic properties, whereas the appearance of translational mobility of molecules around the glass transition results in a frequency-dependent  $\alpha$ -relaxation measured by the mechanical and dielectric techniques (Figure 2). These spectroscopic techniques provide information on chemical bonding and molecular mobility (Roos, 2010a,b). Again, the mechanical changes during the glass transition are heating rate and measurement frequency dependent and occur over a much wider temperature range than the corresponding heat capacity change. The  $\alpha$ -relaxation temperature ( $T_\alpha$ ) has been reported in various food, sugar and polysaccharide systems using dielectric measurements (Noel *et al.*, 1996, 2000; LeMeste *et al.*, 2002; Shinyashiki *et al.*, 2008; Roudaut *et al.*, 2004) and dynamic mechanical analysis (DMA) (Silalai and Roos, 2011). In this work, the glass transitions of the frozen and freeze-dried materials were measured using a DSC and mechanical relaxations around  $T_g$  were determined by DMA.

Figure 2 shows that the rapid increase in molecular mobility around the glass transition in heating of a material can be observed in an exponential decrease in modulus and viscosity (storage modulus). In dielectric measurements, this appears as an  $\alpha$ -relaxation and rapidly increasing permittivity. The  $\alpha$ -relaxation in both dynamic dielectric (thermal) (DEA/DETA) and dynamic mechanical (thermal) analysis (DMA/DMTA) can be identified from a peak in loss modulus.  $\beta$ -relaxation below the glass transition often suggests some changes in molecular mobility in the solid state (Roos, 2010b).

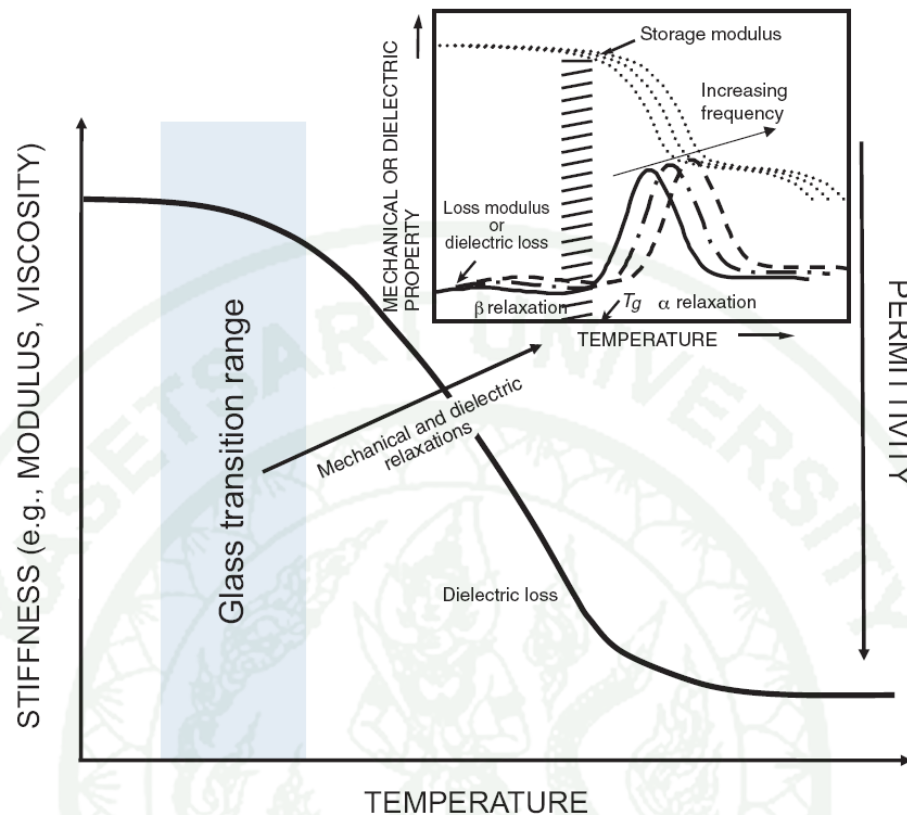


**Figure 2** Changes in dielectric and mechanical properties of materials at and above the glass transition.

**Source:** Roos (2010b)

#### 1.4 Physical changes and food stability above $T_g$

Glass transition is a determinant for food stability during processing and storage. It is generally accepted that food is most stable at and below its glass transition, and a higher  $T - T_g$  contributes to a higher deterioration or reaction rate (Roos, 1995; Rahman, 2006). Amorphous solids are very sensitive to heat and moisture which contributed physical changes, such as flow, collapse, stickiness and sugar crystallization, as well as chemical reaction such as non-enzymatic browning (Bhandari and Howes, 1999; Ling *et al.*, 2005; Telis and Martínez-Navarrete, 2009). The molecular motions above  $T_g$  increased instantly in glass-forming solids which

contained small molecular weight sugars, as was determined from dielectric relaxations (Noel *et al.*, 1996; 2000). Changes in mechanical properties above  $T_g$  were shown to relate to component plasticization and physical stability of dried solids, including stickiness in milk powder systems (Silalai and Roos, 2011). Various structural changes including sugar crystallization and structural collapse have been shown to increase as temperature increases above  $T_g$  ( $T-T_g$ ).

The sugar crystallization of dehydrated foods strongly depends on environmental humidity and  $T_g$  of solids which could contribute to the loss of product qualities and release of encapsulated components. Volatile diffusivity is greatly increased continually as the temperature exceeds the  $T_g$  (Roos and Karel, 1991b). The rubbery matrix above  $T_g$  accelerates the diffusion due to the increased free volume and change in transport and solution behavior of volatiles (Bhandari and Howes, 1999).

As pointed out by Le Meste *et al.* (2002), loss of crispness and brittleness of low moisture foods, e.g., potato chips, breakfast cereals and crackers was attributed to the drop in rigidity modulus that occur at and above  $T_g$ . Moreover, the amorphous form of low molecular weight carbohydrates and protein hydrolysates are very hygroscopic. When a local portion in a packaging absorbs moisture, the  $T_g$  of the portion is locally depressed and hence accelerate crystallization. Once crystallization occurs, tight and orderly molecular packing are formed resulting in release of adsorbed water and further water absorption at the surface of neighboring particles. This creates interparticulate liquid bridges resulting in “caking”. Surrounding particles, which absorb moisture, can also be crystallized and proceed as a chain phenomenon (Bhandari and Howes, 1999). Crystallization process rejects impurities including volatiles. Levi and Karel (1995) found increased rate of loss of a volatile 1-n-propanol encapsulated in an amorphous sucrose system as a result of crystallization. In an enclosed condition, crystallization increases the water activity of the system, which may influence the deteriorating reaction rates and microbial quality of the product (Chirife and Buera, 1995).



For encapsulated compounds which contained two- phased separated of lipophilic-hydrophilic components, more complex interactions was taken into account than for a single soluble components. In systems containing encapsulated lipids, the protective action of the solid matrix is lost when crystallization occurs. In non-crystalline sugar systems, the stability of encapsulated lipids may be increased upon collapse of the samples above the glass transition temperature. A compromise between structural collapse (favorable for retention of encapsulated compounds) and matrix crystallinity (promoting the release of encapsulated compounds) was always observed. It is interesting to note that the loss of encapsulated compound was related to the crystallization of the sugar matrix, but the moisture content of the amorphous phase was determinant of the extent of compound remaining encapsulated (Elizalde *et al.*, 2002; Prado *et al.*, 2002). The effect of crystallization on the release of volatiles and lipids is attributed to the exclusion and release of the compounds (Buera *et al.*, 2005).

Structural collapse of dried products results in the reduction in volume and porosity, which give undesirable appearance and poor rehydration. Powder stickiness and caking are phenomena related to collapse which have been demonstrated to obey WLF equation (LeMeste *et al.*, 2002). The collapse temperature ( $T_c$ ) as well as the sticky point temperature ( $T_s$ ) (the temperature at which the force to stir the powder in the tube increases sharply) has been shown to well correlate with the  $T_g$  of solids (To and Flink, 1978; Roos and Karel, 1993). Roos and Karel (1993) demonstrated that the  $T_s$  of the amorphous sucrose/fructose (7:1) mixture powder were close to the endset temperature and slightly above  $T_g$ . Likewise, the  $T_c$  values were found to be 30 to 70°C above onset  $T_g$  (Roos and Karel, 1991b). However, Le Meste (2002) stated that the addition of small amounts of high molecular weight substances may prevent the collapse during freeze-drying without changing the DSC  $T_g$ . This could possibly due to the reduction of the unfrozen water content.

These previous studies indicated the structural changes during food processing and storage above  $T_g$ . Only limited studies indicated or confirmed the crystallization in dried fruit systems. Although fruits contain high amount of sugars,

the high amount of polysaccharide might retard the crystallization. In this work, the sugar crystallization of freeze-dried mangoes was monitored during storage at various  $a_w$  corresponding to the glass and rubbery state of solids (Part 1). This research also demonstrated the structural collapse of freeze-dried solids during freeze-drying (Part 2, 3, 4, 5) and storage (Part 5).

### 1.5 Phase and state transitions in frozen and freeze-dried materials

In this work, the various freeze-drying conditions (freezing and freeze-drying parameters) were applied to form various material structures. In practice, food materials reveals one of the two behaviors during freezing or the solidification process which depends upon the amount of water component as shown in Figure 3.

(1) The solvent crystallizes at the temperature depending on their compositions

(2) No crystallization of solvents; instead, the solution became more viscous and very stiff as temperature decreases and finally approaches the highly viscous liquid or so called 'glass formation'.

As cooling is the first step in the freeze-drying process and this work also focused on the freezing behavior of materials, these transitions and the solution behavior upon cooling will be discussed in more detail. Considering solution 1 which concentration is less than maximally concentrated solution,  $C_g'$ , once applying the slow cooling rate (process a) then the ice can crystallize resulting in the decrease of water or increase of solution concentration. The equilibrium melting point (line  $T_m$ ) shows the maximum temperature at which this process can be achieved. As the temperature reduced towards  $T_m'$ , more and more ice is formed. When the temperature reached  $T_m'$ , the remaining solution around the ice is maximally freeze-concentrated to  $C_g'$ . Below  $T_m'$  the rubbery solution is rigid and viscosity is high enough to support the structure without flow for a finite time of observation. Upon further cooling, the maximally freeze-concentrated solution transforms into solid glass

at the true glass transition,  $T_g'$ , of the freeze-concentrated matrix surrounding by the ice crystals in a maximally frozen solutions.

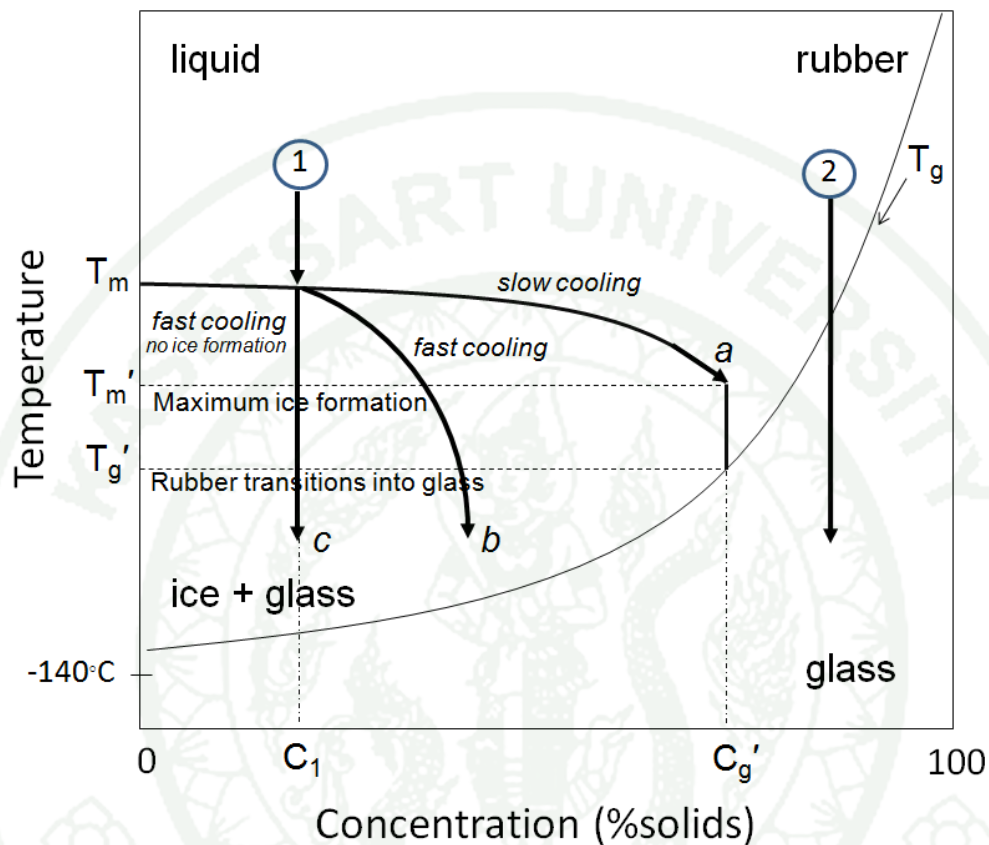


**Figure 3** State diagram showing various cooling behavior of food materials at various concentration. Process 1 represents systems contains freezable water and therefore, the cooling rate strongly affects the amount of unfrozen water as well as the glass formation of the unfrozen solutes; whereas, process 2 represents systems contains unfreezable water. ( $T_m$  = equilibrium melting point,  $T_m'$  = onset temperature of ice melting,  $T_g$  = glass transition temperature,  $T_g'$  = glass transition temperature of maximally freeze-concentrated systems,  $C_g'$  = maximally concentrated solution)

Applying a faster cooling rate (process b), the ice is not be able to maximally form ( $C < C_g'$ ). Some amount of unfrozen water is available in the frozen solution which acts as plasticizer and reduced the glass transition of the systems. Therefore, the glass transition,  $T_g$  of such systems vary upon the concentration of the solution and the available of unfrozen water which can not considered as a true glass transition or  $T_g'$ . This  $T_g$  is less than the  $T_g'$  because of the plasticization effect by the available unfrozen water. Moreover, if the fastest cooling is applied and there is no nucleation of ice (process c), the concentration of the solution does not change ( $C_1$ ). The highest amount of unfrozen water in such systems leads to a high depression of  $T_g$  resulting in the low  $T_g$  of such systems. The available of unfrozen water also determine the stability of frozen, i.e. physical changes and chemical reactions, including ice recrystallization and enzymatic activity. These transitions are completely reversible on slow cooling/ heating. However, in the fast cooling systems, once the temperature increases, the water mobility also increases which can cause the further ice formation. Therefore, upon recooling, this can change  $T_g$  of the solution. In the DSC measurements, the maximum ice formation of the solution can be achieved by controlling the cooling rate as well as the annealing process at temperature below  $T_m'$ . Moreover, the state diagram also showed the concentration of solute or the amount of frozen water which depends on the temperature during freezing.

During cooling of the highly concentrated solutions 2 (i.e., non-freezable water,  $C > C_g'$ ), no crystallization of the solvent occurs and the solution became more and more viscous. Finally, the further reduced temperature causes the transform of materials into a glass below  $T_g$ . The  $T_g$  of such systems depends on concentration of the solutions or in terms of most food systems the water content and plasticization. These types of transitions occur in dehydrated materials including freeze-dried foods.

## 2. Water activity and food stability

Water is omnipresent in food materials and the surrounding atmosphere which significantly impacts the quality and safety of foods. Water activity is defined as the ratio of partial pressure of water vapor in the product ( $p$ ) to that of pure water ( $p_o$ ):  $a_w = p/p_o$ . The influences of  $a_w$  on the rate of chemical reactions in food systems have been extensively studied such as non-enzymatic browning, several enzymatic activities and microbial growth (Nelson and Labuza, 1994; Chirife and Buera, 1995). Labuza (1971) developed a so called ' $a_w$  stability map' to describe the general relationship between  $a_w$  and several chemical reactions as shown in Figure 4.

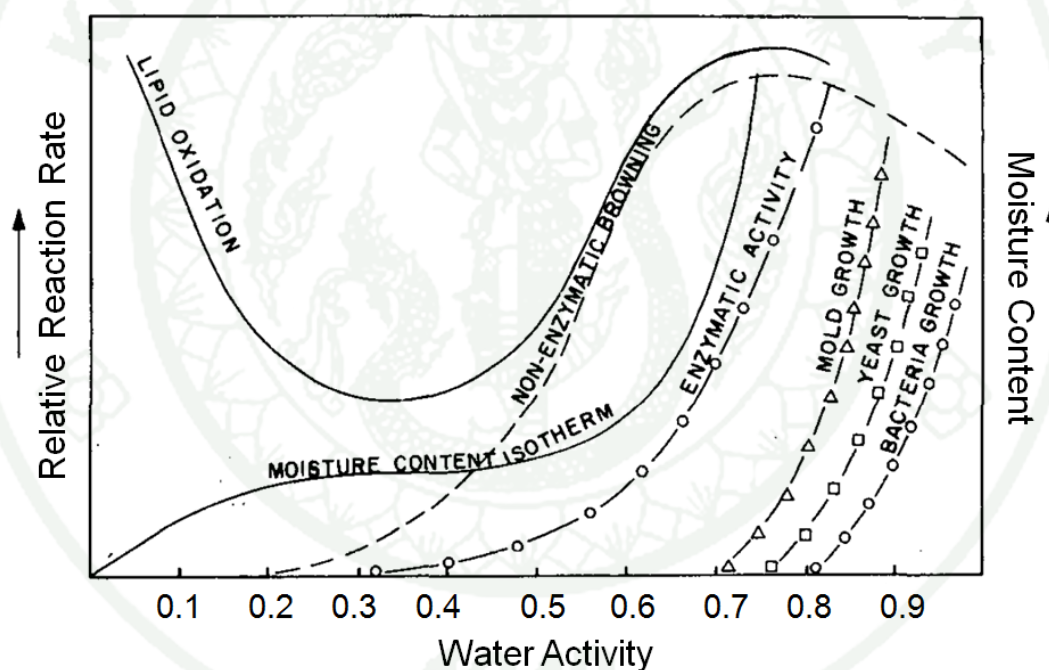


**Figure 4** The original stability map of food showing the relative rate of reactions and moisture content as a function of water activity.

**Source:** Labuza (1971)



At low  $a_w$ , water is tightly bound to the surface sites of polar molecules making it unavailable to solvate reactions (Nelson and Labuza, 1994). The upper limit of this  $a_w$  region is generally referred to as the monolayer moisture ( $m_m$ ) which can be derived from several relationships such as Brunauer-Emmett-Teller (BET) and Guggenheim-Anderson-DeBoer (GAB) equations. The BET equation is applicable to predict the water sorption of dehydrated materials at  $0.05-0.45a_w$ ; whereas, a more complicate GAB equation has been extensively utilized for the prediction of water sorption up to  $0.9a_w$  (Chirife and Iglesias, 1978). At higher  $a_w$ , water exists in multilayer or as a condensed phase in capillaries which increased the mobility of reactant and increases the reaction rate. The available water acts as a reaction medium in which sufficient reactant mobility occurs to allow reactant interactions. As  $a_w$  further increases, the rate of some reactions decrease as a result of the dilution of reactant species in the aqueous phase (Nelson and Labuza, 1994). However, the oxidation of the unsaturated lipids showed the main exception as stated by Labuza (1971) who showed that the reaction rates increased below the  $m_m$  due to increased catalytic activity of metal ion when sufficient water is removed from the hydration sphere around these ions.

As previously mentioned, the humidity induced structural changes above  $T_g$  of dehydrated materials subsequently impacts the physico-chemical properties and stability of foods. For instance, the sugar crystallization and maillard reaction cause the release of adsorbed water from food matrices and consequently increase the product  $a_w$  which accelerates further deteriorative reactions (Chirife and Buera, 1995). The sugar crystallization also causes the release of bioactive ingredients, accelerates chemical reactions and protein denaturation including enzymatic loss and reduces the solubility of bulk materials (Hancock and Shamblin, 1998; Buera *et al.*, 2005). The crystallization of amorphous sugars were commonly observed by the loss of adsorbed water during storage of sugar containing solids at intermediate and high  $a_w$  for various food powders, such as milk powders (Jouppila and Roos, 1994; Jouppila *et al.*, 1997) and sugar systems, including glucose and sucrose (Makower and Dye, 1956), lactose (Omar and Roos, 2007), and trehalose (Iglesias *et al.*, 1997; Schebor *et al.*, 2010); however, lack of study demonstrated the sugar crystallization in fruit powder during

storage including mango. In this work, the loss of adsorbed water as an indication of sugar crystallization of mango powder was monitored during storage at various  $a_w$ . In addition, the crystallization of sugar components was also confirmed by the application of X-ray powder diffraction and scanning electron microscope (Part 1).

The development of functional ingredients including  $\beta$ -carotene has been extensively investigated in the recent decades; however, the investigations of their stability at various  $a_w$  are still scarce. Desobry *et al.* (1999) demonstrated the stability of  $\beta$ -carotene in spray-dried maltodextrin powder at the same dextrose equivalent (DE) stored at 11% and 33% RH. Glucose, galactose and lactose were added to two maltodextrins, 15 DE and 4 DE, to prepare six maltodextrins of different composition but with the same DE (25 DE). A commercial maltodextrin 25 DE was also studied as a reference. Trans- $\beta$ -carotene was mixed with these maltodextrins and was spray-dried. Stability was evaluated during storage in the air at 11 % and 33% RH, at 25°C, 35°C and 45°C. No significant difference was observed between storage at 11 % and 33% RH. In addition, the authors also stated that the addition of mono- and disaccharides to maltodextrins reduces pore size in the maltodextrin network and limits oxygen diffusion. The best preservation was reported with maltodextrin '4 DE + Glucose ' which gave a carotene half-life of 87 weeks, at 25°C (Desobry *et al.*, 1999).

Rascon *et al.* (2011) evaluated the performance of gum arabic (GA) and soy protein isolate (SPI) on paprika oleoresin microcapsules preparation and their storage at 0.11, 0.32, 0.52 and 0.74 $a_w$  at 35°C. Paprika oleoresin (formed by glycerides, liposoluble polyphenolic and carotenoids pigments) emulsions with a ratio of paprika oleoresin/wall material of 1:4 (w/w) were prepared using high-pressure homogenization, and then spray-dried. Maximal stability for carotenoid oxidation was found at  $a_w$  0.74 for both microcapsules prepared with GA and SPI. They stated that at this humidity level, sufficient water was absorbed by the microcapsules to form a dough-like mass which acts as a shell opposed to oxygen diffusion into the microcapsule core, in as much as water is absorbed without initiating the wall dissolution process and led to the highest carotenoid stability (Rascon *et al.*, 1999).

Bechoff *et al.* (2010) reported the effects of water activity (0.13, 0.30, 0.51, and 0.76) during storage at 40°C under air on the degradation of carotenoids during storage of air sun dried sweet potato chips. The results showed that the lower the  $a_w$  the faster the  $\beta$ -carotene degradation. Samples stored at 0.13 $a_w$  showed greater losses of  $\beta$ -carotene, and the degradation decreased as  $a_w$  increased to 0.76 $a_w$ . The highest retention was found at 0.76 $a_w$  in agreement with the finding by Rascon *et al.* (1999). However, no structural integrity of solids was discussed. At such high  $a_w$  (0.76) the enzymatic activity such as peroxidase and lipoxygenase which capable to degrade  $\beta$ -carotene into aroma compounds should be increased as stated by the Labuza (1971). However, the high temperature during drying process might potentially inactivate or denature these enzymes resulted in the highest stability at 0.76 $a_w$ .

These results confirmed the previous finding by Goldman *et al.* (1983) who reported the discolorization of  $\beta$ -carotene solution in methylene chloride dispersed in carboxy methyl cellulose (CMC) matrices stored at dry, 0.33 and 0.84 $a_w$ . The authors found the highest retention in systems stored at 0.84 $a_w$ ; whereas, the dry condition gave the lowest  $\beta$ -carotene retention. However, Gloria *et al.* (1995) showed the insignificant difference of bixin stability in annatto extract-microcrystalline cellulose during storage among 0.33, 0.57 and 0.75 $a_w$  at 21°C in the presence of light air. These data reported varying results as the various matrix components.

Apart from carotenoids, Uddin *et al.* (2002) studied the retention of ascorbic acid (vitamin C) in freeze-dried guava during storage at various  $a_w$  (0.43, 0.75, 0.84, 0.97) and temperature (30°C, 40°C, 50°C). The degradation of ascorbic acid follows a pseudo-first-order reaction. They found that the rate constant increased about four to six fold when storage  $a_w$  increased from 0.43–0.97 $a_w$ . The  $a_w$  effects on rate of ascorbic degradation was described by a second-order polynomial equation. In addition, the effect of temperature on the rate constant followed the Arrhenius relationship. This finding reported a contradict results of the  $a_w$  effects on stability of bioactive components possibly caused by the diverse properties of substances such as the lipophilic-hydrophilic compounds.

Garzon and Wrolstad (2001) determined the stability of anthocyanin pigments namely pelargonidin 3-glucoside, pelargonidin 3-sophoroside and pelargonidin 3-sophoroside 5-glucoside acylated with malonic and cinnamic acids at varying  $a_w$  (0.44, 0.66, and 0.89). Model systems, containing purified anthocyanin in pH 3.4 citrate buffer and glycerol, were stored at 25°C in the dark for 242 days. Changes in pigment, degradation index, and anthocyanin profile were monitored by high-performance liquid chromatography (HPLC). They found that anthocyanin degradation followed first order kinetics and the degree of anthocyanin degradation increased with  $a_w$ . Half lives of the anthocyanins ranged from 56 to 934 days. In addition, changes in the chromatographic profile showed hydrolysis of pelargonidin 3-sophoroside to pelargonidin 3-glucoside and production of malonic acid from the acylated anthocyanin. This was in agreement with the previous finding by Erlandson and Wrolstad (1972) found the increased degradation of anthocyanins in freeze-dried strawberry puree as storage humidity increased.

Li *et al.* (2011) determined the stability of catechins in spray-dried green tea extract powders stored under various RH of 43, 75, 80 and 97% and 25-60°C conditions for up to 16 weeks. They found catechin losses followed first-order kinetics and increased with increasing temperatures and RH values which was due to the increased molecular mobility and the diffusion rate. The activation energy ( $E_a$ ) which indicated the temperature dependence on catechin stability was also derived for each RH. They found that the  $E_a$  remained the same in green tea powder systems stored at low RH conditions ( $RH \leq 75\%$ ) for the temperature range of 25-60°C; whereas, the  $E_a$  of catechin degradation was significantly lower at 97% RH. This indicated that the degradation patterns of green tea catechins were altered by excess moisture absorbed in the powder system, that is, degradation mechanisms of green tea catechins are different between powder systems and concentrated solution systems. They stated that the  $E_a$  could be lowered due to the dramatically increased molecular mobility, or the temperature dependent changes of mobility, that affect the slope of the Arrhenius relationship in samples at 97% RH (Li *et al.*, 2011).



In addition, recent debates have emerged on whether it is  $a_w$  or the state of the system as dictated by the  $T_g$  that impacts the rates of chemical reactions in reduced-moisture solid systems. Bell and Hageman (1994) studied the kinetics of aspartame degradation in the PVP model system. By PVP of different molecular weights, the effect of  $a_w$  and glass transition on chemical reactions can be studied independently and at a constant temperature. The authors found that the rates of aspartame degradation are not significantly different at a given  $a_w$  despite the differences in  $T_g$ . At  $0.33a_w$  which corresponded to the glassy state, the reaction still occurred. Furthermore, at  $0.54 a_w$ , the rate of degradation is similar in both the glassy and rubbery states. However, the two systems having a  $T_g$  near  $50^\circ\text{C}$  have significantly different reaction rates, with the faster rate occurring in the higher  $a_w$  system. The authors stated that the intramolecular rearrangement of aspartame appeared to be more dependent on  $a_w$  than on the  $T_g$ . They also claimed that it was possible that the free volume, even within the glassy system, exceeds that necessary for aspartame to rearrange. Hence, the free volume, and therefore mobility, as dictated by the  $T_g$  of the system is not rate limiting; rather, some factor influenced by the  $a_w$  predominates. Thus, the rate of aspartame degradation depends upon  $a_w$  rather than the state of the systems (Bell and Hageman, 1994).

The water activity is a significant parameter affects stability of functional ingredients in dehydrated systems. In addition, the structural changes of dried solids potentially affect the physico-chemical properties such as oxygen diffusion; therefore, the  $a_w$  as well as the state of materials should be considered simultaneously. The stability of  $\beta$ -carotene in freeze-dried materials during storage at various  $a_w$  and the structural changes in real foods (Lavelli *et al.*, 2007) and model systems (Prado *et al.*, 2006; Ramoneda *et al.*, 2011) are discussed later.



### 3. Freeze-drying

#### 3.1 The classical freeze-drying process

Freeze-drying or lyophilization is a process in which a solvent (usually water) is removed from the frozen foodstuff or a frozen solution by sublimation and by desorption (unfrozen solvent), generally under reduced pressure (Figure 5). In general, freeze drying give amorphous solid food with disorder structure due to a rapid removal of water from the matrix. In freeze-drying, water is removed from the frozen substances directly as vapor without becoming liquid. Consequently, it is necessary that the temperature and pressure of the sublimation interface is held below the triple point of the water or aqueous solution in the material being dried. Many types of freeze-dryer are available, e.g., industrial or laboratory scale, shelf-temperature control and non-temperature control; however, the principle of freeze-drying process consists of 3 stages; freezing, primary drying or sublimation and secondary drying or desorption of unfrozen water.

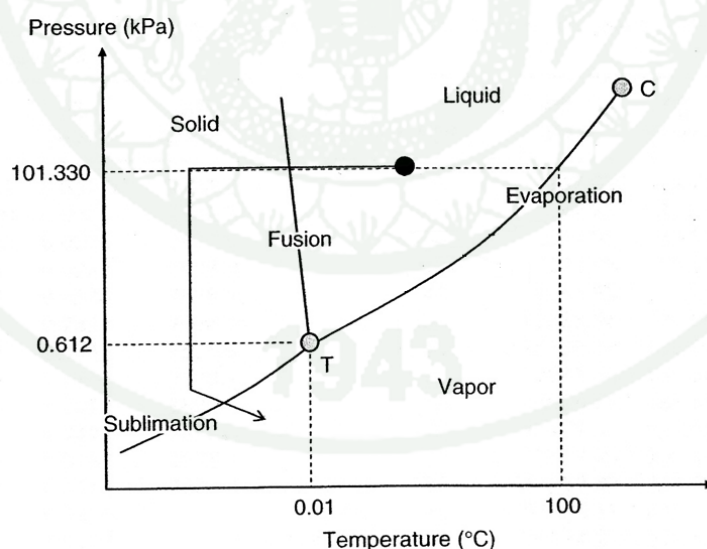


**Figure 5** Phase diagram of water showing the classical freeze-drying pathway (T: triple point, C: critical point of water).

**Source:** Modified from Ratti (2008)

### 3.1.1 The freezing stage

The freezing stage represents the first step in the freeze-drying process. The foodstuff is cooled to a temperature at which the crystallization of the solvent is achieved. The freezing behavior of material was discussed earlier in the previous section. The ice crystals formed during the freezing stage or subsequent frozen storage determine the size and shape of the pores, the pore size distribution, and the pore connectivity of the porous network of the dried layer (Sadikoglu *et al.*, 2006). The mass and heat transfer rate of water vapor are significantly influenced by the porous structure of the dried layer. If the ice crystals are small and discontinuous, then the mass transfer rate of the water vapor is further limited by the material surrounding the pores. On the other hand, if large and homogeneously distributed dendritic ice crystals are formed in the frozen solution, the mass transfer rate of the vapor is high due to the open or sponge-like porous structure. Consequently, the products dry faster in the following drying process (Witschi, 1999). The freezing temperature must be lower than the  $T_m'$  in a food to prevent melting of ice crystals.

### 3.1.2 The primary drying stage or sublimation

The frozen solvent (ice) is removed by sublimation in a reduced pressure or evacuated system. Achieving sublimation, the temperature and pressure must be less than or near the equilibrium vapor pressure of the frozen solvent to remain solids. In other word, the temperature and pressure of the ice need to be less than triple point values in order to allow sublimation of ice rather than evaporation of unfrozen water (Figure 5). When the ice is sublimated and become vapor, they also keep with them the latent heat of sublimation (2840 kJ/kg ice) and thus the temperature of the frozen product again decrease. If there is no heat supplied to the product by a heat source, then the vapor pressure of water at the product temperature reaches the same value as that of the partial pressure of the vapor in the drying chamber. The system reaches equilibrium and no additional ice is sublimated (Witschi, 1999). Therefore, some amount of heat is necessary to achieve the continuous sublimation; however, the amount of heat must be controlled to not

causing the ice melting or remaining product temperature at temperature less than the  $T_m'$ . In addition, the vapor needs to be removed from the drying chamber in order to maintain the non-equilibrium conditions in the systems, generally, by fitting a refrigerated condenser between the condenser and the vacuum pump.

The maximum allowable drying temperature in the frozen layer is determined by the structural collapse which occurs above  $T_m'$ . This temperature also determines the maximum pressure to maintain ice solid at and below  $T_m'$ , and is considerably less than 6.1 mbar. For example, if  $T_m' = 20^\circ\text{C}$  the maximum pressure will be 1 mbar (Witschi, 1999).

### 3.1.3 The secondary drying stage or desorption of unfrozen water

This stage involves the removal of unfrozen water (often referred to as “bound” or “un-freezable” water) which amount (referred as  $1 - C_g'$  on the state diagram) depends upon their components such as sugar and molecular weight of solids. Typically, the lower molecular weight of solids contributes to higher amount of unfrozen water. The desorbed water vapor is transported through the pores of the material that is dried (Pikal *et al.*, 2002). As primary drying, the amount of heat supplied must be control to avoid the structural collapse. It should be considered that food temperature should be lower than  $T_g$  of the dried layer to prevent any chemical and physical changes including structural collapse. The primary and secondary drying usually occur concurrently, as ice is removed from a region, secondary drying arises but the bulk of secondary drying occurs after primary drying is completed and the product temperature has increased (Tang and Pikal, 2004).

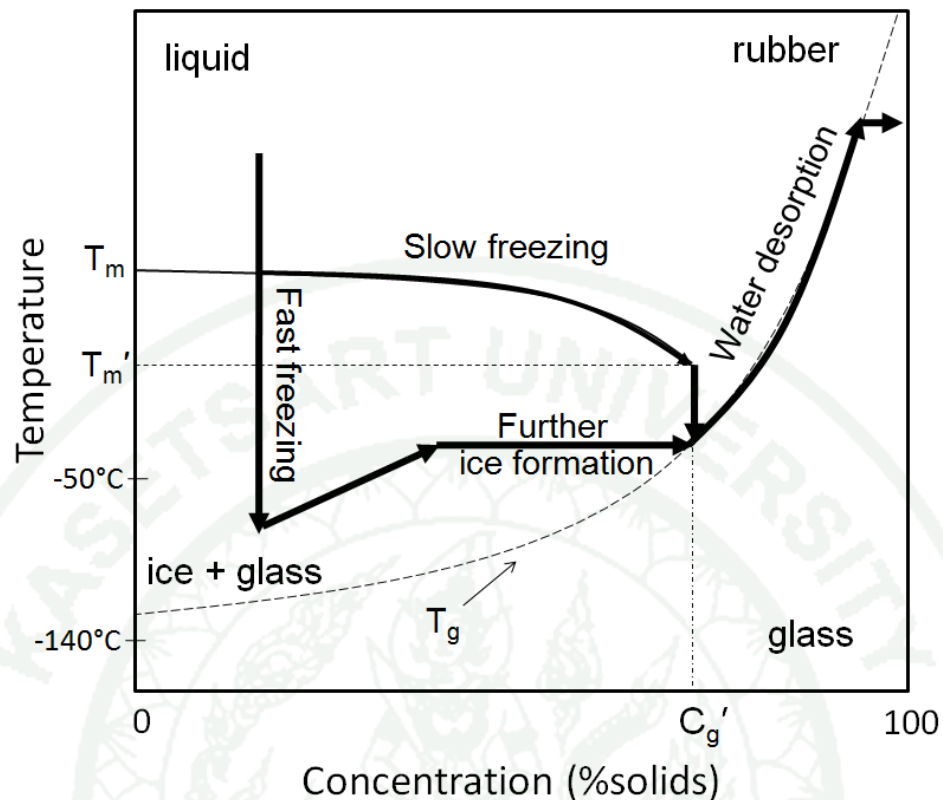


**Figure 6** Typical state diagram supplemented with the freeze-drying pathway of a freeze-concentrated solution to be freeze-dried ( $X=20\%$ ). In case of fast freezing, further ice formation can occur as temperature increases during freeze-drying.

The supplemented phase diagram or so called “state diagram” provides useful maps for the observation of changes in the glass transition as a function of varying temperature, water content or levels of freeze-concentration (Roos and Karel, 1991a,c; Roos, 2010). Several studies established state diagrams for several sugars, polysaccharide, protein as well as complex food systems such as fruits and dairy powders (Roos, 1995, 2010; Rahman, 2006). The state diagram shows the behavior of food components undergo processing and storage.

Figure 6 shows the state diagram supplemented with solution concentration and temperature changes during a freeze-drying process. As mentioned earlier about the freezing of solutions, the slow freezing causes the solution to concentrate

following the  $T_m$  line towards the maximally freeze-concentrated solute ( $C_g'$ ) state. In case of fast freezing, the solution does not reach the  $C_g'$  during the freezing process but a larger amount of unfrozen water vitrifies with the solutes. However, as the temperature rises during freeze-drying, ice can further form because of increased mobility of the unfrozen phase. This may result in the maximally freeze-concentrated state at temperatures approaching the  $T_m'$  with solute concentration of  $C_g'$ . The state diagram, however, cannot show the removal of the ice during sublimation or primary drying. After the ice is removed, solids temperature increases while the unfrozen water is further desorbed. The increase of product temperature needs to be maintained to less than  $T_g$  of solids to prevent the structural collapse (Witschi, 1999). In this work, the freezing conditions were also applied to control porosity and structural collapse of freeze-dried materials (Part 2 and 3).

### 3.2 Structure formation of freeze-dried systems

In the freeze-drying process, while sublimating the water, the freeze-dried solids become porous in nature (Bhandari and Howes, 1999). The most common terminology used in characterizing pores is porosity (volume fraction of pores) (Rahman, 2001). It expresses the ratio of open (empty) space of the material to that of total volume (Karathanos *et al.*, 1996) which is calculated from the solid and bulk density of material. However, this method requires specific instruments and the calculation might lead to high variation among replicate samples. In addition, the porosity calculated from different methods (i.e. mercury porosimetry and gas pycnometer) may give different results. To better understand the porous structure, the microstructure could be also determined, especially in plants where the disruption of cell walls is also an issue. Recently, other terminology, such as the number of pores; pore size, shape, and distribution; the number of walls or faces of pores, and the wall thickness of pores as characterized by image analysis of microstructure has become more pronounced (Rahman, 2001). Void spaces are formed from spaces previously occupied by ice crystals (Petzold and Aguilera *et al.*, 2003). This reflects that the porous freeze-dried structure is formed at the freezing stage; therefore the



modification of freezing parameters might be an effective way to control the porosity of freeze-dried products.

Many studies compared the porous characteristics of foods dehydrated by different drying methods (Karathanos *et al.*, 1996; Krokida and Maroulis, 1997; Krokida *et al.*, 1998; Tsami *et al.*, 1998) and it has been accepted that freeze-drying gave the highest porosity among others. However, the study about the pore formation of freeze-dried food is still limited. This includes the effect of solid components and freeze-drying process parameters on pore formation and microstructure. Previous researches considering freeze-dried food structure focused on the effects of freeze-drying conditions, especially freezing stage in non-food model systems (Hottot *et al.*, 2004; O' Brien *et al.*, 2004; Van Vlierberghe *et al.*, 2007), such as chitosan (Madihally and Mathew, 1999), gelatin gels (Chevalier *et al.*, 2000) and collagen (O'Brien *et al.*, 2005). It is possible that for model systems it is easier to control some parameters, such as water and solids content that may affect the pore formation. There were only little studies addressing the effects of freeze-drying condition on the porous structure of freeze-dried foods.

Acevedo *et al.* (2007) compared the use of different freezing rates on the microstructure of freeze-dried apples. For fast freezing, the apples were frozen by immersion in liquid nitrogen immediately before the freeze-drying process. In slow freezing, they were frozen at approximately -20°C in a home freezer for 12 h and then freeze-dried. The results indicated that after freeze-drying the apple matrices with fast freezing had a larger surface/volume ratio than systems slowly frozen which was derived from the higher water sorption capacity. During fast-freezing many small water crystals were rapidly formed which left a very porous material after ice sublimation (Tsami *et al.*, 1998). Scanning electron microscopy (SEM) micrographs also showed that the slow freezing rate caused severe changes in product microstructure which probably resulted from the larger ice crystals formed during slow freezing. However, there were no results on the pore size of dried apples.

Khalloufi and Ratti (2003) also studied the effect of freezing temperature on structure of various freeze-dried fruits. They compared between the various freezing temperatures of  $-17^{\circ}\text{C}$  and  $-27^{\circ}\text{C}$  on microstructure of freeze-dried strawberries, apples and pears. The image processing of SEM micrographs showed that the pore radii of pear samples frozen at low freezing temperatures were smaller. They stated that the result was in agreement with the theory that lower freezing rates lead to larger pores. For strawberries and apples, the freezing temperature had insignificant effect on pore size. This might be explained by the differences in composition and the strengths of fruit's cell walls. From this viewpoint, the pore formation of freeze-dried solids not only reflected by the freezing process but also the components of food solids.

Sablani and Rahman (2002) investigated the porosity and density of abalone, potato, apple, and two varieties of dates as a function of shelf temperature during freeze-drying. The pore formation showed two diverse results when shelf temperatures during drying were maintained at a constant level in the range of  $-45$  to  $15^{\circ}\text{C}$ . Abalone, potato, and brown dates showed a decreasing trend, whereas apples and yellow dates showed an increasing trend in pore formation. Later in 2007, Sablani *et al.* studied the influence of shelf temperature on pore formation in garlic during freeze-drying. Garlic dried at  $-5^{\circ}\text{C}$  showed significantly lower open pore porosity compared with samples dried at  $-15$  and  $-25^{\circ}\text{C}$ , respectively. Pore-size distribution and scanning electron micrographs also supported that most of the pores formed at  $-5^{\circ}\text{C}$  were much smaller in size as compared to the samples dried at  $-25^{\circ}\text{C}$ . This showed that not only the freezing stage but also the drying temperature during drying stage had an effect on pore formation.

These aforementioned studies suggested that the components as well as the freeze-drying process effectively modify the structure of freeze-dried foods. In addition, previous studies also indicated that the pore formation of freeze-dried solids was reflected by the ice formation during freezing which could have been controlled by the freezing parameters prior to freeze-drying. The following studies conducted the

pore formation in freeze-dried polymer systems and determine the pore morphology of freeze-dried solids with SEM.

Madhally and Matthew (1999) studied pore formation of freeze-dried chitosan materials prepared by controlled freezing and lyophilization of chitosan solutions and gels. The porous structures of materials were characterized via light microscope and SEM. Mean pore diameters could be controlled within the range of 40-250  $\mu\text{m}$ , by varying the freezing conditions. Fresh samples were frozen by immersion in freezing bath with subsequent temperature of  $-20^{\circ}\text{C}$ ,  $-78^{\circ}\text{C}$  and  $-196^{\circ}\text{C}$  prior to freeze-drying. As expected, the results clearly showed that the lower temperature freezing gave a lower mean pore diameter. These authors stated that the resulted pore formations given by various temperatures freezing was reflected by the various cooling rate.

Similarly, Kang *et al.* (1999) also showed that the lower freezing temperature gave a smaller pore size of freeze-dried gelatin. They prepared the gelatin gels and frozen at  $-20^{\circ}\text{C}$ ,  $-80^{\circ}\text{C}$  and liquid nitrogen freezing prior to freeze-drying. Interestingly, the liquid nitrogen freezing was also reported to give highly elastic gels in the dried state whereas the mechanical behavior of other systems was very brittle. These authors stated that the differences in the pore size and inner structure of gelatin gels reflect the differences in heat transfer rates during the freezing process of the gel. It is possible that at a higher freezing temperature; the number of nuclei of ice crystallization initially formed is smaller than that at a lower freezing temperature, leading to an increased final size of ice crystals. Since the larger ice crystals push to expand gelatin chains to a greater extent, the pore size of gels will be increased, while the structure will be destroyed. On the contrary, it is possible that a rapid cooling causes formation of many nuclei of ice crystals, resulting in the formation of smaller-sized pores. The fast freezing process in liquid nitrogen for 20 min produced sponges with smaller pores than those obtained through the slow freezing process in a freezer kept at  $-20^{\circ}\text{C}$  for 24 h. In other words, the difference in pore size and inner structure between these two sponges reflects the different rates of heat transfer during the freezing process of the gels. It follows that a sufficiently rapid rate of cooling, such as

in liquid nitrogen, can extract the heat of crystallization, thus preventing the formation of large ice crystals. In the final stage of gel preparation, frozen materials are dried by sublimation of ice crystals under vacuum at a temperature below the ice freezing point. Therefore, the pore size of the freeze-dried gels can be controlled only by the size of ice crystals formed during the freezing process. Probably, larger ice crystals were formed at a lower freezing rate attained in a freezer, leading to the formation of a larger porous structure with brittle and ruptured walls, while the faster cooling process in liquid nitrogen produced a larger number of small-sized ice crystals (Kang *et al.*, 1999).

The above studies described the influence of the cooling rate on the nucleation and growth of ice crystals and thus on the resulting pore size. In most studies, the samples were incubated in a freezer for several h at different temperatures and the results indicated that the pore size decreased with a decreasing freezing temperature. Whether the underlying cause of this phenomenon was the actual final freezing temperature, the cooling rate, or a combination of both was not discussed.

O'Brien *et al.* (2005) studied the effect of freezing temperature on pore morphology of freeze-dried collagen. Collagen suspensions were frozen at various freezing temperature (-40°C, -30°C, -20°C and -10°C) prior to freeze-drying. The similar initial cooling rate was controlled by the freeze-dryer shelf temperature (approximately 1.4°C/min) for all freezing protocols. The freezing profiles confirmed a similar initial cooling rate of samples; however, the further decreased freezing temperature resulted in less duration of ice formation. The final freezing temperature of -40°C, -30°C, -20°C and -10°C contributed to mean pore size of 95.9, 109.5, 121.0 and 150.5  $\mu\text{m}$ , respectively (O'Brien *et al.*, 2005). The lower temperature freezing gave smaller pore sizes which were in agreement with other aforementioned studies. These authors clearly revealed the effect of freezing temperature on the pore size of freeze-dried solids.

A contrast finding was reported in freeze-dried gelatin gels by Van Vlierberghe *et al.* (2007). They varied the final freezing temperature of -10 and -30°C



while keeping the cooling rate constant ( $0.2^{\circ}\text{C}/\text{min}$ ) of gelatin gels. The results indicated that the final freezing temperature did not significantly influence the gel pore size and porosity as analyzed by SEM image. The same study also implemented a procedure to examine the effect of the cooling rate on the pore size and morphology in freeze-dried gelatin gels. They reported that a decrease of the cooling rate from  $0.83$  to  $0.15^{\circ}\text{C}/\text{min}$  resulted in an increase in the average pore diameter from  $65$  to  $135\text{ }\mu\text{m}$ . The authors stated that the slower the cooling rate, the lower the undercooling (difference between the freezing temperature and the actual temperature of the material) and the nucleation rate and the higher the rate of heat and protein transfer which led to a lower amount of large pores.

From these viewpoints, the explanation whether the freezing temperature or cooling rate predominantly impact the pore morphology of freeze-dried solids was still in contradiction; however, the literature clearly stated that the porosity of freeze-dried solids can be controlled by the size of ice crystal formed during freezing which was governed by the process parameters. Most of the study investigated the freezing and/or freeze-drying parameter effects on the pore formation of freeze-dried solids; however, no studies demonstrate the effect of various solute particularly food components, e.g., sugars on the structure formation of freeze-dried solids. As the solutes also affect the amount of unfrozen water and the state transitions, more investigation on these issues should be more explored. This research also showed the effect of sugar components as well as the freeze-drying protocols, i.e., freezing and freeze-drying parameters on the microstructure formation of freeze-dried solids (Part 3).

Rassis *et al.* (1998) showed that the presence of sucrose by diffusion into alginate-starch gel resulted in decrease porosity after freeze-drying. The gels were immersed in various concentration of sugar solutions prior to freeze-drying. They found that diffusion of sucrose into the gels affected the distribution of the open and closed pores in the dried cellular solids. They stated that the wet gel lost water to their surrounding during immersion in sucrose solution, with resultant diffusion of sucrose into the specimen. This proved that the presence of sucrose and water content also had



an effect on pore formation in freeze-dried foods. However, this study might not be the case of most food, especially fruits which high amount of sugar naturally present in their structures.

The freezing step in freeze-drying is extremely important in defining ice crystal size and the extent of ice formation. Ice crystal size depends mainly on nucleation. In addition, the material properties often have an effect on ice crystal formation at various freezing conditions and particularly on ice recrystallization during storage. In this work, the effects of various freezing conditions and material components of maltodextrin and sugar mixture (glucose, fructose and sucrose) were demonstrated (Part 3).

### 3.3 Structural collapse of freeze-dried materials

Collapse as a physicochemical phenomenon can be defined as viscous flow at which results from a decreased viscosity above the glass transition. The loss of structure occurs since the material becomes unable to support its own weight (Roos, 1995). The term “collapse” has been used to describe loss of structure, reduction of pore size, and volumetric shrinkage in dried food materials. Freeze-drying under sub-optimal conditions can also lead to collapse (Levi and Karel, 1995). During freeze-drying, collapse occurs when, as a result of an increase in water pressure for instance, the heat input exceeds the drying needs. Structural collapse in the course of freeze-drying was shown to happen when the viscosity of the cryoconcentrated phase decreased to the range of  $10^7$  to  $10^4$  Pa s (Bellows and King, 1973; Le Meste, 2002). Below this limit, the interstitial network could not withstand the collapse of the capillary forces. The same critical viscosity range was shown to determine collapse in freeze-dried materials (Tsourouflis *et al.*, 1976; Le Meste *et al.*, 2002). Collapse has been reported to occur above  $T_g$  with a rate that is defined by the  $T-T_g$  (Levi and Karel, 1995; Roos, 1995; Prado *et al.*, 2006).

Krokida *et al.* (1998) stated that the physical properties of freeze-dried materials depend upon the temperature applied during freeze-drying. The

aforementioned study further established the collapse of a plant material after freeze-drying above its  $T_g$ . In the freeze-drying process, the removal of ice by sublimation creates pores, the walls of which may collapse because either of the force of the surfaces or gravity. The viscosity of the freeze-concentrated matrix, which is usually the major component of the pore wall, prevents or retards collapse (Karathanos *et al.*, 1996).

Karathanos *et al.* (1996) studied the structural collapse of plant materials. Fresh and osmotically dehydrated plant materials were freeze-dried at several chamber pressures to achieve initial sample temperatures that were below ( $-55^{\circ}\text{C}$ ), near ( $-45^{\circ}\text{C}$ ), or above ( $-28^{\circ}\text{C}$ ) their  $T_g'$  ( $-45^{\circ}\text{C}$ ). Freeze-drying at  $-55^{\circ}\text{C}$  gave products that retained their original volume. Conversely, as the initial sample temperature was increased to above  $T_g'$ , the resulting freeze-dried samples collapsed. Moreover, the further structural collapse was found when the initial sample temperature was increased to above the  $T_m'$ . Likewise, Krokida *et al.* (1998) reported the structural properties, such as particle density, bulk (or apparent) density and porosity of apples, banana, carrots and potatoes after freeze-drying under various conditions. The materials were freeze-dried at various pressures to achieve an initial sample temperature ranging between  $-50$  and  $-5^{\circ}\text{C}$ . They found that for temperatures above the  $T_g'$  ( $-45^{\circ}\text{C}$ ), the size of freeze-dried materials decreased.

Later in 2002, Shishegarha *et al.* determined the volume of whole and sliced strawberries after freeze-drying under various shelf temperatures ( $30$ ,  $40$ ,  $50$ ,  $60$  and  $70^{\circ}\text{C}$ ). The strawberries had a volume reduction of  $8\%$  (whole) and  $2\%$  (sliced) in freeze-drying, although the level of shrinkage was independent of the freeze-drying temperature. However, the percentage of collapsed strawberries increased with increasing process temperature. At heating temperatures higher than  $50^{\circ}\text{C}$ , the strawberries' dry layer temperature was higher than the estimated  $T_g$  of the dried fruit and increasing the risk of collapse.

These results confirmed that structural collapse during freeze-drying would occur when process temperature was higher than ice melting and glass

transition temperatures. However, structural collapses in model systems, such as sugar or other polysaccharides may occur differently as the plants. Fruits and vegetables contain cell wall which also plays an important role to improve their structural stability (Roos, 1995). In addition, structural collapse of solids can occur during storage above  $T_g$  by water and thermal plasticization and corresponding to the sharply decrease of matrix viscosity above  $T_g$  as stated earlier.

Levi and Karel (1995) demonstrated the effects of glass transition on the rates of collapse of non-crystallizing carbohydrates of sucrose, raffinose and maltodextrin. The structural collapse was determined from the decrease in bulk specific volume ( $v$ ) which was measured as a function of temperature and moisture content. Solids were humidified over the  $a_w$  of 0-0.85 and measured the magnitude of shrinkage and  $T_g$  using DSC. They found the decrease in specific volume with time followed first-order behavior, and calculated specific relaxation times for collapse ( $\tau_c$ ) using Williams-Landel-Ferry (WLF) equation. The results indicate a strong dependence of rates of collapse on temperature and on the quantity of  $T - T_g$  as stated by the decrease of  $\tau_c$  above  $T_g$ . They suggested that the rates of collapse could be predicted using the WLF equation which predicts the relaxation time above  $T_g$ . Most of the effect of moisture was due to the depression of  $T_g$ , and the resultant increase in  $T - T_g$  at constant temperature. This finding clearly indicated the correlation of  $T - T_g$  and the structural collapse of dried materials during storage at various humidity.

Similarly, Prado *et al.* (2006) observed the structural collapse in freeze-dried polyvinylpyrrolidone (PVP-40) stored at high  $a_w$ . The collapse was expressed by the volume reduction of freeze-dried solids during storage over the range of humidity (0.11-0.75 $a_w$ ) at room temperature. The samples stored at  $a_w$  lower than 0.44 did not collapse because the  $T_g$  values of solids were above storage temperature. Conversely, solids stored at  $a_w$  corresponding to the depression of  $T_g$  to well below room temperature visually showed the structural collapse. In addition, the degree of collapse increased as the storage time increased and showed an initial phase of fast collapse followed by a phase of slow collapse, approaching an almost constant value (or plateau) at long times (Prado *et al.*, 2006). After 35 days of storage, the results

also indicated that the magnitude of structural collapse also depended on the magnitude of  $T-T_g$ . This confirmed that structural collapse is the time dependent phenomena and the rate and magnitude increase with increasing  $T-T_g$ .

Structural collapse in freeze-dried matrices adversely affects properties of the freeze-dried materials. However, some recent studies showed that collapse can reduce the rate of some chemical reactions, such as glucose loss via Maillard browning (White and Bell, 1999), browning in lactose and lactose-protein matrices (Burin *et al.*, 2004), lipid oxidation (Bell and White, 2000), carotenoids degradation (Selim *et al.*, 2000; Prado *et al.*, 2006) and slower release of some entrapped volatile compounds (Levi and Karel, 1995). Prado *et al.* (2006) observed lower  $\beta$ -carotene degradation in collapsed systems than in non-collapsed freeze-dried polymeric matrices. However, the effect of collapse was studied as a result of various storage conditions, namely the humidity accelerated structural collapse during storage (Selim *et al.*, 2000; Prado *et al.*, 2006). Moreover, there were no studies related the pre-collapsed structure prior to storage and  $\beta$ -carotene stability during storage in either model or real food systems. The additional effects of structural collapse as well as the porous structure of freeze-dried solids on various reaction rates and stability of bioactive compounds are discussed later. In this research, the effect of pre-collapsed structure of freeze-dried mangoes prior to storage on  $\beta$ -carotene stability was studied (Part 2). Only a limited number of studies relating the degradation of bioactive compounds and food structure including collapse are available.

#### 4. Mangoes

Mangoes (*Mangifera indica*) cultivar ‘Nam Dok Mai’ is one of the most famous Thai fruits due to their great unique taste, flavor and appealing color. As a seasonal fruit, the processing such as drying is necessary to conserve such product for off-season consumption as well as the value-addition. Thailand produced a large number of fresh mangoes as well as processed mangoes particularly dried products. Table 1 shows some nutritional qualities of fresh mangoes (Tharanathan *et al.*, 2006)



**Table 1** The nutritional qualities of fresh mangoes.

Quality	values per 100 g of ripe mango pulp
Calories	62.1–63.7 Cal
Moisture	78.9–82.8 g
Protein	0.36–0.40 g
Fat	0.30–0.53 g
Carbohydrates	16.20–17.18 g
Fiber	0.85–1.06 g
Ash	0.34–0.52 g
Calcium	6.1–12.8 mg
Phosphorus	5.5–17.9 mg
Iron	0.20–0.63 mg
Vitamin A (carotene)	0.135–1.872 mg
Thiamine	0.020–0.073 mg
Riboflavin	0.025–0.068 mg
Niacin	0.025–0.707 mg
Ascorbic Acid	7.8–172.0 mg
Tryptophan	3–6 mg
Methionine	4 mg
Lysine	32–37 mg

**Source:** Tharanathan *et al.* (2006)

The yellow color of ripened mango attributes to the carotenoid components (Mercadante *et al.*, 1997). Among others,  $\beta$ -carotene is the major carotenoid compound which amount in the range of 6,544–11,249  $\mu\text{g}$  /100g mesocarp dried weight (Vasquez-Caicedo *et al.*, 2005).  $\beta$ -carotene is widely distributed in plant tissues as chloroplast and chromoplasts. In chloroplasts, carotenoids are mainly associated with proteins as chlorophyll-carotenoid-protein complexes and serve as necessary pigments in photosynthesis, as photoprotective pigments, and as membrane stabilizers (Ötles and Çagindi, 2007; Pott *et al.*, 2003; Schieber and Carle, 2005). In chromoplasts, this lipophilic molecule exists in various physical forms, as it may be



non-crystalline in lipid droplets in mangoes and it appears in crystalline forms, e.g., in carrots and tomatoes (Harris and Spurr, 1969; Schieber and Carle, 2005; Vásquez-Caicedo *et al.*, 2006). The bioavailability and bioconversion of  $\beta$ -carotene into retinal is affected by its absorption, which can be enhanced by dietary fat. Although the crystalline structure of  $\beta$ -carotene results in poor absorption, only a small amount of dietary fat (3-5 mg) has been reported to effectively enhance absorption (Ribaya-Mercado, 2002).

Figure 7 indicated that carotenoids exist naturally in both crystalline and non-crystalline forms in plant chromoplasts. The oil droplets containing carotenoid particles located inside the mango cell (Figure 7a); whereas, the crystalline carotenoid particles (rod like) was clearly observed in the carrot cells (Figure 7b). Therefore, this research focused the stability of both crystalline and oil-solubilized forms of  $\beta$ -carotene dispersed in freeze-dried materials (Part 4 and 5).

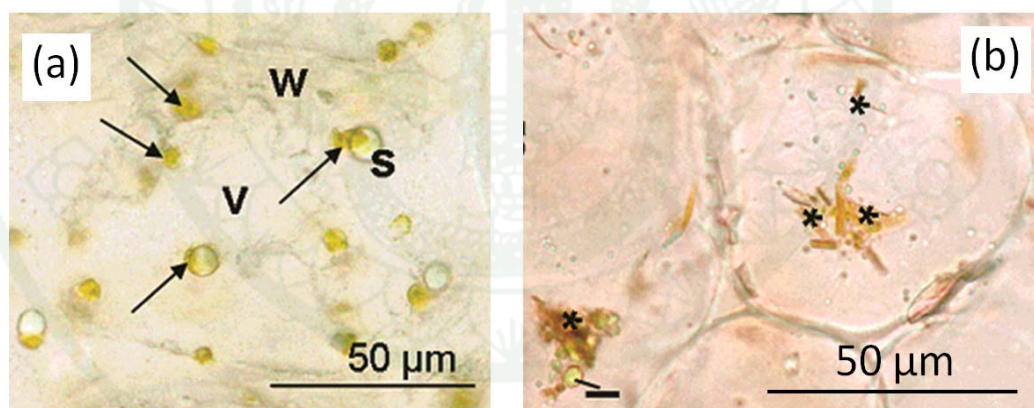


**Figure 7** Light micrograph of ripe mango mesophyll cell (a) showing the typical color of mango chromoplasts (arrows), some starch grains (s), soft cell wall (w) and vacuole (v), and cortex cells of carrot root (b) showing typical color and structure of the crystalline type of chromoplasts (asterisks).

**Source:** Vásquez-Caicedo *et al.* (2006)

## 5. $\beta$ -carotene and modes of degradation

$\beta$ -carotene ( $C_{40}H_{56}$ ) is a lipid soluble substance consisting of a long conjugated double bond carbon skeleton (Figure 8).

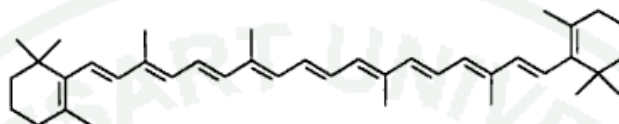


**Figure 8** Structure of all trans- $\beta$ -carotene

The conjugated portion of the molecule (chromophore) is responsible for the molecular shape, chemical reactivity and light absorption in the visible region of the spectra and hence the color (Britton, 1995). It gives yellowish color to most variety of plants and animals. The structure contains two  $\beta$ -ionone rings thus providing the highest vitamin A activity among other carotenoids (Pott *et al.*, 2003). Moreover, their long-chain conjugated polyene structures also provide the antioxidant functions (Caris-Veyrat, 2007).

The large numbers of double bonds contribute to the sensitivity to oxidation which is the major cause of carotenoid loss. Various factors including light, heat, peroxides, metals such as iron, and enzymes had been reported to accelerate the oxidation of carotenoids (Ötles and Çagindi, 2007). The oxidative cleavage may occur at various carbon positions and gives various products called ‘apocarotenal’. The possible mechanisms for  $\beta$ -carotene degradation are given in Figure 9.

The reaction of a molecule with ground state oxygen is commonly called autoxidation, defined as “spontaneous oxidation” in air of substance. Typically, direct reaction between  $\beta$ -carotene and oxygen is very slow but will be quicken as catalyzed by metal traces or light (Caris-Veyrat, 2007) which suggests that autoxidation is the major oxidation in dried foods during storage. The autoxidation of carotenoids begins

with epoxidation and cleavage to apocarotenals (Mordi *et al.*, 1991; Rodriguez and Rodriguez-Amaya, 2007). The investigations on oxidation of  $\beta$ -carotene by various oxidants have been reported in the literature (Handelman *et al.*, 1991; Rodriguez and Rodriguez-Amaya, 2007).

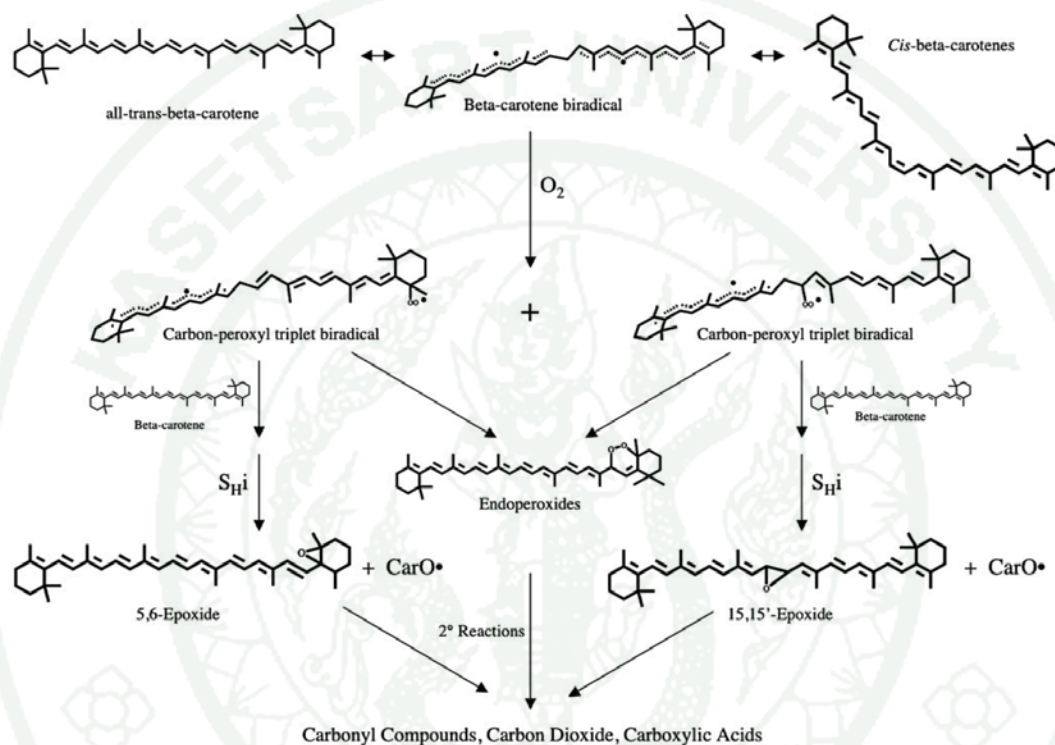


**Figure 9**  $\beta$ -carotene degradation pathway and their products

**Source:** Boon *et al.* (2010)

Moreover,  $\beta$ -carotene can also isomerize from all-trans isomer, which is usually found in nature, into cis-conformation. This is the major consequence of food thermal processing (Mercadante, 1997). During last decade, there had been more research on the isomerization of carotenoids in foods including  $\beta$ -carotene. Pott *et al.* (2003) found that there were also 9-cis and 13-cis conformation in some fresh cultivars of mangoes including 'Nam Dok Mai'. The amount was around 19-30% as compared to all-trans form. They also showed that after drying (air dried at  $75^\circ C$  and solar drying), the amount of cis-isomer could increase up to 2 fold. Vasquez-Caicedo

*et al.* (2005) also investigated the accumulation of 13-cis and 9-cis- $\beta$ -carotene in various Thai mango cultivars as fresh and during postharvest ripening. They found some amounts of cis-isomers in some cultivars but the amount of them was just slightly varying throughout the ripening process. However, lack of investigation reported the isomerization of  $\beta$ -carotene in dried solids during storage possibly because of the specific methods and instruments are required for the analysis.

## 6. Stability of $\beta$ -carotene in freeze-dried materials

Kinetic modeling had been used to report the rate of component formation as well as degradation. In the literature,  $\beta$ -carotene degradation in freeze-dried foods during storage between 20 – 60°C and 0-0.8 $a_w$  was reported to follow first order kinetics (Eq.3) in carrots (Koca *et al.*, 2007; Lavelli *et al.* 2007), guava (Ferreira and Rodriguez-Amaya, 2008), dried sweet potato chips (Bechoff *et al.*, 2010) or when encapsulated in starch (Ferreira and Rodriguez-Amaya, 2008) and trehalose matrix (Elizalde *et al.*, 2002; Prado *et al.*, 2006). This might suggest that in freeze-dried systems, which have a highly porous structure, oxygen could freely penetrate through the matrices resulting in an excessive amount of oxygen for oxidation processes.

$$\ln \frac{C}{C_0} = -kt \quad (\text{Eq.3})$$

where  $C$  and  $C_0$  refer to the concentration at  $t$  and initial concentration at  $t = 0$ , respectively.  $k$  is the rate constant derived from the slope of the regression.

Mostly, the studies investigated the kinetics study of  $\beta$ -carotene as a function of temperature and water activity. Lavelli *et al.* (2007) revealed the plot of first-order rate constants at 40°C for  $\beta$ -carotene against  $a_w$  as an U-shaped curve which was typical of most oxidative reactions. A decrease in rate constants was observed with an increase in  $a_w$  up to about 0.314. In addition, the  $a_w$  range of 0.341–0.537 showed the maximum stability of  $\beta$ -carotene corresponding to the range microbial growth is arrested, enzymatic activity and non-enzymatic browning were minimum. Above these  $a_w$  values  $\beta$ -carotene stability decreased with a further increase in  $a_w$  up to



0.754. In the  $a_w$  range of 0.537–0.754 the microbial growth rate and the enzymatic activity are still at minimum; however the occurrence of non-enzymatic browning could result in  $\beta$ -carotene loss. The  $a_w$  range corresponding to maximum  $\beta$ -carotene stability was next to the monolayer  $a_w$  (Lavelli *et al.*, 2007). Nevertheless, the structural changes of dried solids were not mentioned in this study. This study could be considered as the crystalline form of  $\beta$ -carotene in real food systems. However, no study about the stability of  $\beta$ -carotene in mangoes over the whole range of  $a_w$  has been reported.

In addition, the dehydrated foods are sensitive to moisture and temperature changes. As water and thermal plasticization of solids to the rubbery state, various reactions are accelerated as well as the structural changes, e.g., crystallization and structural collapse. These factors affect the stability of dispersed encapsulant compounds in solids as demonstrated by the previous researches (Buera *et al.* 2005, Prado *et al.*, 2006).

Typically, the encapsulation of functional lipid ingredients including  $\beta$ -carotene in hydrophilic solids has been extensively achieved in the forms of emulsion. As the poor water solubility, some amount of the oil is required to dissolve  $\beta$ -carotene prior to disperse in water and prepared as an emulsion systems. Several studies demonstrated factors affecting stability of dispersed  $\beta$ -carotene in emulsion systems (Tan and Nakajima, 2005; Helgason *et al.*, 2009; Boon *et al.*, 2010; Cornacchia and Roos, 2011; Qian *et al.*, 2012). For instance, the crystallization of lipid carrier which nucleated from the internal core can expel  $\beta$ -carotene to the droplet surface where it is in closer proximity to prooxidants in the aqueous phase (Helgason *et al.*, 2009). The droplet size and subsequent interface area of the emulsion also plays key role on the degradation of  $\beta$ -carotene which means the contact surface between  $\beta$ -carotene and surrounding aqueous (Tan and Nakajima, 2005; Qian *et al.*, 2012). In addition, the manipulation of interfacial properties using various emulsifiers contributed to a significant stabilization of  $\beta$ -carotene by, for instance, modification of thickness and multilayer of interface which acted as physical barriers, radical scavenging as well as



controlling the size and surface area of the droplets (Cornacchia and Roos, 2011; Qian *et al.*, 2012).

In dehydrated systems, however, other factors such as the structural changes and matrix mobility resulting from water plasticization could have been taken into account. The hydrophilic components are the main determinants for physicochemical stability of dehydrated matrix. The crystallization of matrix was reported to cause the release of encapsulant compounds to exposure of oxygen contributing to the degradation (Buera *et al.*, 2005); whereas, the structural collapse could enhance the stability of dispersed compounds by the prevention of oxygen diffusion (Nelson and Labuza, 1994, Prado *et al.*, 2006). Mostly, the stability studies of  $\beta$ -carotene in dehydrated systems were performed by storage of solids under various  $a_w$  conditions and monitored the amount of  $\beta$ -carotene during storage at a single temperature.

Elizalde *et al.* (2002) reported the retention of  $\beta$ -carotene encapsulated in an freeze-dried amorphous trehalose-gelatin during storage at 0.11, 0.44 and 0.75  $a_w$  at 25°C. First-order reaction kinetics indicated the higher retention of  $\beta$ -carotene (about 80% in 6 months) in solids which were not crystallized during storage, while for trehalose-crystallized samples exposed to 0.75  $a_w$  the loss was almost complete. Moreover, in partially crystalline sugar matrices containing exactly the water content to form the dihydrate crystals of trehalose (10%, at  $a_w = 0.44$ ), the loss of  $\beta$ -carotene was lower to those matrix with a similar crystallization degree, but of higher moisture content. The kinetics of  $\beta$ -carotene loss was strongly accelerated in samples with excess of water above that necessary to crystallize. The authors stated that the ability of water to disrupt the hydrogen bonded network formed by the non-crystalline carbohydrate matrix, allowed the entrapped components to escape from micro regions of the dried matrix. In the trehalose matrix, when water content is < 10%, the dihydrate crystal was formed and water was not available to liberate the encapsulated carotene. Above 10% water content, once the degree of crystallization was high, water caused the liberation of carotene from the remaining non-crystalline matrix. Consequently, the rate of  $\beta$ -carotene loss was high (Elizalde *et al.*, 2002). This study

indicated that matrix crystallization resulted in the released of encapsulated  $\beta$ -carotene to exposure of oxygen and subsequent degradation.

Prado *et al.* (2006) studied the kinetics degradation of  $\beta$ -carotene encapsulated in a polymeric matrix (PVP-40) with gelatin and its relationship with physical changes (manifested as structural collapse as measured by the reduction of solid volume) of the matrix during storage. Samples were stored at several  $a_w$  at 25°C. The degradation rate constants decreased with an increased  $a_w$ .  $\beta$ -carotene losses were observed mainly at storage  $a_w$  which  $T_g$  of samples were lower than storage temperature (i.e., glassy), and the lower degradation constant rates were observed under conditions where the matrices were fully plasticized (i.e., rubbery) and collapsed (RH, 64 and 75%). The results indicated that the structural collapse by humidity plasticized effectively enhanced stability of  $\beta$ -carotene. The authors stated that the molecular mobility of the matrix was not rate limiting for the degradation of  $\beta$ -carotene. Factors such as microstructure and porosity of the polymeric matrix may be more important as modifiers of kinetic reactions.

Recently, Ramoneda *et al.* (2001) reported a contradict findings on kinetics  $\beta$ -carotene loss as a function of humidity and structural collapse.  $\beta$ -carotene was dissolved in sun flower oil and dispersed in maltodextrin solids with gum arabic as well as gelatin as emulsifiers. Freeze-dried solids were stored at 0.11, 0.44, 0.75 and 0.92  $a_w$  at 25°C. In their study,  $\beta$ -carotene loss was found in systems stored above  $T_g$  at which water plasticized matrices and corresponding structural collapse occurred. It was possible that the increased mobility in the systems caused the released of the oil from matrices which were faster than the efficiency of collapse to retain the encapsulated compound stability. In addition they also found that the  $\beta$ -carotene was best retained in solids emulsified with gum arabic. This suggested the effects of interface properties between maltodextrin-emulsifier on the stability of  $\beta$ -carotene. However, there was no available information on other factors such as the particle size or interface properties of droplet particles.

Accordingly, the previous studies reported diverse results on the stability of oil-solubilized  $\beta$ -carotene dispersed in freeze-dried systems stored at various  $a_w$ ; however, other factors such as the oil particle size as well as the effect of other solutes have rarely been discussed. In this work we also found the relationship of the lipid droplet size on the stability of dispersed  $\beta$ -carotene in freeze-dried solids (Part 5).

Moreover, several studies also indicated that the pore structure of freeze-dried solids as well as the structural collapse of solids also gave a significant effect on the rate of various chemical reactions during storage. White and Bell (1999) studied the effects of porosity and collapse on the kinetics of glucose loss and brown pigment formation via the Maillard reaction in solid low-water food systems. Equimolar glucose and glycine were incorporated into amorphous polyvinylpyrrolidones (PVP) with different porosities obtained by altering the amount of water in the formulation. These ranged from high porosity to totally collapsed structures after freeze-drying. Samples were equilibrated and stored in desiccators at 0.33  $a_w$  or 0.44  $a_w$  and 25°C. Glucose loss and brown pigment development were monitored for 3 months. Glucose loss rate constants were lower in collapsed systems compared to non-collapsed systems but the various porosities did not affect glucose loss rate constants. However, collapse and porosity had minimal effects on the browning rate constants. These results also coincided with the earlier findings by Bell *et al.* (1998). They studied the rate constants for glycine loss and brown pigment formation resulting from the Maillard reaction using the same systems. Similarly, rate constants for glycine loss decreased upon matrix collapse, but browning rate constants were not affected by collapse. In the glassy state, the rate constants were higher in systems with lower  $T_g$  at a constant  $a_w$ ; however, the glycine loss decreased as the systems became rubbery. These results indicated that porosity and collapse as well as the  $T_g$  of solids affected the chemical reactivity in low-water solids.

Later in 2000, Bell and White studied the stability of thiamin encapsulated in solid PVP model systems stored in the dark at 20°C as a function of  $a_w$  and  $T_g$ . They found that in the glassy state, thiamin degradation rate constants decreased as  $T_g$  increased. However, above the 0.4  $a_w$  at which solids became rubbery, the rate

constants decreased. They hypothesized that this could be attributed to glass transition-induced structural collapse that enhanced the stability of thiamin.

Selim *et al.* (2000) suggested that collapse could decrease saffron carotenoid degradation. These authors studied kinetics of degradation of water soluble carotenoids in saffron (mainly crocins) which were encapsulated in three different amorphous matrices (pullulan and PVP40, PVP360) and stored at various  $a_w$  conditions (0.43, 0.53, 0.64 and 0.75) in the dark at 35°C. Degradation of the polar pigments was monitored by periodic measurements of the coloring strength. They found that carotenoid loss occurred even at temperatures below the  $T_g$  of the polymeric matrices where the matrices were in the glassy state. In the vicinity of the  $T_g$  zone, where pullulan and PVP360 underwent state transformations, there was a change in the reaction rate. The lower degradation rates were observed for PVP40 under conditions where this matrix was fully plasticized (i.e. rubbery) and “collapsed”. They suggested that PVP40 may provide high protection for saffron carotenoids because it collapsed rapidly during storage and, thereby, it might become a more effective barrier to oxygen permeation. It is the fact that collapse of freeze-dried materials is associated with the disappearance of micropores and cavities through which oxygen enters the amorphous matrix. On the other hand, pullulan as wall material, being relatively stable in storage, could be more permeable to oxygen and thus less effective than the PVP systems in protecting saffron carotenoids.

In 2001, Serris and Biliaderis investigated kinetics of degradation of water-soluble beetroot pigments, mainly consisting of the betalain betanin, encapsulated in three different matrices (pullulan and two maltodextrin of DE5 and DE20). systems were freeze-dried and stored at various  $a_w$  (0.23, 0.43, 0.64, 0.75 and 0.84) and temperature (30, 40 and 50°C) conditions. The highest values of the rate constants for degradation were observed at an intermediate water activity 1 ( $a_w = 0.64$ ) for all matrices and all three storage temperatures. They also showed that pigment losses were observed even at temperatures below the  $T_g$  of the polymeric matrices, although degradation was largely slowed down in the glassy state. In the vicinity of the  $T_g$  zone, where all polymers go through a glass-rubber transition, there was not a distinct



change in the reaction rate, which could reflect the pronounced changes in molecular mobility of the wall material. They also found that some of the lower degradation rates were observed mostly under conditions where the matrices were fully plasticized (i.e., rubbery) and collapsed. They implied that the molecular mobility and reactivity of some reactants were not governed by the physical state of the wall material; for example, the diffusion of oxygen was not hindered through a glassy matrix. Depending on the preparation of the freeze-dried glassy materials and possibly aging effects, it was likely that the matrix porosity and microstructure were more important than modifiers of the degradation kinetics of beetroot pigments. However, they also claimed that in addition to structural modification caused by sorbed water, water sorption on the matrix might alter its oxygen barrier properties.

While in 2000, Rassis *et al.* showed that oxidation of encapsulated oil in freeze-dried alginate-oil gel did not affect by porosity at storage 0 and 22% RVP. However, oxidation was increased significantly when stored at 75% RVP and porosity above a critical value of 0.45. They showed that the porosity of the freeze-dried gel was not different for all storage RVP, so it should be noted that no collapse occurred in such system. This might be the reason that at high RVP the oxidation was not decreased as other studies. Their results also showed that water content played a significant role in both sorption and diffusion of oxygen through the alginate matrix.

These studies have shown that porosity and also collapse of structure of freeze-dried foods may diversely affect the rate of chemical reactions involving a contact area. Moreover, the structure resulting from freeze-drying in model systems may differ from real foods, for example, the effect of ice formation is crucial. In model systems, ice will give a porous dried structure, while in foods freezing may also disrupt cellular structures which in turn can cause deterioration, for example because of increased enzymatic activity (i.e. lipoxygenase as carotene oxidase; Pott *et al.*, 2003) and release of some components. Moreover, foods are complex systems in which the presence of various solutes can delay or accelerate reactions. This study investigated the effect of freeze-dried food structures on stability of  $\beta$ -carotene in food and model systems as well as the crystalline and non-crystalline forms of  $\beta$ -carotene.



## MATERIALS AND METHODS

### Materials

The researches contained in this work were conducted at 2 following department:

**1. Department of Food Science and Technology, Faculty of Agro-Industry, Kasetsart University, Thailand (Period: December 2007 to December 2010, Part 1 and 2)**

#### 1.1 Materials

1.1.1 Mango (*Mangifera indica*) cultivar “Nam Dok Mai” (purchased from a freeze-dried fruit industry in Chantaburi, Thailand)

1.1.2  $\beta$ -carotene standard solution ( $\beta$ -carotene type II synthetic  $\geq 95\%$  crystalline;  $C_{40}H_{56}$ , HPLC)

1.1.3 Saturated salt solution (LiCl,  $CH_3COOK$ ,  $MgCl_2$ ,  $K_2CO_3$ , NaBr, KI, and KBr)

1.1.4 Hexane (HPLC grade, RCI Labscan, Bangkok, Thailand)

1.1.5 Methanol (HPLC grade, RCI Labscan, Bangkok, Thailand)

1.1.6 Acetonitrile (HPLC grade, RCI Labscan, Bangkok, Thailand)

1.1.7 Agar powder (Pearl Mermaid<sup>®</sup>, Bangkok, Thailand)

#### 1.2 Equipments

1.2.1 Freeze dryer (Freeze dryer Dura-Top/ Dura Stop MP, Dura Dry MP, FTS Systems<sup>™</sup>, Stone Ridge, NY, USA)

1.2.2 High performance liquid chromatography (HPLC, Model 600, Waters, Milford, MA, USA)

1.2.3  $C_{18}$  HPLC column (XTerra<sup>®</sup> RP18, 5 $\mu$ m, 3.9 x 150 mm) (Waters, Milford, MA, USA)

1.2.4 Differential scanning calorimeter (DSC, Perkin Elmer Pyris 1 DSC)

1.2.5 X-ray powder diffraction (XRD, PHILIPS X'Pert MPD, Netherlands)

1.2.6 Gold sputter coater (PSI sputter coater, PA, USA)

1.2.7 Refrigerated centrifuge (Sorvall RC 5C Plus Superspeed Centrifuge, MN, U.S.A.)

1.2.8 Scanning electron microscope (SEM, JEOL JSM-6480LV, Tokyo, Japan)

1.2.9 Stereo microscope (Leica S8APO, Leica Microsystems<sup>®</sup>, Switzerland)

1.2.10 High-speed homogenizer (IKA T10 basic, Ultra Turrax, Germany)

## **2. School of Food and Nutritional Sciences, University College Cork, Cork, Ireland (Period: January 2011 to December 2011, Part 3, 4 and 5)**

### **2.1 Materials**

2.1.1 Agar (microbiology grade, Fluka, Switzerland)

2.1.2 Maltodextrin (M40, DE6; M100, DE11; M250 or DE25.5; Grain Processing Corporation, Iowa, USA)

2.1.3 Glucose (Sigma-Aldrich Ireland Ltd, Dublin, Ireland)

2.1.4 Fructose (Sigma-Aldrich Ireland Ltd, Dublin, Ireland)

2.1.5 Sucrose (Sigma-Aldrich Ireland Ltd, Dublin, Ireland)

2.1.6 De-ionized water (KB Scientific, Ireland)

2.1.7  $\beta$ -carotene (crystalline Type II, synthetic, 95% HPLC, Sigma-Aldrich Ireland Ltd., Dublin, Ireland)

2.1.8 Polysorbate 20 (Tween 20, Merck, Germany)

2.1.9 Saturated salt solutions of LiCl, CH<sub>3</sub>COOK, MgCl<sub>2</sub>, K<sub>2</sub>CO<sub>3</sub>, Mg(NO<sub>3</sub>)<sub>2</sub>, NaNO<sub>2</sub> and NaCl (Sigma-Aldrich, St. Louise, MO, U.S.A.)

2.1.10 Sunflower oil (Pan Euro Foods, EU)

2.1.11 Methanol (HPLC grade, Sigma-Aldrich Ireland Ltd., Dublin, Ireland)

2.1.12 Hexane (HPLC grade, Sigma-Aldrich Ireland Ltd., Dublin, Ireland)

2.1.13 Acetonitrile (HPLC grade, Fischer Scientific, UK).

2.1.14 Dichloromethane (HPLC grade, Sigma-Aldrich Ireland Ltd., Dublin, Ireland)

2.1.15 Butylated hydroxytoluene ( $\geq 99\%$ , SAFC, USA)

2.1.16 Triethylamine (Fluka, Switzerland, Sigma-Aldrich Ireland Ltd., Dublin, Ireland)

## 2.2 Equipments

2.2.1 Freeze-dryer (Steris Lyovac GT2, Germany with Leybold Trivac, Germany vacuum pump)

2.2.2 Scanning electron microscope (SEM, Carl Zeiss AG, Darmstadt, Germany)

2.2.3 Differential scanning calorimeter (DSC, Mettler Toledo 821e with liquid N<sub>2</sub> cooling, Schwerzenbach, Switzerland)

2.2.4 Dynamic mechanical analyzer (Tritec 2000 DMA version 1.43.00 software, Triton Technology Ltd., Loughborough, UK)

2.2.5 Spectrophotometer (Varian Cary 300 Bio UV-Visible Spectrophotometer, Varian Inc., Middelburg, The Netherlands)

2.2.6 High performance liquid chromatography with photodiode array detector (HPLC, Dionex ICS3000, Sunnyvale, CA., USA)

2.2.7 Laser diffraction particle size analyzer (Malvern Master Sizer MSS, Malvern Instruments Ltd., U.K.)

2.2.8 Two-stage valve homogenizer (APV-1000 high-pressure homogenizer, Denmark)

2.2.9 High-speed homogenizer (T 25 Digital Ultra-Turrax, Germany)

## Methods

The methods are given in 5 parts according to the results and discussion.

### 1. Sugar crystallization and $\beta$ -carotene stability of freeze-dried mango powder

#### 1.1 Freeze-dried mango powder preparation

Ripe mangoes (cultivar ‘Nam Dok Mai’) were purchased from a freeze-dried fruit industry in Chantaburi, Thailand and were selected by homogeneity in size (approximately 14cm x 9cm), weight (400-500g), and peel color (homogeneous yellow). The total soluble solids of mangoes were determined to be in the range of 16–20 °Brix. The fruits were peeled, cut into 1-cm cubes, and freeze-dried using a freeze dryer (Freeze dryer Dura-Top/ Dura Stop MP, Dura Dry MP, FTS Systems™, Stone Ridge, NY, USA). The mango pieces were frozen at -35°C and held for 2 h to achieve ice crystallization and subsequently dried at a shelf temperature of -40°C. Then, all samples were stored in evacuated desiccators for 3 days, which contained silica gel to remove residual water. After that, the samples were considered to have “zero” water content (as adapted from Burin *et al.*, 2004). Subsequently, the freeze-dried mango pieces were packed in aluminum foil in a partial vacuum and crushed into powder using a mortar. The particle size of mango powder was determined to be in the range of 199.8-27,629.1  $\mu\text{m}^2$ . Mango powder was used for the analysis.

#### 1.2 Water sorption behavior of freeze-dried mangoes

##### 1.2.1 Water sorption as a function of time

Mango powder (1–2 g) was transferred into containers and equilibrated in evacuated desiccators, which contained saturated salt solutions of LiCl, CH<sub>3</sub>COOK, MgCl<sub>2</sub>, K<sub>2</sub>CO<sub>3</sub>, NaBr, KI, and KBr to obtain various RVP values (11.3%, 22.5%, 32.8%, 43.2%, 57.6%, 68.9%, and 80.9% (Fontana, 2007). Samples were removed from the vacuum desiccators at intervals, as shown in Figure 10.

Triplicate samples were weighed for each RVP value. After the release of the vacuum from desiccators, the containers were immediately sealed with caps to minimize the transfer of water by air. The amount of water absorption was calculated from the weight gain of the powder (Jouppila and Roos, 1994; Omar and Roos, 2007).

### 1.2.2 Water sorption isotherm (Omar and Roos, 2007).

The Guggenheim-Anderson-DeBoer (GAB) models (Equation 1) were fitted to the experimental water sorption data (Omar and Roos, 2007). The GAB monolayer water content ( $m_m$ ) and constants ( $C$  and  $K$ ) were derived from the experimental sorption data over  $a_w$  range of 0.113–0.432, where  $m$  refers to the moisture content at specific  $a_w$ .

$$\frac{m}{m_m} = \frac{C K a_w}{(1 - K a_w)(1 - K a_w + C K a_w)} \quad (\text{Eq.4})$$

## 1.3 Crystallization in freeze-dried mangoes

Mango powder was humidified at 11.3%, 43.2%, 57.6%, and 68.9% RVP for 7 days at 25°C, which was followed by further drying in an evacuated desiccator that contained silica gel for 7 days. Samples were ground with a mortar and pestle and stored in an evacuated desiccator at 25°C until the analyses were performed. The freeze-dried mango powder prior to storage was analyzed as uncrystallized samples.

### 1.3.1 X-ray diffraction measurement (XRD)

The XRD patterns of freeze-dried mango powder were used to monitor the crystallization process with an X-ray diffractometer (XRD, PHILIPS X'Pert MPD, Netherlands) with an input energy of 40 kV and 30 mA, as described by Cano-Chauca *et al.* (2005). The powder was slightly pressed on an aluminum sample tray using a glass slide and scanned at a diffraction angle ( $2\theta$ ) between 4 and 50°, with a stepped increase of 0.02°  $2\theta$  / 0.5S.



### 1.3.2 Scanning electron microscope (SEM)

The physical structures of freeze-dried amorphous and crystalline samples were assessed with an SEM (JEOL JSM-6480LV, Tokyo, Japan). Small amounts of samples were atomized on silver-painted sample holders with double-sided adhesive tape. Samples were covered with a fine layer of gold in a sputter coater (PSI sputter coater, PA, USA) in a high vacuum. The coated samples were photographed with an SEM at 10 kV with a magnification of 1,000.

### 1.4 $\beta$ -carotene degradation during storage

Freeze-dried mango powder samples were transferred into vials (diameter 10 mm and sample thickness 10-13 mm) and stored at 11.3%, 22.5%, 32.8%, 43.2%, 57.6%, and 68.9% RVP at room temperature. Duplicate samples were extracted and determined for  $\beta$ -carotene content with a method adapted from Ferruzzi *et al.* (1998) using a high performance liquid chromatography (HPLC). Freeze-dried mango powder (1 g) was extracted with 10 mL of methanol and hexane (1:1) by a homogenizer (IKA T10 basic, Ultra Turrax, Germany) for 2 min. The solutions were centrifuged (Sorvall RC 5C Plus Superspeed Centrifuge, MN, U.S.A.) at 4,500 g for 10 min at 4°C. The supernatant (hexane layer) was collected and the precipitant was re-extracted. The collected hexane layer was dried by purging with N<sub>2</sub> gas. Dried residues were added with 2 mL of hexane prior to subjection into an HPLC amber vial. Each sample (20  $\mu$ L) was injected to an HPLC column C18 (XTerra® RP18, 5 $\mu$ m, 3.9 x 150 mm, Waters, Milford, MA, USA). Methanol and acetonitrile (9:1) with 0.1% trimethylamine were used as a mobile phase at a flow rate of 1.5 mL/min. The  $\beta$ -carotene content was analyzed by an HPLC with UV diode-array detector (Model 600, Waters, Milford, MA, USA) at a wavelength of 450 nm (Appendix Figure 1). The amounts of  $\beta$ -carotene were calculated from the standard curve of all-*trans*- $\beta$ -carotene (Appendix Figure 2).

## **2. Influence of collapsed structure on stability of $\beta$ -carotene in freeze-dried mangoes**

### **2.1 Freeze-drying of mangoes**

Fresh ripe mangoes (cultivar 'Nam Dok Mai') were purchased from a freeze-dried fruit industry in Chantaburi, Thailand. They were selected for their homogeneity in size (approximately 14cm x 9cm), weight (400-500g), peel color (homogeneous yellow), and density by floatation in a 4-5% NaCl solution. The total soluble solids of mangoes were determined to be in the range of 16–20 °Brix.

Mangoes were washed, peeled, and cut into 1-cm cubes and freeze-dried (Freeze dryer Dura-Top/ Dura Stop MP, Dura Dry MP FTS Systems™, Stone Ridge, NY, USA) with the application of the 3 freeze-drying protocols, i.e., various freezing methods and freeze-drying temperatures (primary drying) (Table 2). The protocol 1 and 2 consisted of freezing at a shelf temperature of the freeze dryer at -35°C, whereas mango cubes in protocol 3 were frozen by immersion in liquid nitrogen prior to transfer to the freeze-dryer at a shelf temperature of -35°C. Frozen cubes of mangoes were kept at -35°C for 120 min for ice formation. Then the mango samples were freeze-dried using shelf temperatures of -40°C (protocol 1 and 3) or -15°C (protocol 2) (primary drying), with the final product temperature (secondary drying temperature) set as 30°C for all protocols. The drying step was done under pressure < 16 Pa (120 mTorr). All freeze-dried samples were stored in evacuated desiccators over silica gel to reduce water uptake for 3 days.

The effect of freeze-drying protocols on freeze-dried food structures were compared using agar gel. Agar solutions (2% and 4% w/w) were heated to 90°C, held for 2 min, and cooled to form gel. Agar gels were cut into 1-cm cubes prior to freeze drying using the identical freeze-drying protocols as those applied for mangoes (Table1). The obtained freeze-dried agar gels were characterized for the external structures with a stereomicroscope.

## 2.2 Characterization of freeze-dried mango structures

The external structures of the freeze-dried mangoes were determined with a Spot camera (Leica S8APO, Leica Microsystems<sup>®</sup>, Switzerland), which was connected to a stereo light microscope (Leica CLS 150 XE Leica Microsystems<sup>®</sup>, Switzerland) at a low magnification (10×).

The internal structures of freeze-dried mangoes were characterized with the application of SEM (JEOL JSM-6480LV, Tokyo, Japan). Cross-sectioned samples were affixed on silver-painted sample holders and covered with a fine layer of gold in a sputter coater (PSI sputter coater, PA, USA) under vacuum. The coated samples were photographed with a SEM at 5 kV.

## 2.3 Thermal transitions of mangoes

Thermal transitions of mangoes and agar gel were determined with a differential scanning calorimeter (DSC). Mango juice were extracted and determined for thermal transitions as described by Lowithun and Charoenrein (2009). Mango pulp (500 g) was blended and centrifuged at 4,500g for the duration of 15 min. The supernatant was taken as mango juice. Sample juice (10-13 mg) was transferred into aluminium DSC pans and hermetically sealed. Duplicate samples were scanned without annealing to locate apparent  $T_g$  and onset of ice melting ( $T_m'$ ) by DSC (Perkin Elmer Pyris 1 DSC). Samples were cooled from 25 to -60°C, held for 15 min, and subsequently heated to 25°C at 5°C/min. The  $T_g'$  and  $T_m'$  were measured after isothermal annealing at  $T_m'-1^\circ\text{C}$  obtained from the first scan. Triplicate samples were scanned from 25 to -60°C, held for 15 min, subsequently heated to  $T_m'-1$  at 5°C/min and held for 30 min. After that, samples were cooled to -60°C, held for 15 min and heated to 25°C at 5°C/min.  $T_g'$  values were taken from the midpoint of the  $C_p$  change over the glass transition and  $T_m'$  from the onset temperature of the ice melting endotherm.

Agar gels (30% w/w) were transferred into a stainless DSC pan. Duplicate samples were scanned from 25 to 110°C at 10°C/min, held for 1 min, then cooled to -40°C at 5°C/min and held for 10 min. Samples were further heated to -20°C at 10°C/min, held for 15 min, cooled to -40°C at 10°C/min and further heated to 25°C at 10°C/min.  $T_g'$  values were taken from the midpoint of the  $C_p$  change over the glass transition.

#### 2.4 Stability of $\beta$ -carotene in freeze-dried mangoes

Freeze-dried mangoes were stored at 11% and 22% relative vapor pressure (RVP) in glass desiccators over saturated solutions of LiCl or CH<sub>3</sub>COOK at room temperature ( $25 \pm 2^\circ\text{C}$ ) in the laboratory. Duplicate samples were prepared from freeze-dried materials to determine  $\beta$ -carotene contents with a HPLC during storage.  $\beta$ -carotene was extracted and measured with a method adapted from Ferruzzi *et al.* (1998). Freeze-dried mango cubes were powdered in an aluminum foil pouch to prevent uptake of water. Sample powder (1 g) was rehydrated with distilled water (5 mL) and extracted with 10 mL of methanol and hexane (1:1) with a homogenizer (IKA T10 basic, Ultra Turrax, Germany) for 2 min. The suspensions were centrifuged (Sorvall RC 5C Plus Superspeed Centrifuge, MN, U.S.A.) at 4,500 g at 4°C for 10 min. The supernatant (hexane layer) was collected and the precipitant was re-extracted. The collected hexane layer was dried by purging with N<sub>2</sub> gas. Dried residues were diluted with 2 mL of hexane prior to preparation into an HPLC amber vial to assess the  $\beta$ -carotene content. The HPLC analyses were performed as described in section 1.4.

#### 2.5 Statistical analysis

A completely randomized blocked design was used and the data were subjected to analysis of variance by using SPSS 12.0 software for windows (SPSS Thailand Co., Ltd., Bangkok, Thailand). Duncan's multiple range tests were used to determine the difference among means ( $p \leq 0.05$ ).



### 3. Microstructure formation of maltodextrin and sugar matrices in freeze-dried systems

#### 3.1 Maltodextrin and maltodextrin-sugar systems

Agar was used as a gelling agent to form a semi-solid fruit-like structure containing carbohydrates. Solutions of system components were prepared using maltodextrin (M40, DE6; M100, DE11; M250 or DE25.5) (18% w/w), maltodextrin (M100) (9%w/w) with fructose, glucose, or sucrose (9% w/w), or sugar mixture (glucose:fructose:sucrose in the ratio of 1:1:4) (9%w/w) and agar (2% w/w) in distilled water (80% w/w). The materials were weighed and dissolved in de-ionized water. Solutions with agar were stirred and hydrated using a magnetic stirrer at room temperature (24°C) for at least 20 min until further heated to 90°C while stirring and held for 5 min to ensure complete melting of the agar. The gelling solutions were cooled and poured into containers and left for gelation at 25°C for at least 1 h.

#### 3.2 Freezing and freeze-drying

Samples of all systems were prepared by cutting the gels into cubic (10x10x10mm) samples with a razor blade. The gels were placed on aluminium trays and frozen in still air at -20°C, -40°C or -80°C for 20 h. All samples subsequently to freezing were tempered at -80°C for 3 h prior to freeze-drying using a laboratory freeze-dryer (Steris Lyovac GT2, Germany with Leybold Trivac, Germany vacuum pump) for 48 hours. This eliminated temperature increases to melting, as the samples were loaded rapidly on freeze-drying shelves operating at room temperature. The chamber pressure was decreased to less than 0.1 mbar in 5 min corresponding to ice sublimation at  $T < -40^{\circ}\text{C}$ . This condition was maintained throughout the freeze-drying to maintain ice temperature below the onset temperatures of ice melting,  $T_m'$ , of any of the materials. At the end of freeze-drying, the vacuum was broken using ambient air. The freeze-dried systems were stored in evacuated desiccators containing  $\text{P}_2\text{O}_5$  for 4 days prior to analysis.



### 3.3 Freezing profile

A data logger with temperature sensor probes Type T (copper-constantan) (Squirrel SQ800, Grant instruments Ltd., England) were used to record sample temperatures during freezing. Five mL of the hot agar suspensions were transferred to flat-bottom glass vials (d 4 x h 4.5cm). The vials were sealed with parafilm and left for solidification at room temperature for at least 1 h. The temperature probes were punctured through the parafilm seals and placed in the samples at a height of 0.75 cm from the bottom. The vials were immediately placed on an aluminium tray and frozen at -20°C, -40°C and -80°C. A temperature probe was also placed on the aluminium tray to record the temperature of the tray during freezing. The freezing temperature data were taken at 10 s intervals at least for 2 h. Triplicate samples were used and the initial cooling rates were read from the initial slopes of the temperature decrease.

### 3.4 Differential scanning calorimetry

Phase and state transitions of the systems were analyzed with a differential scanning calorimeter (DSC, Mettler Toledo 821e with liquid N<sub>2</sub> cooling). Samples of the freshly prepared hot solutions (25-55 mg) were transferred to preweighed 40 µl DSC aluminium pans (Mettler Toledo, Switzerland) and the pans were hermetically sealed. The DSC was calibrated for temperature and heat flow using n-hexane, mercury, water, gallium and indium, as reported by Haque and Roos (2004). An empty pan was used as a reference.

Samples in DSC pans were first scanned from 25°C to -80°C (10°C/min) and held for 2 min, then heated to 25°C (5°C/min) to determine the onset temperature of ice melting,  $T_m'$  (Roos and Karel, 1991a). Duplicate samples were then scanned from 25°C to -100°C (10°C/min), held isothermally at -100°C for 2 min, heated to  $T_m'$  -2°C, held for 15 min, then cooled to -100°C and held isothermally at -100°C for 2 min prior to heating to 25°C at 5°C/min. The glass transition,  $T_g'$  and onset temperature of ice melting,  $T_m'$  of the maximally freeze-concentrated systems were determined from the final heating scan using STARe software (Mettler Toledo,

Switzerland; version 8.10). The  $T_g'$  values were taken from the onset temperatures of the endothermic change in heat flow (heat capacity,  $C_p$ ) over the glass transition temperature range.

### 3.5 Scanning Electron Microscopy

Freeze-dried samples (10 x 10 x 3 mm thick) were cut with a razor blade and fixed to an aluminium stub using double-sided carbon tape and sputter coated with chromium for 15 min. Samples were examined in a Carl Zeiss Supra 40VP field emission scanning electron microscope (Carl Zeiss AG, Darmstadt, Germany) at 10 kV. Digital Images at 8 bit grey level were acquired by secondary electron detector.

### 3.6 Texture analysis

The rheological characteristics of the 'anhydrous' freeze-dried systems were obtained using a Texture Analyzer model TA-XT2i (Texture Technologies, USA). The freeze-dried cubes were removed from the desiccator containing  $P_2O_5$  and immediately compressed with a metal probe (SMS P/50) to a constant deformation (displacement) of 80% (Nussinovitch *et al.*, 1993; Jaya and Durance, 2009) at a rate of  $0.1 \text{ mm s}^{-1}$ . The data were converted to and presented in stress values (kPa) by dividing the compressive force (N) by the sample surface area ( $0.001 \text{ m}^2$ ). Peak force and modulus values were calculated using data measured for 5 to 7 replicate samples. It should also be noted that, the penetration test is not suitable for the measurement of our solid samples as the data showed high variation among replicate. Therefore, the compression test which showed a good repeatability was chosen for the measurement.

### 3.7 Statistical analysis

Compressive force and modulus were subjected to statistical analysis. A one-way analysis of variance (ANOVA) and Duncan's multiple range tests were used to analyze the differences in data at 95% confidence level with SPSS 12.0 software for Windows (SPSS Thailand Co., Ltd., Bangkok, Thailand).

#### 4. Porosity and Water Activity Effects on Stability of Crystalline $\beta$ -carotene in Freeze-dried Solids

##### 4.1 Gel preparation

Suspensions of  $\beta$ -carotene (crystalline Type II) were prepared by dispersing  $\beta$ -carotene crystals (1.2%w/w) in polysorbate 20 (Tween 20, 2% w/w) in water. Suspensions were stirred with a magnetic stirrer for at least 3 h in dark.

Agar was used as a gelling agent to form a semi-solid, fruit-like structure composed of carbohydrates. Carbohydrate solutions were prepared using maltodextrins (M40, DE6; M100, DE11; M250, DE25.5) (18% w/w), maltodextrin (M100) (9%w/w) with glucose, fructose, or sucrose (9% w/w), and maltodextrin (M100) (9% w/w) with glucose:fructose:sucrose mixture (1:1:4) (9%w/w) and agar (2% w/w) in distilled water (80% w/w). Carbohydrates were weighed and dissolved in de-ionized water. Solutions with agar were stirred and hydrated using a magnetic stirrer at room temperature (24°C) for at least 20 min until further heated to 90°C while stirring and held for 5 min to ensure complete dissolving of the agar. The  $\beta$ -carotene suspensions (0.5%w/w) were poured into carbohydrate solutions during cooling at 60°C. After stirring for further 5 min, a clear and homogeneous pink color of agar systems was visually observed. The gelling systems were poured into containers and left for gelation at 24°C for at least 1 h. Agar served as a gelling agent which fixed the dispersed crystalline  $\beta$ -carotene particles homogeneously in the carbohydrate matrix.

##### 4.2 Freezing and freeze-drying

Samples of all systems were prepared by cutting the gels into cubes (10x10x10mm) with a razor blade. The cubic samples were placed on aluminium trays and frozen for 20 h in still air using temperatures of -20°C, -40°C and -80°C. All samples were subsequently to freezing tempered at -80°C for 3 h prior to rapid loading to freeze-drying carried out using a laboratory freeze-dryer (Steris Lyovac

GT2, Germany with Leybold Trivac, Germany vacuum pump) for 48 h. This eliminated possible ice melting during loading on freeze-drying shelves. The chamber pressure was decreased to less than 0.1 mbar corresponding to ice sublimation at  $T < -40^{\circ}\text{C}$ . This condition was maintained throughout the freeze-drying to keep ice temperature below the onset temperature of ice melting,  $T_m'$ , in any of the materials. The freeze-dryer was operated at ambient room temperature, and at the end of freeze-drying, the vacuum was broken using ambient air. The freeze-dried systems were stored in evacuated desiccators containing  $\text{P}_2\text{O}_5$  for at least 4 days in dark prior to further analysis.

### 4.3 Freeze-dried solids characterizations

#### 4.3.1 Scanning electron microscopy

Freeze-dried solids were analyzed for microstructure with a scanning electron microscope (SEM). Freeze-dried samples (10 x 10 x 3 mm thick) were cut with a razor blade and fixed to an aluminium stub using double-sided carbon tape and sputter coated with chromium for 15 min. Samples were examined in a Carl Zeiss Supra 40VP field emission scanning electron microscope (Carl Zeiss AG, Darmstadt, Germany) operating at 10kV. Digital Images at 8 bit grey level were acquired using the secondary electron detector.

#### 4.3.2 Water sorption

The gels frozen at  $-20^{\circ}\text{C}$  and freeze-dried were analyzed for water contents after storage at various relative vapor pressures (RVP). Approximately 1 g of freeze-dried solid cubes was transferred into glass vials and stored in evacuated desiccators over various saturated salt solutions at room temperature ( $24^{\circ}\text{C}$ ). The salts used were LiCl,  $\text{CH}_3\text{COOK}$ ,  $\text{MgCl}_2$ ,  $\text{K}_2\text{CO}_3$ ,  $\text{Mg}(\text{NO}_3)_2$ ,  $\text{NaNO}_2$  and NaCl with respective RVP of 11.3, 22.5, 32.8, 43.2, 52.9, 66.2% and 75.3%. Triplicate samples were weighed ( $\pm 0.0001\text{g}$ ) at intervals during storage for 360 h. After removal from

desiccators, the vials were immediately closed with caps to prevent water transfer with ambient air.

The Brunauer-Emmett-Teller (BET) sorption isotherm model given in Eq. (5) was fitted to the experimental steady state data at 120 h of storage. The experimental sorption data over the  $a_w$  range of 0.11–0.44 were used. The parameters  $m_m$  (BET monolayer water content) and  $C$  (constant) were derived as described by Bell and Labuza (2000).

$$m = \frac{m_m \cdot C \cdot a_w}{(1 - a_w) (1 + (C - 1)a_w)} \quad (\text{Eq.5})$$

The BET  $m_m$  parameters were obtained by plotting  $a_w/(m(1-a_w))$  against  $a_w$  (Roos, 1993). Linear regression analysis of experimental data over the water activity ( $a_w$ ) range from 0.11 to 0.44 was used.

#### 4.3.3 Glass transition temperature

Freeze-dried agar gels were crushed into powder and glass transition temperatures ( $T_g$ ) using a differential scanning calorimeter (DSC, Mettler Toledo 821e with liquid  $N_2$  cooling, Schwerzenbach, Switzerland) were determined. The DSC was calibrated for temperature and heat flow using n-hexane, mercury, water, gallium and indium, as reported by Haque and Roos (2004). An empty aluminium pan was used as a reference. Samples (7-15mg) were transferred into 40  $\mu$ l aluminum pans and equilibrated over saturated salt solutions with various RVP to corresponding water activities,  $a_w$ . The samples in open pans were stored in evacuated desiccators as in the water sorption study for 4-6 days. DSC pans were immediately sealed after removal from the desiccators. Triplicate samples were scanned at 5°C/min from at least 40°C below to well above the glass transition. The anhydrous samples were analyzed using pans with a punctured lid. The samples were transferred to the DSC and initially heated to 120°C to remove the residual water, then cooled to below the  $T_g$  and reheated to well above the  $T_g$  at 5°C/min. All samples were rescanned over the same temperature range to confirm the location of the glass transition in heating and



cooling, and determine possible enthalpic relaxations around the glass transition (Appendix Figure 3). The  $T_g$  values were determined from the second heating scan onset temperature of the endothermic change in heat flow over the glass transition range using a STAR Software (Mettler Toledo, Switzerland; version 8.10).

#### 4.3.4 Dynamic mechanical analysis (DMA)

The thermal mechanical properties of freeze-dried gels were determined with a dynamic mechanical analyzer (Tritec 2000 DMA version 1.43.00 software, Triton Technology Ltd., Loughborough, UK). Freeze-dried gels were crushed into powder and loaded to the DMA sample pocket made from a sheet of stainless steel (Triton Technology Ltd., Loughborough, UK), which did not have any relaxations or phase transitions over the temperature range used. The powders on metal sheets were equilibrated over saturated salt solutions over various RVP to corresponding  $a_w$  for 4-5 days in evacuated desiccators. After removal from the desiccators, the metal sheets were immediately closed by folding along a prescored line and clamped into the DMA instrument. The anhydrous samples were further vacuum dried in a vacuum oven at 55°C for 24 h. Dried powders were then loaded to the material pocket and immediately closed prior to mounting to the DMA.

The single cantilever bending mode was used to determine the storage modulus ( $E'$ ), loss modulus ( $E''$ ) and  $\tan \delta$  ( $E'/E''$ ) as a function of temperature. Freeze-dried materials were cooled to at least 120°C below the  $T_g$  as measured by DSC. The data were collected during dynamic heating at a heating rate of 3°C/min using frequencies of 0.5, 1, 5, 10 and 20 Hz. Samples were heated to at least 50°C above the onset of the  $\alpha$ -relaxation. The samples were analyzed within the temperature range of -150 to 120°C.

The  $\alpha$ -relaxation temperatures ( $T_\alpha$ ) were taken from the peak values of the loss modulus. The relaxation times of the  $\alpha$ -process ( $\tau_\alpha$ ) were derived from data at various frequencies ( $f$ ) using the relationship  $\tau_\alpha = 1/(2\pi f)$  (Noel *et al.*, 2000). The  $\log \tau_\alpha$  was plotted as a function of  $1/(T-T_g)$ . The frequencies of 0.5, 1, 5, 10 and 20

Hz correspond to the  $\log \tau_a$  of -0.4973, -0.7984, -1.4973, -1.7984 and -2.0994 s, respectively.

#### 4.4 $\beta$ -carotene stability during storage

Freeze-dried maltodextrin-agar gels without sugars frozen at  $-20^{\circ}\text{C}$ ,  $-40$  and  $-80^{\circ}\text{C}$  and with sugars frozen at  $-20^{\circ}\text{C}$  and  $-80^{\circ}\text{C}$  were studied for  $\beta$ -carotene stability. The  $\beta$ -carotene content in freeze-dried gels was determined during storage at different RVP conditions. Freeze-dried cubic gels were placed on an open and transparent petri dish and stored in desiccators over various saturated salt solutions at controlled  $a_w$  of the samples. Vacuum was applied to the desiccators for 30 s. The samples were exposed to normal light from the laboratory at the same environment at room temperature ( $24^{\circ}\text{C}$ ).

$\beta$ -carotene was extracted from freeze-dried gels at intervals during storage using a solvent extraction method. Triplicate samples were removed from the desiccators and transferred to 13 mL screw-capped polypropylene test tubes. Sample cubes (approximately 0.2 g each) were rehydrated with 3 mL of deionized water at room temperature for at least 30 min to ensure complete rehydration. The rehydrated samples were crushed with a spatula in the tubes. Methanol and hexane (HPLC grade, Sigma-Aldrich Ireland Ltd, Dublin, Ireland) in the ratio of 1:1 (6 mL) were added to the mixture prior to vortexing for 2 min. Approximately 1 mL of methanol was added after mixing to enhance the separation of the hexane layer. The clear yellow supernatant of  $\beta$ -carotene in hexane was collected using a transfer pipette. The residues were added to 3 mL of hexane and re-extracted again with the same procedure. The collected hexane solution was transferred to an acrylic cuvette and  $\beta$ -carotene content was determined spectrophotometrically.

A spectrophotometer (Varian Cary 300 Bio UV-Visible Spectrophotometer, Varian Inc., Middelburg, The Netherlands) was used to determine from optical density at 450 nm. The  $\beta$ -carotene content was calculated from the standard curve prepared with  $\beta$ -carotene in hexane. The amount of  $\beta$ -carotene was

taken as a mean of triplicate samples. The first-order kinetics model was fitted to data and the degradation rate constants ( $k$ ) were calculated (Appendix Table 1).

#### 4.6 Statistical analysis

The analysis of  $\beta$ -carotene was performed in triplicate from individual solid samples. The degradation of  $\beta$ -carotene during storage was fitted to first-order kinetic model as described above and linear regressions as well as the rate constants for  $\beta$ -carotene loss were calculated. Statistical differences were determined among linear regressions by analysis of covariance (ANCOVA) using the SPSS Statistics 12.0 software for Windows (SPSS Thailand Co., Ltd., Bangkok, Thailand). The statistical analysis indicated the difference among the regression slopes ( $p < 0.01$ ); whereas, insignificant difference of intercept was observed for all systems. The confidence intervals at 95% were reported with the experimental data.

### **5. Structural effects on stability of dispersed $\beta$ -carotene emulsion in freeze-dried maltodextrin systems**

#### 5.1 Pre-emulsion with $\beta$ -carotene

Emulsions with  $\beta$ -carotene were prepared according to Cornacchia and Roos (2011).  $\beta$ -carotene (crystalline Type II, synthetic, 95% HPLC, Sigma, USA) was dissolved in sunflower oil (Pan Euro Foods, EU) at 0.05% (w/w) at 50°C under continuous stirring with a magnetic rod in the dark for at least 2 h to complete dissolving. A solution of Polysorbate 20 (2.4%w/w) (Tween 20, Merck, Germany) in deionized water was prepared and heated to 50°C. Sunflower oil- $\beta$ -carotene solution was pre-emulsified to water-polysorbate solution at 40:60 ratio using a high speed homogenizer (T 25 Digital Ultra-Turrax, Germany) for 30s. The pre-emulsions (40% w/w oil) were subsequently homogenized at 50°C using a two-stage valve homogenizer (APV-1000 high-pressure homogenizer, Denmark) with 3 cycles at 250 bar (approximately 10% of the total pressure was applied for the second stage). The emulsions with  $\beta$ -carotene were cooled to room temperature and mixed with solutions

of respective maltodextrins and maltodextrin-agar systems. The homogenized emulsions had the normal distribution characteristic of the dispersed phase (Appendix Figure 4).

## 5.2 Maltodextrin and maltodextrin-agar gel systems

The gel and liquid systems containing  $\beta$ -carotene particles were prepared by dispersed the  $\beta$ -carotene emulsion into the solution of maltodextrin-agar and maltodextrin mixtures. Agar (microbiology grade, Fluka, Switzerland, Sigma-Aldrich Ireland Ltd, Dublin, Ireland) and various maltodextrins (M40, DE6; M100, DE11; M250, DE25.5; Grain Processing Corporation, Iowa, USA) were premixed, stirred and hydrated in de-ionized water (KB Scientific, Ireland) using a magnetic stirrer at room temperature (24°C) for at least 20 min until further heated to 90°C while stirring and held for 5 min to ensure complete melting of the agar. The  $\beta$ -carotene emulsions (20%w/w of 40:60 oil:water containing 0.02% w/w  $\beta$ -carotene) were poured into the carbohydrate solutions during cooling at 60°C. Consequently, the gel solutions contained 2% (w/w) agar, 18% (w/w) maltodextrins and 8% (w/w) oil contents. After stirring for further 5 min, a homogeneous turbid yellow color of agar solutions was obtained. The gelling solutions were poured into containers and left for gelation at 24°C for at least 1 h. The emulsion systems containing no agar were prepared with the same maltodextrin ratio (18%w/w) in the final liquid systems and procedures for the measurement of the droplet particle size with laser diffraction particle analyzer. The final  $\beta$ -carotene content of the systems was 0.01%, i.e., 0.05% (w/w) in the oil phase.

## 5.3 Freezing and freeze-drying

Samples of maltodextrin systems were prepared by cutting the gels into cubes (10x10x10mm) with a razor blade. The cubic samples were placed on aluminium trays and frozen in still air at -20°C, -40°C or -80°C for 20 h. All samples were subsequently to freezing tempered at -80°C for 3 h prior to rapid loading to freeze-drying carried out using a laboratory freeze-dryer (Steris Lyovac GT2, Germany with Leybold Trivac, Germany vacuum pump) for 48 h. This eliminated



possible ice melting during loading on freeze-drying shelves. The chamber pressure was decreased to  $< 0.1$  mbar corresponding to ice sublimation at  $T < -40^{\circ}\text{C}$ . This condition was maintained throughout the freeze-drying keeping ice temperature below the onset temperatures of ice melting,  $T_m'$ , of any of the materials. The freeze-dryer was operated at ambient room temperature, and at the end of freeze-drying, the vacuum was broken using ambient air. The freeze-dried systems were stored in evacuated desiccators containing  $\text{P}_2\text{O}_5$  for at least 4 days in dark prior to further analysis.

#### 5.4 Emulsion particle size characterization

The emulsion systems were characterized for the particle size distribution and the average particle diameter was measured by using a laser diffraction particle size analyzer (Malvern Master Sizer MSS, Malvern Instruments Ltd., U.K.) as described by Cornacchia and Roos (2011). The refractive index of the emulsion droplets was 1.456, while the refractive index of the dispersion medium was 1.33. The absorbance value of the emulsion droplets was 0.1. Droplet size measurements are reported as particle size distribution and the surface-weighted or Sauter mean diameter,  $d_{3,2}$ . As the storage stability study, the emulsion solids were stored in evacuated desiccators containing  $\text{P}_2\text{O}_5$  as well as saturated salt solutions of  $\text{MgCl}_2$  and  $\text{NaCl}$  (Sigma-Aldrich, St. Louise, MO, U.S.A.) with respective anhydrous condition and RVP of 32.8 and 75.3%. The solids were reconstituted with 3 mL of deionized water at  $24^{\circ}\text{C}$  for 30 min and immediately measured for the droplet size of dispersed lipid particles.

#### 5.5 Differential scanning calorimetry

As the glass transition is a likely event of the hydrophilic phase components only, freeze-dried maltodextrin solids without dispersed oil were crushed into powder and the glass transition temperatures ( $T_g$ ) were measured using a differential scanning calorimeter (DSC, Mettler Toledo 821e with liquid  $\text{N}_2$  cooling, Schwerzenbach, Switzerland). The DSC was calibrated for temperature and heat flow



using n-hexane, mercury, water, gallium and indium, as reported by Haque and Roos (2004). An empty aluminium pan was used as a reference. Samples (7-15mg) were transferred into 40  $\mu$ l aluminum pans (Mettler Toledo, Schwerzenbach, Switzerland) and equilibrated over saturated salt solutions of  $\text{MgCl}_2$  and  $\text{NaCl}$  (Sigma-Aldrich, St. Louise, MO, U.S.A.) with respective RVP of 32.8 and 75.3%. The samples in open pans were stored in evacuated desiccators as in the water sorption study for 4-6 days. DSC pans were immediately sealed after removal from the desiccators. Triplicate samples were scanned at  $5^\circ\text{C}/\text{min}$  from at least  $40^\circ\text{C}$  below to well above the glass transition. All samples were rescanned over the same temperature range to confirm the location of the glass transition in heating and cooling, and to determine possible enthalpic relaxations around the glass transition. The  $T_g$  values were determined from the second heating scan onset temperatures for the endothermic change in heat flow over the glass transition using a STAR Software (Mettler Toledo, Switzerland; version 8.10).

#### 5.6 $\beta$ -carotene extraction and HPLC analysis

Freeze-dried cubic gels (10x10x10 mm) containing dispersed emulsion of  $\beta$ -carotene were placed on an open and transparent petri dish and stored in desiccators in anhydrous and over saturated salt solutions of  $\text{MgCl}_2$  and  $\text{NaCl}$  to controlled the respective 0.33 and 0.75 $a_w$  of the samples. Vacuum was applied to the desiccators for 30 s. The samples were exposed to normal light from the laboratory at the same environment at room temperature ( $24^\circ\text{C}$ ).

$\beta$ -carotene was extracted from freeze-dried gels at intervals using a solvent extraction method. Duplicate samples were removed from the desiccators at intervals and transferred to 13 mL screw-capped polypropylene test tubes. Sample cubes (approximately 0.2 g each) were then rehydrated with 3 mL of deionized water at room temperature for at least 30 min to ensure complete rehydration. The rehydrated samples were crushed with a spatula in the tubes. Methanol and hexane (HPLC grade, Sigma-Aldrich) containing 0.1% of butylated hydroxytoluene ( $\geq 99\%$ , SAFC, USA) were added to the mixture in the ratio of 1:1 (6 mL) prior to mixing with

a vortex for 2 min. The residues were added with 3 mL of hexane and re-extracted with the same procedure. Approximately 2 mL of methanol were further added after mixing to enhance separation of the hexane layer. The clear yellow supernatant of  $\beta$ -carotene in hexane and the corresponding colorless precipitate were obtained. Additional hexane was added to the  $\beta$ -carotene in hexane solutions to adjust the volume and transferred to HPLC vials for the HPLC analysis.

$\beta$ -carotene contents were quantified with a HPLC systems (Dionex ICS3000, Sunnyvale, CA, U.S.A.) connected with a dual pump (DP-1, Dionex, Sunnyvale, CA, U.S.A.), autosampler (AS-1, Dionex, Sunnyvale, CA, U.S.A.) and photodiode-array detector (PDA ICS Series, Dionex, Sunnyvale, CA, U.S.A.). The analytical condition was modified from Liu, Lin and Yang (2009). A reversed-phase Acclaim C30 analytical column (4.6 x 250mm, 5 $\mu$ m) (Dionex, Sunnyvale, CA, U.S.A.) was used for the analysis. A gradient solvent system of MeOH/ACN/H<sub>2</sub>O (84/14/2, v/v/v) (solvent A) and CH<sub>2</sub>Cl<sub>2</sub> (solvent B) was used: a mixture of 80% A and 20%B was used initially, and then the mixing was programmed linearly to 55%B within 5 min and retained from 5 to 12 min. The flow rate was 1.0 mL/min and detection was performed at 450 nm. The amounts of  $\beta$ -carotene were calculated from the standard curve of all-trans  $\beta$ -carotene.

### 5.7 Statistical analysis

The analysis of  $\beta$ -carotene stability was conducted in two separate experiments with duplicate samples for each. The first-order rate constants shown were calculated from each experiment and shown with SD bars of two separate experiments. A one-way analysis of variance (ANOVA) and Duncan's multiple range tests were used to analyze the differences in data at 95% confidence level with SPSS 12.0 software for windows (SPSS Thailand Co., Ltd., Bangkok, Thailand).

## RESULTS AND DISCUSSION

### 1. Effect of water activity on sugar crystallization and $\beta$ -carotene stability of freeze-dried mango powder

The water sorption determines the stability of amorphous materials. The structural transitions such as crystallization of amorphous sugar components are accelerated by the water plasticization which could possibly affect the stability of bioactive ingredients. This part aimed to monitor the crystallization of sugars in freeze-dried mango powder as well as the stability of  $\beta$ -carotene during storage at various  $a_w$ . The humidity of solids and the environment were assumed to be at the equilibrium conditions; therefore, the direct relationship between the relative vapor pressure (RVP) and  $a_w$  was derived as  $a_w = \%RVP/100$ .

#### 1.1 Water sorption of freeze-dried mango powder

To investigate the behavior of water sorption in freeze-dried mango powder, the water content in the samples was monitored for 240 h. Figure 10 A shows the different water sorption behaviors for each RVP value. At 11.3-32.8% RVP, samples normally absorbed water until they had reached a constant weight. At 43.2-68.9% RVP, an unexpected peak of water sorption was observed at 100 h (Figure 10A), which indicated that some water was absorbed and subsequently released from the freeze-dried mango powder. The loss of adsorbed water during storage at such high RVP has also been reported previously for various food powders, such as milk powders (Jouppila and Roos, 1994; Jouppila *et al.*, 1997) and sugar systems, including glucose and sucrose (Makower and Dye, 1956), lactose (Omar and Roos, 2007), and trehalose (Iglesias *et al.*, 1997; Schebor *et al.*, 2010). The aforementioned authors stated that the loss of sorbed water was due to the crystallization of sugars. Sugars in some processed foods such as spray-dried, freeze-dried, and milled products usually present in the amorphous state. All amorphous sugars are hygroscopic and have a strong tendency to absorb the surrounding water. Once relevant amounts of water are absorbed, the  $T_g$  of the powders decreases to well below the storage

temperature and crystallization can occur, resulting in the release of sorbed water (Buera *et al.*, 2005; Hancock and Shamblin, 1998; Makower and Dye, 1956). Freeze-dried mango powder contains high amounts of sugar; thus, the sugar crystallization was hypothesized to cause the loss of sorbed water. This hypothesis was confirmed by SEM micrographs and XRD analysis, as discussed later in section 1.2.

Moreover, the final water content after sugar crystallization depends on the type of sugar crystalline structure and other components. Sugars that form hydrated crystals (trehalose dihydrates and raffinose tri, tetra or penta hydrates) retain higher amounts of water, whereas sugars that form anhydrous crystals (sucrose and lactose) release all water once crystallization is achieved (Buera *et al.*, 2005; Makower and Dye, 1956). Although sucrose, which forms anhydrous crystals, is the predominate sugar in mango, the results showed that the water was released to a certain level and some sorbed water was found to be present in the samples subsequent to the release of water. Mangoes contain high amounts of polysaccharide, including pectic substances and organic acids (Nararin *et al.*, 1998). The result could have been due to the adsorption of water by such uncrystallized components resulting in a slight increase in the water content during storage time. Sample stored at 80.9% RVP revealed no peak in water loss, which suggested that at such a high RVP, the increased amounts of surrounding water dissolve the formed sugar crystals resulting in increased water uptake.

The water contents of samples stored at all RVP were constant after 200 h of storage. Pseudo equilibrium conditions were considered at 250 h and the pseudo equilibrium water content of freeze-dried mango powder was plotted as a function of  $a_w$  (Figure 10B). A Guggenheim-Anderson-DeBoer (GAB) model was applied to predict the sorption isotherms of mango powder, as it has been shown to adequately represent experimental data in a range of  $a_w$  between 0 and 0.95, which is the range of most interest in food studies (Labuza and Altunakar, 2007; Timmermann *et al.*, 2001). As stated earlier, the crystallization causes the release of sorbed water; thus, the observed equilibrium water content was collected after crystallization. This gave a lower degree of accuracy in the prediction of the sorption isotherms. Therefore, only

the equilibrium water content at RVP less than or equal to 32.8% was used to model the GAB isotherms.

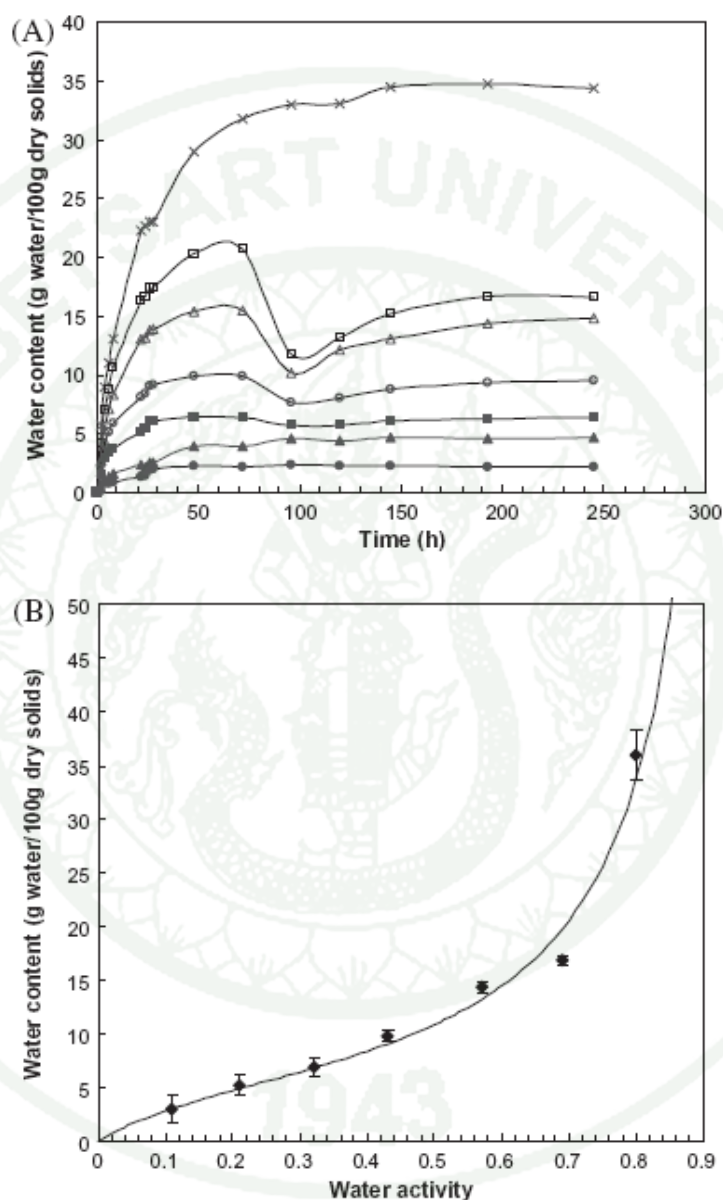


**Figure 10** Water content (A) and water sorption isotherms (mean  $\pm$  standard deviation bars;  $n = 3$ ) (B) of freeze-dried mango powder at various RVP levels at 25°C. Data corresponded to the water content after sugar crystallization. (◆ 11.3% RVP, ▲ 22.5% RVP, ■ 32.8% RVP, ◇ 43.2% RVP, △ 57.6% RVP, □ 68.9% RVP, X 80.9% RVP)



Although crystallization of sugar results in a loss of adsorbed water, the sorption isotherm did not clearly indicate such a loss of water, which is typical for pure amorphous sugars (Omar and Roos, 2006; Roos, 1993a). Only the sample stored at 68.9% RVP revealed a shift below the predicted values (Figure 10B). These results reflect that the lack of discontinuities in the water sorption isotherms is not indicative of the absence of crystallinity.

## 1.2 Determination of sugar crystallization

Confirmation of the phenomenon of sugar crystallization caused by the water loss in freeze-dried mango powder during storage was attempted by means of SEM and XRD analysis.

### 1.2.1 X-ray powder diffraction

Due to the fact that the amorphous materials show no X-ray patterns that are typical of crystalline materials (Roos, 1995); the XRD patterns for dehydrated mango powders were measured for crystallization of sugar (Figure 11). The XRD patterns clearly revealed a sharp peak in the samples stored at 57.6% and 68.9% RVP and thus, disclosed the crystalline morphologies in the samples. As expected, the sample taken prior to storage showed amorphous characteristics and no crystalline peak was observed. This indicated that freeze drying resulted in amorphous mango powder. This finding coincided with Haque and Roos (2005), who found that freeze drying results in amorphous lactose powder. After storage for 7 d at 11.3% RVP, the mango powder still showed amorphous characteristics. This meant that there was no change in the physico-chemical properties of the freeze-dried mango powder under such storage conditions. At such an RVP value for storage, samples are in a glassy state and some phenomena, such as sugar crystallization, are not expected to occur. Samples stored at 43.2% RVP are expected to show crystalline characteristics; however, no crystalline peaks as 57.6% or 68.9% RVP were observed. This possibly due to the amount of formed crystals in the sample at 43.2% RVP was not sufficient for detection by XRD analysis. Moreover, the intensity of 68.9% RVP samples was

determined to be substantially elevated in comparison to the 57.6% RVP samples. Haque and Roos (2005) and Jouppila *et al.* (1997) elaborated on the intensity of the XRD pattern as an indication of crystal formation in their samples. These authors also stated that the intensity values depend on the storage RVP. Thus, in the present study, the intensity indicated that the amount of crystal formation during storage at 68.9% RVP is higher.

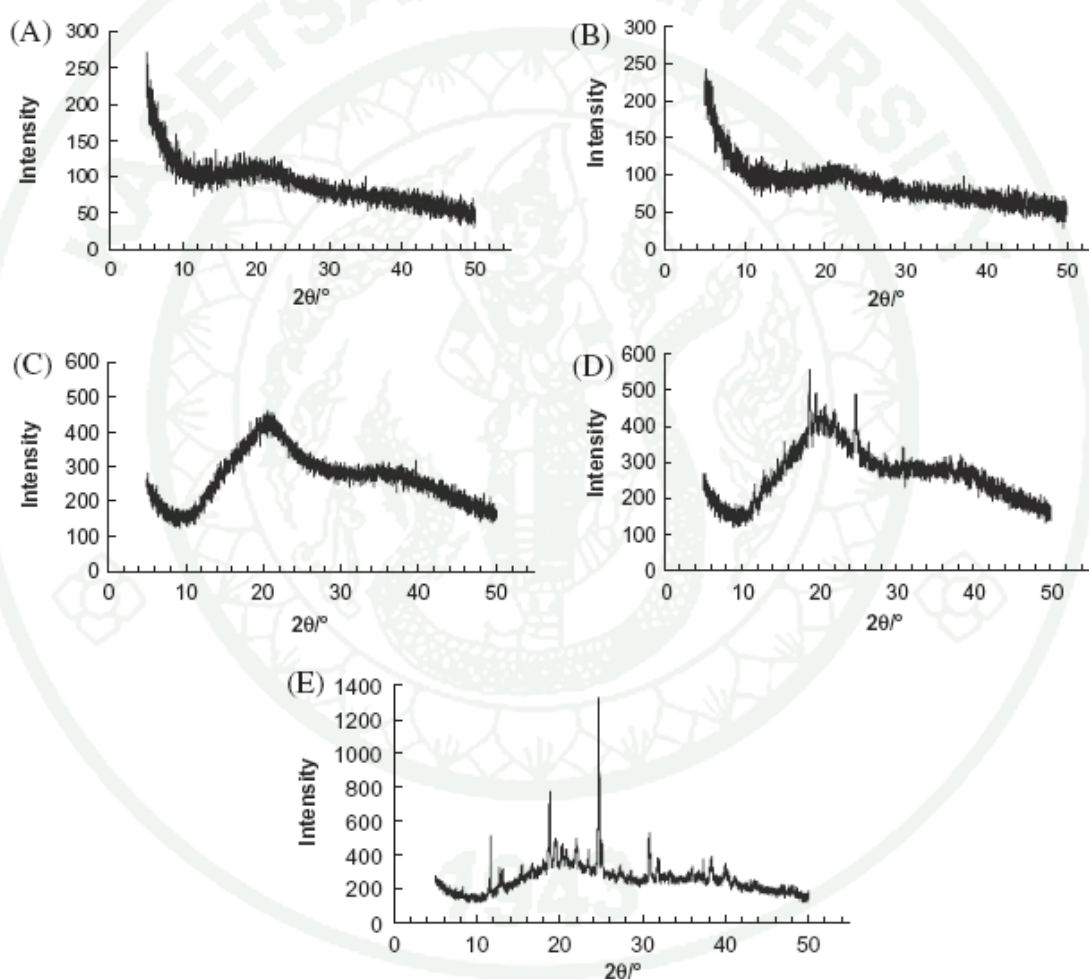


**Figure 11** X-ray diffraction pattern of freeze-dried mango powder: uncrystallized (A), stored at 11.3% RVP (B), 43.2% RVP (C), 57.6% RVP (D), and 68.9% RVP (E) for 7 d at 25°C.

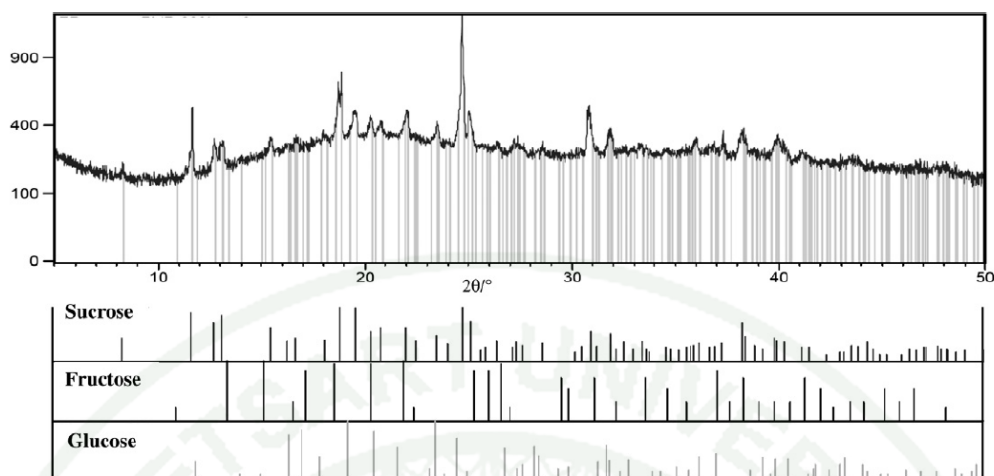


**Figure 12** X-ray diffraction pattern of freeze-dried mango powder stored at 68.9% RVP for 7 d at 25°C compared to XRD standard peaks of sucrose, fructose, and glucose.

The XRD patterns of the sample at 68.9% RVP were compared to sugar present in mangoes (glucose, fructose and sucrose), and subsequently corresponded to the crystalline peak of the standard sucrose (Figure 12). This indicated that most of the crystalline regions in freeze-dried mango powder consist of sucrose crystals, which is the predominate sugar in mango. Moreover, the XRD patterns revealed a curve at 10–30°, which indicated the presence of some amorphous regions in the samples which failed to crystallize, such as soluble pectin.

### 1.2.2 Scanning electron microscopy (SEM)

Figure 13 compares the micro-surface of freeze-dried mango powder both prior and subsequent to storage at different RVP values for 7 d. The mango powder samples segregated prior to storage (Figure 13 A) revealed surfaces that were as smooth as those samples which were stored at 11.3% RVP. Again, samples stored at RVP 43.2% showed very few coarse particles, whereas rough surfaces were clearly detected on the samples stored at 57.6% and 68.9% RVP. This is an indication of the occurrence of physico-chemical changes in freeze-dried mango powder, particularly sugar crystallization. All SEM results were in agreement with the

XRD analysis. In conclusion, the coarse particles formed on the surface of the mango powder were sugar crystals.

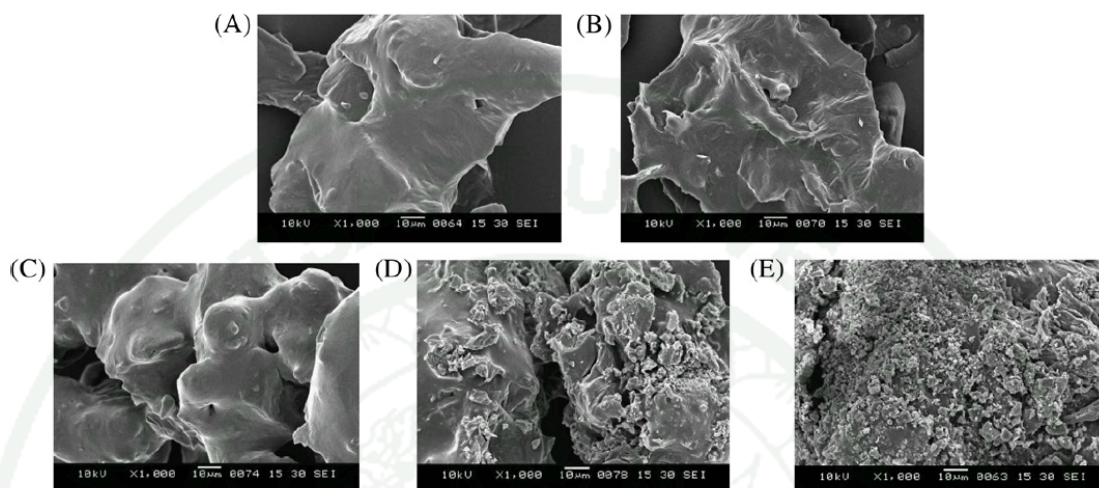


**Figure 13** SEM images of freeze-dried mango powder: (A) uncrystallized, stored at (B) 11.3% RVP, (C) 43.2% RVP, (D) 57.6% RVP and (E) 68.9% RVP for 7 d at 25°C.

### 1.3 Degradation of $\beta$ -carotene during storage

The  $\beta$ -carotene content in freeze-dried mangoes decreases over time during storage. To compare the degradation of  $\beta$ -carotene among different storage RVP values, the rate constants were plotted as a function of water activity (Figure 14). As the humidity of solids and the environment were assumed to be at the equilibrium conditions, the  $a_w$  values were calculated from  $a_w = \%RVP/100$ . Freeze-dried mango powder was in glassy state while stored at 11.3% RVP (Appendix Figure 5), whereas it was plasticized by water and subsequently rendered into a rubbery state while stored above an RVP of 11.3%. The decrease in the rate constant was found at higher levels of storage RVP of up to 43.2%, which coincided with the transition into the rubbery state. This was in agreement with Prado *et al.* (2006), who observed a decrease in the rate constant of  $\beta$ -carotene degradation in the encapsulated freeze-dried polymeric matrix when stored at higher RVP levels. In the glassy state, the rate



constant of  $\beta$ -carotene degradation was determined to be higher than that in the rubbery state. These authors pointed out that the reduction in the rate constant is due to the structural collapse of the samples (Prado *et al.*, 2006). Bell and White (2000) also observed a reduction in the rate constant of thiamin degradation when samples are rendered into a rubbery state. They stated that it can be attributed to the collapse of the matrix (Bell and White, 2000). Selim *et al.* (2000) also observed a lower degradation rate of saffron carotenoids encapsulated in polymeric matrices where they were fully plasticized and collapsed. In addition, Serris and Billiaderis (2001) found similar results in encapsulated beetroot pigment.

In the present study, the collapse (sticky aspect) of mango powder was also observed at storage values for RVP greater than or equal to 22.5%. The possible reason for the lower  $\beta$ -carotene degradation was that the collapse is responsible for the decrease in the micropores of samples, at which oxygen can enter or move into the matrices. The oxygen diffusion into food matrices is thus hindered and with the absence of oxygen,  $\beta$ -carotene is stable. Several studies indicated that in the glassy state, the high porosity of matrices allows oxygen diffusion and therefore,  $\beta$ -carotene degradation occurs quickly. In addition to the structural collapse, water sorption on the matrix alters its oxygen barrier properties (Prado *et al.*, 2006; Selim *et al.*, 2000; Serris and Biliaderis, 2001).

Collapse phenomena in food can be found during processing and storage and are directly related to the respective  $T_g$ . Collapse results in the loss of some desirable qualities (Bhandari and Howes, 1999), such as the rehydration capacity and product appearance. However, some previous studies showed that the collapse of food matrices can reduce the rate constant of some reactions, such as reactant loss via the Maillard reaction (White and Bell, 1999), tyrosinase loss (Chen *et al.*, 1999), and a decrease in the rate of non-enzymatic browning in food (Acevedo *et al.*, 2006). These suggest that collapse has benefits in the retardation of some undesirable reactions and the degradation of some bioactive compounds.



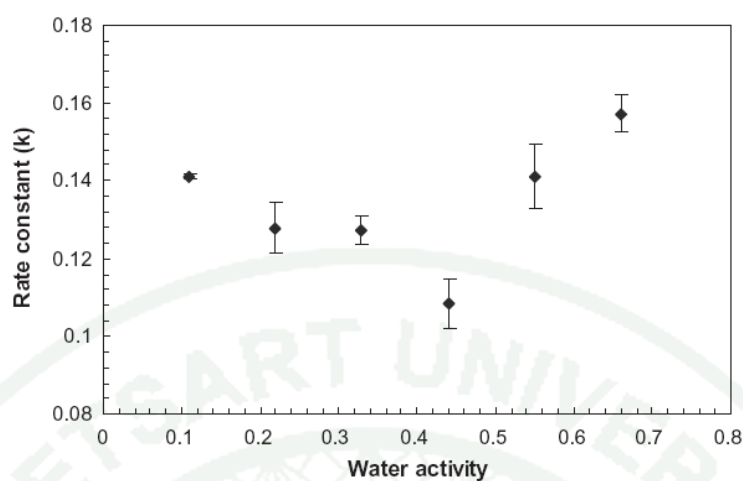


**Figure 14** First-order rate constant of  $\beta$ -carotene degradation at various  $a_w$ , at 25°C (Mean  $\pm$  standard deviation;  $n=2$ ). The humidity of the mango powders and the environment were assumed to be at the equilibrium conditions; therefore, the direct relationship between the relative vapor pressure (RVP) and  $a_w$  was derived from  $a_w = \%RVP/100$ .

The rate constant was found to increase sharply beyond the attainment of the minimum point at (43.2% RVP), with the highest rate constant being determined at 68.9% RVP. These findings diverge from the previous studies in a model system, mentioned earlier. This shows the disparities between the investigation of food and model systems. However, similar degradation behavior was previously established in freeze-dried carrots by Lavelli *et al.* (2007), who observed a U-shape curve subsequent to plotting the rate constant for  $\beta$ -carotene against  $a_w$  and furthermore, they stated this to be typical of most oxidative reactions, as similarly elaborated on by Labuza (1971). These findings suggested that  $\beta$ -carotene degradation in freeze-dried mango powder occurs due to the oxidation process. Sablani *et al.* (2007) further observed an increased rate constant for the loss of vitamin C in fortified formula powder stored at  $a_w$  values in the range 0.431–0.877. Such behavior was explained by an increase in the water content in dry matrices that potentially augments the rate of oxidation by an enhancement of the mobility of reactants. However, the water can slow down the oxidation process by hydration, or the dilution of heavy metal catalysts or their precipitation as hydroxides. Water also has the potential to counteract

peroxide decomposition by the formation of hydrogen bonds with hydroperoxide, and thus, encourages a radical recombination, which potentially interrupts the oxidation reaction chain (Lavelli *et al.*, 2007). This causes a minimum degradation at 43.2% RVP, whereas above this RVP, the rate constant increases sharply again. Mango also contains oxidative enzymes which accelerate the degradation of  $\beta$ -carotene, such as polyphenol oxidase, and peroxidase (Narain *et al.*, 1998). Alternatively, from the perspective of  $T_g$ , several enzymatic reactions were considered as diffusion-controlled in dried foods. As the water plasticization increases the molecular diffusion in food, it thus promotes the enzymatic activity (Champion *et al.*, 2000). Consequently, the degradation of  $\beta$ -carotene was promoted at 57.6% and 68.9% RVP.

Moreover, the pronounced increase in the rate constant of  $\beta$ -carotene at 57.6% and 68.9% RVP was coincident with the pronounced occurrence of sugar crystallization in samples. In a model system, previous authors indicated that the matrix crystallization results in the loss of some encapsulated bioactive compounds. The exclusion of these compounds from the crystalline matrices makes them more susceptible to oxygen exposure and consequent degradation (Buera *et al.*, 2005; Elizalde *et al.*, 2002; Shimada *et al.*, 1991b). Elizalde *et al.* (2002) reported higher retention of  $\beta$ -carotene (about 80% in 6 month) in the non-crystallized trehalose/gelatin matrices, while for crystallized samples exposed to water activity of 0.75, the loss was almost complete. However, the effect of sugar crystallization on  $\beta$ -carotene stability has not been proven in real food systems. Moreover, the structure of the plant is more complex. The cellular structure and protein complexes in nature provide a certain degree of  $\beta$ -carotene stability (De Oliveira-Alves *et al.*, 2010). Thus, the exclusion of  $\beta$ -carotene from matrices is not expected to be the cause of  $\beta$ -carotene loss as in a model system. Based on the present study, it is hypothesized that the crystallization of sugar enhances  $\beta$ -carotene loss by affecting the plant cell integrity. Sugars potentially move towards outer mango cell to form crystals which increased leakage of the cell and the consequent promotion of the  $\beta$ -carotene to oxygen exposure. These findings also suggest that the collapse of samples at high RVP levels does not show any protective effect on  $\beta$ -carotene retention, as appeared in low RVP systems.

The results of this part confirmed the hypothesis that the crystallization of sugar components resulted in the water loss of freeze-dried mango powder as confirmed by the XRD and SEM analysis. As the environmental humidity increased above  $T_g$ , the sugar crystallization as well as the collapse of powder was accelerated. The  $a_w$  at which  $\geq 0.4$  caused the sugar crystallization which was coincident with the increased  $\beta$ -carotene degradation rate in freeze-dried mangoes.

## **2. Influence of collapsed structure on stability of $\beta$ -carotene in freeze-dried mangoes**

This part aimed to modify the structures of freeze-dried mangoes to enhance the stabilization of  $\beta$ -carotene during storage. The previous part indicated the structural changes including sugar crystallization and matrix collapse when stored above  $T_g$ ; in this part, therefore, the stability test of  $\beta$ -carotene in freeze-dried mangos were monitored during storage at and below  $T_g$  to prevent any possible structural changes. In addition, the agar gels which form a semi solids mimics the fruit-like structures were conducted to determine the effect of freeze-drying protocols on the structure formation of freeze-dried materials. The freeze-drying protocols were modified and the various freeze-dried mango and agar gel structures were reported.

### **2.1 Thermal transition of mangoes**

Mango juice samples showed two endothermic transitions prior to ice melting peak during the DSC scan (Appendix Figure 6) which were typical of sugar-containing materials (Rahman, 2004). In the literature, the two transitions were interpreted in various ways; however, the lower transition ( $T_g'$ ) was the glass transition of the freeze-concentrated solids phase;  $T_g'$  was obtained after annealing to obtain maximum freeze-concentration of solids. The second, higher temperature transition ( $T_m'$ ), showed the onset of ice melting.

Mangoes contain high amount of small molecular weight sugars that are sucrose, glucose, and fructose which gave the low  $T_g'$  and  $T_m'$  of - 53.3 and -38.0°C,

respectively. Conversely, agar consists of high molecular weight carbohydrate, and therefore has a high  $T_g'$  ( $-11.3^\circ\text{C}$ ). These thermal transitions, particularly the  $T_m'$  that controls ice melting, directly affect the freeze-dried product structure.

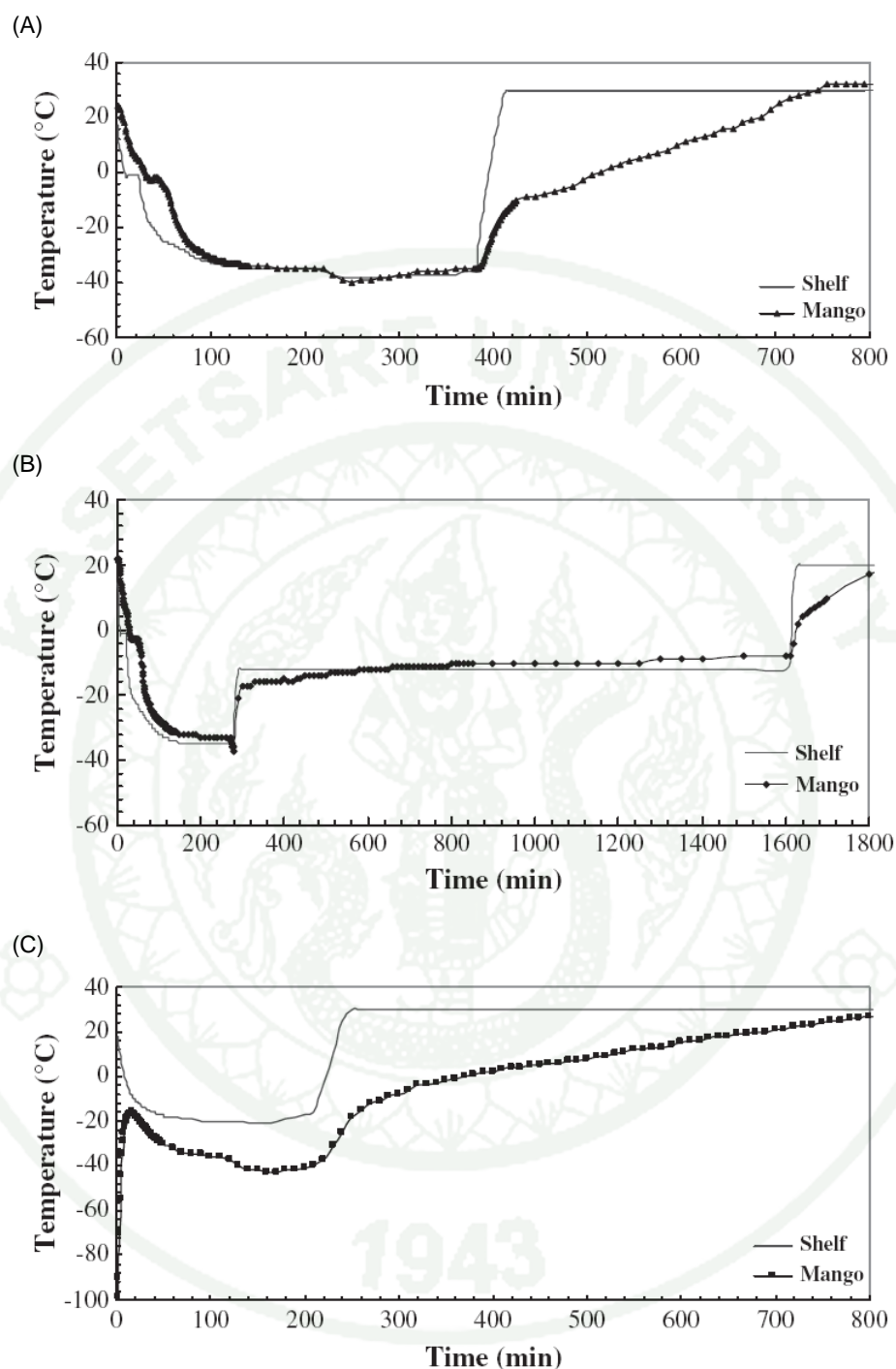
## 2.2 Influence of freeze-drying protocols on freeze-dried mango structure

Table 2 shows the freeze-drying protocols and obtained freeze-dried solid structures. The collapsed structure was observed in freeze-dried mangoes when frozen at  $-35^\circ\text{C}$  and freeze-dried at the shelf temperature of  $-15^\circ\text{C}$  (protocol 2) and when frozen with liquid nitrogen and freeze-dried using the shelf temperature of  $-40^\circ\text{C}$  (protocol 3); freezing at  $-35^\circ\text{C}$  followed by freeze-drying at the shelf temperature of  $-40^\circ\text{C}$  (protocol 1) gave a non-collapsed structure.

**Table 2** Freeze-drying protocols and obtained freeze-dried mango and agar gel (2% and 4% w/w) structures. The secondary drying temperature applied for all protocols was  $30^\circ\text{C}$ .

Freeze drying protocol	Freezing method	Freeze-dried shelf temperature <sup>1</sup>	Freeze-dried matrix structures		
			Mangoes	Agar gel 2%w/w	Agar gel 4% w/w
1	$-35^\circ\text{C}$	$-40^\circ\text{C}$	Non-collapse	Non-collapse	Non-collapse
2	$-35^\circ\text{C}$	$-15^\circ\text{C}$	Collapse	Non-collapse	Non-collapse
3	Liquid nitrogen (liq.N <sub>2</sub> )	$-40^\circ\text{C}$	Collapse with cracking	Collapse with cracking	Non-collapse with cracking

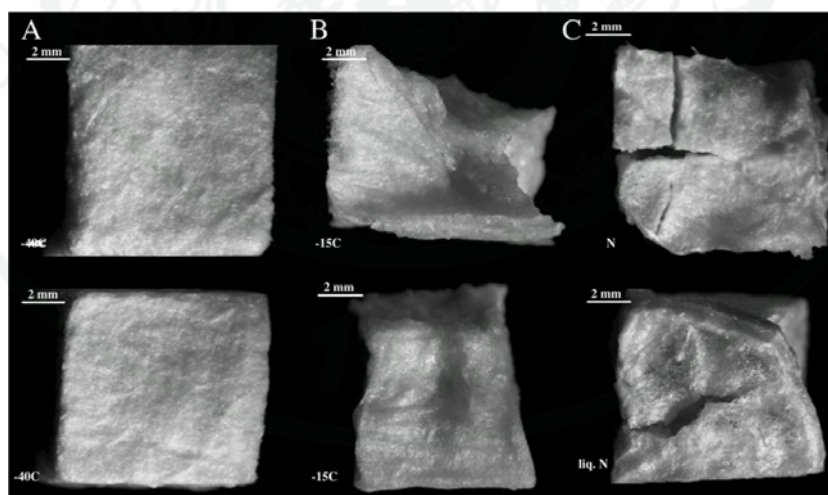
<sup>1</sup>Freeze-dried shelf temperature during primary drying



**Figure 15** Freeze-drying temperature profile of mangoes with the application of  
 (A) protocol 1: freezing at -35°C and shelf temperature of -40°C,  
 (B) protocol 2: freezing at -35°C and shelf temperature of -15°C and  
 (C) protocol 3: freezing by immersion in liquid nitrogen and shelf temperature of -40°C.

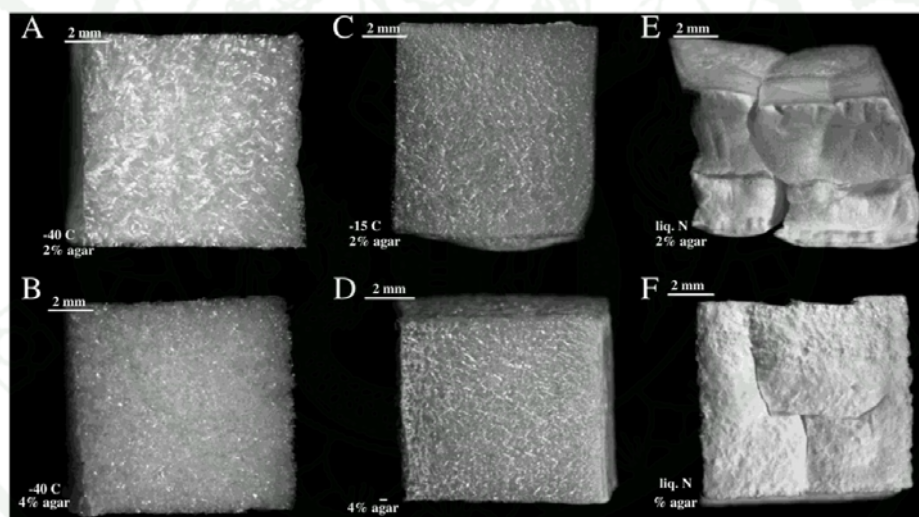


Figure 15 shows the freeze-drying temperature profile of mango samples. Mangoes freeze-dried by the application of protocol 1 underwent the freezing stages at temperatures higher than  $T_g'$  ( $-53.3^\circ\text{C}$ ) but drying at a temperature lower than  $T_m'$  ( $-38.0^\circ\text{C}$ ) (Figure 15A). This observation was coincident with the non-collapsed structures of freeze-dried mangoes (shelf temperature  $-40^\circ\text{C}$ ). The loss of product structure or collapse during freeze drying typically occurs when the temperature of the subliming interface is maintained above the “collapse temperature” (Bellows and King, 1972) which is related to the  $T_m'$ . Sacha and Nail (2009), with the aid of a freeze-dry microscope, observed that the onset of structural collapse in frozen sugar solution associated with the higher transition temperature or  $T_m'$ . The result shows that the sample temperature exceeded the  $T_g'$ ; however, it was below that of  $T_m'$ , thus no structural collapse occurred. Moreover, the strength of mango cell walls and polymers also supported the physical structure in food tissues (Roos, 1995). The external structures of the samples are shown in Figure 16 A. The application of freeze-drying protocol 1 was proven successfully for the retention of the tissue structures of the mango samples.



**Figure 16** Stereomicrographs of freeze-dried mangoes using freeze-drying (A) protocol 1: freezing at  $-35^\circ\text{C}$  and shelf temperature of  $-40^\circ\text{C}$ , (B) protocol 2: freezing at  $-35^\circ\text{C}$  and shelf temperature of  $-15^\circ\text{C}$  and (C) protocol 3: freezing by immersion in liquid nitrogen and shelf temperature of  $-40^\circ\text{C}$  at a magnification of 10x.

The freeze-drying protocol 2 resulted in collapsed structures (Figure 16B), which was due to the melting of the ice during freeze-drying. The ice formed in the samples during the freezing stage at  $-35^{\circ}\text{C}$ . Freeze-drying was controlled by the shelf temperature of  $-15^{\circ}\text{C}$ , which was above the  $T_m'$ . The ice consequently melted, and the samples were dried by evaporation from a partially freeze-concentrated state rather than by sublimation which resulted in the loss of structure (Bellows and King, 1972). In addition, food matrices are plasticized by unfrozen water, thus the viscosity of the freeze concentrated matrix was decreased. This was responsible for the acceleration of the collapse during freeze-drying (Karathanos *et al.*, 1996). In addition, the result showed that the duration of the drying stage of the freeze-drying protocol 2 exceeded that of protocol 1.



**Figure 17** Stereomicrographs of freeze-dried agar gel surface with the application of freeze-drying protocol 1: freezing at  $-35^{\circ}\text{C}$  and shelf temperature of  $-40^{\circ}\text{C}$  of (A) 2%w/w, (B) 4%w/w, protocol 2: freezing at  $-35^{\circ}\text{C}$  and shelf temperature of  $-15^{\circ}\text{C}$  of (C) 2%w/w, (D) 4%w/w and protocol 3: freezing by immersion in liquid nitrogen and shelf temperature of  $-40^{\circ}\text{C}$  of (E) 2%w/w, (F) 4%w/w at a magnification of 10x.

Mangoes frozen by liquid nitrogen prior to freeze drying at the shelf temperature of  $-40^{\circ}\text{C}$  (protocol 3) resulted in collapsed structures, although the freeze-drying temperature of protocol 1 and 3 were identical ( $-40^{\circ}\text{C}$ ). This was an evident indication of the negative effects of liquid nitrogen freezing on the structural consistency of mangoes. The result showed that after freezing in liquid nitrogen, the sample temperature increased during the freezing stage in the freeze dryer to exceed  $T_g'$ . Freezing in liquid nitrogen produced small ice crystals and fine porosity after initial stages of the freeze-drying. This presumably increased resistance for vapor removal and a higher sublimation temperature at the sublimation interface. In addition, the liquid nitrogen freezing resulted in formation of a crust at the mango surface, which further prevented the mass transfer during sublimation. Furthermore, the cracking on surface was observed in samples which were frozen in liquid nitrogen (Figure 16C). When the internal portion of the water underwent phase transition, it caused an internal stress as a result of expansion to the surface and once the resistance of the mango was overcome, cracking of the mango surface occurred (Hung, 1997). Chassagne-Berces *et al.* (2009) also observed the cracking of apple tissue frozen by immersion in liquid nitrogen. This indicated that a too fast freezing rate provoked breakage of food surfaces.

The effect of freeze drying protocols on freeze-dried food structures were also investigated in agar gel. Agar gels (2% and 4% w/w) were freeze dried using the identical freeze-drying protocols applied to mangoes. The obtained structures are shown in Figure 17. The freeze drying protocol 1 resulted in non-collapsed structures at both gel concentrations, which was in agreement with the finding in mangoes. As expected, protocol 2 also rendered non-collapsed structures because the  $T_g'$  of agar is  $-11.3^{\circ}\text{C}$  which was above the freeze-dried process temperature (shelf temperature  $-15^{\circ}\text{C}$ ). During drying, agar gels were in the glassy state at which the viscosity of the solids is high enough to support its own weight. In addition, the solid concentration of agar as low as 2%w/w shows no structural collapse by freeze-drying at  $-15^{\circ}\text{C}$ . In contrast, liquid nitrogen freezing resulted in a structural collapse of the 2%w/w freeze-dried agar gel. However, for 4%w/w samples, no structural collapse occurred. This indicated that the increasing solid contents of agar potentially prevented

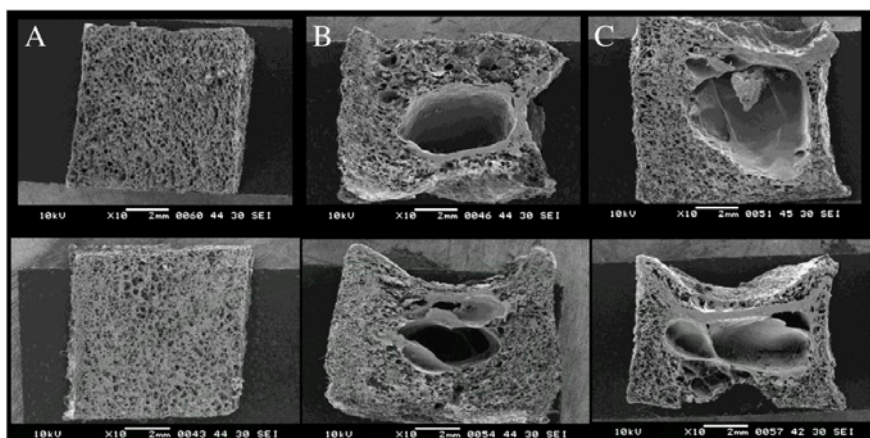
structural collapse by the exposure to liquid nitrogen. However, cracking on freeze-dried agar surface was observed at both gel concentrations. Moreover, stereomicrographs showed the crust on surface of freeze-dried agar samples frozen by means of liquid nitrogen which differed from other freeze-drying protocols (Figure 17C). The results suggest that an increase in the solid content of agar gels can prevent structural collapse, although the cracking of surface still occurs in agar frozen with liquid nitrogen. In summary, agar underwent the freeze drying (all protocols) at lower process temperatures than  $T_g'$ , the high viscosity in the glassy state helped to prevent any structural changes. Mangoes and agar samples frozen by means of liquid nitrogen caused the crust formation due to a rapid freezing and the cracking of samples.

Figure 18 shows the SEM micrographs of the internal structure of the freeze-dried mangoes. The protocol 1 rendered non-collapsed samples with porous internal structures as shown in Figure 18A. The collapse structure caused by the application of protocols 2 and 3 revealed large gaps and dense dry layer structures because the sublimation could not be achieved; the internal water vapor pressure caused melting and water was instead removed by evaporation. This unfrozen water plasticized the dry layer formed at the beginning of drying and the internal pressure contributed to formation of a large hollow inside the structure (Figure 18B). Jaya and Durance (2009) showed the internal structure of dried hydrocolloid gels using different drying methods. The freeze drying showed the continuous matrix of dried hydrocolloid gel whereas the vacuum-dried gel gave one big hollow in the centre of the dried gel (Jaya and Durance, 2009). This was in agreement with the formation of large hollows in freeze-dried mangoes using protocol 2 and 3.

### 2.3 Stability of $\beta$ -carotene in freeze-dried mangoes

HPLC analysis showed that the amount of  $\beta$ -carotene in mango samples amounted to 3,708  $\mu\text{g}/100\text{g}$  dried weight which was in agreement with Vásquez-Caicedo *et al.* (2005) who reported that mangoes (cultivar 'Nam Dok Mai') contained 1,658 -11,249  $\mu\text{g}$   $\beta$ -carotene /100g dried weight; however such contents fluctuate with the ripeness of the fruit.





**Figure 18** SEM images of cross-sectioned freeze-dried mangoes using freeze-drying (A) protocol 1: freezing at  $-35^{\circ}\text{C}$  and shelf temperature of  $-40^{\circ}\text{C}$ , (B) protocol 2: freezing at  $-35^{\circ}\text{C}$  and shelf temperature of  $-15^{\circ}\text{C}$  and (C) protocol 3: freezing by immersion in liquid nitrogen and shelf temperature of  $-40^{\circ}\text{C}$  at a magnification of 10x.

Freeze-dried mangoes which were exposed to the three diverse freeze-drying protocols were kept at 11% and 22% RVP to determine  $\beta$ -carotene stability over time (Figure 19). Generally, storage at high RVP led to various changes in dried foods such as structural collapse and sugar crystallization. To exclude these effects, inclusive structural transformations, the storage RVP was selected in accordance to the previous work which showed that freeze-dried mangoes stored at  $25^{\circ}\text{C}$  at 11% RVP were in the glassy state, whereas they become rubbery at 22% RVP (Harnkarnsujarit and Charoenrein, 2011a). However, no structural change including collapse was observed, thus both RVP were selected for monitoring the stability of  $\beta$ -carotene in freeze-dried mangoes during storage.



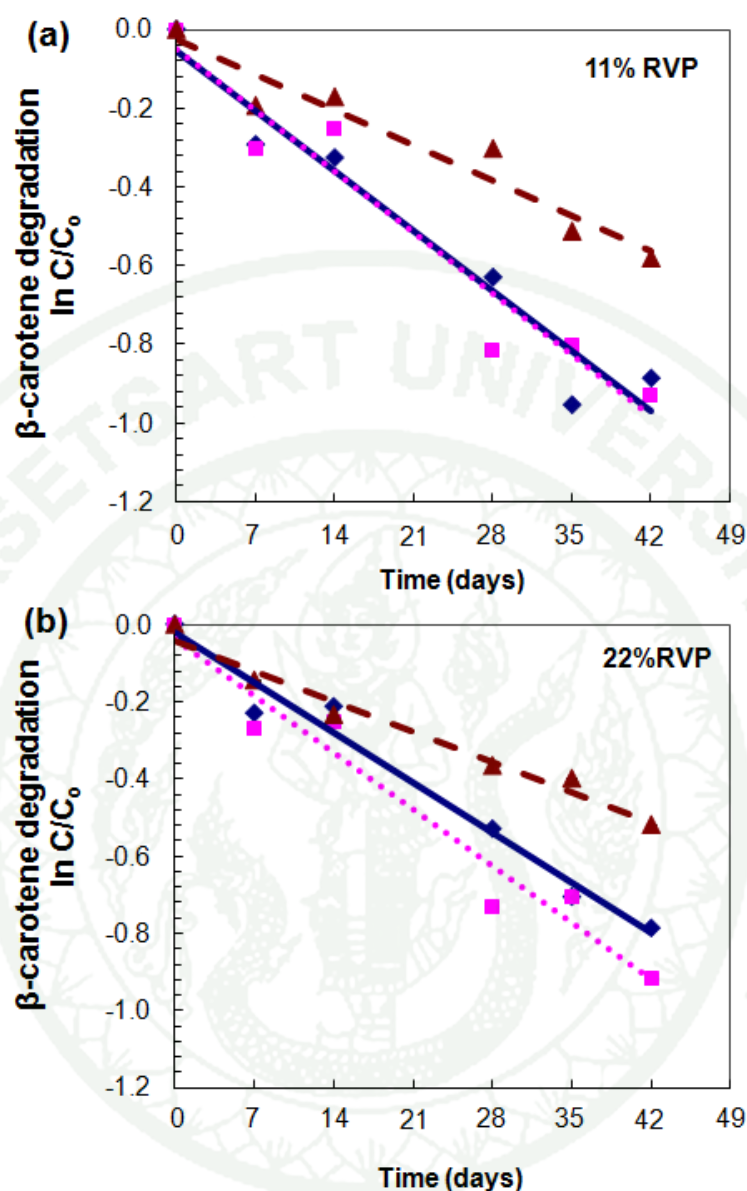


**Figure 19** Degradation of  $\beta$ -carotene in freeze-dried mangoes underwent various freeze-drying protocols during storage at (a) 11% and (b) 22% RVP.

- ◆ protocol 1: freezing at  $-35^{\circ}\text{C}$  and shelf temperature of  $-40^{\circ}\text{C}$ ,
- ▲ protocol 2: freezing at  $-35^{\circ}\text{C}$  and shelf temperature of  $-15^{\circ}\text{C}$  and
- protocol 3: freezing by immersion in liquid nitrogen and shelf temperature of  $-40^{\circ}\text{C}$ .

$\beta$ -carotene is naturally unstable in the presence of oxygen and light. After six weeks of storage,  $\beta$ -carotene in samples freeze-dried by the application of protocols 1, 2, and 3 decreased approximately 56.6-56.8%, 42.2-42.8%, and 57.9-59.4% respectively for both RVP. The degradation rate at both RVP was similar.  $\beta$ -carotene degradation followed first order kinetics which was in agreement with previous studies in both food and model systems such as carrots (Lavelli *et al.*, 2007), and a trehalose matrix (Elizalde *et al.*, 2002; Prado *et al.*, 2006).

Rate constants of  $\beta$ -carotene degradation at both storage RVP are shown in Table 3. Increased rate constants indicated higher degradation rates. The results showed that the freeze-drying protocol 1 and 3 rendered similar degradation rates. In contrast, protocol 2 decreased  $\beta$ -carotene degradation rate significantly ( $p < 0.05$ ), which attributed to the collapsed structure of the freeze-dried mangoes. Structural collapse gave a dense internal matrix (Figure 18B) and that has been found to increase the stability of  $\beta$ -carotene and other carotenoids in model systems. Prado *et al.* (2006) observed that storage RVP at which structural collapse was found increased the stability of encapsulated  $\beta$ -carotene in freeze-dried polyvinylpyrrolidone. Selim *et al.* (2000) also suggested that matrix collapse could decrease the degradation of saffron carotenoids. Similarly, Serris and Biliaderis (2001) observed the lower degradation kinetics of water-soluble beetroot pigments in a collapsed matrix. Collapse of freeze-dried materials is associated with the loss of micropores and cavities through which oxygen can diffuse, so collapse of freeze-dried materials builds a barrier against oxygen penetration (Selim *et al.*, 2000).  $\beta$ -carotene is naturally more stable in the absence of oxygen. Contrarily, the higher rate constant in samples freeze-dried with protocol 1 is explained by the high porosity (Figure 18A) which allowed a higher rate of oxygen diffusion (Prado *et al.*, 2006). Surprisingly, structural collapse induced by liquid nitrogen renders no protection from the degenerative effects on  $\beta$ -carotene. It is hypothesized that the cracking of sample surface can have a potential to increase the oxygen exposure through food matrix, which results in the rapid  $\beta$ -carotene degradation.

**Table 3** Rate constant of  $\beta$ -carotene degradation in freeze-dried mangoes stored at 11% and 22% RVP.

Freeze-drying protocol	Rate constant ( $\text{day}^{-1}$ )	
	11% RVP	22% RVP
1	$0.0210 \pm 0.0011\text{a}$	$0.0199 \pm 0.0020\text{a}$
2	$0.0130 \pm 0.0002\text{b}$	$0.0217 \pm 0.0010\text{b}$
3	$0.0203 \pm 0.0027\text{a}$	$0.0119 \pm 0.0010\text{a}$

Values with the different superscripts within the same column are significantly different ( $p \leq 0.05$ ).

The results of this part confirmed the hypothesis that the structural collapse resulted in the loss of matrix micropores which effectively enhanced stability of  $\beta$ -carotene in freeze-dried mangoes. However, the cracking on the surface of the collapsed systems could not provide the stabilizing effects on  $\beta$ -carotene.

### 3. Microstructure formation of maltodextrin and sugar matrices in freeze-dried systems

The previous part indicated that the stability of  $\beta$ -carotene in freeze-dried mangoes was influenced by the matrix microstructures. Therefore the deep understanding of component effects on microstructure formation of freeze-dried solids is required to develop the structure modification of freeze-dried materials. As fruits contain high amount of sugars (glucose, fructose and sucrose) and polymeric substances, these components as well as the freezing properties were determined for the influence on microstructure formation and the mechanical properties of freeze-dried solids. As agar is a polysaccharide which potentially forms a semi-solid gel and served a fruit-like structure, it exists in the carbohydrate formulation as the gelling agent forming the fruit type structure.

### 3.1 Frozen state transitions

The frozen state transitions were dependent on the carbohydrate composition and molecular weight of frozen systems components (Levine and Slade, 1986; Roos, 1995). In the present study, the solutes of the systems were composed of different maltodextrins and maltodextrin-sugar mixtures which showed clear glass transitions of the unfrozen solute phases below the onset temperatures of ice melting at the maximally freeze-concentrated state (Levine and Slade, 1986; Roos and Karel, 1991c). The  $T_g'$  and  $T_m'$  values are given in Table 4. Annealing at  $T_m' - 2$  affected the glass transition by completing ice formation and the  $T_g'$  was obtained, but the effect of the isothermal annealing on  $T_m'$  was negligible. The glass transition was extremely sensitive to water and the results showed that the annealing effectively increased ice formation (Roos and Karel, 1991c), i.e., increased the  $T_g$  to  $T_g'$ .

The results showed that the  $T_m'$  of the systems were affected by the composition of the solids. Maltodextrins are starch hydrolysis products, which at various DE clearly showed the effect of molecular weight on the  $T_m'$ . The higher DE values refer to higher degrees of hydrolysis and higher amounts of smaller molecular weight glucose polymers, including glucose and oligosaccharides. The  $T_m'$  decreased with increasing DE and decreasing average molecular weight of the solids. Maltodextrin M40 was of the highest average molecular weight and gave the highest  $T_m'$  values, whereas M250 had the lowest average molecular weight and gave the lowest  $T_m'$  in accordance with the data of Roos and Karel (1991c). The presence of small molecular weight sugars in a mixture with maltodextrin M100 in a ratio of 1:1 decreased the average molecular weight significantly corresponding to the lower  $T_m'$ . Monosaccharides, glucose and fructose, which had the lowest individual  $T_m'$  also gave the lowest  $T_m'$  for the maltodextrin-sugar mixtures. The results indicated that the lower was the molecular weight of the solids, the lower was the  $T_m'$ .

**Table 4** Glass transition ( $T_g'$ ) and onset temperature of ice melting ( $T_m'$ ) of maltodextrin–agar gels with and without sugars, and compression characteristics of freeze-dried solids frozen at  $-20^\circ\text{C}$  prior to freeze-drying.

Material	$T_m'$ ( $^\circ\text{C}$ )	$T_g'$ ( $^\circ\text{C}$ )	Compression Test	
			Peak Force (kPa)	Modulus (MPa)
M40 ( $M_w$ 3600)	-13	N/A	$65.3 \pm 14.6$ a	$9.6 \pm 1.4$ abc
M100 ( $M_w$ 1800)	-16	N/A	$57.6 \pm 14.2$ a	$7.9 \pm 1.2$ a
M250 ( $M_w$ 720)	-24	N/A	$46.0 \pm 7.8$ a	$8.6 \pm 2.5$ ab
M100-Glucose	-36	-64	$159.5 \pm 16.4$ d	$11.2 \pm 1.7$ cd
M100-Fructose	-37	-64	$144.3 \pm 19.6$ d	$11.8 \pm 1.1$ d
M100-Sucrose	-28	-49	$87.6 \pm 14.5$ b	$11.9 \pm 1.1$ d
M100-Mixture	-31	-55	$111.4 \pm 19.6$ c	$10.2 \pm 1.3$ bcd

$M_w$ : molecular weight that indicated by the manufacturer.

N/A: Not available data

The values for  $T_g'$  and  $T_m'$  were  $\pm 1^\circ\text{C}$ .

Different letters show significant differences within the same columns ( $p \leq 0.05$ ).

The glass transition of the maximally freeze-concentrated unfrozen solute phase appeared as a small endothermal step below the  $T_m'$  (Appendix Figure 7). Roos and Karel (1991c) found that the temperature difference between  $T_g'$  and  $T_m'$  decreased with increasing molecular weight, and the  $T_g'$  and  $T_m'$  merged for high molecular weight carbohydrate systems. High molecular weight compounds commonly showed a broad glass transition and relatively small change in heat capacity,  $\Delta C_p$  (Roos and Karel, 1991d). However, the change in heat capacity cannot always be measured for the maximally freeze-concentrated solutes, as the glass transition may overlap with ice melting (Roos, 1993a). The glass transitions of sugar systems were more pronounced and could be clearly observed below  $T_m'$ . Glucose and fructose had a strong effect on the  $T_g'$  of the systems, whereas sucrose had the highest  $T_g'$  of the sugar systems. The  $T_g'$  of the sugar mixture was closed to sucrose, because of the highest ratio of sucrose (glucose:fructose:sucrose in the ratio of 1:1:4). Sugars



effectively depressed the  $T_m'$  and  $T_g'$  of the maltodextrin-sugar systems. Roos (1993a) showed that glucose, fructose and sucrose had  $T_m'$  at -46, -46 and -34°C, and  $T_g'$  at -57, -57 and -46°C, respectively. The  $T_m'$  and  $T_g'$  values of the sugar systems in the present study agreed with the previous values. However, higher  $T_g'$  and  $T_m'$  were found when high amounts of maltodextrin (M100) were used with sugars as the system components (Table 4).

### 3.2 Freezing profile and microstructure

The freezing profiles of the maltodextrin systems with and without sugars are shown in Figure 20a and b. The initial supercooling temperature,  $T_s$ , and the freezing temperature at -20°C, -40°C or -80°C freezing,  $T_i$ , as determined from the cooling curves (Figure 20a and b) are given in Table 5. The  $T_s$  and  $T_i$  values were insignificantly different for carbohydrates at each freezing temperature. The freezing temperatures of -80°C and -20°C gave similar  $T_s$  whereas slightly higher  $T_s$  were found at -40°C. The lower freezing temperature decreased the  $T_i$ . These data were used to relate the freezing properties of the systems to their freeze-dried structures. The cooling rates were derived from the initial slopes of the cooling curves to  $T_s$ . The system components showed insignificant differences in cooling rates, which were 1.2, 3 and 5.4°C/min in freezing at -20°C, -40°C and -80°C, respectively. The cooling rate to  $T_s$  was the determinant of the rate of nucleation of water molecules to form ice and showed an increase as the freezing temperature was decreased. The time for the ice crystal growth was temperature-dependent, but almost component independent at all freezing temperatures.

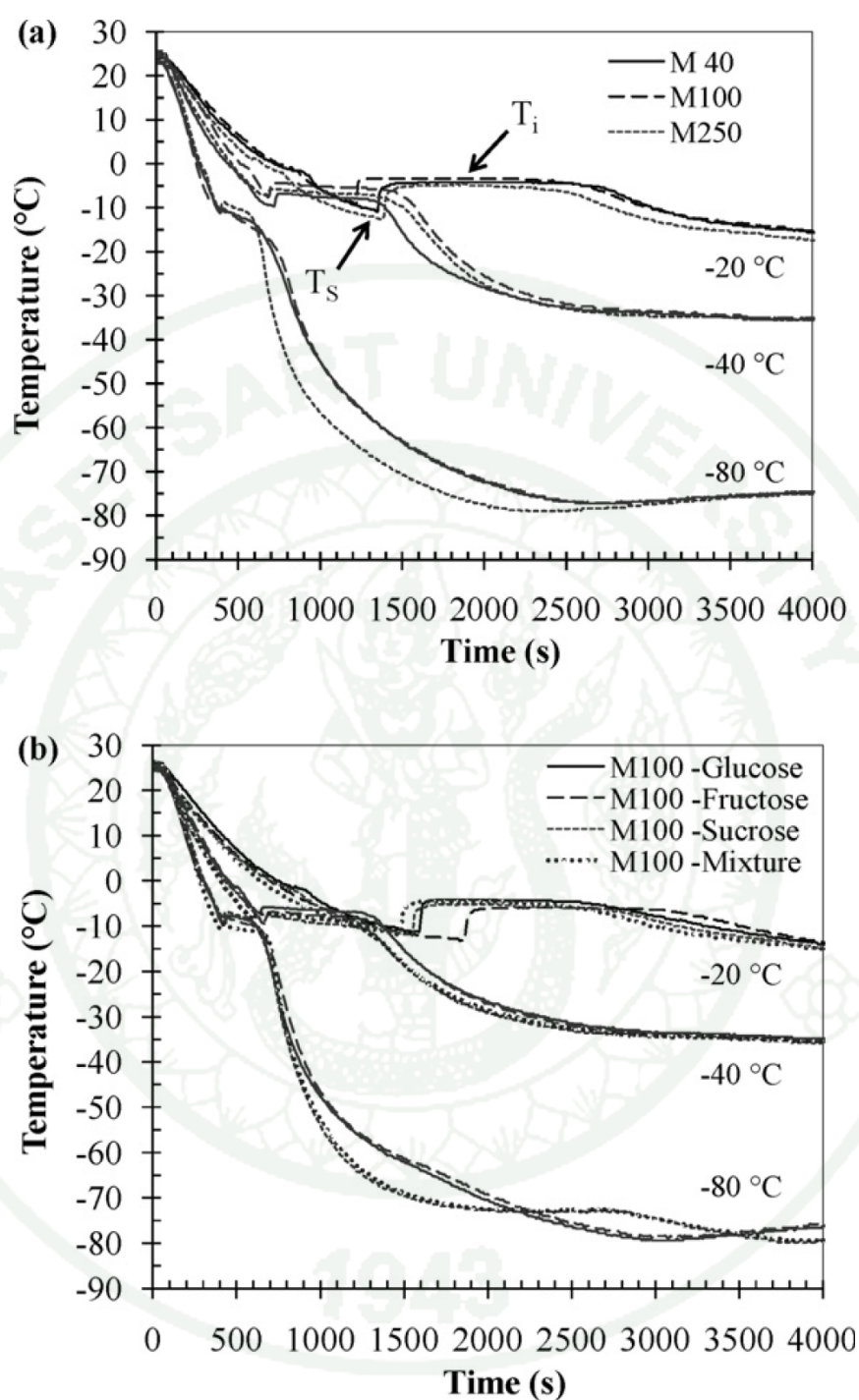


**Figure 20** Freezing profiles of (a) maltodextrin–agar gels and (b) maltodextrin–agar gels with sugars at freezing temperatures of -20, -40 and -80 °C.

The porous structures of the freeze-dried systems are shown in Figure 21. The SEM micrographs revealed the interconnected network structure of solids and embedded pores formed by ice crystals during the prefreezing step and vacated as a result of ice sublimation. The direction of pore channels was identical to the formation of dendritic ice crystals (Kang *et al.*, 1999). Heterogeneous pores were found in freeze-dried systems frozen at -20°C, whereas more homogeneous pores were formed at the freezing temperatures of -40°C and -80°C. The lower freezing temperature and resultant high nucleation rate gave more uniform, smaller and homogeneous pore structures in agreement with previous studies (Kang *et al.*, 1999; Ma and Zhang, 1999).

**Table 5** Freezing properties derived from freezing profiles: supercooling temperature ( $T_s$ ) and freezing temperature ( $T_i$ ) of fresh maltodextrin-agar gels with and without sugars frozen at -20°C, -40°C and -80°C prior to freeze-drying.

Material	-20°C		-40°C		-80°C	
	$T_s$ (°C)	$T_i$ (°C)	$T_s$ (°C)	$T_i$ (°C)	$T_s$ (°C)	$T_i$ (°C)
M40	-11±0	-3±1	-9±1	-6±2	-10±1	-8±3
M100	-10±2	-4±0	-8±2	-8±3	-7±3	-7±2
M250	-12±1	-6±2	-8±2	-10±5	-12±2	-10±3
M100-Glucose	-13±1	-6±2	-9±3	-7±2	-9±3	-10±4
M100-Fructose	-12±1	-6±1	-9±1	-8±1	-11±2	-12±2
M100-Sucrose	-12±0	-5±1	-7±2	-7±2	-8±0	-12±4
M100-Mixture	-12±1	-5±1	-9±1	-7±1	-11±1	-11±1

Values shown were mean ± SD of triplicate samples

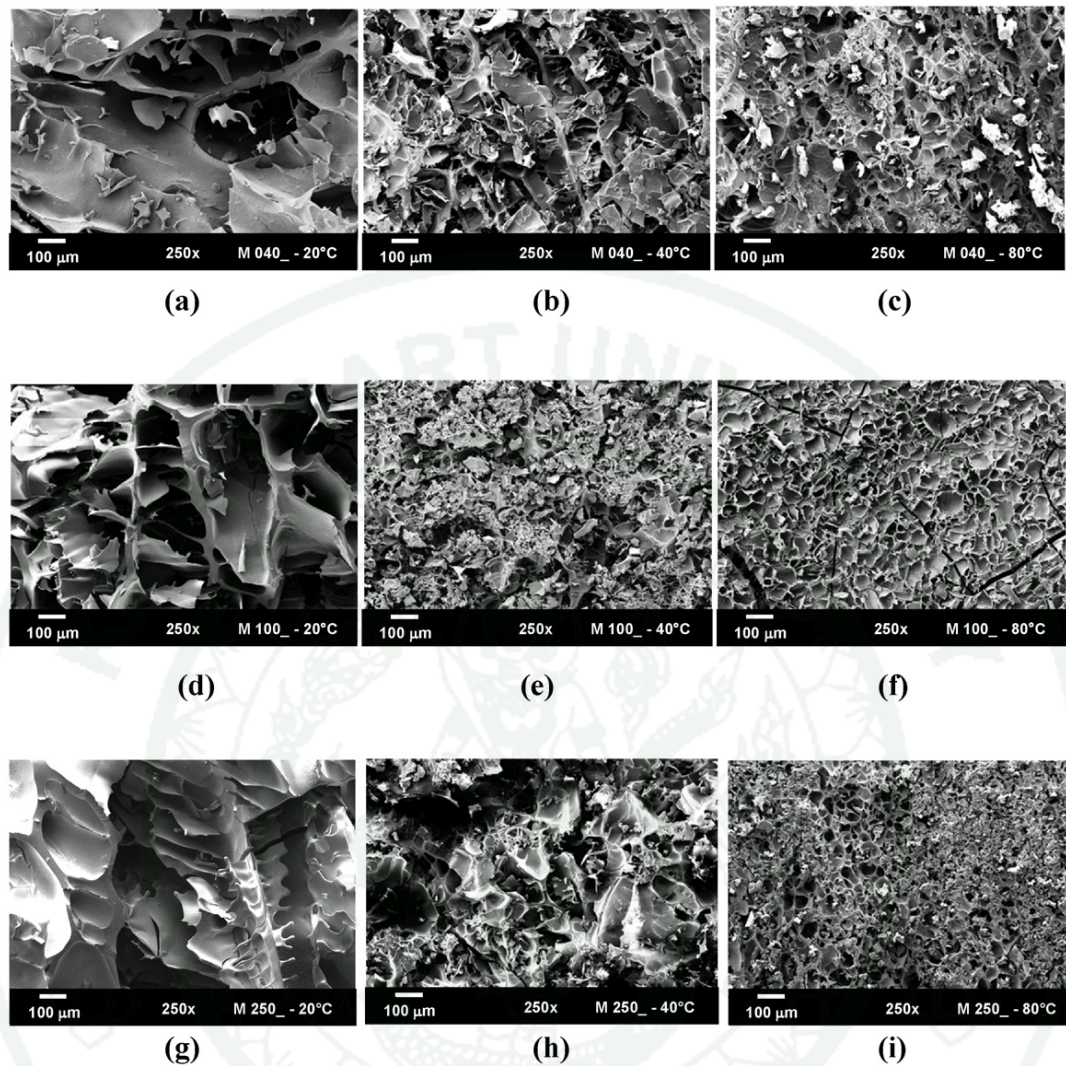


**Figure 21** SEM micrographs of freeze-dried maltodextrin–agar systems: M40 frozen at (a)  $-20^{\circ}\text{C}$ , (b)  $-40^{\circ}\text{C}$  and (c)  $-80^{\circ}\text{C}$ ; M100 frozen at (d)  $-20^{\circ}\text{C}$ , (e)  $-40^{\circ}\text{C}$  and (f)  $-80^{\circ}\text{C}$ ; and M250 frozen at (g)  $-20^{\circ}\text{C}$ , (h)  $-40^{\circ}\text{C}$  and (i)  $-80^{\circ}\text{C}$  prior to freeze-drying at  $250\times$  magnification.

The pore size of freeze-dried systems was reduced as the freezing temperature was decreased to give a higher cooling rate and increased nucleation. Freeze-dried systems frozen at  $-20^{\circ}\text{C}$  had the largest pores and channels as shown in Figure 21 a, d, g. This higher freezing temperature gave a lower cooling rate, less rapid nucleation and the longest time for ice crystal growth (Figure 20), and consequently the largest pores left by the ice crystals (Figure 21). However, the



microstructure of the freeze-dried materials was highly dependent on their composition, and the wall membranes represented the unfrozen solute phase formed during prefreezing. The results in Figure 21 and Figure 22 show that the thickness of the pore membranes decreased as freezing temperature was decreased following the pore size decrease, and corresponding increase in surface area. The inner structure of the freeze-dried systems frozen at  $-20^{\circ}\text{C}$  showed the thickest pore membranes, but also the biggest composition-dependent variations in the number of pores and wall thicknesses (Figure 22). In contrast, the high cooling rate of freezing at  $-40^{\circ}\text{C}$  and  $-80^{\circ}\text{C}$  gave thinner wall membranes. The results confirmed that a smaller number of ice nuclei were initially formed at the higher freezing temperature leading to formation of larger ice crystals (Kang *et al.*, 1999). Moreover, Figure 20 reveals that the time of freezing decreased as the freezing temperature was decreased.

Similar effects of freezing temperature on the pore size of freeze-dried polymers have been reported (Shapiro and Cohen, 1997; Kang *et al.*, 1999; Ma and Zhang, 1999; Madhally and Matthew, 1999; O'Brien *et al.*, 2005). These studies found the decrease in pore size of freeze-dried matrices as freezing temperature was decreased. Van Vlierberghe *et al.* (2007) demonstrated that at the same final freezing temperature, a decrease of the cooling rate from  $0.83$  to  $0.15^{\circ}\text{C}/\text{min}$  resulted in a significant increase in the average pore diameter of a freeze-dried gelatin hydrogel. The same study also found that the final freezing temperature between  $-10^{\circ}\text{C}$  and  $-30^{\circ}\text{C}$  (at the same cooling rate of  $0.2^{\circ}\text{C}/\text{min}$ ) did not influence the pore size of the freeze-dried hydrogel (Van Vlierberghe *et al.*, 2007). In the present study, the decreasing pore size of freeze-dried systems, as the freezing temperature was decreased from  $-20^{\circ}\text{C}$  to  $-80^{\circ}\text{C}$ , was significantly influenced by the increase of cooling rate from  $1.2$  to  $5.4^{\circ}\text{C}/\text{min}$ . A sufficiently rapid rate of cooling increased the number of nuclei and removed the heat of crystallization, thus preventing the formation of large ice crystals (Kang *et al.*, 1999; Shapiro and Cohen, 1997).



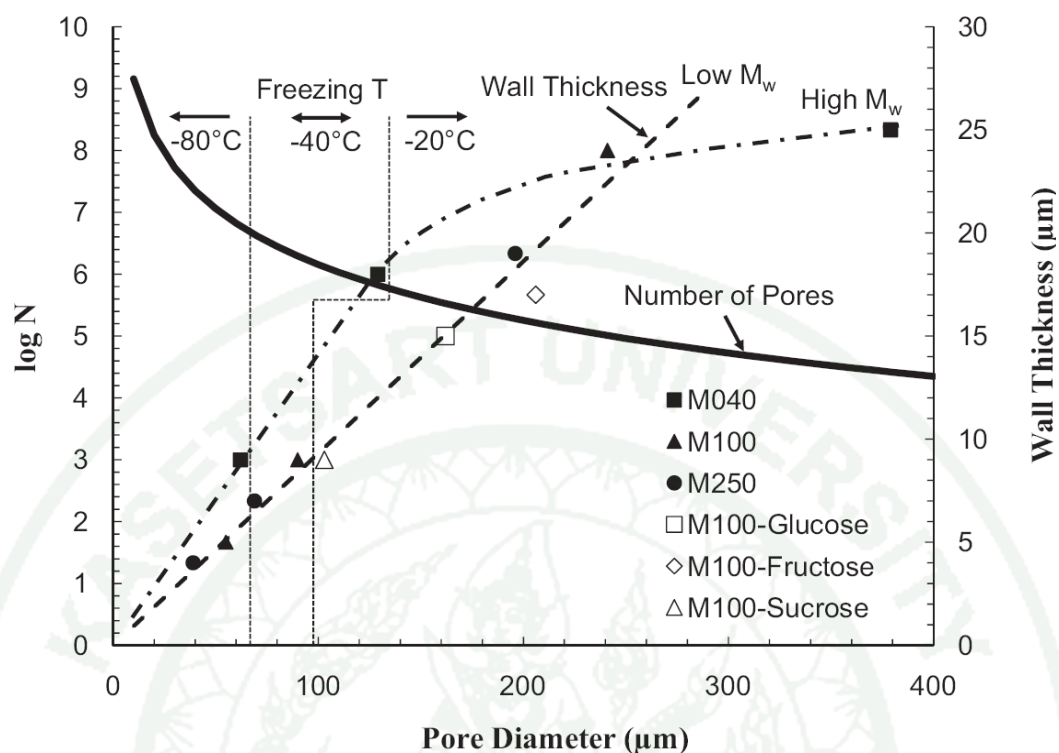


**Figure 22** Number of pores and wall thickness as a function of pore diameter of freeze-dried maltodextrin–agar systems with and without sugars. The number of pores ( $\log N$ ) is given for 10 mm  $\times$  10 mm  $\times$  10 mm samples. The wall thickness for low molecular weight ( $M_w$ ) solids correlated with a 43.5% surface coverage of spherical ice crystals by the unfrozen fluid giving the wall thickness shown. A high molecular weight maltodextrin system (M40) had a higher surface coverage of spherical ice crystals at low freezing temperatures. The calculations were shown in Appendix Table 2 and 3).

There is still lack of evidence on the effects of composition and freezing properties of solutes ( $T_g'$  and  $T_m'$ ) on the pore size and morphology of freeze-dried solids. The average molecular weight of maltodextrin affected the pore size and wall thickness of freeze-dried solids as well as the presence of various mono- and disaccharides (Figure 23). An assumption of formation of spherical ice crystals was used to derive the number of ice crystals formed at maximum freeze-concentration of

the systems that was maintained throughout freeze-drying. This presumed freezing of water to form an unfrozen phase with 80% solutes and 20% water (Roos and Karel, 1991b; Roos, 1993a). Accordingly 75% of the initial weight (volume) was water frozen to ice and 5% of the weight (volume) was unfrozen water. The number of spherical ice crystals that could be formed in each of the 10 mm x 10 mm x 10 mm samples of the 0.75 mL of freezing water is shown in Figure 22. An expansion of the spheres based on the  $0.917 \text{ kg/m}^3$  density of ice could be used to derive the frozen radius of the same number of spheres on which a proportion of the unfrozen fluid (0.25 mL) could form a surface coverage to a final radius with half thickness of the interparticle walls. The wall thicknesses measured for the freeze-dried systems excluding the M40 systems increased linearly with increasing pore diameter, as shown in Figure 22. It was shown that the wall thickness experimentally and theoretically for spherical pores increased linearly with increasing pore diameter. The linear fit to experimental data showed that 43.5% of the unfrozen fluid was on surfaces and 56.5% was located in interparticle voids. For M40 systems frozen at  $-80^\circ\text{C}$  and  $-40^\circ\text{C}$  the unfrozen fluid at particle surfaces increased to 65%, but this decreased to 30% when M40 system was frozen at  $-20^\circ\text{C}$  locating more unfrozen fluid in the interparticle voids. The results indicated that for maltodextrins a smaller molecular weight gave a smaller pore size and thinner pore membranes at all freezing temperatures. Table 5 showed minor differences in freezing points for maltodextrins, but their molecular size (DE) affected the amount of unfrozen water during freezing at the same temperature and their viscosities could also differ which accounted for the differences in pore sizes. M250 contained a higher amount of small molecular weight solutes retarding ice crystal growth and more unfrozen water during freezing above the  $T_m'$ . In contrast, M40 had a higher amount of water that formed ice at the same temperature and larger ice crystals were produced during initial freezing.

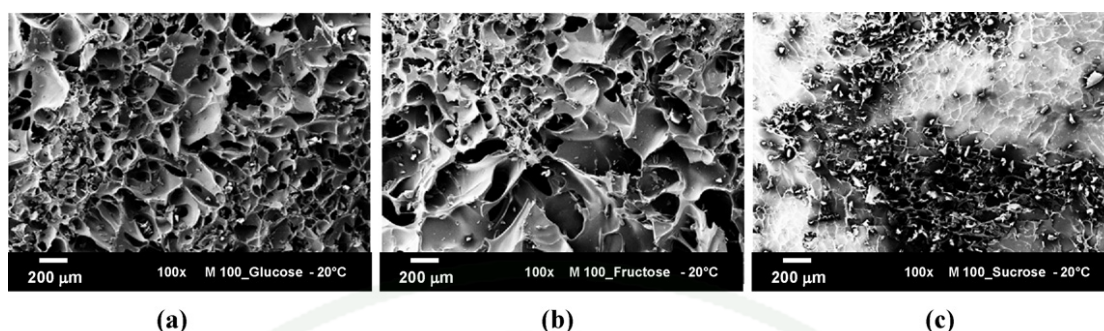


**Figure 23** SEM micrographs of freeze-dried maltodextrin–agar (M100) solids with (a) glucose, (b) fructose, and (c) sucrose frozen at  $-20^{\circ}\text{C}$  prior to freeze-drying at 100x magnification.

Freezing of the maltodextrin systems at  $-80^{\circ}\text{C}$  and  $-40^{\circ}\text{C}$  showed that a relatively similar freezing point depression, but differences in  $T_g'$  and  $T_m'$  in freezing at a temperature well below the  $T_m'$  affected the rate of nucleation (number and size of pores). M40 systems showed a smaller number and larger pore sizes. It may be expected that nucleation in M40 was retarded in conditions close to maximum freeze-concentration in a shorter time and crystal growth became more rapid, because of a lower DE and higher molecular weight increasing the driving force for the crystal growth after nucleation close to the  $T_m'$  conditions. Also a larger quantity of water could crystallize in these systems at the same temperatures than in systems with lower molecular weight further increasing crystal size. This also applied to the differences in the pore sizes and wall thicknesses found for the M100 and M250 systems. It should also be noted that the pore sizes and wall thicknesses in freezing at  $-40^{\circ}\text{C}$  and  $-80^{\circ}\text{C}$  followed more closely the theoretical values (Figure 22) confirming that a more rapid nucleation produced smaller, more spherical ice crystals than conditions producing large and more dendrite structured ice crystals.

Interestingly, the DE values of the maltodextrins (molecular size) and the molecular size of the sugars were found to affect the freezing properties and freeze-dried structures of the systems. These materials are commonly used in cryopreservation and as protective matrices in freezing and freeze-drying of

pharmaceutical preparations, proteins, bacteria strains and sensitive food components. The results show that the entrapment of dispersed components may become better protected in thicker walls and larger interparticle voids of the high molecular weight carbohydrate systems. These systems are easier to freeze-dry because of the higher  $T_m'$  and they are less sensitive to water in the dehydrated state (Roos and Karel, 1991d). However, such high molecular weight components may show less interactions with sensitive components and provide less protection to, for example, native protein structures and cell membranes that may require flexibility during freeze-concentration and freeze-drying.

### 3.3 Collapse in Freeze-Drying

The different freezing temperatures,  $-20^{\circ}\text{C}$ ,  $-40^{\circ}\text{C}$  and  $-80^{\circ}\text{C}$ , showed no significant effects on the macroscopic appearance of the freeze-dried systems (Figure 24). But some hardening was observed in maltodextrin systems. A similar observation was reported in freeze-dried alginate and agar gels containing starch (Göğüş and Lamb; 1998; Rassis *et al.*, 2002). A rapid cooling of a surface could cause the formation of a crust as water could flow out of the gel and freeze at the surface leaving a shrunken gel (Scherer, 1993). The higher amount of frozen water in M40 system surfaces could lead to a hard crust formation and a high strength to the freeze-dried material. This could also result from smaller pores at the freezing surface of the samples. Sugars gave the structural collapse of freeze-dried solids. Systems frozen at  $-20^{\circ}\text{C}$  had least collapse. As freezing temperature was decreased to  $-40^{\circ}\text{C}$ , structural collapse was clearer but was almost negligible in M100-sucrose systems. The highest degree of collapse resulted from freezing at  $-80^{\circ}\text{C}$ . The degree of collapse was influenced by both freezing temperature and types of sugars, and was particularly the consequence of the pore size effects on mass transfer during freeze-drying.

During freeze drying, ice supported the frozen structure. Once sublimation removed the ice, the remaining pores did not collapse due to the high viscosity of the concentrated amorphous solution or the unfrozen solutes (Bellows and King, 1972). If the viscosity of the unfrozen solutes decreased to a level that facilitated deformation,



the matrix could flow and collapse of the pore could occur (Levi and Karel, 1995). It has been shown that collapse increases above the  $T_g$  since the viscosity of the amorphous matrix decreases drastically, as described by the Williams-Landel-Ferry (WLF) relationship (Williams *et al.*, 1955; Levi and Karel, 1995). The presence of sugars plasticized the materials and decreased the  $T_m'$  and  $T_g'$  of the systems. The dried systems, which contained glucose and fructose, had lower glass transition temperatures ( $T_g$ ) than sucrose (Roos and Karel, 1991d). Therefore, the higher temperature difference between process  $T$  and  $T_g$  ( $T - T_g$ ) of dried systems containing glucose and fructose also accelerated the structural collapse. The presence of small molecular weight solutes decreased the temperature at which collapse occurred (Tsourouflis *et al.*, 1976; To and Flink, 1978). Rassis *et al.* (2002) found that there was more total shrinkage of freeze-dried alginate gels, which contained solutes with smaller average molecular size.

As the freeze-dried sugar systems frozen at  $-40^\circ\text{C}$  and  $-80^\circ\text{C}$  visually showed structural collapse and loss of porous structure, it was expected that the pores left by small ice crystals gave a high resistance to mass transfer. This could increase ice temperature at the ice interface and result in partial ice melting, which led to plasticization of solids and structural collapse during freeze-drying. The sublimation of small ice crystals resulted in small pores in the dry layer which effectively resisted mass transfer and hence acted as a barrier against sublimation (Pikal *et al.*, 2002). Moreover, the very rapid freezing also caused the crust formation during freezing which produced an additional barrier against vapor flow. As a result, the partial melting of the ice was a major cause for structural collapse during freeze-drying. This led to the high degree of structural collapse during freeze-drying of the systems, which had low  $T_m'$  and  $T_g'$  and were frozen at low temperature.

The least collapse in sucrose systems, particularly frozen at  $-40^\circ\text{C}$ , was caused by the highest  $T_m'$  and  $T_g'$  of M100-sucrose systems. In contrast, M100 with glucose, fructose and a mixture of sugars showed similar degree of structural collapse at all freezing temperatures because of the similar  $T_m'$  and  $T_g'$ .

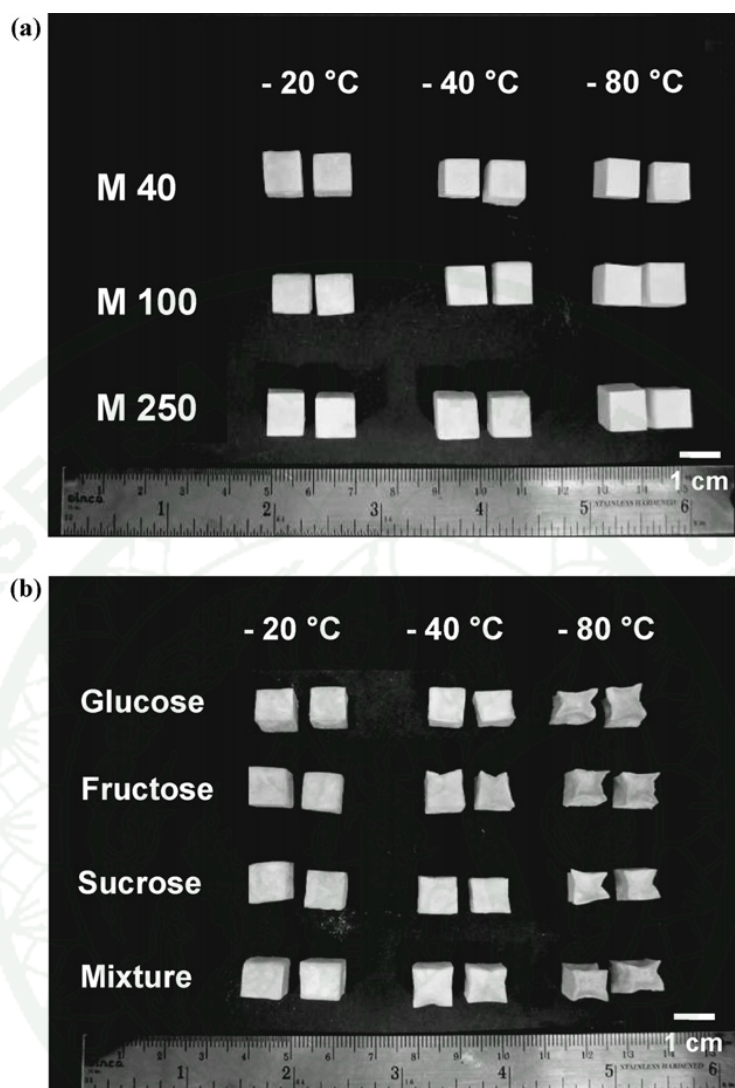


**Figure 24** Appearance of freeze-dried solids: (a) maltodextrin (M40:DE6, M100:DE11 and M250:DE25.5); (b) maltodextrin (M100) with sugar (glucose, fructose, sucrose and mixture) at the ratio of 1:1 frozen at  $-20$ ,  $-40$  and  $-80$  °C prior to freeze-drying.

### 3.4 Texture analysis

Freeze-dried maltodextrin-agar systems frozen at  $-80^{\circ}\text{C}$ ,  $-40^{\circ}\text{C}$  and  $-20^{\circ}\text{C}$ , were analyzed for mechanical strength under compression force using a texture analyzer. The typical compressive stress *versus* strain curves are shown in Figure 25. When the compressive force was applied, breaking of the brittle pore wall material

caused fractures. The freeze-dried systems showed the irregular jagged shape characteristics of a brittle solid foam (Peleg, 1997). These oscillations of stress during compression were denoted as 'jagged' with shape slightly differing among materials due to the wall properties of the pores (Peleg, 1997; Nussinovitch *et al.*, 2001; Laurindo and Peleg, 2007). Either compressive peak force and/or modulus were found to explain the strength of freeze-dried solids (Rassis *et al.*, 1998; Ma and Choi, 2001; Hou *et al.*, 2003). The peak in stress-strain curves corresponded to the highest resistance to compression (hardness). Systems frozen at  $-80^{\circ}\text{C}$  were the most resistant to compression followed by those frozen at  $-40^{\circ}\text{C}$  and  $-20^{\circ}\text{C}$ , respectively (Figure 26). The higher cooling rate gave higher resistance to compression. This was coincident with the finding of Shapiro and Cohen (1997), who showed that a higher compressive force was needed to deform freeze-dried alginate gels produced by a higher cooling rate using liquid nitrogen freezing. The higher peak forces of systems frozen at low freezing temperature were coincident with the smaller pores and thinner wall membranes. In addition, the very rapid freezing could cause the crust formation and increase the resistance against a compressive force.

Maltodextrin M40 systems had the highest strength at freezing temperatures of  $-40^{\circ}\text{C}$  and  $-80^{\circ}\text{C}$ . This was caused by the crust formation on the freezing surface during very rapid freezing which provided with the strength and enhanced the resistance against compression. The strength of freeze-dried systems composed of M100 and M250 showed only insignificant differences. This was coincident with Corveleyn and Remon (1997) who reported the insignificant differences of maximum penetration force to deform the tablet of xanthan gum, which contained different DE maltodextrins (DE 12, 24 and 38).

The pore size and wall thickness (Figure 22) affected the strength of the freeze-dried systems. After the maximum peak force plateau, the compressive stress-strain curve showed the typical drop of stress (Figure 25). The jagged characteristics indicated the strength of pore walls in freeze-dried solids. At above 30% strain, freeze-dried systems frozen at  $-80^{\circ}\text{C}$  clearly revealed the highest force followed by those frozen at  $-40^{\circ}\text{C}$  and  $-20^{\circ}\text{C}$ , respectively. This reflected the highest strength of

pore walls in systems frozen at low temperatures. Although the walls of freeze-dried systems frozen at -80 °C were thinner than at -20 °C, the gap between the walls was smaller owing to the formation of smaller ice crystals. This gave the higher strength to freeze-dried solids. Moreover, the smaller pore size distributed stresses in the system more evenly allowing it to resist the compressive force leading to bigger amplitude of each jagged peak. Therefore, the smaller pore size and increase in the number of pores provided strength against compressive crack propagation under applied compressive force (Kim *et al.*, 2004). Freeze-dried systems frozen at -80 °C revealed the highest strength of the pore walls.

In this study, the amount and concentration of solids were the same. However, systems frozen at -80 °C gave higher compressive modulus than all maltodextrin systems frozen at -20 °C (Figure 26B), whereas, the systems frozen at -40 °C showed insignificant differences to -20 °C and -80 °C. The lowest modulus indicated the highest deformation rate, which referred to high brittleness and lower strength of solids. The DE of maltodextrins showed no effect on modulus values.

The compressive peak force and modulus of freeze-dried maltodextrin systems with sugars frozen at -20 °C are shown in Table 4. Sugars increased solid strength as reflected by higher peak force and modulus values than were measured for the M100 system. It is possible that the sugar-containing glass potentially enhanced the strength of freeze-dried solids. Moreover, the small molecular weight sugars interacted compatibly with maltodextrins and/or agar which enhanced the strength of solids. Sucrose-containing dry solids revealed the lowest peak force. Glucose and fructose as components showed no differences in peak forces, whereas mixtures of sugars gave values in between these sugars and sucrose. This was possibly due to the smallest pore size of sucrose-based systems.



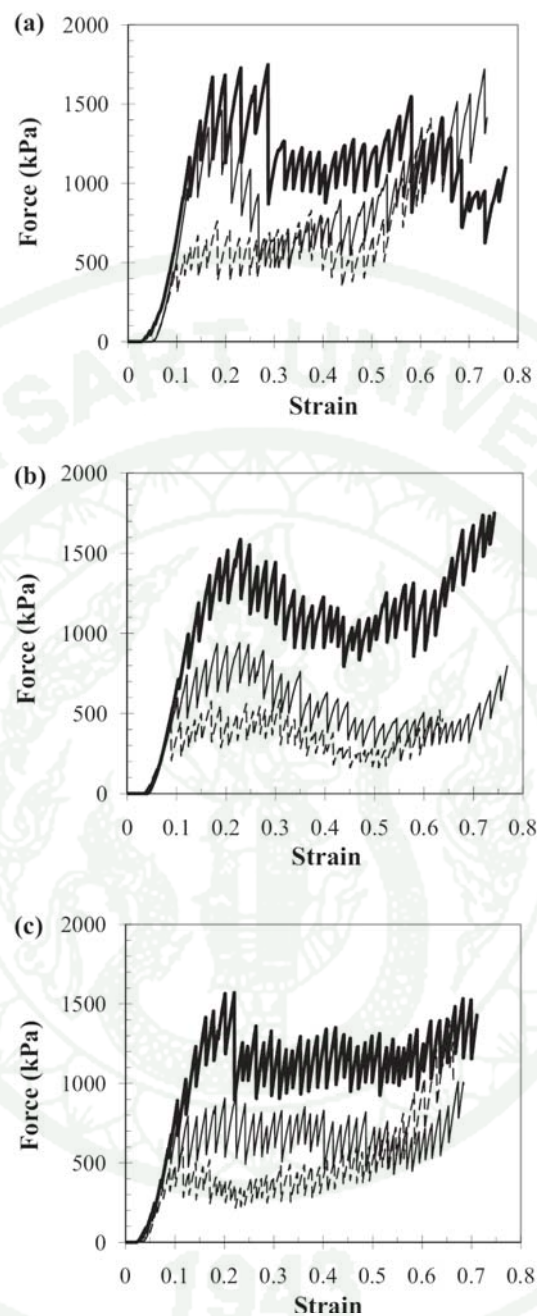


**Figure 25** Compressive force–displacement curves of ‘anhydrous’ freeze-dried maltodextrin–agar systems: (a) maltodextrin M40:DE6; (b) M100:DE11; (c) M250:DE25.5 frozen at  $-20\text{ }^{\circ}\text{C}$  (dotted line),  $-40\text{ }^{\circ}\text{C}$  (normal line) and  $-80\text{ }^{\circ}\text{C}$  (thick line) prior to freeze-drying.

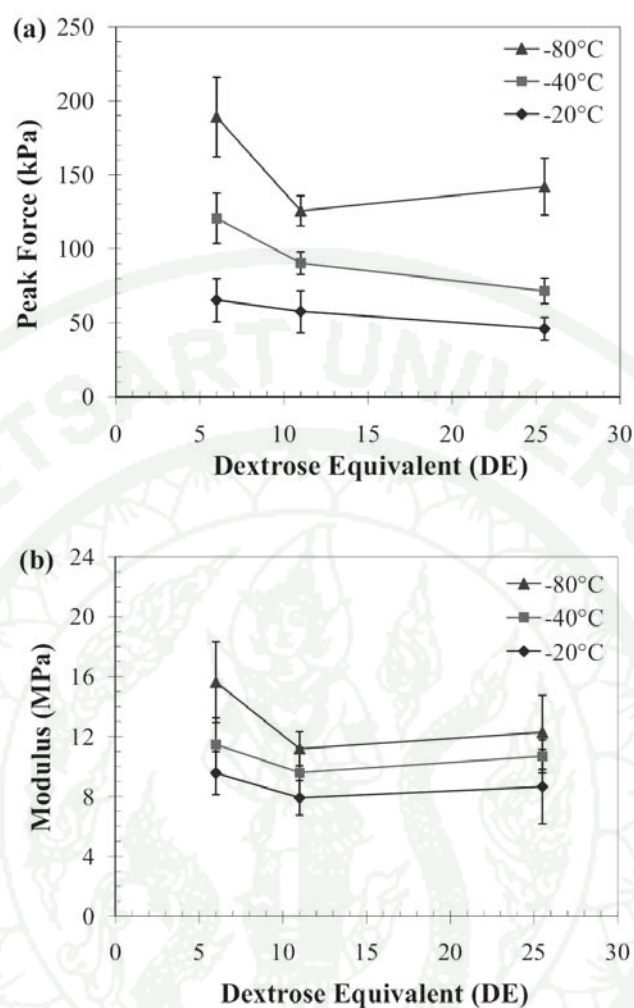


**Figure 26** Compressive (a) peak force and (b) modulus of ‘anhydrous’ freeze-dried maltodextrin–agar systems (M40, M100 and M250) frozen at –20°C, –40°C and –80 °C prior to freeze-drying as a function of dextrose equivalent (DE).

The results in this part indicated the relationship between process-induced structure formations in freeze-dried carbohydrate systems. They confirmed the hypothesis that the pore formation of freeze-dried solids was reflected by the rate of water nucleation which was strongly dependent on the freezing properties of solids. In addition, the freezing at a lower temperature increased the rate of water nucleation resulting in a large number of ice nuclei and consequently gave a large number of small pores in freeze-dried solids.

#### 4. Porosity and Water Activity Effects on Stability of Crystalline $\beta$ -carotene in Freeze-dried Solids

The previous part indicated that the freezing parameters and solids components potentially controlled the microstructure of freeze-dried solids. In this part, the crystalline  $\beta$ -carotene was dispersed in the freeze-dried carbohydrate matrix and determined for the effect of microstructure and water activity on the stability of  $\beta$ -carotene. The microstructures of freeze-dried matrices were formed as described in the previous part. As  $\beta$ -carotene naturally distributed in plants as both crystalline and non-crystalline forms, this part investigated the stability of crystalline type of  $\beta$ -carotene in freeze-dried solids.

##### 4.1 Microstructure of freeze-dried solids

Microstructures of freeze-dried maltodextrin systems frozen at  $-20^{\circ}\text{C}$ ,  $-40^{\circ}\text{C}$  and  $-80^{\circ}\text{C}$  are shown in Figure 27. The SEM micrographs indicated that the pore size and membrane thickness of freeze-dried solids were strongly dependent on the freezing temperature prior to freeze-drying. A higher freezing temperature of  $-20^{\circ}\text{C}$  gave larger pores and thicker walls to freeze-dried solids. Conversely, the smaller size of ice crystals formed at the lower freezing temperatures gave smaller pores and thinner walls, as discussed by Harnkarnsujarit *et al.* (2012a). We found that sugars affected significantly the freezing properties and pore formation in the freeze-drying of maltodextrin systems frozen at  $-20^{\circ}\text{C}$  (Harnkarnsujarit *et al.*, 2012a). M100-fructose and M100-glucose systems had corresponding pore structures with heterogeneities. In contrast, smaller and more homogeneous pores were found in M100-sucrose systems. The previous part indicated that the nucleation of water and ice crystal growth were reflected by the component-dependent freezing properties governed by the respective glass transition temperature and ice melting temperature,  $T_g'$  and  $T_m'$ , of the maximally freeze-concentrated systems (Harnkarnsujarit *et al.*, 2012a). Freezing at  $-80^{\circ}\text{C}$  caused structural collapse during freeze-drying of all sugar-maltodextrin systems. The low temperature freezing formed small ice crystals, which decreased pore size and increased the resistance of vapor flow during sublimation that

could increase ice temperature to above the  $T_m'$  causing viscous flow and accelerated structural collapse during freeze-drying.

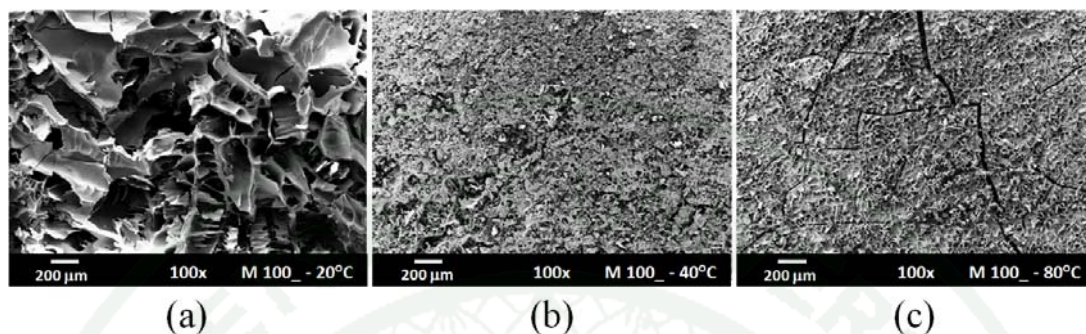


**Figure 27** SEM micrographs of freeze-dried maltodextrin systems (M100) prefrozen at (a)  $-20^{\circ}\text{C}$ , (b)  $-40^{\circ}\text{C}$  and (c)  $-80^{\circ}\text{C}$  prior to freeze-drying at 100x magnification indicate pore size and wall thickness of the solids.

#### 4.2 Water sorption and glass transition

Water contents and glass transition temperatures ( $T_g$ ) of freeze-dried systems at various water activity ( $a_w$ ) values are given in Table 6. Sugars (glucose, fructose and sucrose) and water affected the  $T_g$  values that were lower for the solids with sugars and confirmed plasticization of maltodextrin components by the smaller molecular weight components. Fructose with the lowest  $T_g$  as solids component depressed the  $T_g$  values most strongly, and was followed by glucose and sucrose, in accordance with their individual  $T_g$  values (Roos, 1993). Sugar mixture systems showed  $T_g$  values intermediate to those of the 3 component sugars while maltodextrin-agar solids effectively increased the  $T_g$  of the mixtures (Appendix Figure 8).



**Table 6** Water content and glass transition temperature ( $T_g$ ) of freeze-dried maltodextrin (M40:DE6, M100:DE11 and M250:DE25.5) and maltodextrin-sugar (glucose, fructose, sucrose and sugar mixture (glucose: fructose: sucrose; 1:1:4) systems (M100: sugars; 1:1) at various water activity,  $a_w$ , values.

Systems	$a_w$	0	0.11	0.22	0.33	0.44	0.55	0.66	0.75
M040	H <sub>2</sub> O <sup>a</sup>	0.00	2.23	4.10	5.43	7.74	8.96	12.22	16.80
	$T_g$ (°C) <sup>b</sup>	N/A	N/A	N/A	77	69	51	50	27
M100	H <sub>2</sub> O	0.00	1.57	2.89	4.87	6.82	8.13	11.37	16.41
	$T_g$ (°C)	N/A	N/A	78	58	50	42	29	20
M250	H <sub>2</sub> O	0.00	0.98	1.96	3.65	5.46	6.24	9.29	14.23
	$T_g$ (°C)	N/A	N/A	42	37	28	20	6	-28
M100 + Glucose	H <sub>2</sub> O	0.00	1.13	1.82	2.57	5.20	8.72	14.30	22.99
	$T_g$ (°C)	38	13	10	0	-12	-29	-42	-61
M100 + Fructose	H <sub>2</sub> O	0.00	1.12	1.89	2.70	5.58	9.13	14.45	23.46
	$T_g$ (°C)	30	6	3	-4	-15	-29	-42	-60
M100 + Sucrose	H <sub>2</sub> O	0.00	1.04	1.69	2.59	4.48	7.08	11.64	18.21
	$T_g$ (°C)	75	32	28	21	15	-2	-12	-39
M100 + Mixture	H <sub>2</sub> O	0.00	1.10	1.74	2.51	4.80	7.69	12.76	19.88
	$T_g$ (°C)	68	24	22	15	3	-15	-24	-46

<sup>a</sup>Water content (g water/100 g dried solids)

<sup>b</sup>The values for  $T_g$  were  $\pm 1^\circ\text{C}$

N/A: Not available data

### 4.3 Dynamic mechanical analysis

The structural relaxation times ( $\tau_\alpha$ ) at the  $\alpha$ -relaxation for the freeze-dried solids are shown in Figure 28. The  $\log \tau_\alpha$  data were plotted against  $(T - T_g)^{-1}$  following the WLF relationship (Williams *et al.*, 1955) of changes of structural relaxation times above the glass transition given by equations (6) and (7). Such presentation may be used to describe “fluidness” of glass-forming substances above the glass transition (Roos, 2012). The  $C_2$  of the WLF equation measures the fluidness above the glass transition while  $C_1$  gives the number of logarithmic decades over which structural relaxation times change above the  $T_g$ , as described for “fragility” of glass formers by Angell (1997). Figure 28 shows the WLF curves at  $C_2$  values of 51.6 K (universal  $C_2$  value), 75 K, 100 K and 125 K. The dielectric relaxation times data of fructose-water systems at solids contents of 77.8% (w/w) and 94.6% (w/w) of Shinyashiki *et al.* (2008) are shown for comparison. The relaxation times derived from the dynamic mechanical analysis data were shown for the anhydrous systems and systems at 0.44  $a_w$ , as crystallization of glucose could take place in systems at higher  $a_w$  during equilibration of samples. According to Bellows and King (1973) collapse in freeze-drying occurred at viscosities lower than  $10^4$  Pa s, which corresponds to relaxation times lower than  $10^{-3}$  s, as shown in Figure 28.

$$\log \alpha_T = \log \left( \frac{\tau}{\tau_g} \right) = \log \left( \frac{\eta}{\eta_g} \right) = \frac{-C_1(T - T_g)}{C_2 + (T - T_g)} \quad (\text{Eq.6})$$

$$\log \tau = -(C_1 - \log \tau_g) + \left( \frac{C_1}{\frac{1}{C_2} + \frac{1}{T - T_g}} \right) \frac{1}{T - T_g} \quad (\text{Eq.7})$$

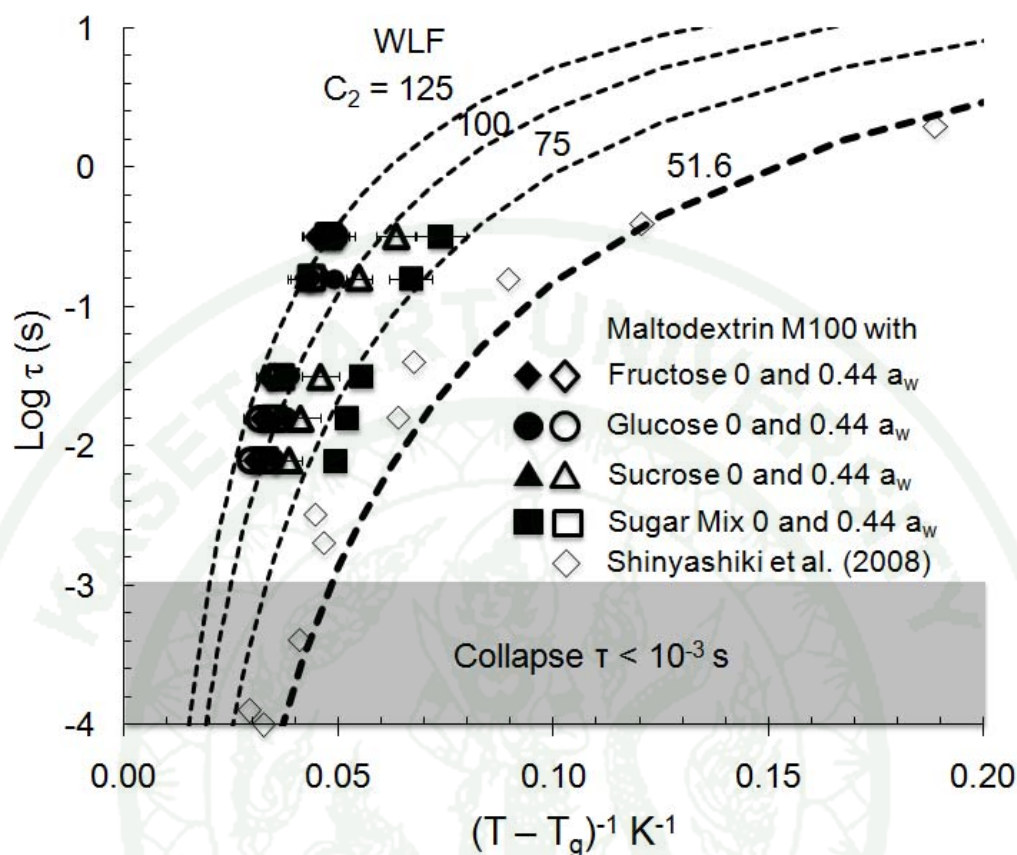


**Figure 28** The  $\alpha$ -relaxation time ( $\tau_\alpha$ ) of freeze-dried maltodextrin-sugar systems (M100: sugar; 1:1) at anhydrous and 0.44  $a_w$  at 24°C. The  $\tau$  values were derived from the loss modulus of dynamic mechanical measurements at frequencies of 0.5, 1, 5, 10, 20 Hz (Appendix Figure 9 and 10). Dotted lines represent predicted structural relaxation times by the WLF equation (Eq.6 and 7) at  $C_2$  constant values of 51.6 K, 75 K, 100 K and 125 K. Symbols:  $\circ$  M100-glucose,  $\diamond$  M100-fructose,  $\Delta$  M100-sucrose and  $\square$  M100-sugar mixture

At a constant temperature an increasing water activity above the critical  $a_w$  increased the molecular mobility of the glass-forming solids, as shown by the decreasing relaxation times (Figure 28) with increasing water activity induced change in  $T - T_g$  above the glass transition corresponding water activity ( $T - T_g = 0$ ). Noel *et*

*al.* (1996) reported that as water content increased, the intermolecular hydrogen bonds between the sugar-maltodextrin molecules were replaced by the water-sugar-maltodextrin bonds (Noel *et al.*, 1996). Water plasticization indicates increasing free volume and a weakening of the molecular interactions of the solute molecules (Oh *et al.*, 2006). Water did not significantly change the relaxation times above the glass transition, i.e., the decrease followed the increasing  $T-T_g$  and the relaxation times were more material than water content dependent (Figure 28). The relaxation time depends on both the hydration level and the molecular structure of the sugar molecules (Jansson *et al.*, 2005). The results revealed that  $\tau_\alpha$  at any water activity was governed by the glass transition and was lower for the small molecular sugars than maltodextrins.

#### 4.4 $\beta$ -carotene stability

The loss of dispersed  $\beta$ -carotene in freeze-dried systems during storage at 24°C and 0, 0.11, 0.44 and 0.66 $a_w$  followed first-order kinetics in agreement with previous studies of oil-soluble  $\beta$ -carotene in foods and model systems (Desobry *et al.*, 1999; Koca *et al.*, 2007; Lavelli *et al.*, 2007; Pesek and Warthesen, 1990; Ramoneda *et al.*, 2011). First order rate constants were calculated for  $\beta$ -carotene degradation (Figures 29 and 30). Freezing temperature showed a clear effect on degradation (Figure 31). The results showed that the lower freezing temperature gave a higher stability to  $\beta$ -carotene particles in freeze-dried maltodextrin systems with sugars (Figure 31). However, maltodextrin systems without sugars showed higher stability for  $\beta$ -carotene when materials were frozen at -20°C, except for M40 system that showed the highest stability when frozen at -80 °C (Appendix Figure 10). This stability was accounted for the crust formation by solids during freeze-drying (Harnkarnsujarit *et al.*, 2012a).

Figure 31 shows the first order rate constants for degradation of  $\beta$ -carotene in M100-sugar systems frozen at -20 °C and -80 °C during storage at 0 and 0.11 $a_w$ . Freezing at -80 °C led to degradation only during the first 13 days followed by stable carotene content up to 34 days of storage (Appendix Figure 11) which indicated



limited degradation of  $\beta$ -carotene. A similar behavior was obtained at 0.11 $a_w$ . The maltodextrin-sugar systems frozen at  $-80^\circ\text{C}$  showed the structural collapse during freeze-drying. The results suggested that only a limited amount of  $\beta$ -carotene on solid surfaces was exposed to oxygen and consequent degradation during the first period of the storage, whereas  $\beta$ -carotene entrapped in the collapsed solids was more protected. The dense collapsed matrix could reduce diffusion and permeation of oxygen through the solids increasing stability of  $\beta$ -carotene (Harnkarnsujarit and Charoenrein, 2011b).  $\beta$ -carotene was fully retained in collapsed structure of solids.

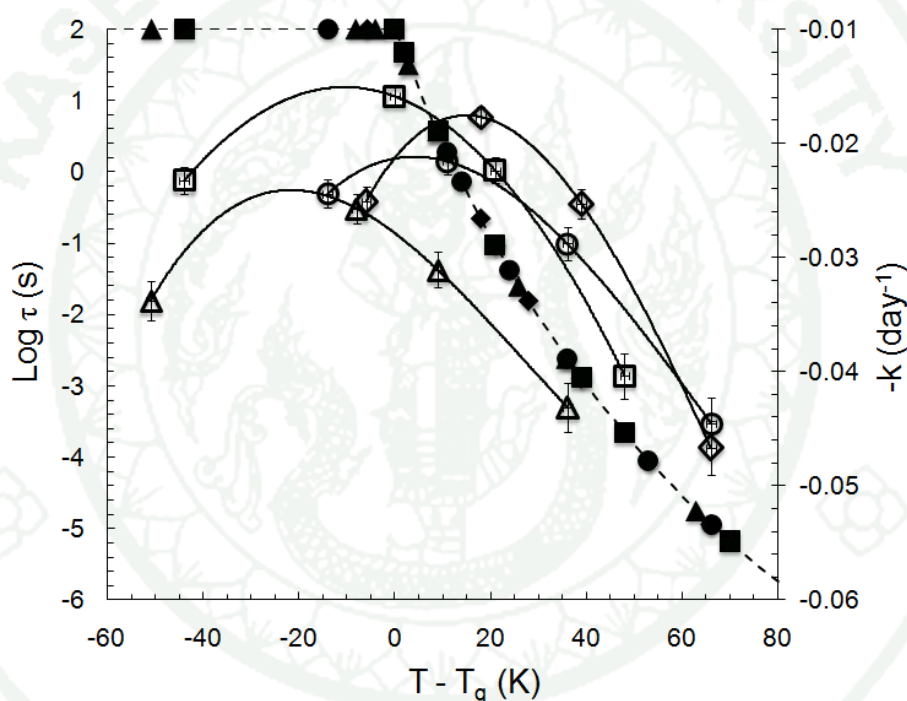


**Figure 29** Log  $\alpha$ -relaxation time ( $\tau_\alpha$ ) (filled symbols) and first-order rate constants ( $-k$ ) of  $\beta$ -carotene degradation (empty symbols) in porous freeze-dried maltodextrin-sugar (glucose, fructose, sucrose and sugar mixture (glucose: fructose: sucrose; 1:1:4) systems (M100: sugars; 1:1) as a function of difference between storage temperature and glass transition temperature ( $T-T_g$ ). Systems were prefrozen at  $-20^\circ\text{C}$  prior to freeze-drying and stored at  $24^\circ\text{C}$  at various humidities.

Symbols:  $\circ$  M100-glucose,  $\diamond$  M100-fructose,  $\Delta$  M100-sucrose and  $\square$  M100-sugar mixture

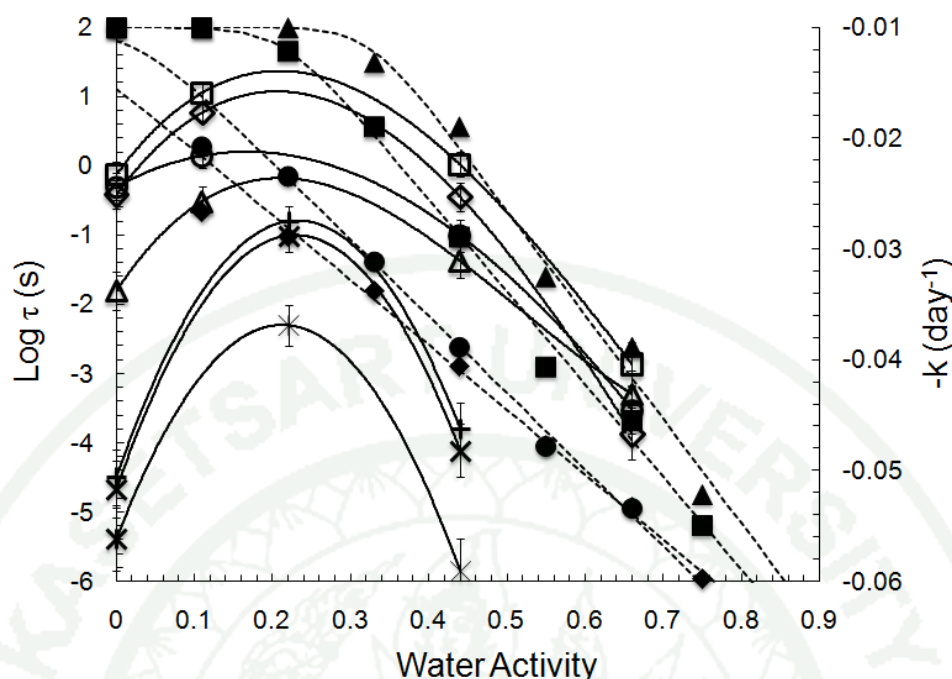


**Figure 30** Log  $\alpha$ -relaxation time ( $\tau_\alpha$ ) (filled symbols) and first-order rate constants ( $-k$ ) of  $\beta$ -carotene degradation (empty symbols) in porous freeze-dried maltodextrin (M40:DE6, M100:DE11 and M250:DE25.5) and maltodextrin-sugar (glucose, fructose, sucrose and sugar mixture (glucose: fructose: sucrose; 1:1:4) systems (M100: sugars; 1:1) as a function of water activity,  $a_w$ . Systems were prefrozen at  $-20^\circ\text{C}$  prior to freeze-drying and stored at  $24^\circ\text{C}$  at various humidity conditions. Arrows with values indicate the critical  $a_w$  of the solid systems.

Symbols: \* M40, × M100, + M250, ○ M100-glucose, ◇ M100-fructose, Δ M100-sucrose and □ M100-sugar mixture

The rate constants decreased as  $a_w$  increased to  $0.22a_w$ , but were increased at  $0.44a_w$  in all freeze-dried maltodextrin and maltodextrin-sugar systems (Figure 30). As  $a_w$  increased to 0.11, lower  $\beta$ -carotene degradation rates were found in all maltodextrin-sugar systems frozen at  $-20^\circ\text{C}$  followed by increasing rate constants as water activity increased up to  $0.66a_w$ . This was in agreement with the findings by Lavelli *et al.* (2007) who reported decreasing  $\beta$ -carotene degradation rates in carrots up to  $a_w$  0.55 prior to increasing degradation at higher  $a_w$ . The present study could be

comparable to losses of  $\beta$ -carotene in dried carrots, which contain crystalline  $\beta$ -carotene. Ramoneda *et al.* (2011) also found the increased degradation rate of oil-solubilized  $\beta$ -carotene encapsulated in freeze-dried maltodextrin-gelatin solids as storage RVP was increased (11 to 75%).

#### 4.5 Structure and stability of $\beta$ -carotene in freeze-dried solids

Solids composition and freezing temperature governed the size of the ice crystals formed and porosity of the freeze-dried materials, as shown in Figure 27 and reported by Harnkarnsujarit *et al.* (2012a). The smaller size of ice crystals formed at the lower freezing temperatures gave smaller pores with a larger surface area and thinner walls (Figure 27). This decreased  $\beta$ -carotene stability in the glassy M100 maltodextrin solids probably because of poorer entrapment and exposure of the particles to oxygen which accelerated the degradation of  $\beta$ -carotene. All maltodextrin systems showed higher rates of  $\beta$ -carotene loss than maltodextrin-sugar systems (Figure 30). Interestingly, the rate decreased with decreasing DE value, which showed that  $\beta$ -carotene was protected by the increase in wall thickness and increased pore size of the M40 and M100 systems (Harnkarnsujarit *et al.*, 2012a). A similar effect of maltodextrin DE on  $\beta$ -carotene stability was previously demonstrated for spray-dried solids, which showed more rapid degradation of  $\beta$ -carotene in lower DE solids (Wagner and Warthesen, 1995; Desobry *et al.*, 1999). In the present study, the smaller average molecular weights gave higher unfrozen water contents at the freezing temperatures used, but also smaller pores left by ice crystals and thinner membranes (Harnkarnsujarit *et al.*, 2012a). Therefore, the freeze-dried structures could provide a larger surface and higher exposure of the carotene particles to oxygen and more rapid degradation was observed in glassy solids. The influence of DE on  $\beta$ -carotene stability was well correlated with the pore size and matrix microstructure.

Maltodextrin-sugar systems gave lower rate constants than plain maltodextrin matrices, but systems frozen at  $-80^{\circ}\text{C}$  showed a lower rate of degradation of  $\beta$ -carotene than systems frozen at  $-20^{\circ}\text{C}$  (Figure 31). This could result from partial flow of the unfrozen matrix during freeze-drying on the carotene particles

forming a protective coating. Such flow (partial collapse) could result from the high resistance of the dry layer to vapor flow and consequent increase of ice temperature and associated plasticization of the dry layer. Therefore, freezing at a lower temperature was beneficial to  $\beta$ -carotene stability in the freeze-dried solids containing sugars.

**Table 7** Brunauer-Emmet-Teller (BET) monolayer water content ( $m_m$ ) and critical water activity,  $a_w$ , which depressed the glass transition temperature,  $T_g$ , of freeze-dried solids to room temperature (24°C).

System	$m_m$ (g water/ 100g dried solids)	critical $a_w$
M040	4.57	0.822
M100	4.43	0.719
M250	3.47	0.482
M100 + Glucose	2.36	0.078
M100 + Fructose	2.59	0.001
M100 + Sucrose	2.55	0.267
M100 + Mixture	2.29	0.189

The first order rate constants for loss of  $\beta$ -carotene vs. pore size and wall thickness, as predicted by Harnkarnsujarit *et al.* (2012a) based on SEM images, are shown in Figure 32. The relationships showed that there was a critical pore diameter of 100  $\mu\text{m}$  corresponding to a wall thickness of 10  $\mu\text{m}$  below which the rate constant of  $\beta$ -carotene loss increased steeply with decreasing values. In addition, an increase in pore size gave a bigger void or solid inter-pore volume in which  $\beta$ -carotene could be dispersed. However, the lowest degradation rate occurred for M40 solids frozen at -80°C. Although the smallest pore size and thinnest walls were obtained in freezing at -80°C, the system showed the highest  $\beta$ -carotene stability. The high stability of  $\beta$ -carotene conformed to hardening of the solids (Harnkarnsujarit *et al.*, 2012a) resulting from partial collapse which could prevent oxygen permeation and diffusion through



the solids thus protecting  $\beta$ -carotene. This was also confirmed by the high retention of  $\beta$ -carotene in fully collapsed structures of maltodextrin-sugar systems. Our previous study also indicated that the collapsed structure of freeze-dried mangoes could enhance the stability of  $\beta$ -carotene during storage (Harnkarnsujarit and Charoenrein, 2011b). The structural collapse as well as the surface hardening gave a dense surface structure which prevented oxygen penetration through solids and effectively protected  $\beta$ -carotene from exposure to oxygen thus enhancing the stability of dispersed  $\beta$ -carotene.

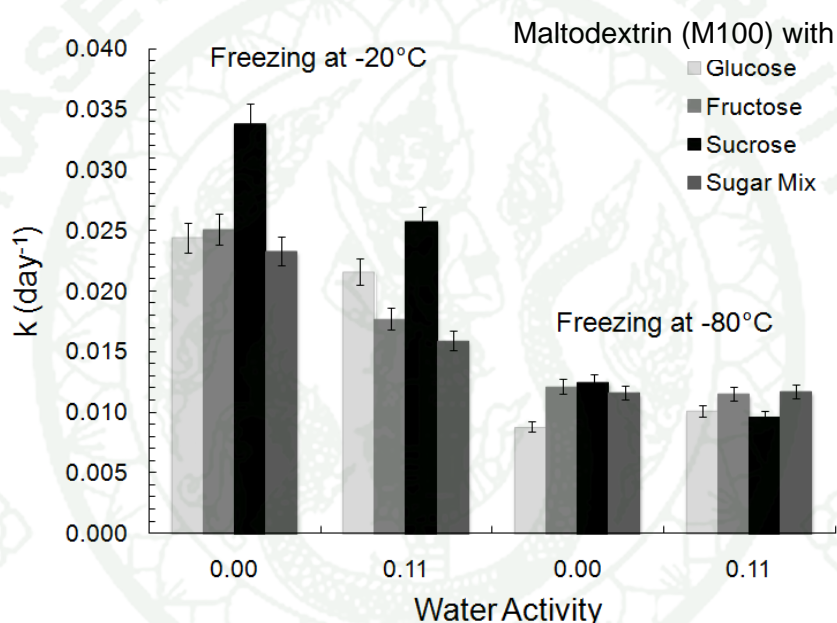


**Figure 31** First-order rate constants ( $k$ ) of  $\beta$ -carotene degradation in freeze-dried maltodextrin-sugar systems (glucose, fructose, sucrose and sugar mixture (glucose: fructose: sucrose; 1:1:4) (M100: sugars; 1:1) prefrozen at  $-20^{\circ}\text{C}$  and  $-80^{\circ}\text{C}$  prior to freeze-drying and stored at  $24^{\circ}\text{C}$  in anhydrous condition and  $0.11a_w$ . The experimental values expressed with 95% confidential intervals. The prefreezing at  $-20^{\circ}\text{C}$  and  $-80^{\circ}\text{C}$  resulted in porous and collapsed structures of freeze-dried maltodextrin-sugar solids, respectively. The lower rate constants were observed in systems prefreezing  $-80^{\circ}\text{C}$  corresponding to collapsed structures of freeze-dried solids.

A comparison of  $\beta$ -carotene loss in the M100 maltodextrin and maltodextrin-sugar systems showed that the highest  $\beta$ -carotene loss rate was in M100 systems frozen at  $-80^{\circ}\text{C}$  followed by the M100 systems frozen at  $-20^{\circ}\text{C}$  which was coincident with the porosity of freeze-dried solids. The presence of sugars (glucose, fructose and sucrose) gave smaller pores and thinner membrane walls to systems frozen at  $-20^{\circ}\text{C}$  (Harnkarnsujarit *et al.*, 2012a). These results suggested that the glass formation by small sugars was more effective in enhancing the stability of  $\beta$ -carotene in freeze-dried systems than the use of larger molecular weight maltodextrins. A corresponding  $\beta$ -carotene loss rate was found for glucose and fructose systems whereas sucrose gave a higher rate which was coincident with the smallest pore size and thinnest membrane walls of the maltodextrin-sucrose system. In contrast, glucose and fructose systems had a larger and similar pore size and membrane thickness (Harnkarnsujarit *et al.*, 2012a).

The  $T_g$  values indicated that all freeze-dried maltodextrin systems up to  $0.44a_w$  were in the glassy state (Table 6). Therefore, in maltodextrin systems water induced structural changes, including collapse during storage, were negligible. Figure 30 shows the rate constant of  $\beta$ -carotene loss in maltodextrin solids as a function of storage conditions after humidification to varying  $a_w$  at room temperature. The results clearly demonstrated a high rate constant for the ‘anhydrous’ systems, a decrease in rate constant towards the monolayer value (Table 7), followed by an increasing rate constant at the higher water activity. This loss of  $\beta$ -carotene occurred in glassy freeze-dried solids, i.e., below the  $T_g$ , and the loss of  $\beta$ -carotene could be accounted for the diffusion and presence of oxygen within the freeze-dried solids. We may also assume that the free volume of the larger molecular (low DE) maltodextrins was higher than the free volume of the higher DE maltodextrin and maltodextrin-sugar systems that showed lower rates of  $\beta$ -carotene loss.

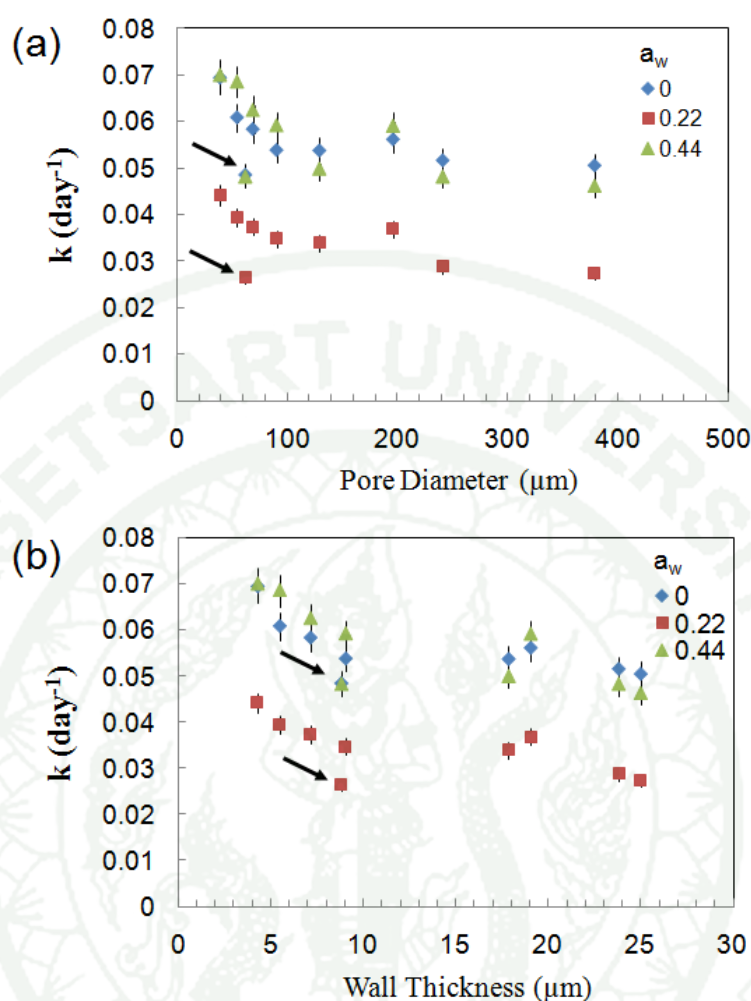


**Figure 32** First-order rate constants ( $k$ ) of  $\beta$ -carotene degradation in freeze-dried maltodextrin systems (prefreezing at  $-20^\circ\text{C}$ ,  $-40^\circ\text{C}$  and  $-80^\circ\text{C}$ ) as functions of (a) solid pore diameter and (b) wall thickness stored at anhydrous condition, 0.22 and 0.44 $a_w$  at  $24^\circ\text{C}$ . The various pore size and wall thickness of solids resulted from the various prefreezing condition prior to freeze-drying. Pore diameter and wall thickness of freeze-dried solids were obtained from the analysis of SEM micrographs as described by Harnkarnsujarit *et al.* (2012a). The experimental values expressed with 95% confidential intervals. Arrows indicate data of the surface hardening solids (M40 prefrozen at  $-80^\circ\text{C}$ ) resulting from the crust formation during freeze-drying which contributed to the highest stability of  $\beta$ -carotene in freeze-dried solids.

The loss of  $\beta$ -carotene showed a minimum for all systems at around 0.22  $a_w$  which showed that the glass transition of the host matrix at low  $a_w$  was not the main factor controlling the loss of  $\beta$ -carotene. At the  $a_w$  which showed the maximum  $\beta$ -carotene loss, most maltodextrin-sugar systems were above the  $T_g$  during storage. The maltodextrin-fructose and maltodextrin-sugar mixture (glucose: fructose: sucrose in the ratio of 1:1:4) systems showed the lowest rates for  $\beta$ -carotene loss and were followed by glucose. Fructose and glucose systems at most  $a_w$  values were stored above the  $T_g$  of the matrix which could allow viscous flow of the sugars and enhance  $\beta$ -carotene protection. The high stability of  $\beta$ -carotene in the maltodextrin-sugar system could have resulted from differences in freezing properties at  $-20^\circ\text{C}$  prior to freeze-drying. The results confirmed that water enhanced  $\beta$ -carotene stability in dehydrated systems at low  $a_w$ . Earlier studies have attributed similar findings to the hydration of metal ions which decreased the efficacy to catalyze the oxidation of  $\beta$ -carotene and the hydrogen bond formation of peroxides slowing the chain reaction (Labuza *et al.*, 1972). The increased degradation from 0.22 to 0.44 $a_w$  was due to the increased mobility of the catalysts (Labuza *et al.*, 1972). The results indicated that a hydration layer initially formed on the solid surfaces and protected  $\beta$ -carotene against oxidation until mobility increased to accelerate degradation.

Maltodextrin-sucrose systems showed the highest loss of  $\beta$ -carotene during storage up to 0.44 $a_w$ . This was caused by the smaller pore size of the solid structure of freeze-dried sucrose systems which increased exposure of  $\beta$ -carotene particles to oxygen. Glucose, fructose and the sugar mixture systems had larger pore sizes (Harnkarnsujarit *et al.*, 2012a) and a better stability for  $\beta$ -carotene. However, as storage  $a_w$  was increased to 0.66 $a_w$ , fructose systems showed the highest loss rate. Maltodextrin-fructose systems had the lowest  $T_g$  and showed the highest increase in the rate of  $\beta$ -carotene loss at high  $a_w$ . This could be accounted for the rapid decrease in structural relaxation times and enhanced diffusion. At high  $a_w$ , the crystallization of sugars could also expel the dispersed  $\beta$ -carotene causing exposure to oxygen and increased loss of  $\beta$ -carotene. These results reflected that stability of  $\beta$ -carotene at high  $a_w$  was dependent on the glass transition, diffusion and structural changes of solids rather than the freeze-dried structure. The increased rate of  $\beta$ -carotene loss was found



in all systems stored above  $T_g$  (Figure 29). As humidity plasticized the solids to above the glass transition, the molecular mobility within the solids increased which could accelerate diffusion and chemical reactions as well as crystallization of sugars and structural collapse of solids.

The results were in agreement with the hypothesis that the stability of dispersed crystalline  $\beta$ -carotene in freeze-dried solids was strongly dependent on the matrix microstructure and water activity. The pore microstructure namely pore size and wall thickness affected the diffusion and permeation of oxygen through solids which subsequently impact the stability of  $\beta$ -carotene. The results also confirmed that the structural collapse of glassy solids effectively stabilized  $\beta$ -carotene during storage. Moreover, water activity affected the rate of  $\beta$ -carotene degradation as a result of the increased molecular mobility above  $T_g$ .

## **5. Structural effects on stability of dispersed $\beta$ -carotene emulsion in freeze-dried maltodextrin systems**

The previous part investigated the stability of dispersed  $\beta$ -carotene as crystalline type in freeze-dried materials. In this part,  $\beta$ -carotene crystals were dissolved in sun-flower oil and prepared as emulsion systems prior to disperse into the carbohydrate systems to form non-crystalline type of  $\beta$ -carotene as found in mangoes. Therefore, other factors, i.e., stability of the emulsion droplets were also investigated.

### **5.1 Stability of frozen emulsion**

The freezing profile of frozen agar gels containing emulsion and maltodextrin (M40, M100 and M250) are shown in Figure 33. The presence of dispersed oil (8%w/w) in maltodextrin-agar gave a similar freezing profile as non-dispersed oil systems which indicated the key role of hydrophilic phase component on the freezing properties of bulk systems. The initial slope indicated the cooling rates affecting the rate of nucleation of water molecules which were insignificantly different for the systems at each freezing temperature. As expected, faster cooling

rates and shorter freezing times were found at the lower freezing temperatures in agreement with our previous study (Harnkarnsujarit *et al.*, 2012a).

Samples of the frozen emulsions were thawed and immediately measured for particle size distributions and compared with those of fresh emulsions. The results showed that freezing significantly increased the size of oil particles in maltodextrin-emulsion systems (Figure 34). Low temperature freezing at  $-40^{\circ}\text{C}$  and  $-80^{\circ}\text{C}$ , gave similar particle size distributions and the particles were larger than in freezing at  $-20^{\circ}\text{C}$  for M100 and M250 systems. M40 systems showed a significant difference in freezing behavior and provided with similar particle sizes at various freezing temperatures. This emphasized the effect of maltodextrin DE on the freezing point depression and the onset of ice melting at the maximally freeze-concentrated state,  $T_m'$ . M40 systems had the highest  $T_m'$  and could become frozen and maximally freeze-concentrated at a higher temperature. Maximum freezing at a higher temperature supported the liquid state of the sunflower oil which was found to reduce destabilization in freeze-thaw cycling of emulsions (Cornacchia and Roos, 2011a). Freezing of M100 and M250 systems at  $-40^{\circ}\text{C}$  and  $-80^{\circ}\text{C}$  produced the maximally freeze-concentrated state at a lower temperature concomitantly to possible crystallization of the lipid phase which could promote emulsion destabilization in the freeze-thaw processes. These results suggest that freezing conditions of delivery systems with sensitive bioactive components need to be optimized using data on component effects on the freezing of water and lipid crystallization. In agreement with this conclusion, the higher DE maltodextrins maintained smaller particle sizes at  $-20^{\circ}\text{C}$  freezing. Mun *et al.* (2011) also found less stable emulsion droplets in systems containing lower DE of maltodextrins. Depending on the freezing conditions, droplet aggregation by the depletion attraction caused by the non-adsorbed free molecules in the aqueous phase may also increase emulsion destabilisation. Attractive forces have been reported to be proportionate to the molecular weight of the free molecules (Klinkesorn *et al.*, 2004; Mun *et al.*, 2011; McClements, 2004). Consequently, the highest DE of M250 system could show least depletion flocculation at  $-20^{\circ}\text{C}$  where it was also the least freeze-concentrated system. The ice formation during freezing concentrated the oil particles and forced them into closed proximity with one another

in the freeze-concentrated solids phase (Ghosh and Coupland, 2008). M250 system with the lowest average molecular weight and  $T_m'$  (Figure 33) had the highest unfrozen water content and most reduced tendency for emulsion droplets adhesion. Upon freezing at  $-20^\circ\text{C}$  the  $T_m'$  of M40 was lower than  $T_m'$  which could result in maximum ice formation and increased aggregation of oil droplets as compared to the M100 and M250 systems.

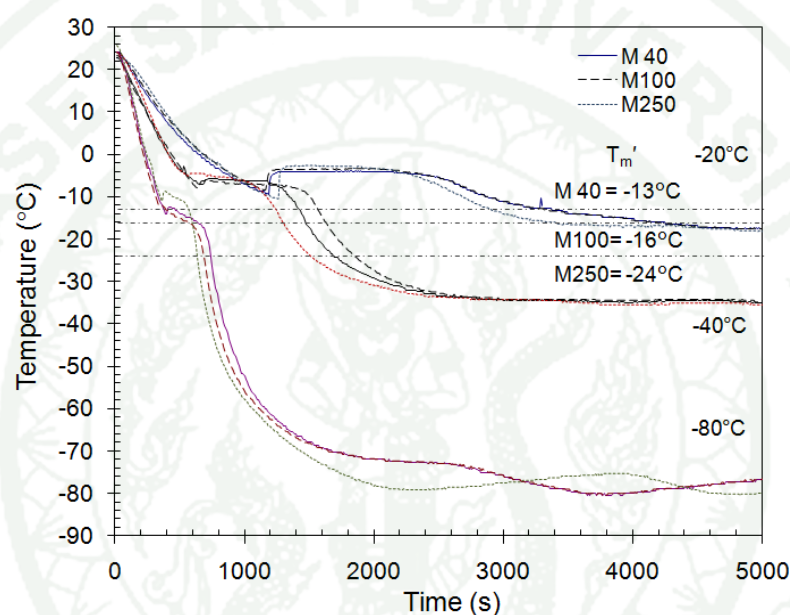


**Figure 33** Freezing profile of maltodextrin-agar gels containing dispersed emulsion of  $\beta$ -carotene at freezing temperature of  $-20^\circ\text{C}$ ,  $-40^\circ\text{C}$  and  $-80^\circ\text{C}$  with corresponding onset of ice melting temperature ( $T_m'$ ) of maltodextrin systems (dotted lines). Gel temperature during freezing was insignificant different among maltodextrin type (M40:DE6, M100:DE11 and M250:DE25.5). As initial slope refers to the cooling rate, the lower temperature freezing gave faster cooling rate and faster water nucleation as discussed by Harnkarnsujarit *et al.* (2012a).

Although the small ice crystals formed by rapid freezing could reduce emulsion destabilisation, the results showed an increased size of emulsion droplets at low temperature freezing (Figure 34). The  $T_g'$  and  $T_m'$  as reported by Roos and Karel

(1991e) and Harnkarnsujarit *et al.* (2012a) for freezing at  $-40^{\circ}\text{C}$  and  $-80^{\circ}\text{C}$  were higher and could support maximum freeze-concentration. This was a primary cause for the increased size of oil particles and it also coincided with the crystallization of the surfactant and lipid particles that all could rupture interphases and cause emulsion destabilization. Cornacchia and Roos (2011) reported the major crystallization of sunflower oil to occur between around  $-50^{\circ}\text{C}$ . In M100 and M250 systems freezing at  $-40^{\circ}\text{C}$  and  $-80^{\circ}\text{C}$  could cause the lipid crystallization and destabilisation by the disruption of the interfacial membranes leading to the formation of lipid bridges and aggregation of particles particularly as the fat melted upon thawing (Vanapalli *et al.*, 2002; Cramp *et al.*, 2004; Thanasukarn *et al.*, 2004; Ghosh and Coupland, 2008; Cornacchia and Roos, 2011).

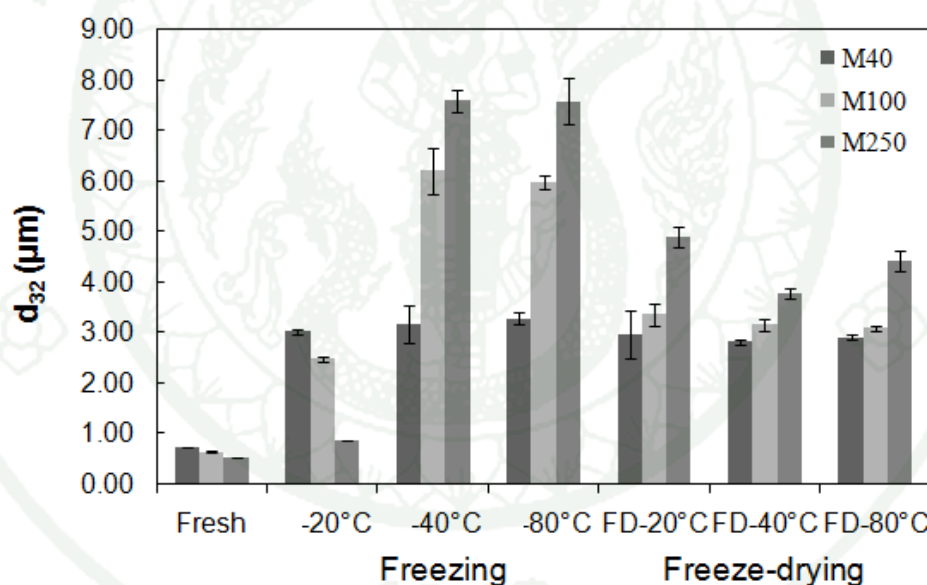


**Figure 34** Influence of freezing at  $-20^{\circ}\text{C}$ ,  $-40^{\circ}\text{C}$  and  $-80^{\circ}\text{C}$ , and freeze-drying (FD) on average particle size  $d_{32}$  of  $\beta$ -carotene emulsion in various maltodextrin solids (M40:DE6, M100:DE11 and M250:DE25.5). Low temperature freezing ( $-40^{\circ}\text{C}$  and  $-80^{\circ}\text{C}$ ) could cause lipid solidification and led to coalescence upon thawing; however, M40 effectively stabilize  $\beta$ -carotene emulsion upon freezing.



## 5.2 Freeze-dried emulsions

The hydrophilic components of maltodextrins formed solid matrices in freezing and contained dispersed emulsion particles after freeze-drying. Figure 35 shows the appearance of freeze-dried emulsions containing maltodextrin solids during storage at 0.75  $a_w$  at room temperature. No changes in visual appearance were found during storage at 0 and 0.33  $a_w$  as the glassy state of the maltodextrins was maintained. Water plasticization depressed the  $T_g$  by increasing the free volume which led to structural changes as a result of viscous flow above the  $T_g$ . Structural collapse was found in M100 and M250 during storage at 0.75 $a_w$ . The results were in agreement with the previous findings which indicated the higher rate of the structural collapse with increasing  $T-T_g$  (Levi and Karel, 1995; Prado *et al.*, 2006).

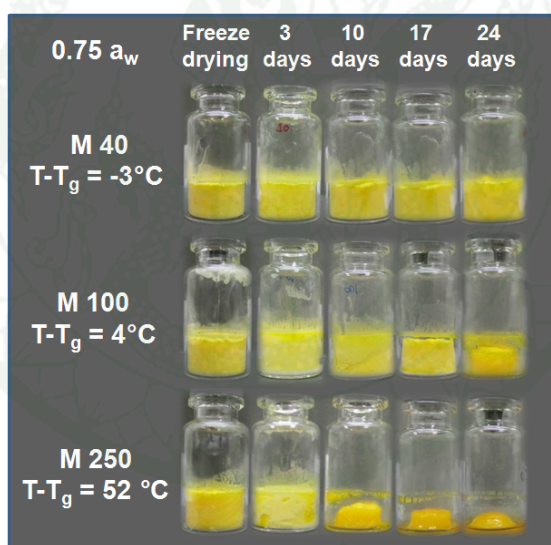


**Figure 35** Appearance of freeze-dried  $\beta$ -carotene emulsions after freeze-drying and subsequent storage for 24 days at 0.75 $a_w$  at room temperature (24°C) with the corresponding  $T-T_g$  values referring to the difference between storage temperature and glass transition temperature. Various prefreezing temperatures gave similar results. All systems showed no structural changes during storage at anhydrous and 0.33 $a_w$  with the corresponding glassy state of maltodextrin solids. The results indicated the higher degree of solid flow and subsequent structural collapse as increased  $T-T_g$ .

M100 and M250 stored at  $0.75a_w$  had the largest particle sizes exceeding significantly those of solids stored at anhydrous and  $0.33a_w$  conditions (Figure 36). The increased particle sizes of droplets were due to structural collapse and appearance of liquid properties allowing separation of the hydrophilic and hydrophobic phases. M250 systems showed the largest lipid particle size which was coincident with the lowest  $T_g$  of the systems and hence the highest  $T-T_g$  during storage. Conversely, emulsion destabilization was not present in systems stored in the glassy state.

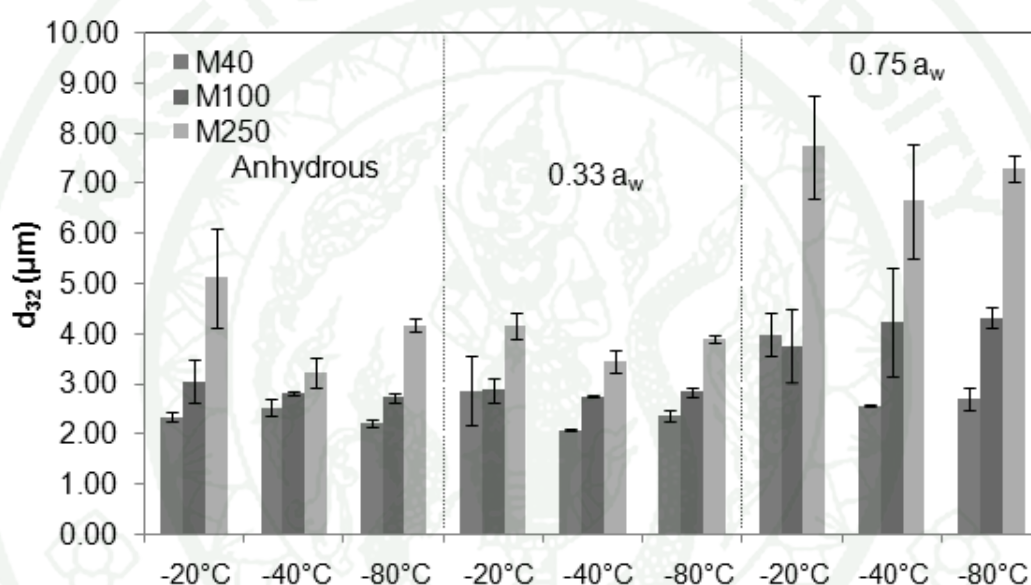


**Figure 36** Average particle size  $d_{32}$  of  $\beta$ -carotene emulsion in various freeze-dried maltodextrin solids (M40:DE6, M100:DE11 and M250:DE25.5) prefrozen at  $-20^\circ\text{C}$ ,  $-40^\circ\text{C}$  and  $-80^\circ\text{C}$  prior to freeze-drying and storage under anhydrous,  $0.33$  and  $0.75a_w$  at room temperature ( $24^\circ\text{C}$ ) for 24 days. Insignificant change of particle size was observed during storage of solids kept in the glassy state ( $T < T_g$ ) except M40 frozen at  $-20^\circ\text{C}$  and stored at  $0.75a_w$  which corresponded to the very low  $T-T_g$  ( $3^\circ\text{C}$ ) and the largest pore left by larger ice crystals (see text). M100 and M250 systems stored at  $0.75a_w$  exceeded the  $T_g$  of solids which caused the flow and resulted in increased average particle size. The particle size distributions are shown in Appendix Figure 12)

### 5.3 $\beta$ -carotene in freeze-dried solids

Stability of noncrystalline  $\beta$ -carotene in freeze-dried maltodextrin-agar systems prefrozen at  $-20^{\circ}\text{C}$ ,  $-40^{\circ}\text{C}$  and  $-80^{\circ}\text{C}$  prior to freeze-drying was monitored during storage at anhydrous, 0.33 and 0.75 $a_w$  conditions using HPLC. The mobile phase and stationary phase of  $\text{C}_{30}$  column used in our study were reported to effectively separate the isomers of  $\beta$ -carotene (Liu *et al.* 2009). However, only a single peak of all-trans- $\beta$ -carotene was found in the HPLC chromatograms which suggested that the isomerization of  $\beta$ -carotene was negligible. The mechanism of  $\beta$ -carotene degradation has been extensively reviewed by previous researchers (Britton, 1995; Gregory III, 2007; Boon *et al.*, 2010). Generally, various factors during food processing and storage, e.g., heat, acid, light, oxygen, metal ions, accelerate oxidation and isomerization of carotenoids leading to the degradation and loss of bioavailability (Britton, 1995; Gregory III, 2007). Autoxidation is known as the major cause of carotenoid losses in dehydrated foods.

To describe the degradation rate of  $\beta$ -carotene during storage, the first-order kinetics was fitted to the experimental data as previously reported for dehydrated fruits and model systems stored at various temperatures ( $20$ - $60^{\circ}\text{C}$ ) and humidities ( $0$ - $0.8a_w$ ) (Prado *et al.*, 2006; Koca *et al.*, 2007; Lavelli *et al.* 2007; Ferreira and Rodriguez-Amaya, 2008; Harnkarnsujarit and Charoenrein, 2011a,b; Ramoneda *et al.*, 2011; Harnkarnsujarit *et al.*, 2012b). The degradation rate of  $\beta$ -carotene in M40 and M100 systems was found to be dependent on the freezing temperature with a clear difference between  $-20^{\circ}\text{C}$  and  $-80^{\circ}\text{C}$  (Figure 38). Our previous study discussed that the lower temperature freezing gave a faster cooling rate and water nucleation which led to smaller pores and thinner wall membranes of freeze-dried maltodextrin-agar solids (Harnkarnsujarit *et al.*, 2012a). This gave a higher  $\beta$ -carotene degradation rate in M40 and M100 solids (Figure 38). The high amount of small pores with corresponding thinner spaces between voids locating solids and entrapped lipids gave higher surface area and oxygen exposure of  $\beta$ -carotene could be reduced. This presumably increased accessibility of oxygen and accelerated degradation of  $\beta$ -carotene (Harnkarnsujarit *et al.*, 2012b). However, the stability of  $\beta$ -carotene in M250

systems was independent on prefreezing conditions. The lowest rate constants for  $\beta$ -carotene loss were found in M250 systems at all freezing and storage conditions. This was accounted for the partial flow or structural collapse during freeze-drying of M250 solids at all freezing conditions (Figure 37). Our previous data (Part 3) showed a non-collapse structure of M250 solids underwent identical prefreezing and freeze-drying conditions; however, the existing of the lipid components resulted in the structural collapse. The hydrophobic lipid particles possibly hinder the vapor diffusion through unfrozen matrix during sublimation which accelerated the structural collapse. The structural collapse of glassy solids has been reported to effectively enhance the stability of dispersed crystalline  $\beta$ -carotene as well as oil-dissolved  $\beta$ -carotene in freeze-dried mangoes by prevention of oxygen permeation through the collapsed solids (Harnkarnsujarit and Charoenrein, 2011b; Harnkarnsujarit *et al.*, 2012b).

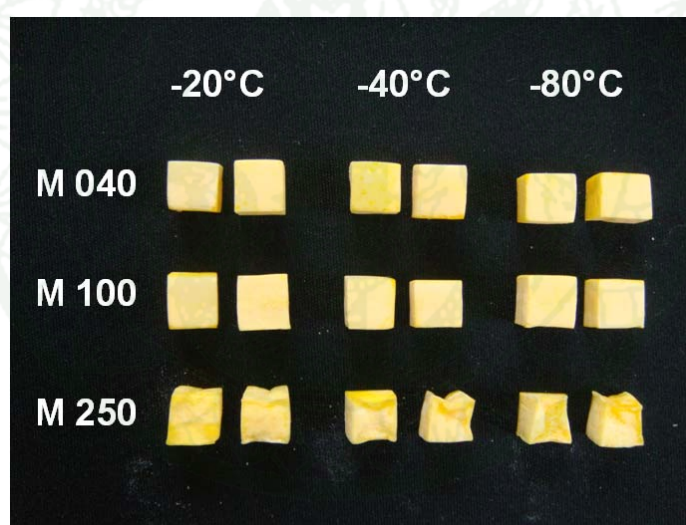


**Figure 37** Appearance of freeze-dried agar-maltodextrin (M040, M100 and M250) solids containing dispersed oil-dissolved  $\beta$ -carotene particles pre-frozen at  $-20^{\circ}\text{C}$ ,  $-40^{\circ}\text{C}$  and  $-80^{\circ}\text{C}$  prior to freeze-drying. The M250 solids clearly show the structural collapse during freeze-drying at all prefreezing conditions which corresponded to the highest  $\beta$ -carotene stability.



M250 and M100 systems stored at  $0.75a_w$  also showed flow of solids plasticized to above  $T_g$  and the structural collapsed was apparent with increased emulsion destabilization and size of oil particles during storage (Figure 35 and 36) which led to lower  $\beta$ -carotene degradation rate. The results agree with Prado *et al.* (2006) who reported a lower degradation rate of oil-solubilized  $\beta$ -carotene in polyvinylpyrrolidone (PVP-40) matrices as humidity increased and the highest retention was found in systems with fully collapsed matrix. Similarly, Selim *et al.* (2000) and Serris and Biliaderis (2001) also observed the highest retention of saffron and beetroot pigments in systems stored at high  $a_w$  at which full collapse of structures of matrices occurred. As water plasticized encapsulant matrices and led to viscous flow and structural collapse, the reduction of matrix micropores and dense structure effectively controlled the amount and rate of oxygen transport through solids giving a higher retention of  $\beta$ -carotene (Selim *et al.* (2000) and Serris and Biliaderis, 2001; Prado *et al.*, 2006). Conversely, Ramoneda *et al.* (2011) demonstrated increased degradation rate of  $\beta$ -carotene emulsion encapsulated in maltodextrin solids with increasing  $a_w$  and the fully plasticized and collapsed matrices gave the highest degradation. The emulsifier effects on  $\beta$ -carotene retention in maltodextrin solids were also reported. Gelatin gave a faster degradation rate than non-emulsifier and gum arabic systems, respectively (Ramoneda *et al.*, 2011). Various solid components, however, gave diverse results which possibly caused by the oxygen water solubility (Whitcombe *et al.*, 2005) and the emulsion stability, i.e., oil droplet size during storage at high humidities.

However, the relationship between the stability of  $\beta$ -carotene and size of emulsion droplets dispersed in dehydrated solids stored at various  $a_w$  has not yet been established. The present study showed that the lowest  $\beta$ -carotene degradation rate of M250 systems at  $0.75a_w$  was coincident with the largest size of lipid particles (Figure 36). Several studies indicated the effect of oil droplet size on the stability of dispersed  $\beta$ -carotene emulsions (Tan and Nakajima, 2005; Qian *et al.*, 2012). Qian *et al.* (2012) reported higher stability of  $\beta$ -carotene nanoemulsion with  $\beta$ -lactoglobulin than Tween 20 stabilised which was possibly due to the larger size of oil particles (80 and 60 nm, respectively after 15 days of storage at  $37^\circ\text{C}$ ). This confirmed the previous finding by

Tan and Nakajima (2005) who observed increased stability of  $\beta$ -carotene nanoemulsion in systems with larger particle size ( $D_{43}$  ranging from 60-140 nm) prepared by various homogenizing conditions (pressure and cycle) after storage at 4°C for 12 weeks. Soottitantawat *et al.* (2005) also demonstrated higher retention as particle size of D-limonene increased in spray-dried powders which could have been explained by the surface area to expose and react with oxygen. The higher  $\beta$ -carotene degradation in small dispersed lipid size systems was contributed to the higher effective surface area between  $\beta$ -carotene particles and the environments. The results indicated that coalescence of lipid particle during storage above  $T_g$  increased the size of emulsion droplets which decreased surface area for oxygen exposure and subsequently increased  $\beta$ -carotene stability. Similarly, M100 systems had similar rate constants between storage at anhydrous and 0.33 $a_w$  whereas, lower degradation was observed at 0.75 $a_w$  which was coincident with the flow of solids and subsequent increase of droplet size.

M40 gave lower  $\beta$ -carotene degradation than M100 systems stored at anhydrous and 0.33 $a_w$ . The stabilizing effect of M40 was also found in the frozen emulsion that underwent freezing at various temperatures (Figure 34). Non-polar part of emulsifiers on droplet interphase can be incorporated into the helical coils formed by maltodextrin in the emulsion systems (Mun *et al.*, 2011); therefore, it could stabilize emulsion droplets upon freeze-thawing. Upon water removal, this structure formed might physically protect  $\beta$ -carotene against reactive oxygen species during storage. In addition, the higher average molecular weight of M40 also gave a larger pore size and membrane thickness which led to a less oxygen expose to dispersed  $\beta$ -carotene particles as described by Harnkarnsujarit *et al.* (2012b). In the glassy solids, the gaseous oxygen highly diffused through solids and expose to  $\beta$ -carotene particles located at the pore surface. Therefore, a smaller pore size and hence a larger surface area of  $\beta$ -carotene expose to oxygen leads to an increased degradation; whereas,  $\beta$ -carotene particles dispersed in the solids membrane were more effectively protected. The present study also shows a higher stability of oil-dissolved  $\beta$ -carotene than the crystalline  $\beta$ -carotene particles reported by Harnkarnsujarit *et al.* (2012b). The results indicated that the oil droplets also give a protection to  $\beta$ -carotene. The oxygen need to

diffuse through the oil particles to interact with  $\beta$ -carotene locating at the core of the lipid droplets and, therefore, retards the degradation. In addition, the sunflower oil dissolving  $\beta$ -carotene contains the antioxidant components such as tocopherols which potentially interact and terminate the radicals formed in the lipid droplets which subsequently increase  $\beta$ -carotene stability.

The present study showed a decrease of  $\beta$ -carotene degradation rate as  $a_w$  increased. Oxidation is the main factor accelerates  $\beta$ -carotene loss in freeze-dried solids as mentioned above. The results could have been agreed well with the classical food stability map showing the oxidative reaction of food established by Labuza *et al.* (1972). They demonstrated that the oxidation rate decreased towards monolayer value which was caused by various factors. First, the hydration of transition metals particularly cation rendering them less active promoters of autoxidation. Second, lipid hydroperoxides move to oil-water boundaries and are taken out of the propagation reactions due to hydrogen bonding with water. Third, the free radical termination reactions increase as polar radicals congregate at the oil-water interface (Labuza *et al.*, 1972). As a result, the intermediate moisture food exhibits higher stability against oxidation. They also suggested that from  $a_w$  0.4-0.7, lipid oxidation rate increases again owing to the increased mobility of transition metal cations and the reduction of viscosity (Labuza *et al.*, 1972). However, the further increased of  $a_w$  above 0.7 contributes to reduced degradation because of the dilution of reacting species (Labuza *et al.*, 1972; Nelson and Labuza, 1994). In addition, the greatest stability to oxidation has been extensively observed at high  $a_w$  at which solids were in the rubbery state and structural collapse or flow occurred which prevented oxygen diffusion through the matrix (Nelson and Labuza, 1994). Therefore, the rate of  $\beta$ -carotene degradation could have been explained as a result of oxidative reaction with the relative high value within the glassy state particularly anhydrous condition. The results indicated that not only the structural collapse of the rubbery systems but also the increased size of lipid particles as well as thicker encapsulate matrix membranes could effectively enhance the stability of dispersed  $\beta$ -carotene in freeze-dried solids.

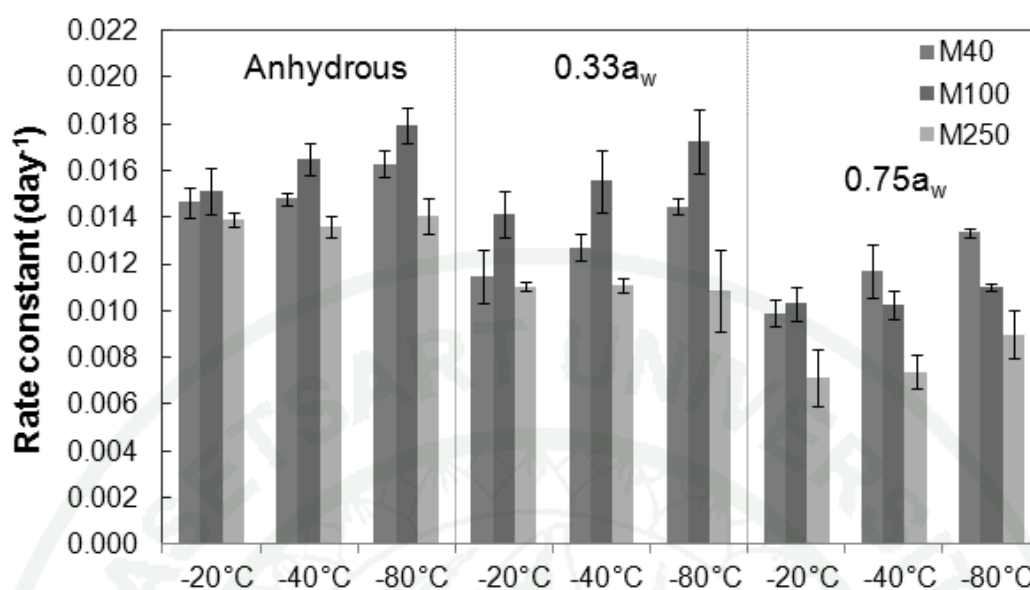


**Figure 38** First-order rate constants for  $\beta$ -carotene degradation in freeze-dried maltodextrin systems stored at anhydrous, 0.33 and 0.75a<sub>w</sub> condition. Systems were prefrozen at -20°C, -40°C and -80°C prior to freeze-drying and stored at room temperature (24°C). The structural collapse during freeze-drying was observed in M250 systems at all prefreezing conditions corresponding to the lowest degradation during storage at anhydrous and 0.33a<sub>w</sub>. M100 and M250 stored at 0.75a<sub>w</sub> also showed significant reduction for the rate of  $\beta$ -carotene loss which was coincident with the largest emulsion particle size in freeze-dried solids.

The results confirmed that the matrix microstructure affected the rate of  $\beta$ -carotene degradation in freeze-dried systems. The increased a<sub>w</sub>, however, increased the stability of  $\beta$ -carotene as a result of the increased size of lipid particle containing  $\beta$ -carotene which reduced the effective surface area for  $\beta$ -carotene to oxygen exposure. This was in agreement with the hypothesis that the size of dispersed lipids also affected the stability of dispersed  $\beta$ -carotene in freeze-dried systems.



## Overall Discussion

This part aimed to discuss the overall data from the previous 5 parts of the results and discussion including the microstructure formation of freeze-dried solids and consequently impact on  $\beta$ -carotene stability during storage. In addition, the effect of water activity on  $\beta$ -carotene degradation is also discussed in both mango and model sugar-maltodextrin systems.

The model systems of sugar-maltodextrin mixtures contained agar to form the semi-solid gels which mimics fruit type structure. Fresh mangoes and model gel systems were comparable in terms of:

- (i) Moisture contents which were approximately 80-85% and 80%w/w for mangoes and model systems, respectively.
- (ii) Solids contents which were approximately 15-20% and 20%w/w for mangoes and model systems, respectively.
- (iii) Texture of the fresh systems by a similar firmness of approximately 6 and 7 N for the mango pulp (Owcharoen, 2012) and the model gels, respectively.
- (iv) As fruits contain high amount of polysaccharide, the semi-solid structure of the model systems was formed with a polysaccharide of agar.

### 1. Microstructure formation of freeze-dried solids

Freeze-drying consists of freezing and sublimation under reduced pressure. Once the ice is removed during sublimation, the pores are left embedding in the solids. The present study shows various factors affecting the ice formation (Part 3) as depicted in Figure 39. The water nucleation and ice growth affect the ice morphology and subsequently impact the pore morphology of freeze-dried materials (Petzold and Aguilera, 2009; Harnkarnsujarit *et al.*, 2012a). However, the structural collapse can occur during freeze-drying as a result of the ice melting which is accelerated by various factors including freeze-drying temperature, solid components and ice crystal size (Figure 39).

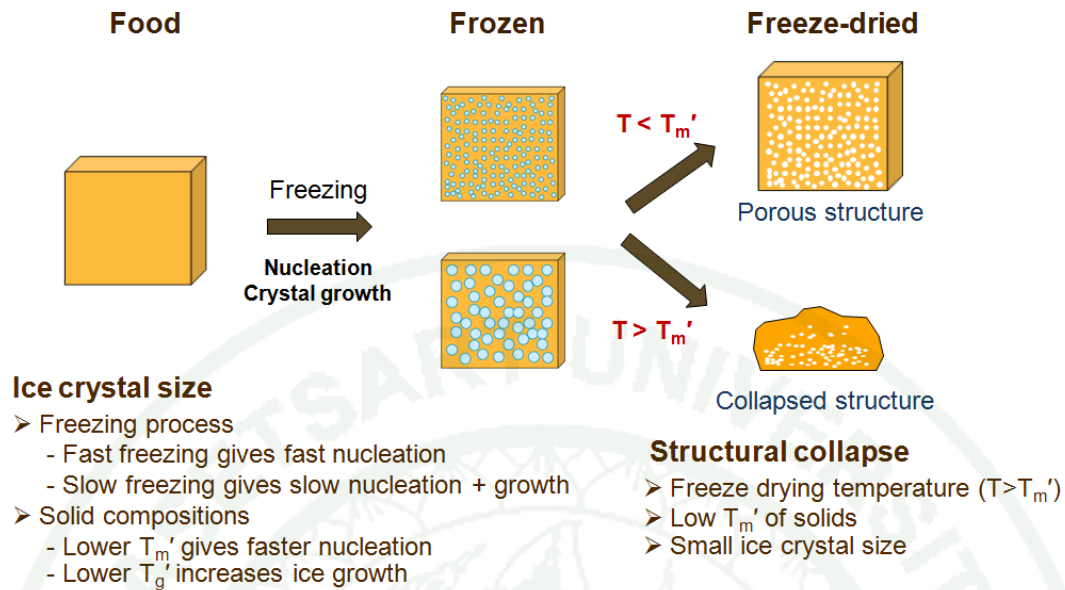


**Figure 39** Schematic diagram shows the microstructure formation (porous and collapsed structure) of freeze-dried solids as reflected by the process parameters (freezing and freeze-drying) and solid components. The nucleation and growth during freezing control the ice morphology which subsequently reflects the pore structure of freeze-dried solids. Moreover, the ice temperature exceed the onset of ice melting temperature  $T_m'$  accelerate the structural collapse during freeze-drying.

The factors influencing the pore morphology of freeze-dried solids as reflected by the ice crystal formed during freezing include:

(i) The freezing process

The freezing temperature controls the rate of water nucleation as well as the ice growth. The results indicated that the lower temperature freezing gave a faster cooling rate as clearly shown in the freezing profile (Part 3). Consequently, a faster rate of water nucleation and a limited time of crystal growth resulted in a high number of small ice crystal formed during freezing. In contrast, the higher freezing temperature gives a slower cooling rate and hence a slower water nucleation. Moreover, the higher freezing temperature also increases the time for the ice growth

during freezing and formed a small number of large ice crystal size. The results were in agreement with the previous findings in various freeze-dried polymer systems indicating a faster cooling rate giving a smaller pore size of freeze-dried systems (Shapiro and Cohen, 1997; Kang *et al.*, 1999; Van Vlierberghe *et al.*, 2007).

Moreover, the crust formation was also observed in mangoes prefrozen by immersion in liquid nitrogen which suggested a very rapid freezing. The hard crust formed during initial freezing consequently gave the cracking on mango surface as a result of the internal expansion once the internal portion underwent phase change (Part 2). The hard crust was also observed in model gel systems with a large molecular weight solutes (M40) prefrozen at  $-80^{\circ}\text{C}$ . The highest amount of freezable water in M40 systems conformed to the hard crust formation which was also indicated by the highest mechanical strength against compression (Part 3). Once a very fast freezing is applied to the gel systems, the water rapidly move to the gel surface which causes the shrinkage at the surface and contributes to the crust formation (Scherer, 1993).

#### (ii) The solid compositions

The results showed the effect of solid components on the pore size of freeze-dried solids in 2 directions. First, the components affect the nucleation and growth of the ice during freezing. The results showed that the small molecular weight sugars (glucose, fructose and sucrose) decreased the pore size of freeze-dried systems by controlling the nucleation and ice growth. Sugars with a low  $T_m'$  give a fast nucleation and hence formed a high number of ice nuclei; whereas, a low  $T_g'$  of solids increases the ice growth which reflected the pore morphology of freeze-dried solids. The results clearly indicate the  $T_g'$  and  $T_m'$  dependent on the ice formation during freezing.

Second, the molecular weight of solutes influences the pore size and wall thickness of freeze-dried solids as caused by the amount of unfrozen water. Higher molecular weight solutes contribute to lower amount of unfrozen water giving a larger

ice crystal formed and hence a larger solid pore size. At the same freezing temperature, the results revealed the largest pore size in M40 systems followed by M100 and M250, respectively.

The structural collapse during freeze-drying occurs once the ice temperature exceeds the  $T_m'$  (Roos, 1997) as shown in Figure 39. The ice melting plasticized food matrix and decreased solid viscosity to well below  $10^7$  to  $10^4$  Pa s which unable to support the gravimetric and capillary force of solids and allows for the structural collapse as reported by Bellows and King (1973). Various factors accelerating structural collapse during freeze-drying are previously reported in this research (Part 2 and 3).

(i) The freeze-drying temperature

The results clearly indicated the structural collapse in freeze-dried mangoes underwent freeze-drying above  $T_m'$  (Part 2). As a result of the ice melting, the structural collapse was observed with a big cavity embedded in solids reflecting the water evaporation rather than the entire sublimation. Moreover, the results also indicate a longer process time than the entire sublimation systems.

(ii)  $T_m'$  of solids

The solids  $T_m'$  also impact the magnitude of the structural collapsed (Part 3). Sugars depressed the  $T_m'$  of maltodextrin systems which showed the structural collapse as the freezing temperature decreased. Sucrose revealed a lower magnitude of the structural collapse than glucose and fructose systems frozen at  $-40^\circ\text{C}$  which corresponded to the highest  $T_m'$  of sucrose systems.



### (iii) The size of ice crystals

The results also suggested that a very fast freezing resulted in the structural collapse of solids during freeze-drying (Part 2 and 3). Mangoes prefrozen in liquid nitrogen not only showed the cracking but also the structural collapse. The very fine ice crystals formed during a very fast freezing retarded the vapor flow during sublimation which increases the pressure and temperature at the sublimation interface and accelerates the structural collapse. Moreover, the hard crust formed resulted from the fast freezing might hinder the vapor flow during sublimation. These findings were confirmed in the model gel systems (Part 3). The lower freezing temperature revealed a higher magnitude of structural collapse. Fully-collapsed was observed in systems frozen at  $-80^{\circ}\text{C}$ ; whereas, a least collapse with the existing pore structure were observed in sugar systems frozen at  $-20^{\circ}\text{C}$ .

## 2. The stability of $\beta$ -carotene in freeze-dried systems

### 2.1 The effect of freeze-dried solid microstructures

The results clearly show the microstructure dependent on the stability of  $\beta$ -carotene in the glassy state of freeze-dried systems (Part 2, 4 and 5) as depicted in Figure 40. In the glassy state, the degradation of  $\beta$ -carotene in solids is strongly dependent on the surface area expose to oxygen and the efficacy of oxygen diffusion and permeation through solids. The crystalline and the oil-dissolved  $\beta$ -carotene particles located within the unfrozen solids as well as the pore interface. A higher surface area for oxygen exposure to  $\beta$ -carotene attributes to a smaller pore size of solids. In addition, a smaller pore was coincident with a thinner membrane walls which allowed for more amount of oxygen permeation and diffusion through solid. The results showed increased  $\beta$ -carotene degradation as pore size and wall thickness of solids decreased (Part 4 and 5).

The structural collapse of glassy mango solids significantly contributed to a higher  $\beta$ -carotene stability than the non-collapsed systems (Part 2). The sugar

systems prefrozen at  $-80^{\circ}\text{C}$  gave a structural collapse and contributed to a lower loss of crystalline  $\beta$ -carotene (Part 4). Similarly, M250 gel solids containing dispersed oil-dissolved  $\beta$ -carotene showed an improved stabilization which attributed to the structural collapse during freeze-drying (Part 5). The model systems confirmed the finding in freeze-dried mangoes that the structural collapse of glassy solids effectively improved stabilization of  $\beta$ -carotene because of the compact solid structure potentially prevents oxygen accessibility through solids. The amount of oxygen expose to  $\beta$ -carotene is very limited contributing to a very low degradation. Moreover, the hard crust formation during freeze-drying (M40 prefrozen at  $-80^{\circ}\text{C}$ ) effectively prevents oxygen accessibility through solids and significantly improved the stabilization of  $\beta$ -carotene (Part 4). The results suggest that the modification of matrix microstructure significantly control the stability of  $\beta$ -carotene in freeze-dried systems.

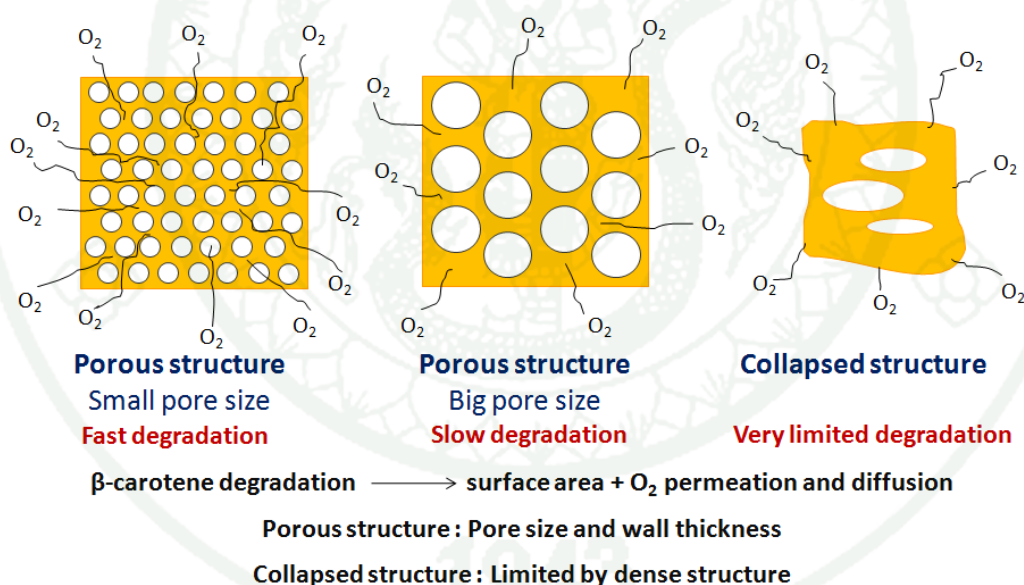


**Figure 40** Schematic diagram shows the effect of solid microstructure on the stability of  $\beta$ -carotene in freeze-dried solids. The smaller pore size gives a higher surface area and thinner membrane walls allowing for a higher amount of oxygen exposed to  $\beta$ -carotene leading to a fast degradation; whereas, the structural collapse limited the oxygen accessibility giving a very low degradation of  $\beta$ -carotene.

## 2.2 The effect of water activity

The rate constants of  $\beta$ -carotene degradation in freeze-dried mangoes and model systems decreased as  $a_w$  increased from anhydrous conditions followed by an increased of the rate constants as further increased of  $a_w$  (Part 1, 4 and 5). This characteristic is similar to that the lipid oxidation as reported by Labuza (1971). Figure 41 reveals the effect of water on the stability of  $\beta$ -carotene in freeze-dried solids. At anhydrous condition, oxygen can penetrate freely through solids as the absence of water and expose with  $\beta$ -carotene giving a fast degradation.

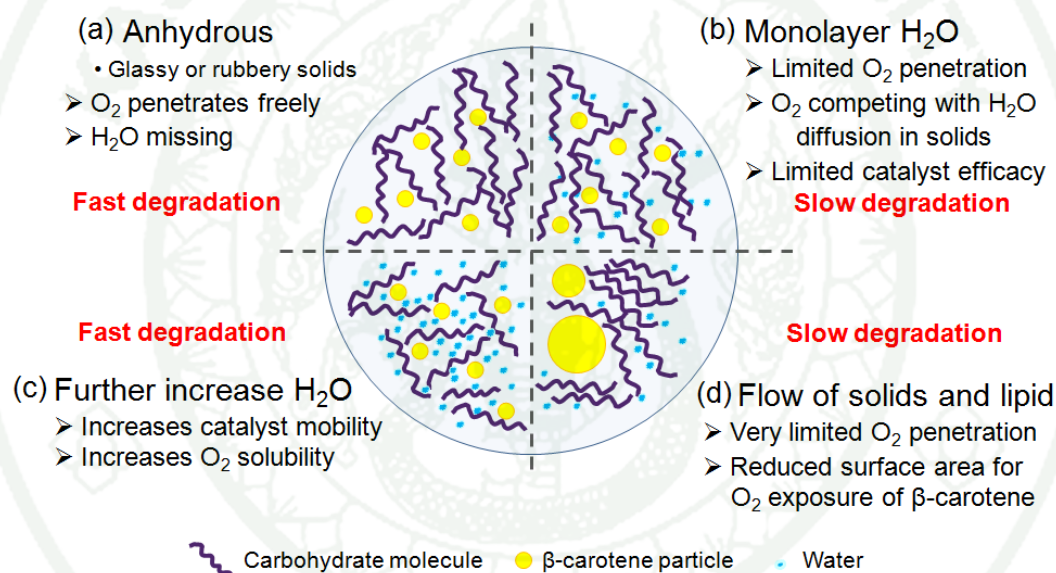


**Figure 41** Schematic diagram shows the effects of water on the stability of  $\beta$ -carotene in freeze-dried systems. The models demonstrate the degradation rate of  $\beta$ -carotene particles dispersed in dehydrated carbohydrate solids at (a) anhydrous, (b) monolayer water content ( $m_m$ ), (c) further increase of water above  $m_m$  and (d) water plasticized matrices and cause the solid and lipid flow.

As water increased towards monolayer water content, the water molecule binds to the hydrophilic site of the solute molecules and, therefore, the oxygen molecules compete with water for the diffusion through solids resulting in a limited

oxygen penetration. In addition, the water potentially limited the catalyst efficacy by (i) hydrating with the transition metals rendering them less active promoters of autoxidation, (ii) lipid hydroperoxides move to oil-water boundaries and are taken out of the propagation reactions due to hydrogen bonding with water and (iii) the free radical termination reactions increase as polar radicals congregate at the oil-water interface (Labuza *et al.*, 1972). The rate constant, therefore, decreases as a result of a slower degradation.

However, a fast degradation corresponding to the increased rate constants was observed as further increased  $a_w$ . The further increased rate constant at higher  $a_w$  attributes to the increased molecular mobility and the catalyst efficacy. In addition, the solubility of oxygen increases as increased amount of water which contributed to a higher exposure to  $\beta$ -carotene particles. The water plasticization increases free volume and decreases solids viscosity (Roos, 1995) which accelerates the sugar crystallization. The SEM micrographs indicated that the crystalline sugar particles of freeze-dried mangoes were larger than the mango cells as reported by Vásquez-Caicedo *et al.* (2006). The results suggest a movement of the amorphous sugars towards outer cell to form sugar crystals causing the cell wall disruption (Figure 42). The loss of cell integrity potentially allowed for higher amount of oxygen expose to  $\beta$ -carotene particles located in the cells. In addition, the enzymatic activity including polyphenol oxidase and peroxidase increased as mobility increased which could also cause a fast degradation. The drastic increased rate constant of  $\beta$ -carotene degradation was coincident with the pronounced sugar crystallization (Part 1).

As water increases, the freeze-dried matrices show a more liquid behavior which allows for the flow of solids and dispersed oil particles (Figure 41). The flow of solids causes the structural collapse and the dense of structure which potentially prevent the oxygen accessibility through matrices giving low  $\beta$ -carotene degradation. Furthermore, the flow of lipid contributes to the coalescence of lipid phase which decreases the surface area for oxygen exposure and, therefore, results in a lower degradation (Part 5). The results indicate the structural collapse and coalescence of lipid improved the stabilization of  $\beta$ -carotene.



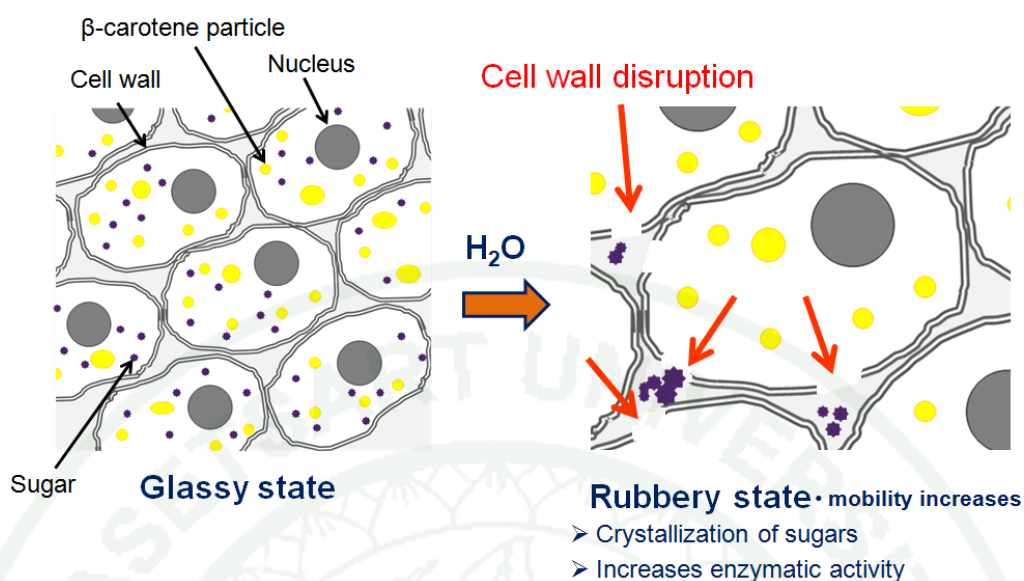


**Figure 42** Water accelerates sugar crystallization causing the cell wall disruption of mangoes. The amorphous sugars and dispersed  $\beta$ -carotene particles remain in the mango cells (left). The increased water activity causes the transition of solids from the glassy to the rubbery state and increases the molecular mobility which accelerates sugar crystallization and enzymatic activity. The crystallization of amorphous sugars causes the cell wall disruption as the amorphous sugars tend to congregate and form the crystalline structures (right).

### 2.3 The stability of crystalline and non-crystalline $\beta$ -carotene

The naturally dispersed  $\beta$ -carotene particles in mangoes showed the highest degradation rate; whereas, the crystalline gave a faster degradation than the oil-dissolved forms of  $\beta$ -carotene (Part 1, 4 and 5). The results could have been explained by the very small size of  $\beta$ -carotene particles in mangoes which conforms to larger surface area for exposure of oxygen. The highest stability of oil-dissolved  $\beta$ -carotene particles possibly attributes to the limitation of oxygen diffusion through the oil phase to expose with  $\beta$ -carotene locating in the core of the oil particles. In addition, the existing antioxidant in the sunflower oil would delay the oxidation of  $\beta$ -carotene and hence improved the stabilization.

## CONCLUSIONS

The aim of this work was to determine the influence of freeze-dried food microstructures and water activity on the stability of  $\beta$ -carotene in freeze-dried foods. Mangoes and agar-maltodextrin-sugar mixtures were studied as a real food and model system, respectively. The various freeze-drying protocols were applied to control the porosity of freeze-dried solids as well as the structural collapse. Freeze-dried solids were kept at various  $a_w$  conditions and monitored for the physicochemical changes including sugar crystallization, structural collapse and droplet coalescence of dispersed emulsion as well as the degradation of  $\beta$ -carotene. From the results and discussions the following conclusions can be drawn.

Part 1: Freeze-dried mango powder contains high amounts of amorphous sugars, which tend to crystallize when stored above their  $T_g$ . Freeze-dried mangoes stored at  $\geq 0.4a_w$  caused the sugar crystallization. The degradation of  $\beta$ -carotene in freeze-dried mangoes followed first-order kinetics. The loss of  $\beta$ -carotene decreased as  $a_w$  increased, up to  $0.4a_w$  and a dramatic increase in  $\beta$ -carotene loss was observed at further increased  $a_w$  which also coincided with pronounced sugar crystallization.

Part 2: The freeze-drying at temperatures above  $T_m'$  led to the structural collapse which subsequently reduced the rate of  $\beta$ -carotene loss in the glassy freeze-dried mangoes because the loss of matrix micropores and compact structure potentially prevented oxygen diffusion. However, the cracking on surface in concurrent with the structural collapse by liquid  $N_2$  freezing could not improve the stability of  $\beta$ -carotene. The results indicated that the structural collapse of glassy solids effectively stabilized  $\beta$ -carotene during storage.

Part 3: The lower freezing temperature increased the nucleation rate of the systems. High cooling rate as well as the higher  $T-T_g'$  generated a large number of small ice crystals which led to a smaller pore size and thinner pore walls. Sugars (glucose, fructose and sucrose) depressed the  $T_g'$  and  $T_m'$  of the systems and caused the structural collapse during freeze-drying of systems frozen at  $-40^\circ\text{C}$  and  $-80^\circ\text{C}$ . A

higher degree of structural collapse was visually observed in freeze-dried systems frozen at a lower temperature and had a low  $T_m'$ . The small ice crystals formed during freezing at low temperatures effectively led to the resistance of vapor flow during sublimation and hence enhanced structural collapse. The freezing temperatures of  $-40^{\circ}\text{C}$  and  $-80^{\circ}\text{C}$  gave a large number of small pores and affected crust formation in freeze-dried solids which enhanced the mechanical strength against compression. The compressive stress-strain curves revealed a good relationship between mechanical strength and pore size.

Part 4: The degradation of crystalline  $\beta$ -carotene in freeze-dried solids was affected by the porous structure and solids composition. A small pore size and thinner pore walls increased an exposure to oxygen and led to higher  $\beta$ -carotene degradation. The formation of crust in freezing and structural collapse of freeze-dried solids reduced  $\beta$ -carotene degradation. In the glassy state, the degradation of  $\beta$ -carotene was governed by the matrix porosity including the pore size and solid wall thickness. The mobility of the materials affected stability of  $\beta$ -carotene above the  $T_g$ . The mechanical  $\alpha$ -relaxation time associated with the structural changes of solids which correlated with degradation of  $\beta$ -carotene above  $T_g$ . The sugar systems with high mechanical  $\alpha$ -relaxation time had a low mobility above  $T_g$  and showed a less rapid  $\beta$ -carotene degradation.

Part 5: The freezing temperature below  $T_m'$  resulted in an increased size of emulsion particles. In particular the solidification of lipid particles at low temperature freezing caused the destabilization of emulsion; however, M40 gave a significant stabilizing effect on emulsion underwent freezing and freeze-drying. Freeze-dried emulsion solids stored at  $a_w$  above  $T_g$  caused the flow and structural collapse as well as the increased size of emulsion particles. The stability of  $\beta$ -carotene was dependent on matrix porosity which controlled by the prefreezing conditions prior to freeze-drying and the structural collapse during freeze-drying was confirmed to effectively stabilized  $\beta$ -carotene during storage at various  $a_w$ . The highest stability of  $\beta$ -carotene at high  $a_w$  of 0.75 was coincident with the increased size of lipid particles during

storage above  $T_g$ . The larger lipid particles resulted in the higher stability because of the lower effective surface area for oxygen exposure.

The freeze-drying process and solid components can control the porosity and structural collapse of freeze-dried materials and subsequently impacted the stability of  $\beta$ -carotene. The freezing process as affected by freezing parameters and matrix formulation can be of high significance in the use of different carbohydrates as protective components and structure forming materials in numerous food and pharmaceutical delivery systems. This research suggested that the stability of  $\beta$ -carotene in freeze-dried solids can be improved by the modification of humidity, matrix porosity and solid components such as sugar as well as molecular weight of solids which can be utilized by the freeze-dried food industry to develop the functional ingredient stability.



## RECOMMENDATION

For further investigations, the rate and amount of oxygen permeation through various solid structures are suggested as well as the studies on some additional factors affecting the stability of  $\beta$ -carotene during storage such as light and oxygen content. The fully collapsed structure is an undesirable characteristic for freeze-dried products; therefore, the further studies should investigate the mechanism to control structural collapse magnitude for both the desirable qualities, e.g., rehydration capacity and appearance as well as the retention of nutrient stability. Furthermore, as fruits contain high amount of pectic substances, the development of pectin-based materials for the encapsulation would possibly be a good alternative system to understand the stabilization effects of microstructure and water activity on  $\beta$ -carotene component.

## LITERATURE CITED

- Acevedo, N., C. Schebor and M.P. Buera. 2006. Water-solids interactions, matrix structural properties and the rate of non-enzymatic browning. **J. Food Eng.** 77: 1108-1115.
- Aguilera, J.M. and P.J. Lillford. 2008. Structure-property relationships in foods *In* J.M. Aguilera and P.J. Lillford, eds. **Food Material Science: Principle and Practice**. Springer Science Business media, New York, USA.
- Aguilera, J.M., T.R. Cuadros and J.M. Del Valle. 1998. Differential scanning calorimetry of low-moisture apple products. **Carbohydr. Polym.** 37: 79-86.
- Al-Muhtaseb, A.H., W.A.M. McMinn and T.R.A. Magee. 2002. Moisture sorption isotherm characteristics of food products: A review. **Food Bioprod. Process.** 80: 118-128.
- Alves, C.C.O., J.V. de Resende, M.E.T. Prado and R.S.R. Cruvinel. 2010. The effects of added sugars and alcohols on the induction of crystallization and the stability of the freeze-dried peki (*Caryocar brasiliense* Camb.) fruit pulps. **Lebensm-Wiss. u.-Technol.** 43: 934-941.
- Angell, C.A. 1997. Why  $C_1=16-17$  in the WLF equation is physical – and the fragility of polymers. **Polym.** 38: 6261-6266.
- Angell, C.A., R.D. Bressel, J.L. Green, H. Kanno, M. Oguni and E.J. Sare. 1994. Liquid fragility and the glass transition in water and aqueous solutions. **J. Food Eng.** 22: 115-142.
- Barbosa-Cánovas G.V., A.J. Fontana, S.J. Schmidt and T.P. Labuza. 2007. **Water Activity in Foods: Fundamental and Applications**. Blackwell Publishing Ltd., Iowa, USA.

- Bechoff, A., C. Dhuique-Mayer, M. Dornier, K.I. Tomlins, R. Boulanger, D. Dufour and A. Westby. 2010. Relationship between the kinetics of  $\beta$ -carotene degradation and formation of norisoprenoids in the storage of dried sweet potato chips. **Food Chem.** 121: 248-257.
- Bell, L.N. and M.J. Hageman. 1994. Differentiating between the effects of water activity and glass transition dependent mobility on a solid state chemical reaction: Aspartame degradation. **J. Agric. Food Chem.** 42: 2398-2401.
- Bell L.N. and T.P. Labuza. 2000. **Practical Aspects of Moisture Sorption Isotherm Measurement and Use**. Egan Press, Minnesota, USA.
- Bell, L.N. and K.L. White. 2000. Thiamin stability in solids as affected by the glass transition. **J. Food Sci.** 65: 498-501.
- Bell, L.N., D.E. Touna, K.L. White and Y.H. Chen. 1998. Glycine loss and maillard browning as related to the glass transition in a model food system. **J. Food Sci.** 63: 625-628.
- Bellows, R.J. and C.J. King. 1972. Freeze-drying of aqueous solutions: Maximum allowable operating temperature. **Cryobiology**. 9: 559-561.
- Bellows, R.J. and C.J. King. 1973. Product collapse during freeze-drying of liquid foods. **AIChE Symp. Ser.** 69: 33-41.
- Bhandari, B.R. and T. Howes. 1999. Implication of glass transition for the drying and stability of dried foods. **J. Food Eng.** 40: 71-79.
- Boon, C.S., D.J. McClements, J. Weiss and E.A. Decker. 2010. Factors influencing the chemical stability of carotenoids in foods. **Crit. Rev. Food Sci.** 50: 515-532.

Britton, G. 1995. Structure and properties of carotenoids in relation to function.

**FASEB J.** 9: 1551-1558.

Buera, P., S. Carolina and B. Elizalde. 2005. Effects of carbohydrate crystallization on stability of dehydrated foods and ingredient formulations. **J. Food Eng.** 67: 157-165.

Burin, L., K. Jouppila, Y.H. Roos, J. Kansikas and M.P. Buera. 2004. Retention of  $\beta$ -galactosidase activity as related to maillard reaction, lactose crystallization, collapse and glass transition in low moisture whey systems. **Int. Dairy J.** 14: 517-525.

Chirife, J. and M.P. Buera. 1995. A critical review of some non-equilibrium situations and glass transitions on water activity values of foods in the microbiological growth range. **J. Food Eng.** 25: 531-552.

Cano-Chauca, M., P.C. Stringheta, A.M. Ramos and J. Cal-Vidal. 2005. Effect of the carriers on the microstructure of mango powder obtained by spray drying and its functional characterization. **Innov. Food Sci. Emerg.** 6: 420-428.

Champion, D., M. Le Meste and D. Simatos. 2000. Towards an improved understanding of glass transition and relaxations in foods: Molecular mobility in the glass transition range. **Trends Food Sci. Tech.** 11: 41-55.

Chassagne-Berces, S., C. Poirier, M.F. Devaux, F. Fonseca, M. Lahaye, G. Pigorini, C. Girault, M. Marin and F. Guillon. 2009. Changes in texture, cellular structure and cell wall composition in apple tissue as a result of freezing. **Food Res. Int.** 42: 788-797.

Chen, B.H. and Y.C. Tang. 1998. Processing and stability of carotenoid powder from carrot pulp waste. **J. Agric. Food Chem.** 46: 2312-2318.



- Chen, Y., J.L. Aull and L.N. Bell. 1999. Invertase storage stability and sucrose hydrolysis in solids as affected by water activity and glass transition. **J. Agric. Food Chem.** 47: 504–509.
- Chevalier, D., A. Le Bail and M. Ghouil. 2000. Freezing and ice crystals formed in a cylindrical food model: Part I. Freezing at atmospheric pressure. **J. Food Eng.** 46: 277-285.
- Chirife, J. and H.A. Iglesias. 1978. Equations for fitting water sorption isotherms of foods: Part I- A Review. **J. Food Technol.** 13: 159-174.
- Chirife, J. and M.P.A. Buera. 1995. Critical review of some non-equilibrium situations and glass transitions on water activity values of foods in the microbiological growth range. **J. Food Eng.** 25: 531-552.
- Contreras, C., Martín, M.E., Martínez-Navarrete, N. and A. Chiralt. 2005. Effect of vacuum impregnation and microwave application on structural changes which occurred during air-drying of apple. **Lebensm-Wiss. u.-Technol.** 38: 471-477.
- Cornacchia, L. and Y.H. Roos. 2011. Lipid and water crystallization in protein-stabilised oil-in-water emulsions. **Food Hydrocolloid.** 25: 1726-1736.
- Cornacchia, L. and Y.H. Roos. 2011. Stability of  $\beta$ -carotene in protein-stabilized oil-in-water delivery systems. **J. Agric. Food Chem.** 59: 7013-7020.
- Corveleyn, S. and J.P. Remon. 1997. Formulation and production of rapidly disintegrating tablets by lyophilisation using hydrochlorothiazide as a model drug. **Int. J. Pharm.** 152, 215-225.
- Cramp, G.L., A.M. Docking, S. Ghosh and J.N. Coupland. 2004. On the stability of oil-in-water emulsions to freezing. **Food Hydrocolloid.** 18: 899-905.

- De Oliveira Alves, C.C., J.V. de Resende, M.E.T. Prado and R.S.R. Cruvinel. 2010. The effects of added sugars and alcohols on the induction of crystallization and the stability of the freeze-dried peki (*Caryocar brasiliense* Camb.) fruit pulps. **Lebensm-Wiss. u.-Technol.** 43, 934-941.
- Desobry S.A., F.M. Netto and T.P. Labuza. 1999. Influence of maltodextrin systems at an equivalent 25DE on encapsulated  $\beta$ -carotene loss during storage. **J. Food Process. Pres.** 23:39-55.
- Desobry, S.A., F.M. Netto and T.P. Labuza. 1997. Comparison of spray-drying, drum-drying and freeze-drying for  $\beta$ -carotene encapsulation and preservation. **J. Food Sci.** 62: 1158-1162.
- Elizalde, B.E., M.L. Herrera and M.P. Buera. 2002. Retention of  $\beta$ -carotene encapsulated in a trehalose-based matrix as affected by water content and sugar crystallization. **J. Food Sci.** 67: 3039-3045.
- Erlandson, J.A. and R.E. Wrolstad. 1972. Degradation of anthocyanins at limited water concentration. **J. Food Sci.** 37: 592–595.
- Fabra, M.J., P. Talens, G. Moraga and N. Martínez-Navarrete. 2009. Sorption isotherm and state diagram of grapefruit as a tool to improve product processing and stability. **J. Food Eng.** 93: 52-58.
- Ferreira, J.E.M. and D.B. Rodriguez-Amaya. 2008. Degradation of lycopene and  $\beta$ -carotene in model systems and in lyophilized guava during ambient storage: Kinetics, structure, and matrix effects. **J. Food Sci.** 73: 589-594.
- Ferruzzi, M. G., L.C. Sander, C.L. Rock and S.J. Schwartz. 1998. Carotenoid determination in biological microsample using liquid chromatography with a coulometric electrochemical array detector. **Anal. Biochem.** 256: 74-81.

- Flink, J.M. and M. Karel. 1972. Mechanisms of retention of organic volatiles in freeze-dried systems. **J. Food Technol.** 7: 199-211.
- Fontana, A.J. 2007. Appendix A: Water Activity of Saturated Salt Solutions. *In* G.V. Barbosa-Cànovas, A.J. Fontana, S. Schmidt, and T. Labuza, eds. **Water Activity in Foods: Fundamental and Applications**. Blackwell Publishing Ltd, Iowa, USA.
- Garzón, G.A. and R.E. Wrolstad. 2001. The stability of pelargonidin-based anthocyanins at varying water activity. **Food Chem.** 75: 185-196.
- Georget, D.M.R., A.C. Smith, K.W. Waldron. 1999. Thermal transitions in freeze-dried carrot and its cell wall components. **Thermochim. Acta.** 332: 203-210.
- Ghosh, S. and J.N. Coupland. 2008. Factors affecting the freeze-thaw stability of emulsions. **Food Hydrocolloid.** 22: 105-111.
- Glória, M.B.A., S.R. Vale and P.A. Bobbio. 1995. Effect of water activity on the stability of bixin in an annatto extract-microcrystalline cellulose model system. **Food Chem.** 52: 389-391.
- Goff, H.D. and M.E. Sahagian. 1996. Glass transitions in aqueous carbohydrate solutions and their relevance to frozen food stability. **Thermochim. Acta** 280/281: 449-464.
- Goff, H.D., Verespej, E. and D. Jermann. 2003. Glass transitions in frozen sucrose solutions are influenced by solute inclusions within ice crystals. **Thermochim. Acta.** 399: 43-55.
- Göğüş, F. and J. Lamb. 1998. Choice of model gel systems for the food dehydration studies. **Dry. Technol.** 16: 297-309.

- Goldman, M., Horev, B. and I. Saguy. 1983. Decolorization of  $\beta$ -carotene in model systems simulating dehydrated foods: Mechanism and kinetic principles. **J. Food Sci.** 48: 751-754.
- Gordon, M. and J.S. Taylor. 1952. Ideal copolymers and the second order transitions of synthetic rubbers. I. Non-crystalline copolymers. **J. Applied Chem.** 2: 493-500.
- Gregory III, J.F. 2007. Minerals. *In* S. Damodaran, K.L. Parkin and O.R. Fennema, eds. **Food Chemistry 4<sup>th</sup> edition**. CRC Press, Folrida, USA.
- Garzón, G.A. and R.E. Wrolstad. 2001. The stability of pelargonidin-based anthocyanins at varying water activity. **Food Chem.** 75: 185-196.
- Hancock, B.C. and S.L. Shamblin. 1998. Water vapour sorption by pharmaceutical sugars. **Pharm. Sci. Technol. Today** 1. 8: 345-351.
- Haque M.K. and Y.H. Roos. 2004. Water sorption and plasticization behavior of spray-dried lactose/protein mixtures. **J. Food Sci.** 69:384-391.
- Haque, M.K. and Y.H. Roos. 2005. Crystallization and X-ray diffraction of spray-dried and freeze-dried amorphous lactose. **Carbohydr. Res.** 340: 293-301.
- Harnkarnsujarit, N. and S. Charoenrein. 2011a. Effect of water activity on sugar crystallization and  $\beta$ -carotene stability of freeze-dried mango powder. **J. Food Eng.** 105: 592-598.
- Harnkarnsujarit, N. and S. Charoenrein. 2011b. Influence of collapsed structure on stability of  $\beta$ -carotene in freeze-dried mangoes. **Food Res. Int.** 44:3188-3194.



- Harnkarnsujarit, N., S. Charoenrein and Y.H. Roos. 2012a. Microstructure formation of maltodextrin and sugar matrices in freeze-dried systems. **Carbohydr. Polym.** 88: 734-742.
- Harnkarnsujarit, N., S. Charoenrein and Y.H. Roos. 2012b. Porosity and water activity effects on stability of  $\beta$ -carotene crystals in freeze-dried solids. **J. Food Sci.** (Submitted).
- Harris W.M. and A.R. Spurr. 1969. Chromoplasts of tomato fruits. II. The red tomato. **Am. J. Bot.** 56:380–389.
- Harris, P.J. and B.G. Smith. 2006. Plant cell walls and cell-wall polysaccharides: structures, properties and uses in food products. **Int. J. Food Sci Technol.** 41: 129–143.
- Helgason, T., T.S. Awad, K. Kristbergsson, E.A. Decker, D.J. McClements and J. Weiss. 2009. Impact of surfactant properties on oxidative stability of  $\beta$ -carotene encapsulated within solid lipid nanoparticles. **J. Agric. Food. Chem.** 57: 8033-8040.
- Hottot, A., S. Vessot and J. Andrieu. 2004. A direct characterization method of the ice morphology. Relationship between mean crystals size and primary drying times of freeze-drying processes. **Dry. Technol.** 22: 2009-2021.
- Hou, Q., D.W. Grijpma and J. Feijen. 2003. Porous polymeric structures for tissue engineering prepared by a coagulation, compression moulding and salt leaching technique. **Biomaterials.** 24: 1937-1947.
- Hung Y.C. 1997. Freeze-cracking, pp. 92-100. *In* M.C. Erickson and Y.C. Hung, eds., **Quality in frozen food**. Chapman and Hall, New York, USA.

- Iglesias, H. A., J. Chirife and M.P. Buera. 1997. Adsorption isotherm of amorphous trehalose. **J. Sci. Food and Agric.** 75: 183-186.
- Jansson H, R. Bergman and J. Swenson. 2005. Dynamics of sugar solutions as studied by dielectric spectroscopy. **J. Non-Cryst. Solids.** 351: 2858-2863.
- Jaya, S. and H. Das. 2009. Glass transition and sticky point temperatures and stability/mobility diagram of fruit powders. **Food Bioprocess Technol.** 2: 89-95.
- Jaya, S. and T.D. Durance. 2009. Compressive characteristics of cellular solids produced using vacuum-microwave, freeze, vacuum and hot air dehydration methods. **J. Porous Mater.** 16: 47-58.
- Johari, G.P., A. Hallbrucker and E. Mayer. 1987. The glass-liquid transition of hyperquenched water. **Nature** 330: 552-553.
- Jouppila K. and Y.H. Roos. 1994. Glass transition and crystallization in milk powders. **J. Dairy Sci.** 77: 2907-2915.
- Jouppila, K., J. Kansikas and Y.H. Roos. 1997. Glass transition, water plasticization, and lactose crystallization in skim milk powder. **J. Dairy Sci.** 80: 3152-3160.
- Kang, H.W., Y. Tabata and Y. Ikada. 1999. Fabrication of porous gelatin scaffolds for tissue engineering. **Biomaterials.** 20: 1339-1344.
- Karathanos, V.T., S.A. Anglea and M. Karel. 1996. Structure collapse of plant materials during freeze drying. **J. Therm. Anal.** 46: 1541-1551.
- Karel, M. and J.M. Flink. 1973. Influence of frozen state reactions on freeze-dried foods. **J. Agric. Food Chem.** 21: 16-21.

- Kasapis, S., I.M. Al-Marhoobi and J.R. Mitchell. 2003. Testing the validity of comparisons between the rheological and the calorimetric glass transition temperatures. **Carbohydr. Res.** 338: 787-794.
- Kawakami, K. and M.J. Pikal. 2005. Calorimetric investigation of the structural relaxation of amorphous materials: Evaluating validity of the methodologies. **J. Pharm. Sci.** 94: 948-965.
- Khalloufi, S. and C. Ratti. 2003. Quality deterioration of freeze-dried foods as explain by their glass transition temperature and internal structure. **J. Food Sci.** 68: 892-903.
- Khalloufi, S., Y. El-Maslouhi and C. Ratti. 2000. Mathematical model for prediction of glass transition temperature of fruit powders. **J. Food Sci.** 65: 842–848.
- Kim, U.J., J. Park, C. Li, H.J. Jin, R. Valluzzi and D.L. Kaplan. 2004. Structure and properties of silk hydrogels. **Biomacromolecules.** 5: 786-792.
- Klinkesorn, U., P. Sophanodora, P. Chinachot and D.J. McClements. 2004. Stability and rheology of corn oil-in-water emulsions containing maltodextrin. **Food Res. Int.** 37: 851-859.
- Koca, N., H.S. Burdurlu and F. Karadeniz. 2007. Kinetics of colour changes in dehydrated carrots. **J. Food Eng.** 78: 449-455.
- Krokida, M.K. and Z.B. Maroulis. 1997. Effect of drying method on shrinkage and porosity. **Dry. Technol.** 15: 2441-2458.
- Krokida, M.K., V.T. Karathanos and Z.B. Maroulis. 1998. Effect of freeze-drying conditions on shrinkage and porosity of dehydrated agricultural products. **J. Food Eng.** 35: 369-380.

- Labuza TP, L. McNally, D. Gallagher and J. Hawkes. 1972. Stability of intermediate moisture foods. I. Lipid oxidation. **J. Food Sci.** 37:154–159.
- Labuza, T.P. 1971. Kinetics of lipid oxidation in foods. **Crit. Rev. Food Sci. Tech.** 2: 355-405.
- Labuza, T.P. and B. Altunakar. 2007. Water activity prediction and moisture sorption isotherms. *In* G.V. Barbosa-Cánovas, A.J. Fontana, S. Schmidt, and T. Labuza, eds., **Water Activity in Foods: Fundamentals and Applications**. Blackwell Publishing Ltd., Iowa, USA.
- Labuza, T.P., L. McNally, D. Gallagher and J. Hawkes. 1972. Stability of intermediate moisture foods. I. Lipid oxidation. **J. Food Sci.** 37: 154–159.
- Laurindo, J.B. and M. Peleg. 2007. Mechanical measurements in puffed rice cakes. **J. Texture Stud.** 38: 619-634.
- Lavelli, V., B. Zanoni and A. Zaniboni. 2007. Effect of water activity on carotenoid degradation in dehydrated carrots. **Food Chem.** 104: 1705-1711.
- Le Meste, M., D. Champion, G. Roudaut, G. Blond and D. Simatos. 2002. Glass transition and food technology: A critical appraisal. **J. Food Sci.** 67: 2444-2458.
- Levi, G. and M. Karel. 1995. Volumetric shrinkage (collapse) in freeze-dried carbohydrates above their glass transition temperature. **Food Res. Int.** 28: 145-151.
- Levine, H. and L. Slade. 1986. A polymer physico-chemical approach to the study of commercial starch hydrolysis products (SHPs). **Carbohydr. polym.** 6: 213-244.



- Lewicki, P.P. 2009. Data and Models of Water Activity. II: Solid Foods. *In* M.S. Rahman, ed. **Food Properties Handbook**. CRC Press, Florida, USA.
- Li, N., L.S. Taylor and L.J. Mauer. 2011. Degradation kinetics of catechins in green tea powder: Effects of temperature and relative humidity. **J. Agric. Food Chem.** 59: 6082-6090.
- Lin, L.S., H.K. Yuen and J.E. Varner. 1991. Differential scanning calorimetry of plant cell walls. **P. Natl. Acad. Sci. USA.** 88: 2241-2243.
- Ling, H., Birch, J. and M. Lim. 2005. The glass transition approach to determination of drying protocols for colour stability in dehydrated pear slices. **Int. J. Food Sci. Technol.** 40: 921-927.
- Liu, S., J. Lin and D. Yang. 2009. Determination of cis- and trans- $\alpha$ - and  $\beta$ -carotenoids in Taiwanese sweet potatoes (*Ipomoea batatas* L.) harvested at various times. **Food Chem.** 116: 605–610.
- Liu, Y., B. Bhandari and W. Zhou. 2006. Glass transition and enthalpy relaxation of amorphous food saccharides: a review. **J. Agric. Food Chem.** 54: 5701–5717.
- Lowithun, N. and S. Charoenrein. 2009. Influence of osmodehydrofreezing with different sugars on the quality of frozen rambutan. **Int. J. Food Sci. Technol.** 44: 2183-2188.
- Ma, P.X. and J.W. Choi. 2001. Biodegradable polymer scaffolds with well-defined interconnected spherical pore network. **Tissue Eng.** 7: 23-33.
- Ma, P.X. and R. Zhang. 1999. Synthetic nano-scale fibrous extracellular matrix. **J. Biomed. Mater. Res.** 46: 60-72.

- Madene, A., M. Jacquot, J. Scher and S. Desobry. 2006. Flavour encapsulation and controlled release: a review. **Int. J. Food Sci. Technol.** 41: 1–21.
- Madihally, S.V. and H.W.T. Matthew. 1999. Porous chitosan scaffolds for tissue engineering. **Biomaterials.** 20: 1133-1142.
- Makower, B. and W.B. Dye. 1956. Sugar crystallization: Equilibrium moisture content and crystallization of amorphous sucrose and glucose. **J. Agric. Food Chem.** 4: 72-77.
- Maltini, E., D. Torreggiani, E. Venir and G. Bertolo. 2003. Water activity and the preservation of plant foods. **Food Chem.** 82: 79-86.
- McClements, D.J. 2004. Protein-stabilized emulsions. **Curr. Opin. Colloid In.** 9: 305-313.
- Meda, L. and C. Ratti. 2005. Rehydration of freeze-dried strawberries at varying temperature. **J. Food Process. Eng.** 28: 233-246.
- Medeni, M. and F. Gogus. 1998. Sorption isotherms and drying characteristics of Mulberry (*Morus alba*). **J. Food Eng.** 37: 437-449.
- Moraga, G., N. Martínez-Navarrete and A. Chiralt. 2006. Water sorption isotherms and phase transitions in kiwifruit. **J. Food Eng.** 72: 147-156.
- Mun, S., D.J. McClements and J. Surh. 2011. Influence of maltodextrin addition on the freeze-dry stability of  $\beta$ -lactoglobulin-based emulsions with controlled electrostatic and/or steric interactions. **Food Sci. Biotechnol.** 20: 1143-1150.
- Nararin, N., P.S. Bora, R. Nararin and P.E. Shaw. 1998. Mango. *In* P.E. Shaw, H.T. Chan, and S. Nagy, eds. **Tropical and Subtropical Fruits**. AgScience, Inc., Florida, USA.

- Nelson, K.A. and T.P. Labuza. 1994. Water activity and food polymer science: Implications of state on Arrhenius and WLF models in predicting shelf life. **J. Food Eng.** 22: 271-289.
- Noel, T.R., R. Parker and S.G. Ring. 1996. A comparative study of the dielectric relaxation behavior of glucose, maltose, and their mixtures with water in the liquid and glassy states. **Carbohydr. Res.** 282: 193–206.
- Noel, T.R., R. Parker and S.G. Ring. 2000. Effect of molecular structure and water content on the dielectric relaxation behavior of amorphous low molecular weight carbohydrates above and below their glass transition. **Carbohydr. Res.** 329: 839–845.
- Nussinovitch, A., M.G. Corradini, M.D. Normand and M. Peleg. 2001. Effect of starch, sucrose and their combinations on the mechanical and acoustic properties of freeze-dried alginate gels. **Food Res. Int.** 34: 871-878.
- Nussinovitch, A., R. Velez-Silvestre and Peleg, M. 1993. Compressive characteristics of freeze-dried agar and alginate gel sponges. **Biotechnol. Prog.** 9: 101-104.
- O'Brien, F.J., B.A. Harley, I.V. Yannas and L. Gibson. 2005. The effect of pore size on cell adhesion in collagen-GAG-scaffolds. **Biomaterials**, 26: 433-441.
- Oh, J., J.A. Seo, H.K. Kim and Y.H. Hwang. 2006. The secondary relaxation in the dielectric loss of glucose-water mixtures. **J. Non-Cryst. Solids.** 352: 4679-4684.
- Ohkuma, C., K. Kawai, C. Viriyarattanasak, T. Mahawanich, S. Tantratian, R. Takai, and T. Suzuki. 2008. Glass transition properties of frozen and freeze-dried surimi products: Effects of sugar and moisture on the glass transition temperature. **Food Hydrocolloid.** 22: 255-262.

- Oikonomopoulou, V.P., M.K. Krokida and V.T. Karathanos. 2011. Structural properties of freeze-dried rice. **J. Food Eng.** 107, 326-333.
- Omar, A.M.E. and Y.H. Roos. 2007. Glass transition and crystallization behaviour of freeze-dried lactose-salt mixtures. **Lebensm-Wiss. u.-Technol.** 40: 536-543.
- Ötles, S. and O. Çargindi. 2007. Carotenoids as natural colorants *In* C. Socaciu, ed. **Food Colorants: Chemical and Functional Properties**. CRC Press, Florida, USA.
- Oungbho, K. and B.W. Müller. 1997. Chitosan sponges as sustained release drug carriers. **Int. J. Pharm.** 156: 229–237.
- Owcharoen, K. 2012. **Effect of Freezing Rates and Freeze-Thaw Cycles on Texture and Pectic Substances of Mango (*Mangifera indica* L. cv. Nam Dok Mai Sri Thong)**, M.S. Thesis, Kasetsart University.
- Peleg, M. 1997. Review: Mechanical properties of dry cellular solid foods. **Food Sci. Int.** 3: 227-240.
- Peleg, M. 1992. On the use of the WLF model in polymers and foods. **Crit. Rev. Food Sci. Nutr.** 32: 59-66.
- Pesek, C.A. and J.J. Warthesen. 1990. Kinetic model for photoisomerization and concomitant photodegradation of  $\beta$ -carotenes. **J. Agric. Food Chem.** 38: 1313-1315.
- Petzold, G. and J.M. Aguilera. 2009. Ice morphology: Fundamentals and technological applications in foods. **Food Biophys.** 4: 378-396.
- Pikal, M.J., S. Rambhatla and R. Ramot. 2002. The impact of freezing stage in lyophilization: Effect of the ice nucleation temperature on process design and product quality. **Am. Pharm. Rev.** 5: 48-53.



- Pott, I., M. Marx, S. Neidhart, W. Mühlbauer and R. Carle. 2003. Quantitative determination of  $\beta$ -carotene stereoisomers in fresh, dried, and solar-dried mangoes (*Mangifera indica* L.). **J. Agric. Food Chem.** 51: 4527-4531.
- Prado, S.M., M.P. Buera and B.E. Elizalde. 2006. Structural collapse prevents  $\beta$ -carotene loss in a supercooled polymeric matrix. **J. Agric. Food Chem.** 54: 79-85.
- Qian, C., E.A. Decker, H. Xiao and D.J. McClements. 2012. Physical and chemical stability of  $\beta$ -carotene-enriched nanoemulsions: Influence of pH, ionic strength, temperature, and emulsifier type. **Food Chem.** 132: 1221-1229.
- Rahman, M.S. 2004. State diagram of date flesh using differential scanning calorimetry (DSC). **Int. J. Food Prop.** 7: 407-428.
- Rahman, M.S. 2006. State diagram of foods: Its potential use in food processing and product stability. **Trends Food Sci. Technol.** 17: 129-141.
- Ramoneda, X.A., P.A. Ponce-Cevallos, M.D.P. Buera and B.E. Elizalde. 2011. Degradation of  $\beta$ -carotene in amorphous polymer matrices: Effect of water sorption properties and physical state. **J. Sci. Food Agric.** 91:2587–2593.
- Rascón, M.P., C.I. Beristain, H.S. García and M.A. Salgado. 2011. Carotenoid retention and storage stability of spray-dried encapsulated paprika oleoresin using gum Arabic and Soy protein isolate as wall materials. **Lebensm.-Wiss. u.-Technol.** 44: 549-557.
- Rassis, D.K., I.S. Saguy and A. Nussinovitch. 1998. Physical properties of alginate-starch cellular sponges. **J. Agric. Food Chem.** 46, 2981-2987.

- Rassis, D.K., I.S. Saguy and A. Nussinovitch. 2002. Collapse, shrinkage and structural changes in dried alginate gels containing fillers. **Food Hydrocolloid**. 16: 139-151.
- Ratti, C. 2008. Freeze and vacuum drying of foods. *In* Chen X.D. and A.S. Mujumdar, eds. **Drying Technologies in Food Processing**. Blackwell Publishing Ltd., UK.
- Ribaya-Mercado, J.D. 2002. Influence of dietary fat on  $\beta$ -carotene absorption and bioconversion into vitamin A. **Nutr. Rev.** 60:104-110.
- Robles-Sánchez, M., H. Astiazarán-García, O. Martín-Belloso, S. Gorinstein, E. Alvarez-Parrilla, L.A. de la Rosa, G. Yepiz-Plascencia and G.A. González-Aguilar. 2011. Influence of whole and fresh-cut mango intake on plasma lipids and antioxidant capacity of healthy adults. **Food Res. Int.** 44: 1386-1391.
- Roos, Y.H. 1993a. Melting and glass transitions of low molecular weight carbohydrates. **Carbohydr. Res.** 238: 39-48.
- Roos, Y.H. 1993b. Water activity and physical state effects on amorphous food stability. **J. Food Process. Pres.** 16: 433–447.
- Roos, Y.H. 1995. **Phase Transitions in Foods**. Academic Press, California, USA.
- Roos, Y.H. 1997. Frozen state transitions in relation to freeze drying. **J. Therm. Anal.** 48, 535-544.
- Roos, Y.H. 2010a. Crystallization, collapse, and glass transition in low-water food systems. *In* D.S. Reid, T. Sajjaanantakul, P. J. Lillford and S. Charoenrein, eds. **Water Properties in Food, Health, Pharmaceutical and Biological Systems: ISOPOW 10**. Wiley-Blackwell, Oxford, UK.

- Roos, Y.H. 2010b. Glass transition temperature and its relevance in food processing. **Annu. Rev. Food. Sci. Technol.** 1: 469-96.
- Roos, Y.H. 2012. Relaxations, glass transition and engineering properties of food solids. *In* S. Yanniotis, P. Taoukis, N. Stoforos, V. Karathanos, eds. **Advances in Food Process Engineering Research and Applications**. Springer, New York, USA.
- Roos, Y.H. and M. Karel. 1991a. Amorphous state and delayed ice formation in sucrose solutions. **Int. J. Food Sci. Technol.** 26: 553-566.
- Roos, Y.H. and M. Karel. 1991b. Applying state diagrams to food processing and development. **Food Technol.** 45: 66, 68-71, 107.
- Roos, Y.H. and M. Karel. 1991c. Nonequilibrium ice formation in carbohydrate solutions. **Cryoletters.** 12: 367-376.
- Roos, Y.H. and M. Karel. 1991d. Phase transitions of mixtures of amorphous polysaccharides and sugars. **Biotechnol. Progr.** 7: 49-53.
- Roos, Y.H. and M. Karel. 1991e. Water and molecular weight effects on glass transitions in amorphous carbohydrates and carbohydrate solutions. **J. Food. Sci.** 56, 1676-1681.
- Roos, Y.H., K. Jouppila and B. Zielasko. 1996. Non-enzymatic browning-induced water plastification: Glass transition temperature depression and reaction kinetics determination using DSC. **J. Therm. Anal.** 47: 1437-1450.
- Roudaut, G., D. Simatos, D. Champion, E. Contreras-Lopez and M. Le Meste. 2004. Molecular mobility around the glass transition temperature: A mini review. **Innov. Food Sci. Emerg. Technol.** 5: 127-134.

- Sá, M.M. and A.M. Sereno. 1994. Glass transitions and state diagrams for typical natural fruits and vegetables. **Thermochim. Acta.** 246: 285–297.
- Sá, M.M., A.M. Figueiredo and A.M. Sereno. 1999. Glass transitions and state diagrams for fresh and processed apple. **Thermochim. Acta.** 329: 31-38.
- Sablani, S.S. and M.S. Rahman. 2002. Pore formation in selected foods as a function of shelf temperature during freeze drying. **Dry. Technol.** 20: 1379-1391.
- Sablani, S.S., K. Al-Belushi, I. Al-Marhubi and R. Al-Belushi. 2007. Evaluating stability of vitamin C in fortified formula powder using water activity and glass transition. **Int. J. Food Prop.** 10: 61–71.
- Sablani, S.S., M.S. Rahman, M.K. Al-Kuseibi, N.A. Al-Habsi, R.H. Al-Belushi, I. Al-Marhubi and I.S. Al-Amri. 2007. Influence of shelf temperature on pore formation in garlic during freeze-drying. **J. Food Eng.** 80: 68-79.
- Sablani, S.S., M.S. Rahman, M.K. Al-Kuseibi, N.A. Al-Habsi, R.H. Al-Belushi, I. Al-Sacha and L.N. Steven. 2009. Thermal analysis of frozen solutions: Multiple glass transitions in amorphous systems. **J. Pharm. Sci.** 98: 3397-3405.
- Sadikoglu, H., M. Ozdemir and M. Seker. 2006. Freeze-drying of pharmaceutical products: Research and development needs. **Dry. Technol.** 24: 849-861.
- Schebor, C., M.F. Mazzobre and M.P. Buera. 2010. Glass transition and time-dependent crystallization behavior of dehydration bioprotectant sugars. **Carbohydr. Res.** 345: 303-308.
- Scherer, G.W. 1993. Freezing gels. **J. Non-Cryst. Solids.** 155: 1-25.



- Searles, J.A. 2010. Freezing and annealing phenomena in lyophilization *In* J.C. May and L. Rey, eds. **Freeze-Drying/Lyophilization of Pharmaceutical and Biological Products**. Informa Healthcare, New York, USA.
- Selim, K., M. Tsimidou and C.G. Biliaderis. 2000. Kinetics studies of degradation of saffron carotenoids encapsulated in amorphous polymer matrices. **Food Chem.** 71: 199-206.
- Serris, G.S. and C.G. Biliaderis. 2001. Degradation kinetics of beetroot pigment encapsulated in polymeric matrices. **J. Sci. Food Agric.** 81: 691-700.
- Shapiro, L. and S. Cohen. 1997. Novel alginate sponges for cell culture and transplantation. **Biomaterials.** 18: 583-590.
- Shimada, Y., Y.H. Roos and M. Karel. 1991. Oxidation of methyl linoleate encapsulated in amorphous lactose-based food model. **J. Agric. Food Chem.** 39: 637-641.
- Shinyashiki, N., M. Shinohara, Y. Iwata, T. Goto, M. Oyama, S. Suzuki, W. Yamamoto, S. Yagihara, T. Inoue, S. Oyaizu, S. Yamamoto, K.L. Ngai and S. Capaccioli. 2008. The glass transition and dielectric secondary relaxation of fructose–water mixtures. **J. Phys. Chem. B.** 112: 15470-15477.
- Shishehgarha, F., J. Makhlouf and C. Ratti. 2002. Freeze-drying characteristics of strawberries. **Dry. Technol.** 20: 131-145.
- Silalai, N. and Y.H. Roos. 2011. Mechanical relaxation times as indicators of stickiness in skim milk-maltodextrin solids systems. **J. Food Eng.** 106: 306-317.
- Sivakumar, D., Y. Jiang and E.M. Yahia. 2011. Maintaining mango (*Mangifera indica* L.) fruit quality during the export chain. **Food Res. Int.** 44: 1254-1263.

- Sobral, P.J.A., V.R.N. Telis, A.M.Q.B. Habitante and A. Sereno. 2001. Phase diagram for freeze-dried persimmon. **Thermochim. Acta.** 376: 83-89.
- Sootitawat, A., F. Bigeard, H. Yoshii, T. Furuta, M. Ohkawara and P. Linko. 2005. Influence of emulsion and powder size on the stability of encapsulated D-limonene by spray drying. **Innov. Food Sci. Emerg.** 6, 107-114.
- Syamaladevi, R.M., S.S. Sablani, J. Tang, J. Powers and B.G. Swanson. 2009. State diagram and water adsorption isotherm of raspberry (*Rubus idaeus*). **J. Food Eng.** 91: 460-467.
- Syamaladevi, R.M., S.S. Sablani and B.G. Swanson. 2010. Aging of amorphous raspberry powder: Enthalpy relaxation and fragility. **J. Food Eng.** 101: 32-40.
- Tan, C.P. and M. Nakajima. 2005.  $\beta$ -Carotene nanodispersions: Preparation, characterization and stability evaluation. **Food Chem.** 92: 661-671.
- Tang, X. and K. Pikal. 2004. Design of freeze-drying processes for pharmaceuticals: practical advice. **Pharm. Res.** 21: 191-200.
- Tang, Y.C. and B.H. Chen. 2000. Pigment change of freeze-dried carotenoid powder during storage. **Food Chem.** 69: 11-17.
- Telis, V.R.N. and N. Martínez-Navarrete. 2009. Collapse and color changes in grapefruit juice powder as affected by water activity, glass transition, and addition of carbohydrate polymers. **Food Biophys.** 4: 83-93.
- Telis, V.R.N. and P.J.A. Sobral. 2001. Glass transitions and state diagram for freeze-dried pineapple. **Lebensm-Wiss. u.-Technol.** 34: 199-205.

- Thanasukarn, P., R. Pongsawatmanit and D.J. McClements. 2004. Impact of fat and water crystallization on the stability of hydrogenated palm oil-in-water emulsions stabilized by whey protein isolate. **Colloid. Surface A**. 246: 49-59.
- Tharanathan, R.N., H.M. Yashoda and T.N. Prabha. 2006. Mango (*Mangifera indica* L.), “The King of Fruits”-An Overview. **Food Rev. Int.** 22(2): 95-123.
- Timmermann, E.O., J. Chirife and H.A. Iglesias. 2001. Water sorption isotherms of foods and foodstuffs: BET or GAB parameters?. **J. Food Eng.** 48: 19-31.
- To, E.C. and J.M. Flink. 1978. ‘Collapse’, a structural transition in freeze-dried carbohydrates: II. Effect of solute composition. **J. Food Technol.** 13: 567-581.
- Tsami, E., M.K. Krokida and A.E. Drouzas. 1998. Effect of drying method on the sorption characteristics of model fruit powders. **J. Food Eng.** 38: 381-392.
- Tsimidou, M. and C.G. Biliaderis. 1997. Kinetic studies of saffron (*Crocus sativus* L.) quality deterioration. **J. Agric. Food Chem.** 45: 2890-2898.
- Tsourouflis, S., J.M. Flink and M. Karel. 1976. Loss of structure in freeze-dried carbohydrates solutions: Effect of temperature, moisture content and composition. **J. Sci. Food Agric.** 27: 509-519.
- Uddin, M.S., M.N.A. Hawlader, L. Ding and A.S. Mujumdar. 2002. Degradation of ascorbic acid in dried guava during storage. **J. Food Eng.** 51: 21-26.
- Van Vlierberghe, S., V. Cnudde, P. Dubruel, B. Masschaele, A. Cosijns, I. De Paepe, P.J.S. Jacobs, L. Van Hoorebeke, J.P. Remon and E. Schacht. 2007. Porous gelatin hydrogels: 1. Cryogenic formation and structure analysis. **Biomacromolecules**. 8: 331–337.

- Vanapalli, S.A., J. Palanuwech and J.N. Coupland. 2002. Stability of emulsions to dispersed phase crystallization: Effect of oil type, dispersed phase volume fraction, and cooling rate. **Colloid. Surface A.** 204: 227-237.
- Vásquez-Caicedo, A.L., Heller, A., Neidhart, S. and R. Carle. 2006. Chromoplast morphology and  $\beta$ -carotene accumulation during postharvest ripening of mango Cv. 'Tommy Atkins'. **J. Agric. Food Chem.** 54: 5769-5776.
- Wagner, L.A. and J.J. Warthesen. 1995. Stability of spray-dried encapsulated carrot carotenes. **J. Food Sci.** 60: 1048-1053.
- Wang, H., S. Zhang and G. Cuen. 2008. Glass transition and state diagram for fresh and freeze-dried Chinese gooseberry. **J. Food Eng.** 84: 307-312.
- Wangsakan, A., P. Chinachoti and D.J. McClements. 2003. Effect of different dextrose equivalent of maltodextrin on the interactions with anionic surfactant in an isothermal titration calorimetry study. **J. Agric. Food Chem.** 51: 7810-7814.
- Wangsakan, A., P. Chinachoti and D.J. McClements. 2001. Maltodextrin - anionic surfactant interactions: Isothermal titration calorimetry and surface tension study. **J. Agric. Food Chem.** 49: 5039-5045.
- Welti-Chanes, J., J.A. Guerrero, M.E. Barcenas, J.M. Aguilera, F. Vergara and G.V. Barbosa-Canovas. 1999. Glass transition temperature ( $T_g$ ) and water activity ( $a_w$ ) of dehydrated apple products. **J. Food Process Eng.** 22: 91-101.
- Whitcombe, M.J., R. Parker and S.G. Ring. 2005. Oxygen solubility and permeability of carbohydrates. **Carbohydr. Res.** 340: 1523-1527.
- White, K.L. and L.N. Bell. 1999. Glucose loss and maillard browning in solids as affected by porosity and collapse. **J. Food Sci.** 64: 1010-1014.

Williams, M.L., R.F. Landel and I.D. Ferry. 1955. The temperature dependence of relaxation mechanisms in amorphous polymers and other glass-forming liquids. **J. Am. Chem Soc.** 77: 3701-3707.

Witschi, F. 1999. **Influence of Microstructure on the Drying Kinetics of a Foamed Amorphous Model Food Concentrate**. Ph.D.Thesis, Swiss Federal Institute of Technology Zürich (ETH Zürich).

Wungtanagorn, R. and S.J. Schmidt. 2001. Phenomenological study of enthalpy relaxation of amorphous glucose, fructose, and their mixture. **Thermochim. Acta.** 369: 95-116.

Zasyrkin, D.V., E.E. Braudo and V.B. Tolstoguzov. 1997. Multicomponent biopolymer gels. **Food Hydrocolloid.** 11: 159-170.





## APPENDIX

**Appendix Table 1** Zeroth-, first- and second-order rate constants ( $k$ ) and coefficients of determination ( $R^2$ ) of  $\beta$ -carotene degradation in freeze-dried maltodextrin solids (M40, M100, M250) prefrozen at various temperature ( $-20^\circ\text{C}$ ,  $-40^\circ\text{C}$  and  $-80^\circ\text{C}$ ) during storage at anhydrous condition at  $25^\circ\text{C}$ . The experimental  $\beta$ -carotene contents were fitted with the equations of various kinetics orders (zero, first and second). The results indicated the highest correlation coefficients of the first-order equations confirming the first-order kinetics degradation of  $\beta$ -carotene.

Systems	Zeroth-order <sup>3</sup>		First-order <sup>4</sup>		Second-order <sup>5</sup>	
	$k$ ( $\text{day}^{-1}$ )	$R^2$	$k$ ( $\text{day}^{-1}$ )	$R^2$	$k$ ( $\text{day}^{-1}$ )	$R^2$
M040 $-20^\circ\text{C}$	2.0571	0.9583	0.0506	0.9843	0.0019	0.9777
M040 $-40^\circ\text{C}$	2.8983	0.9712	0.0538	0.9901	0.0016	0.9476
M040 $-80^\circ\text{C}$	2.5797	0.9378	0.0486	0.9712	0.0013	0.8780
M100 $-20^\circ\text{C}$	2.4228	0.8251	0.0517	0.9494	0.0019	0.9560
M100 $-40^\circ\text{C}$	3.8465	0.9075	0.0539	0.9562	0.0015	0.9626
M100 $-80^\circ\text{C}$	5.7312	0.9307	0.0609	0.9693	0.0013	0.9371
M250 $-20^\circ\text{C}$	3.1233	0.9486	0.0562	0.9675	0.0019	0.9602
M250 $-40^\circ\text{C}$	3.5101	0.8538	0.0584	0.9463	0.0019	0.9682
M250 $-80^\circ\text{C}$	6.2517	0.9308	0.0694	0.9742	0.0016	0.9190

<sup>1</sup> The kinetics equations were transformed into linear regressions and the experimental  $\beta$ -carotene contents were plotted as a function of storage time. The rate constants,  $k$  were derived from the slope of the linear relationship.

<sup>2</sup> The coefficients of determination,  $R^2$  ranges from 0 to 1.

<sup>3</sup>  $[A] = -kt + [A_0]$

<sup>4</sup>  $\ln[A] = -kt + \ln[A_0]$

<sup>5</sup>  $\frac{1}{[A]} = \frac{1}{[A_0]} + kt$

**Appendix Table 2** The calculation of number of pores (log N) in freeze-dried solids within the range of the pore size from 0.01 to 400  $\mu\text{m}$  as shown in Figure 22. The calculation based on the assumption that the ice homogeneously formed in a spherical shape.

Diameter ( $\mu\text{m}$ )	Pore size <sup>1</sup>		Pore Volume <sup>2</sup> ( $\text{m}^3$ )	Total pores <sup>3</sup>	
	Diameter (m)	Radius (m)		number of pores (N)	Log N
0.01	0.00000001	5E-09	5.23599E-25	1.43239E+18	18.1561
0.1	0.0000001	5E-08	5.23599E-22	1.43239E+15	15.1561
1	0.000001	0.0000005	5.23599E-19	1.43239E+12	12.1561
10	0.00001	0.000005	5.23599E-16	1432394488	9.1561
20	0.00002	0.00001	4.18879E-15	179049311	8.2530
30	0.00003	0.000015	1.41372E-14	53051647.7	7.7247
40	0.00004	0.00002	3.35103E-14	22381163.87	7.3499
50	0.00005	0.000025	6.54498E-14	11459155.9	7.0592
60	0.00006	0.00003	1.13097E-13	6631455.962	6.8216
70	0.00007	0.000035	1.79594E-13	4176077.224	6.6208
80	0.00008	0.00004	2.68083E-13	2797645.484	6.4468
.	.	.	.	.	.
.	.	.	.	.	.
.	.	.	.	.	.
340	0.00034	0.00017	2.05795E-11	36443.98758	4.5616
350	0.00035	0.000175	2.24493E-11	33408.61779	4.5239
360	0.00036	0.00018	2.4429E-11	30701.18501	4.4872
370	0.00037	0.000185	2.65218E-11	28278.57161	4.4515
380	0.00038	0.00019	2.87309E-11	26104.28794	4.4167
390	0.00039	0.000195	3.10594E-11	24147.31347	4.3829
400	0.0004	0.0002	3.35103E-11	22381.16387	4.3499

<sup>1</sup> The pore diameters in solid were transformed into radius.

<sup>2</sup> The radii were calculated for the pore volume (V) by the relationship of  $V = (4/3)\pi r^3$ .

<sup>3</sup> The total pores of solids were derived on the assumption that 0.75 mL of 10 mm-cubic samples was the frozen phase. Therefore, the number of the pores came from the volume of the frozen phase ( $0.01 \times 0.01 \times 0.01 \times 0.75$ ) divided by the volume of the pores.

**Appendix Table 3** The calculation of pore wall thickness in freeze-dried solids as a function of pore diameter as shown in Figure 22. The calculation based on the assumption that the ice homogeneously formed in a spherical shape.

Pore diameter ( $\mu\text{m}$ )	Frozen volume <sup>1</sup> ( $\text{m}^3$ )	Frozen radius <sup>2</sup> (m)	Total number of pores <sup>3</sup>	Unfrozen fluid between particles		Final Radius <sup>6</sup> (m)	Wall thickness <sup>7</sup> (m)
				unfrozen/pore <sup>4</sup> ( $\text{m}^3$ )	Total Volume <sup>5</sup> ( $\text{m}^3$ )		
0.01	5.710E-25	1.104E-08	1.432E+18	7.531E-26	6.463E-25	1.150E-08	9.309E-10
0.1	5.710E-22	1.104E-07	1.432E+15	7.531E-23	6.463E-22	1.150E-07	9.309E-09
1	5.710E-19	1.104E-06	1.432E+12	7.531E-20	6.463E-19	1.150E-06	9.309E-08
10	5.710E-16	1.104E-05	1.432E+09	7.531E-17	6.463E-16	1.150E-05	9.309E-07
20	4.568E-15	2.208E-05	1.790E+08	6.025E-16	5.170E-15	2.301E-05	1.862E-06
30	1.542E-14	3.312E-05	5.305E+07	2.033E-15	1.745E-14	3.451E-05	2.793E-06
.	.	.	.	.	.	.	.
.	.	.	.	.	.	.	.
.	.	.	.	.	.	.	.
260	1.004E-11	2.870E-04	8.150E+04	1.324E-12	1.136E-11	2.991E-04	2.420E-05
270	1.124E-11	2.981E-04	7.277E+04	1.482E-12	1.272E-11	3.106E-04	2.513E-05
280	1.253E-11	3.091E-04	6.525E+04	1.653E-12	1.419E-11	3.221E-04	2.607E-05
290	1.393E-11	3.201E-04	5.873E+04	1.837E-12	1.576E-11	3.336E-04	2.700E-05

<sup>1</sup> As the ice density is  $0.917 \text{ kg/m}^3$ . The frozen volume was derived by dividing the pore volume (Appendix Table 2) by 0.917.

<sup>2</sup> The frozen radii were calculated by the relationship of  $V = (4/3)\pi r^3$ .

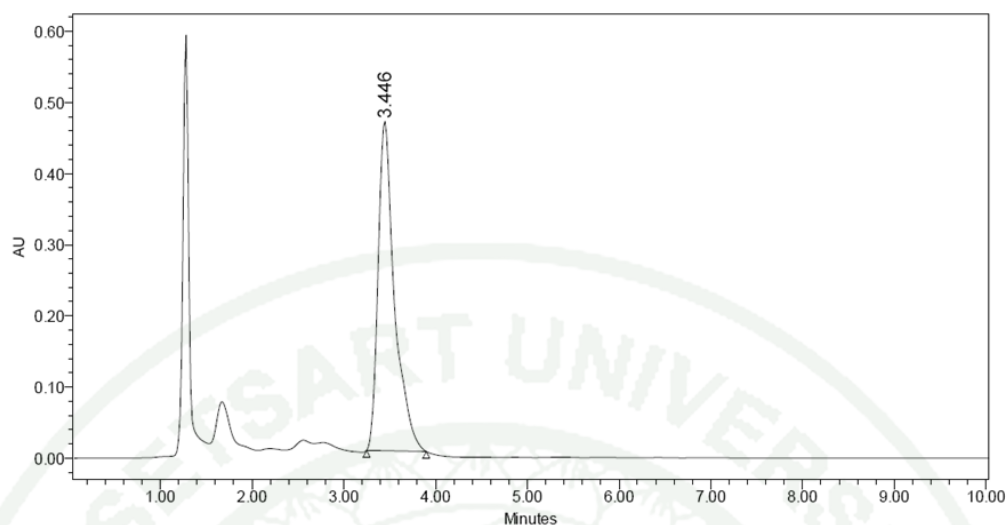
<sup>3</sup> The calculation made by Appendix Table 2.

<sup>4</sup> The unfrozen volume per pore was derived on the assumption that 0.25 mL of 10 mm-cubic samples was the unfrozen phase and approximately 43.5% of the unfrozen fluid was on pore surface. Therefore, the unfrozen fluid at the pore came from the volume of the unfrozen phase at the pore ( $0.01 \times 0.01 \times 0.01 \times 0.25 \times 0.43$ ) divided by the number of the pores.

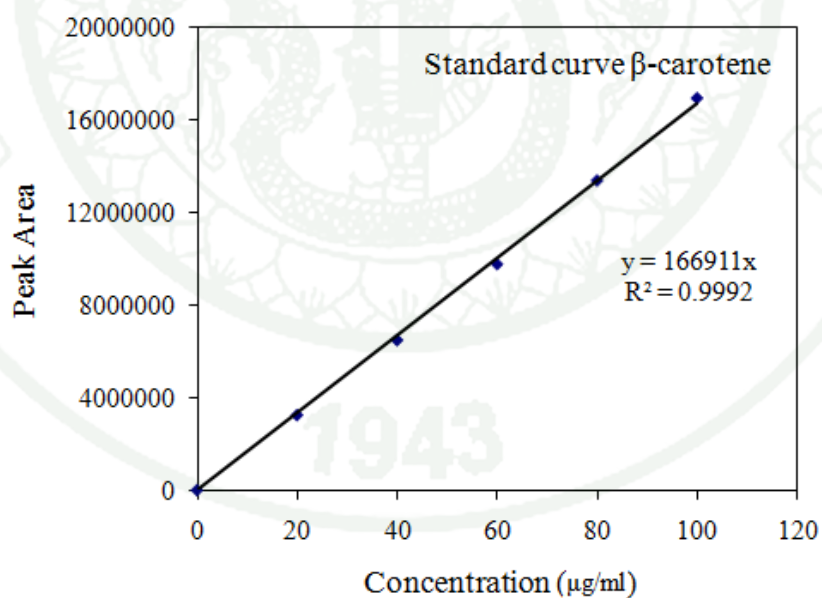
<sup>5</sup> The total volume of a pore came from the sum of frozen and unfrozen pore volume calculated from <sup>1</sup> and <sup>4</sup>, respectively.

<sup>6</sup> The final pore radii were calculated by the relationship of  $V = (4/3)\pi r^3$ .

<sup>7</sup> The wall thickness between 2 pores came from (Final radius-Frozen radius) $\times 2$

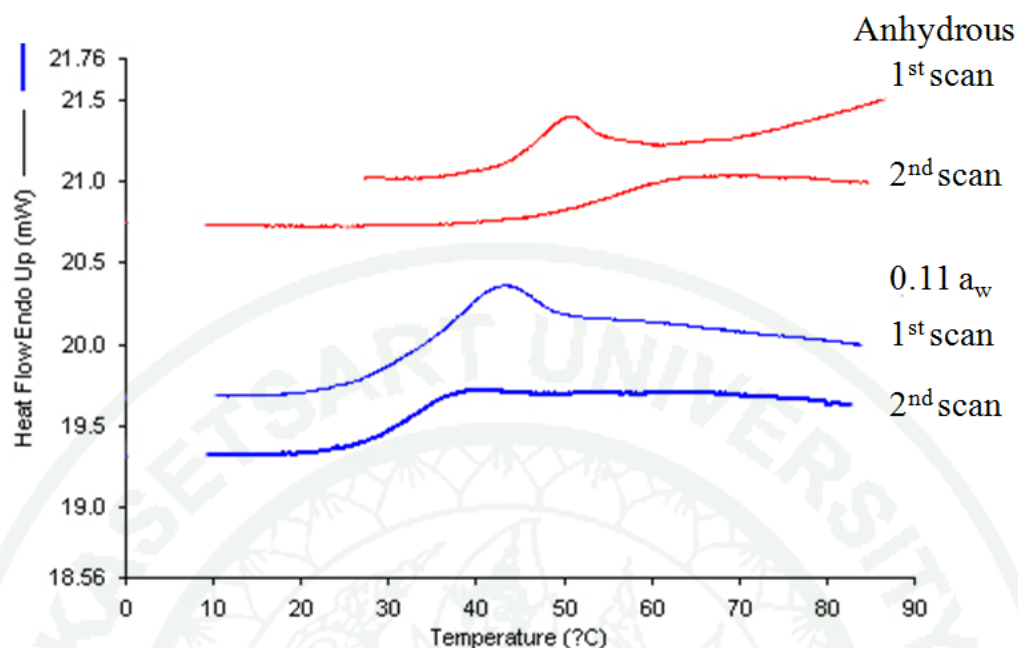


**Appendix Figure 1** Experimental HPLC chromatogram shows the eluting peak and retention time (~3.5 min) of  $\beta$ -carotene in freeze-dried mangoes.

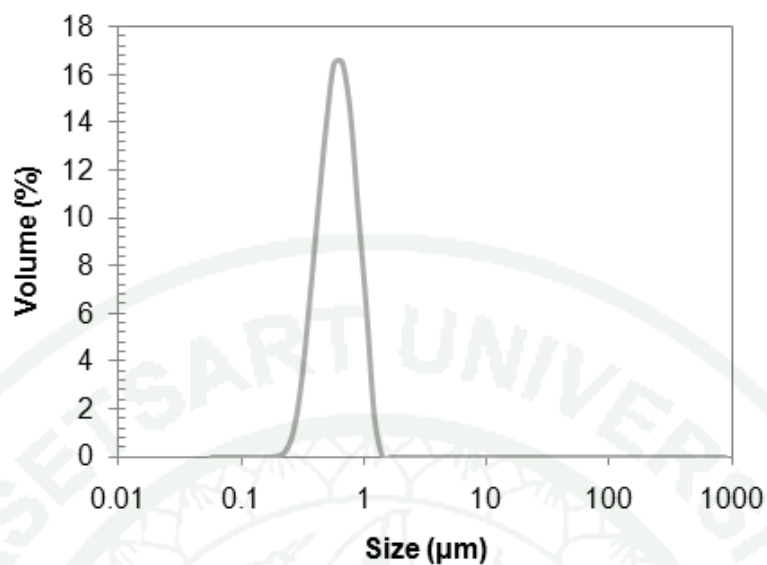


**Appendix Figure 2** Experimental standard curve for  $\beta$ -carotene analysis using a HPLC

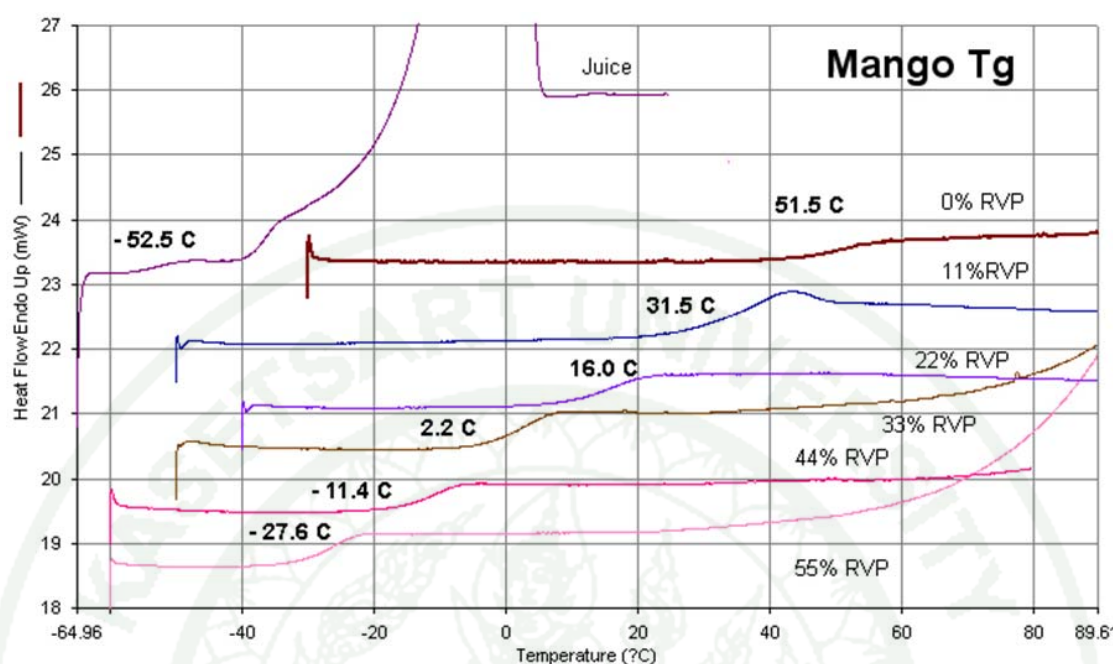




**Appendix Figure 3** First and second DSC scan of freeze-dried mangoes stored under anhydrous and 0.11a<sub>w</sub> conditions. The first scan shows the enthalpy relaxation of freeze-dried mango solids as a result of storage under T<sub>g</sub> at room temperature (25°C); while the relaxation was disappear in the second scan after heating towards the glass transition of the first scan. The enthalpy relaxation suggested the available of molecular mobility in the glassy state of mango solids.

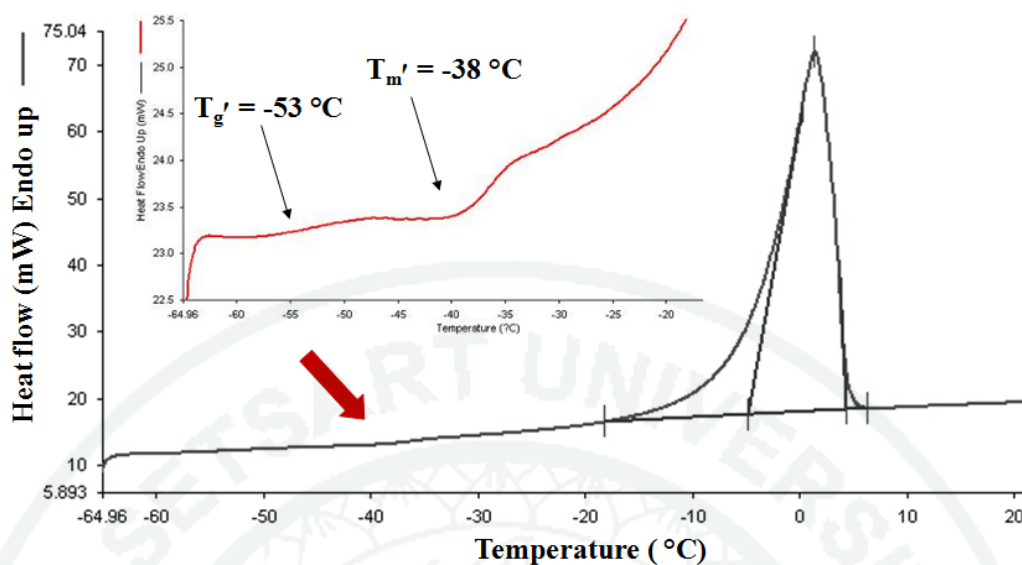


**Appendix Figure 4** Particle size distribution of dispersed phase of emulsion (40:60 oil: water) containing 0.02%w/w  $\beta$ -carotene after homogenized with a two-stage valve homogenizer prior to mixing with maltodextrin systems. The emulsion system had the normal distribution of disperse particles within the range of 0.1-2  $\mu\text{m}$ .

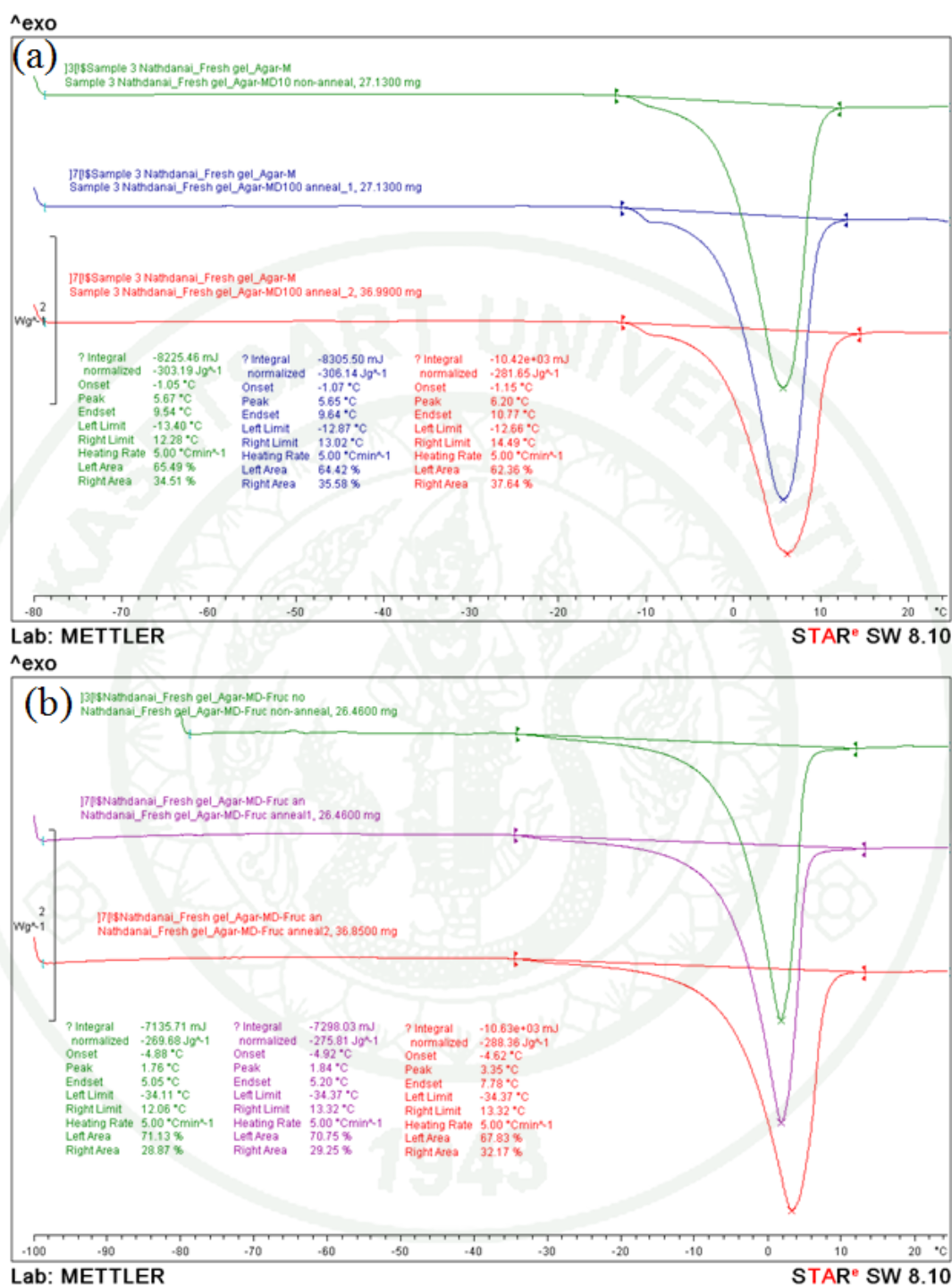


**Appendix Figure 5** DSC thermograms of mango juice and freeze-dried mangoes stored at various relative vapor pressure (RVP) with the corresponding T<sub>g</sub> values. The freeze-dried samples showed the endothermic shift of heat flow at glass transition regions. The figure shows the effect of water plasticization on decreasing T<sub>g</sub> of solids. The mango juice shows a small glass transition prior to a peak of the ice melting.

1943

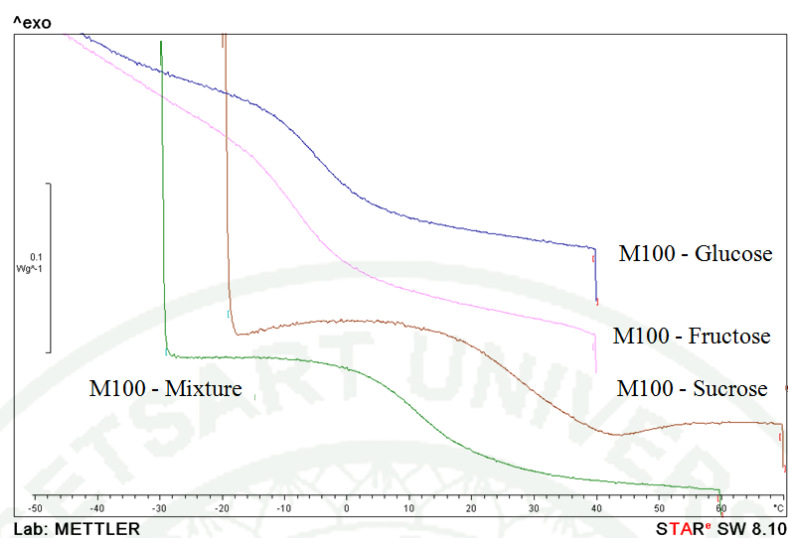


**Appendix Figure 6** DSC thermogram of fresh mango juice showing phase and state transitions of mangoes. The inset figure shows the glass transition and ice melting region with the corresponding glass transition and onset temperature of ice melting of the maximally freeze-concentrated systems ( $T_g'$  and  $T_m'$ ) as a result of annealing. The figure shows the glass transition of juice solids follows by the endothermic peak of ice melting.

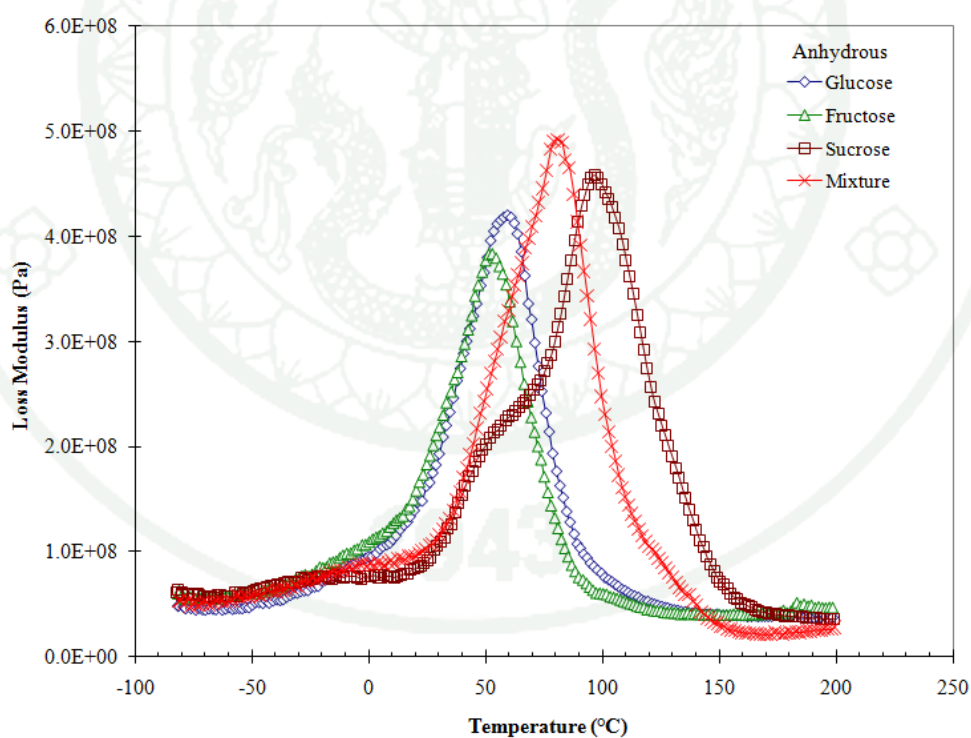


**Appendix Figure 7** DSC thermograms of agar-maltodextrin (M100) (a) and agar-M100-fructose (b) systems shows the ice melting peak during a heating scan and some experimental parameters. The figures clearly indicated the depression of the onset of ice melting in the presence of sugar (fructose).

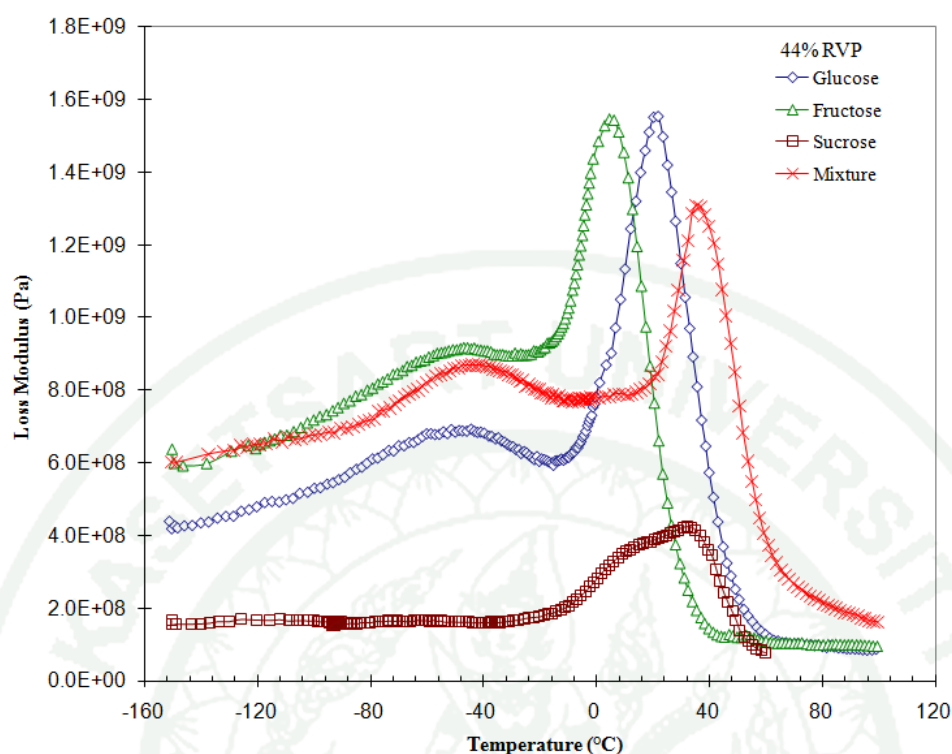




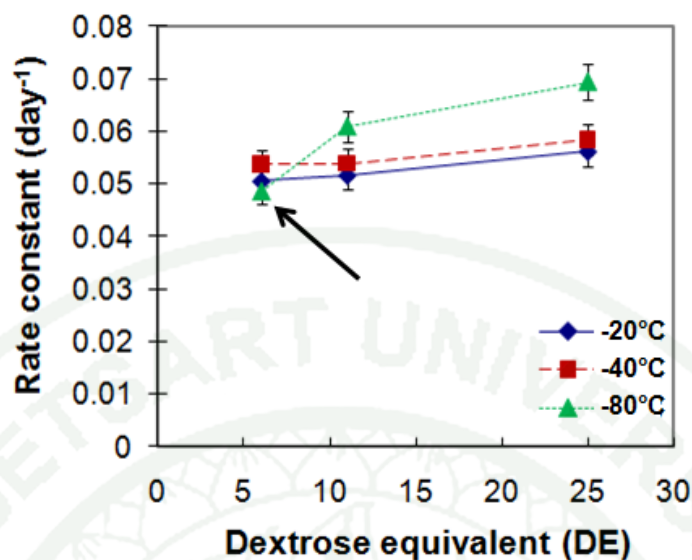
**Appendix Figure 8** DSC thermograms of freeze-dried maltodextrin-sugar systems (M100: sugar, 1:1) at  $0.44a_w$ .



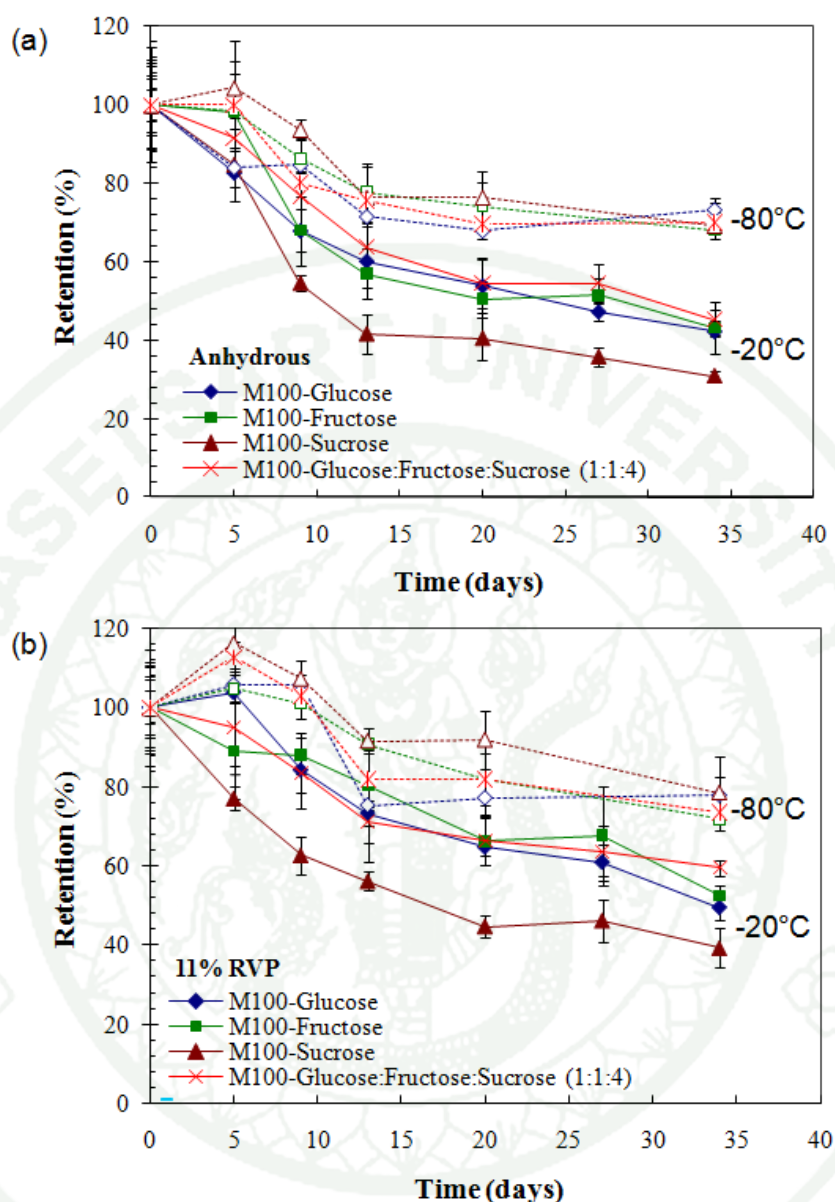
**Appendix Figure 9** The loss modulus as a function of temperature of anhydrous freeze-dried maltodextrin (M100)-sugar systems at a frequency of 0.5 Hz. The peaks of loss modulus indicate the  $\alpha$ -relaxation temperature of solids.



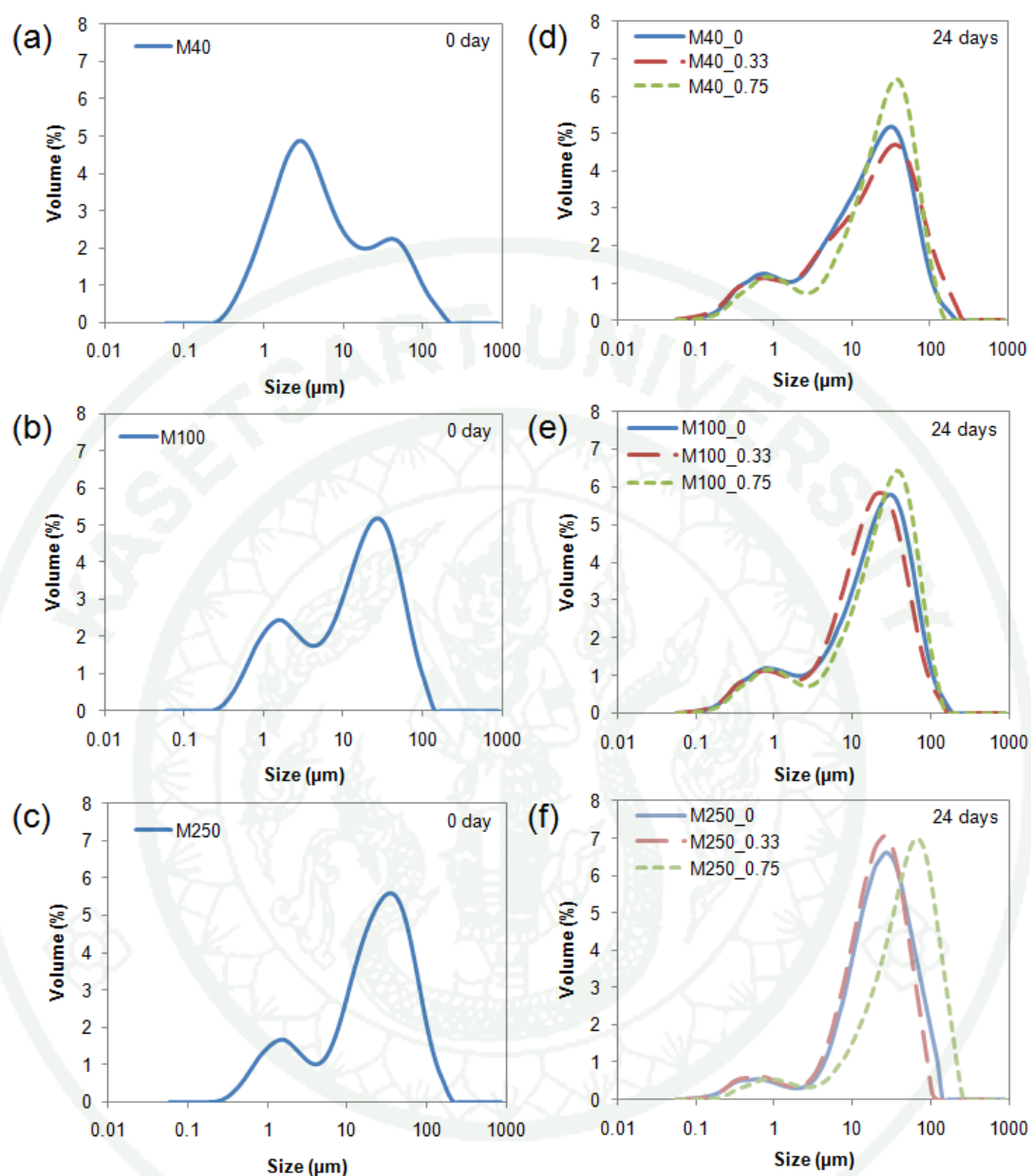
**Appendix Figure 10** The loss modulus as a function of temperature of 0.44a<sub>w</sub> freeze-dried maltodextrin (M100)-sugar systems at a frequency of 0.5 Hz. The figure shows 2 peak of loss modulus. The former peaks suggest the sub-T<sub>g</sub> relaxations; whereas, the latter indicate the α-relaxation temperature of solids. The increased water content gave clearer sub-T<sub>g</sub> relaxations.



**Appendix Figure 11** The rate constant for  $\beta$ -carotene degradation in freeze-dried maltodextrin systems as a function of dextrose equivalent (M040: DE6, M100: DE11, M250: DE25.5) at 25°C. Maltodextrin gels were prefrozen at -20°C, -40°C and -80°C prior to freeze-drying. Lower freezing temperature showed higher  $\beta$ -carotene degradation in all DE of maltodextrin. However, the exception was found in M40 systems prefrozen at -80°C which gave the highest stability (arrow). The most effective stabilization was coincident with the hard crust formation of M40 solids.



**Appendix Figure 12** Retention (%) of  $\beta$ -carotene in sugar-maltodextrin systems prefrozen at  $-20^{\circ}\text{C}$  and  $-80^{\circ}\text{C}$  during storage at (a) anhydrous and (b) 11% RVP at  $25^{\circ}\text{C}$ . Sugar systems prefrozen at  $-80^{\circ}\text{C}$  gave higher stability than  $-20^{\circ}\text{C}$  which attributed to the structural collapse of solids. The collapsed systems showed the gradation only the first 13 days followed by a limited degradation.



**Appendix Figure 13** Particle size distribution of lipid particles in maltodextrin systems (M040, M100 and M250) measured with a laser diffraction particle size analyzer at (a, b and c) 0 day and (d, e and f) 24 days of storage at various  $a_w$  (0, 0.33 and 0.75 $a_w$ ).



## Personal information

Birth Date May 27, 1985

Birth Place      Bangkok, Thailand

## Education

2007	Kasetsart University	B.Sc. (Food Science and Technology) with first class honors
------	----------------------	--

## Work and research experience

- May 2010 – January 2012, Position: Research assistant in project “Effect of Freezing conditions on  $\beta$ -carotene contents in freeze-dried mangoes” funded by Kasetsart University Research and Development Institute (KURDI), Kasetsart University, Bangkok, Thailand.
- October 2007- November 2007, Position: Research assistant in project “Rheology of Fat for Coating Applications”, Technical University of Munich, Freising, Germany.
- April 2007 - September 2007, Position: Food Regulatory Executive, Fonterra Brands Co., Ltd., Thailand.

### Award and scholarship

- The outstanding oral presentation award entitle “Microstructure and water activity effects on stability of  $\beta$ -carotene in freeze-dried systems” at the Royal Golden Jubilee Ph.D. Congress XIII, Jomtein Palm Beach Hotel, Chonburi, Thailand. 6-8 April 2012.
- The Royal Golden Jubilee Ph.D. grant from Thailand Research Fund during 2007-2012.
- DAAD award for the international student exchange from the Government of Germany (Conducting research at Technical University of Munich, Freising, Germany; research project “Rheology of Fat for Coating Applications”, 1 Oct – 30 Nov 2007).

### List of publications

- **Harnkarnsujarit, N.**, Charoenrein, S. and Roos, Y.H. 2012. Microstructure formation of maltodextrin and sugar matrices in freeze-dried systems. Carbohydrate polymers, 88, 734-742.
- **Harnkarnsujarit, N.** and Charoenrein, S. 2011. Influence of collapsed structure on stability of  $\beta$ -carotene in freeze-dried mangoes. Food Research International, 44, 3188-3194.
- **Harnkarnsujarit, N.** and Charoenrein, S. 2011. Effect of water activity on sugar crystallization and  $\beta$ -carotene stability of freeze- dried mango powder. Journal of Food Engineering, 105, 592-598.
- **Harnkarnsujarit, N.** and Charoenrein. 2009. Effect of pretreatment on glass transition temperature of freeze-dried mangoes. Proceeding of Asian Conference on Thermal Analysis and Applications, 134-138.

### Conference and academic presentation

- **Harnkarnsujarit, N.**, Charoenrein, S. and Roos, Y.H. 2012. Microstructure and water activity effects on stability of  $\beta$ -carotene in freeze-dried systems. The Royal Golden Jubilee Ph.D. Congress XIII, Jomtein Palm Beach Hotel, Chonburi, Thailand. 6-8 April 2012. (oral presentation)
- **Harnkarnsujarit, N.**, Charoenrein, S. and Roos, Y.H. 2012. Degradation of  $\beta$ -carotene in glassy porous solid polymers. International Congress on Food Engineering and Technology (IFET) 2012, Impact Convention Center, Bangkok, Thailand. 28-30 March 2012. (poster presentation)
- **Harnkarnsujarit, N.**, Charoenrein, S. and Roos, Y.H. 2012. State transitions and freeze-dried food structures. International Conference on Food and Applied Biosciences, Kantary Hill Hotel, Chiang Mai, Thailand. 6-7 February 2012. (oral presentation)

- **Harnkarnsujarit, N.**, Charoenrein, S. and Roos, Y.H. 2011. Freezing effects on structure and stability of  $\beta$ -carotene in freeze-dried solids. European Federation of Food Science and Technology (EFFoST) annual meeting 2011, Technical University of Berlin, Germany, 9-11 November 2011. (oral presentation)
- **Harnkarnsujarit, N.** and Charoenrein, S. 2011. Influence of collapsed structure on stability of  $\beta$ -carotene in freeze-dried mangoes. International Congress of Engineering and Foods (ICEF) 11, Hilton Hotel, Athens, Greece, 22-26 May 2011, (poster presentation)
- **Harnkarnsujarit, N.**, Charoenrein, S. and Roos, Y.H. 2011. Freeze-drying protocols affect stability of  $\beta$ -carotene in freeze-dried mangoes. 40<sup>th</sup> Annual UCC Food Research Conference, University College Cork, Ireland, 31 March - 1 April 2011. (oral presentation)
- **Harnkarnsujarit, N.** and Charoenrein. 2009. Effect of pretreatment on glass transition temperature of freeze-dried mangoes. Asian Conference on Thermal Analysis and Applications, Bangkok Pullman Hotel, Bangkok, Thailand, 17-18 December 2009. (oral presentation)